Quantification and seasonal variation of colored dissolved organic matter (CDOM) in the coastal and estuarine waters of Goa

A Thesis submitted in partial fulfillment for the Degree of

DOCTOR OF PHILOSOPHY

In the School of Earth, Ocean and Atmospheric Sciences

Goa University

By

Albertina Balbina Dias

CSIR- National Institute of Oceanography

Dona-Paula, Goa

December, 2021

Quantification and seasonal variation of colored dissolved organic matter (CDOM) in the coastal and estuarine waters of Goa

A Thesis submitted in partial fulfillment for the Degree of

DOCTOR OF PHILOSOPHY

In the School of Earth, Ocean and Atmospheric Sciences

Goa University

By

Albertina Balbina Dias

CSIR- National Institute of Oceanography
Dona-Paula, Goa

Research Guide

Dr. Siby Kurian

Principal Scientist
CSIR-National Institute of Oceanography
Dona-Paula, Goa, India

December, 2021

DECLARATION

I, Albertina Balbina Dias hereby declare that this thesis represents work which has been carried out by me and that it has not been submitted, either in part or full, to any other University or Institution for the award of any research degree.

Place: Dona Paula

December, 2021 Albertina Balbina Dias

CERTIFICATE

I hereby certify that the above Declaration of the candidate, name of the candidate is true and the work was carried out under my supervision.

Dr. Siby Kurian

CSIR-National Institute of Oceanography

Dona Paula, Goa, India

This thesis is dedicated to my parents, Andrew and Adriana; my sister, Anthia, and to my mentor Suresh sir,

For their endless support…..

Acknowledgment

This work would have not been accomplished without the guidance, help, and support of many people. It is an immense pleasure to thank all of them to whom I sincerely want to pay my gratitude.

I would like to offer my deepest appreciation and gratitude to my research supervisor, Dr. Siby Kurian, who accepted me willingly as her student. Her patient understanding, timely encouragement, guidance, and advice helped me in tackling and achieving my research objectives. She always kept my work as her priority, despite her busy schedule and commitments. She put in a lot of effort and time in meticulously correcting my manuscripts and thesis. I have learned a lot from her, which I will always remember and carry forward in my life.

I am deeply indebted to Dr. T Suresh, who introduced me to the subject of ocean color. He has been my backbone throughout my research, and it would have been difficult to complete this work without his support. I thank him for always standing by me, trusting that I could do much more. He taught me to look at the problem and tackle it and not to stop at the solution but to think beyond.

I am extremely grateful to my doctoral research committee members, Dr. Harilal Menon, present Vice-Chancellor of Goa University, and Dr. Mangesh Gauns, HOD of Biological Oceanography Department (CSIR-NIO) for their constructive comments, positive approach, encouragement, and guidance throughout my Ph.D. tenure.

I thank Director, CSIR-NIO for providing the facilities required to carry out my work. I am also very grateful to Dr. Damodar Shenoy for his constant support and for providing me with the required supporting data. I thank Dr. Anil Pratihary for his help in setting up the laboratory experiment and Dr. Rajdeep Roy for providing HPLC training on pigment analysis.

I am very much grateful to the chief scientists Dr. Hema Uskaikar and Dr. Anil Pratihary, participants, and crew members for their support during the cruises, and biogeochemistry group during CaTS field trips. Also, I acknowledge Ms. Alnilam Fernandes for her help onboard during the SSD 052 cruise.

I am very much thankful to all my colleagues of the Ocean color group especially Mitilesh and Ashvesh, and the biogeochemistry group for all the help rendered during field measurements. I would like to thank Mr. Vijay Kumar Kanojia, Dr. Madhubala, Shreya, Nupoor, and Shubam for their help in Matlab and programming. I am also thankful to Mrs.Supriya, Mr.Anand, and Mr.Dalvi for all the technical assistance and help provided whenever needed.

Distance is not a bar and I would like to thank the scientific advice and help received from Dr. Rossana DelVecchio. Though she has left for the heavenly adobe, I will always remember the lengthy conversation we had on PARAFAC analysis. Dr. Kathleen Murphy and Dr. Urban Wunch are also acknowledged for their help on PARAFAC analysis. Dr. Nagur Cherukuru, Dr. Collin Roesler, Dr. Ajit Subramanium, Dr. Joaquim Goes, Dr. Micheal Goinsor, and Dr. Jennifer Canninzaro are thanked for the discussions during my research work.

I thank Dr. Richita for comforting me during difficult times and motivating me to write my thesis. I am also very thankful to Dr. Suhas Shetye for his constant encouragement to finish the thesis on time. I owe my friends Dr. Madhubala, Amanda, Mithilesh, Ashvesh, Priya, Shreya, Janvi, Nandini, Ankita, Jonathan, Noah, Nupoor, Reshmita, Bhagyashri, Chndrasekhara Rao, Mithila, Dr. Amara, Snehal, Sidhesh, Adnan, Siddharth, SaiPrasad, Aseem, Sujatha, Apsara, Sethu, Dr. Anbuselvan and Nandakumar, who always stood by me and helped me during the journey of my Ph.D.

CSIR is acknowledged for granting me the Senior Research Fellowship. Space Application Center (ISRO), Indian National Centre for Ocean Information Services (INCOIS), and Ministry of Earth Sciences (SIBER-INDIA project) are acknowledged for the project funding.

The faculty members and staff (Mr. Yeshwant, Ms. Joaninha, and Ms. Namita Naik) of the Marine Science department at Goa University, and NIO who helped me in some way or the other are acknowledged for their support throughout my Ph.D tenure. I also acknowledge the help provided by the HRM and the library staff of NIO during my Ph.D. tenure.

I am also thankful to Ms. Sushama Sonak, Ms. Shradada Uchil, and Sr. Moncia Cardozo for their help in the compilation of my thesis.

Finally, I wish to thank my parents, especially my mother for always striving to give me the best and being by my side in good and bad times during this journey. My sister, Anthia, and brother-in-law Raymond are acknowledged for their love, continuous encouragement, and support during my anguish. A special thanks to my sweet little niece, Rebecca for being my stress reliever. I thank my family members, near and dear friends, and well-wishers who always supported me with their prayers.

Above all, I would like to thank God, the almighty, for giving me wisdom, his innumerable blessings and grace, and loving comfort through this journey of my life.

Albertina Dias

Table of contents

Abstract

The ocean is one of the largest sinks of bioactive carbon on earth, storing as much as 700 petagrams (Pg) of carbon, and hence plays an important role in the carbon cycle and global climate. The amount of dissolved organic carbon (DOC) in the aquatic environments is comparable to the carbon reservoir in the atmosphere. Although colored dissolved organic matter (CDOM) represents a small fraction of DOM, absorption of light in the aquatic environment is controlled by the colored and particulate organic matter in water and hence can have a profound impact on the marine environment. The rivers and estuaries form an important conduit transporting organic carbon between the terrestrial and marine ecosystems. Keeping this in mind, spatial and temporal variations of the optically important fraction of carbon in the estuarine and coastal waters of Goa, on the west coast of India are presented in this study. The estuarine waters of Goa have two -fold higher CDOM absorption than the coastal waters of Goa, with the maximum absorption observed during the south west monsoon (SWM) and spring inter-monsoon (SIM). Both the seasons have contrasting hydrographic and biogeochemical variations, with CDOM originating from the terrigenous origin with low spectral slopes and low S_R values indicating the dominance of high molecular weight organic matter coinciding with low salinity, high river runoff, and lower residence time during SWM. However, during SIM, the CDOM origin is mostly autochthonous favored by the longer residence time of water, mangrove inputs, and anthropogenic activities in the estuaries, as indicated by higher spectral slopes and S_R values. Principal component analysis was used to successfully differentiate the sources of CDOM, with the samples during non-monsoon clustering together indicating the dominant autochthonous source, while samples during monsoon clustered together indicating the terrestrial nature of DOM. A prominent non-conservative mixing behavior between the estuarine and coastal waters was observed with large additions of CDOM in the mid-stream region of the estuaries, while removal of CDOM was observed in the coastal waters by photobleaching during all the seasons and due to flocculation in the estuaries at very low salinities during SWM. The Influence of CDOM was observed in the modulation of the spectral quality of underwater light by shifting the underwater light penetration to a longer wavelength (570 nm) in the estuaries as compared to the coastal waters (540 nm).

In the marine environment, autochthonous production arising from phytoplankton is an important source of organic matter. The coastal waters of Goa witness blooms of phytoplankton, of which *Trichodesmium* has been reported in these waters since the 1970s. In this study, the spectral and fluorescence characteristics of CDOM during *Trichodesmium* blooms observed during SIM of 2014-2018 are presented. The CDOM during *Trichodesmium* blooms was unique with distinct peaks in the UV and visible region and deviated from the normal exponential behavior. The peaks in the UV region were attributed to the mycosporine -like amino acids (MAA) and visible region due to phycobiliproteins. Some characteristics of the CDOM spectra during the *Trichodesmium* bloom, helped to differentiate the stages of bloom. The peaks in the visible region were observed only during the senescence phase of the bloom due to the leaching of the phycobiliprotein pigments which are water-soluble, while these were not observed during the growing phase and only peaks due to MAA were present. Three FDOM components (2 humic-like and 1 protein-like fluorescence) were identified during *Trichodesmium* blooms using PARAFAC. One of the humic-like components was linked to the degradation product of tetrapyrroles and the other was similar to the marine humic-like component. The protein-like component resembled tryptophan-like amino acid. Our field study proves the production of humic-like organic matter by phytoplankton which was earlier thought to arise only from terrestrial sources. In addition, *in-situ* experiments proved that bacteria play an important role in the degradation of organic matter along with photodegradation.

The western continental shelf of India (WCSI) experiences upwelling during the SWM which results in nutrient enrichment in the euphotic zone further driving high productivity in the region. A strong stratification is observed due to the low saline water arising from local precipitation and land-driven runoff above the high saline, low temperature upwelled waters. Rapid microbial remineralization reduces the oxygen content in the water column resulting in hypoxic to anoxic conditions in the subsurface layer during the late SWM. The studies on CDOM absorption and characterization were carried out along the WCSI during the upwelling and seasonal hypoxia. High CDOM absorption (a_g412 m^{-1}) was observed in the bottom waters, which coincided with hypoxic/suboxic conditions. During the seasonal hypoxia, it is presumed that anoxic sediments would lead to the release of iron oxide -bound organic matter to the overlying water column. This could be one of the reasons for high CDOM absorption in the bottom waters. Spectral slope, $S_{250\text{-}600}$ also showed a significant difference between the oxygen -rich and low oxygenated waters. Three

fluorescent DOM components were identified from PARAFAC analysis. Component 1 (C1) and 2 (C2) were humic-like with emissions in the longer wavelength, while component 3 (C3) was protein-like with excitation and emission in the UV region. CDOM absorption (a_g412) and humic-like fluorescent component (C1) showed a positive correlation with apparent oxygen utilization (AOU), indicating the role of microbial respiration for CDOM production. Laboratory experiments also shed light on the CDOM production in low oxygenated waters when sufficient organic matter is available. This study gives insight into understanding the cycling of DOM under varying oxygen conditions prevailing in these waters.

List of Tables

List of Figures

List of Abbreviations

Abbreviation	Description
OM	Organic matter
DOM	Dissolved organic matter
DOC	Dissolved organic carbon
CDOM	Colored dissolved organic matter
CDM	CDOM + detrital matter
FDOM	Fluorescent dissolvent organic matter
POM	Particulate organic matter
a_g412	CDOM absorption (m^{-1}) at 412 nm
$S_{250-600}$	Spectral slope (nm^{-1}) in the range of 250-600 nm
$S_{275-295}$	Spectral slope (nm^{-1}) in the range of 275-295nm
$S_{350-400}$	Spectral slope (nm^{-1}) in the range of 350-400 nm
S_R	Slope ratio
$a_d(\lambda)$	Absorption by detritus (m^{-1})
$a_{ph}(\lambda)$	Absorption by Phytoplankton pigment (m^{-1})
E_s	Surface solar irradiance ($Wm^{-2}nm^{-1}$)
k_d	Diffuse attenuation coefficient (m^{-1})
L_u	Upwelling radiance ($Wm^{-2}nm^{-1}sr^{-1}$)
E_d	Downwelling irradiance ($Wm^{-2}nm^{-1}$)
R_{rs}	Remote sensing reflectance at the surface of water (sr^{-1})
Z_{90}	Penetration depth (m)
PAR	Photosynthetically available radiations
WCSI	Western continental shelf of India
AS	Arabian Sea
OMZ	Oxygen minimum zone
SIM	Spring-inter monsoon
SWM	Southwest monsoon
FIM	Fall inter monsoon
NEM	Northeast monsoon

CTD	Conductivity, temperature, depth
AOU	Apparent oxygen utilization ($\mu molkg^{-1}$)
DO	Dissolved oxygen (mL/L)
SST	Sea surface temperature (^oC)
SSS	Sea surface salinity
EEM	Excitation emission matrix
IFE	Inner filter effect
PARAFAC	Parallel factor analysis
PCA	Principal component analysis
ANOVA	One way analysis of variance
RU	Raman units
FI	Fluorescent index
SNR	Signal to noise ratio
ECV	Essential climate variables
ETM	Estuarine turbidity maxima
HPLC	High performance liquid chromatography
FCC	fluorescent chlorophyll catabolites
MAA	Mycosporine-like amino acid
PC	Phycocyanin
PUB	Phycourobilin
PEB	Phycoerythrobilin
TEP	Transparent exopolymeric particles
PCD	Programmed cell death

Chapter 1

Introduction

1. Introduction

1.1. General Overview

Oceans are one of the largest ecosystems, occupying about 70% of the surface on earth of which, only about 7-10% is present as coastal oceans (Walsh, 1991; Borges et al., 2005; Muller-Karger et al., 2005) and contribute substantially to the biogeochemical cycles. The coastal oceans are unique having interconnection with multiple ecosystems forming a conduit between the land and the oceans. Moreover, coastal waters are one of the most productive marine ecosystems accounting for 13-33% of the oceanic production and 80% of the organic matter (OM) burial (Gattuso et al., 1998), and offer great control on the global climate, by maintaining the CO_2 balance in the atmosphere.

Typically, OM is operationally differentiated based on their retention on the filter (0.2 or 0.7 micron) as particulate OM (POM), and that which passes through the filter is termed as dissolved OM (DOM). The major fraction of POM is the detrital matter with a small portion of living biomass generally suspended in the water column which sinks to the bottom sediments over time. While the dissolved fraction is majorly lifeless, though it includes some prokaryotes and viruses (Hedges, 2002) and has a very long residence time in water which contributes significantly to the carbon pool. DOM is one of the largest available pools of organic carbon on earth, carrying a percentage of carbon equivalents to that available in the atmosphere as CO_2 (Hedges, 1992), and hence play a vital role in the global carbon cycle. DOM comprises organic compounds arising from the remains of plants, animals, and their waste products having varied molecular weights. In the oceans, a major fraction of DOM exists in the form of dissolved organic carbon (DOC) and accounts for around 700 Pg of carbon in the ocean (Hansell et al., 2002). The fraction of DOM that interacts with light is defined as colored DOM (CDOM). Initially, it was termed as gelbstoff (A German term meaning “yellow substance”) by Kalle in 1966, gilvin (in Latin meant pale yellow) by Kirk, (1976) since it imparts yellow color to the water. In particular, CDOM absorbs light over a broad range of wavelengths with the strongest absorption in the UV region (200-380 nm) and decreases exponentially to near-zero absorption in the red region of visible light (700-850 nm). CDOM mostly constitutes humic substances, which can further be classified into humic acids, fulvic acids, and humins, and is responsible for around 70-90% of DOC in the coastal waters (Coble, 2007). The fractions of organic matter are pictorially depicted in figure 1.1. CDOM can be easily

characterized based on its optical characteristics of absorption and fluorescence (Stedmon and Markager, 2003). These methods of characterization of CDOM are affordable, and offers a non-destructive means for acquiring sensitive estimations of a diverse group of organic compounds.

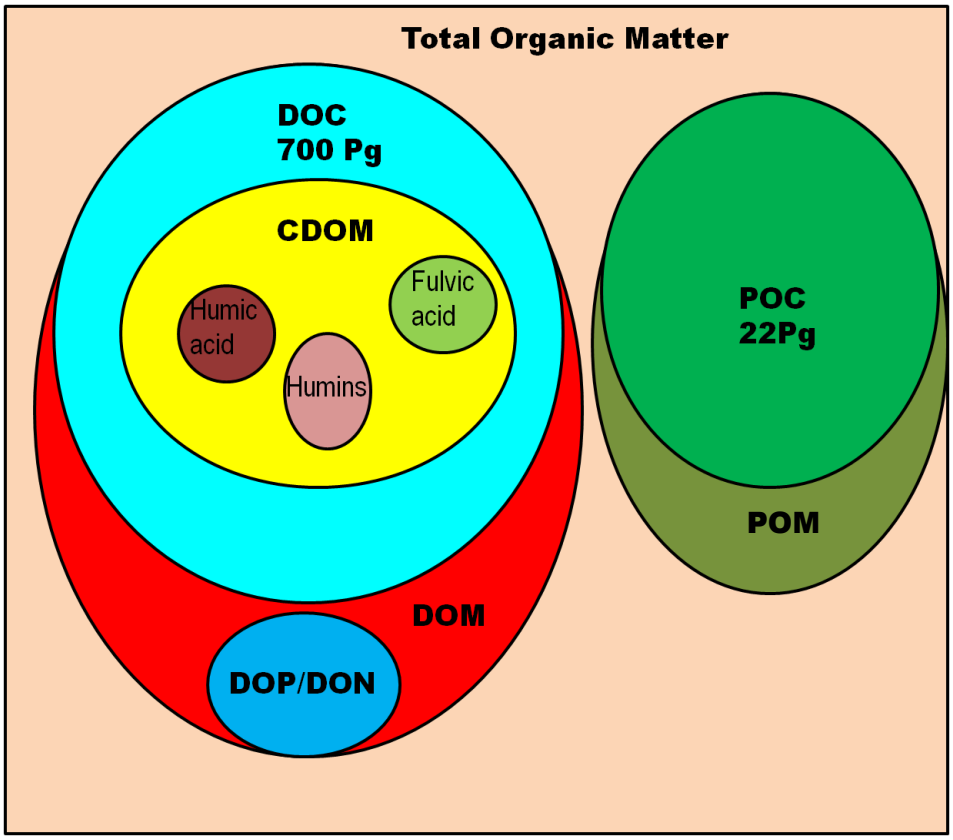

Figure 1.1: The distribution of various fractions of organic carbon in the water.

1.2. Sources and Sink of CDOM

In the marine system, CDOM can originate either from autochthonous or allochthonous sources. The autochthonous sources comprises plankton exudates arising from grazing and excretion, extracellular release by algae, degradation and exudation of macrophytes, viral lysis of bacteria and algae, and benthic fluxes (Kawasaki and Benner, 2006, Lonborg et al., 2009; Fig. 1.2). While the allochthonous sources predominantly include the terrestrially derived organic matter, augmented by groundwater, atmospheric inputs, and OM arising from anthropogenic activities (Willey et al., 2000; Raymond and Spencer, 2015). Specifically, terrestrial DOM comprises soil-derived humic substances and also incorporates material leached from plants exported during rain events. Bacteria are not only the consumers of DOM but also produce DOM during cell division and viral lysis

(Iturriaga and Zsolany, 1981; Ogawa et al., 2001; Kawasaki and Benner, 2006). In addition, marine sediments are one of the dominant sites for OM degradation, hosting 1000 times more microbial density than found in the water column (Hewson et al., 2001). The concentration of DOM in the sediments are also several magnitudes higher than that found in the overlying water column (Burdige and Gardner, 1998), resulting in diffusive fluxes and hence are a major DOC source (350 Tg C yr^{-1}) equivalent to inputs received from rivers (Burdige and Komada, 2015).

The important pathways which are responsible for the removal of CDOM from the water column include abiotic degradation through photochemical reactions, flocculation into micro-particles or sorption to particles, and biotic degradation by heterotrophic micro-organisms. It is estimated that the combined effect of photobleaching and microbial degradation is responsible for the removal of the major fraction of CDOM from the water column (Carlson and Hansell, 2015; Fig. 1.2). The CDOM being coherent between the chemical and biological world plays a vital role in the functioning of the ecosystem. It is therefore utmost necessary to study the impact of global climate change on the cycling of this fraction of DOC.

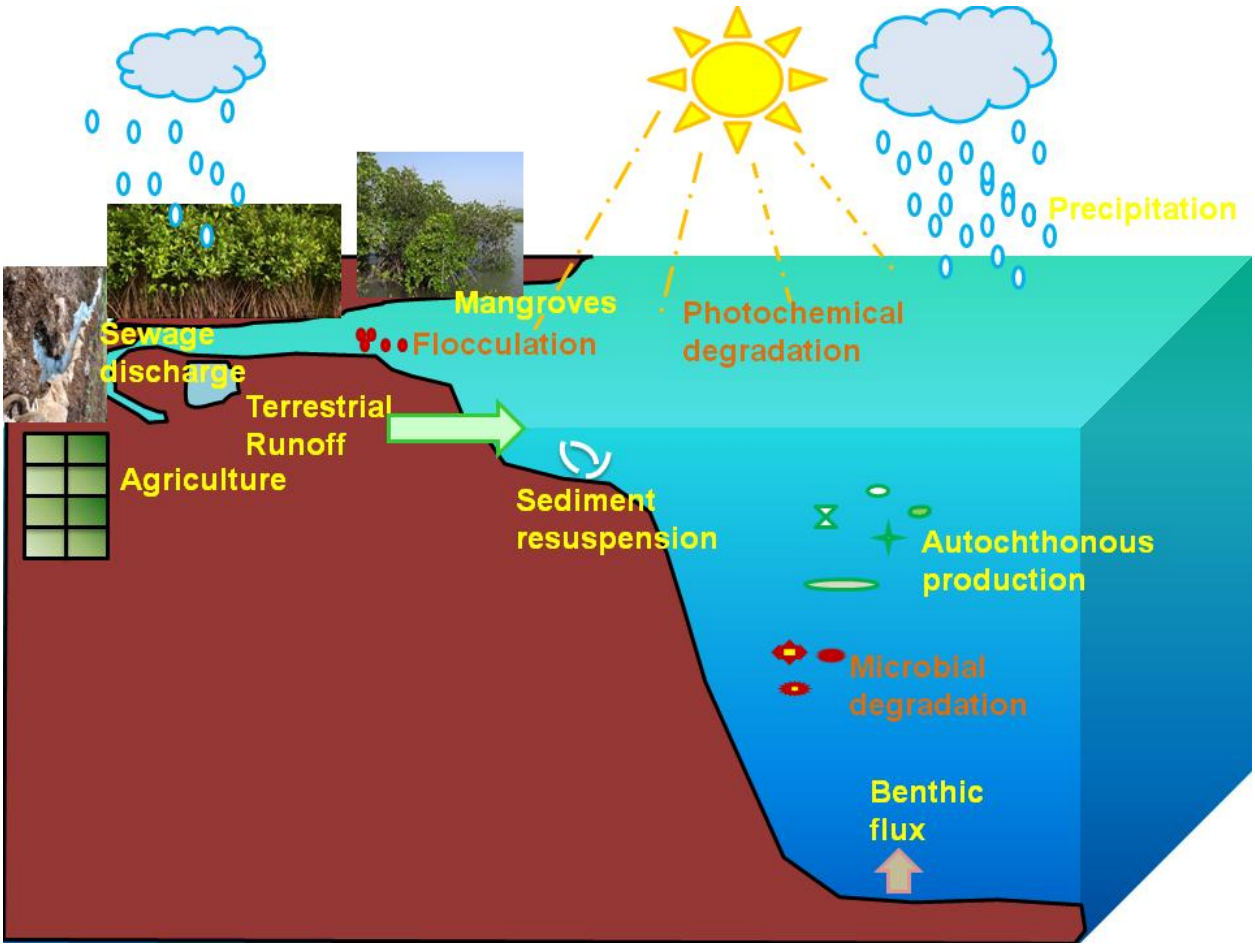

Figure 1.2: The potential sources (indicated in yellow color) and sinks (indicated in orange color) of CDOM in the water are depicted.

1.3. CDOM and environmental significance

CDOM greatly influences the aquatic light field as it absorbs highly in the UV and visible region (Del Vecchio and Blough, 2002), and hence can pose positive and negative effects on the environment. CDOM can thus provide photoprotection to phytoplankton and other sensitive organisms from the damaging UV radiations (Del Vecchio and Blough, 2002; Coble, 2007). It also regulates the penetration of photosynthetically available radiations (PAR) which can influence the primary production (DeGrandpre et al., 1996; Vodacek et al., 1997).

The estimation of phytoplankton from ocean color satellites has received widespread application for various studies across the globe. CDOM can have a profound influence on the remote estimation of chlorophyll from satellites. It is estimated that a CDOM absorption signal of 0.005 m^{-1} at 440 nm would result in the satellite signal equivalent to

0.1 mgm^{-3} concentration of chlorophyll-*a* (Carder et al., 1989). Hence precise estimates of CDOM on regional scales are important for the necessary corrections to be done in the remote estimation of chlorophyll-*a*. CDOM is photoreactive (Mopper and Kieber, 2002) resulting in the loss of absorption (Del Vecchio and Blough, 2002; Vodacek et al., 1997) and in turn production of biologically available low molecular weight compounds that can propel the growth of micro-organisms. CDOM photodegradation can also result in the production of several important trace gases such as CO_2 and CO, as well as the photosensitized loss of gases such as dimethyl sulfide (Mopper and Kieber, 2002; Nelson and Siegel, 2002). Therefore, net oxidation of only 1% of the total oceanic DOM pool within one year would lead to a larger CO_2 flux to the atmosphere than that produced annually by fossil fuel burning (Hedges et al., 2001).

CDOM comprises diverse functional groups like aromatics, phenols, quinines which can provide binding sites for various organic, inorganic pollutants, metals and thus decrease their bioavailability and toxicity (Wu et al., 2011; Zhang et al., 2019; Yuan et al., 2019). CDOM acts as a carrier of nutrients either directly or via the microbial loop and hence regulates the availability of nutrients in the water.

1.4. CDOM and climate change

Climate change is real and various parameters of the ocean are changing, with dissolved oxygen reducing, methane increasing by a factor of 2.5, nitrous oxide by a factor of 1.2, and CO_2 being absorbed by the ocean resulting in acidification. Ocean color parameters, which include CDOM are now part of the 54 Essential Climate Variables (ECV) (Dutkiewicz et al., 2019; Bojinski et al., 2014). Since CDOM is already listed as ECV, monitoring its variations and other studies of CDOM on regular basis will be required.

1.5. Ocean Warming

Light in the water is attenuated either by scattering or absorption by optically active fractions in the water. The attenuation of light affects the near-surface vertical temperature distribution (Zaneveld et al., 1981). An increase in atmospheric CO_2 in recent years due to human activity has been observed (Boucher et al., 2013), resulting in the warming of oceans (Levitus et al., 2000) and ocean acidification (Caldeira and Wickett, 2003). Among the oceans, the Indian Ocean is one of the most rapidly warming oceanic basins (Gnanaseelan et al., 2017; Beal et al., 2020). A rapid increase in sea surface temperature (SST) has been observed with an average rise of 1ºC during 1951-2015 in the tropical Indian Ocean (Roxy et al., 2020). In the Arctic, biologically induced surface warming has been observed (Pefanis et al., 2020). Due to global warming, India too has witnessed an increase in the number of cyclones and catastrophic events in recent years. The increase in precipitation and subsequent land-driven runoff will result in an increase of the optically active fractions (CDOM + detritus), which may have a positive feedback on ocean warming.

On the contrary, ocean warming would result in the highly stratified surface ocean and strengthening of thermocline favoring CDOM photobleaching with the present and future increase in Earths' UV radiations (Herman, 2010; Watanabe et al., 2011; Lonborg et al., 2020). As a result of which a net loss of carbon pool to the atmosphere is expected.

1.6. Ocean acidification

As a result of industrialization and an increase in the combustion of fossil fuels, 40% rise in atmospheric CO_2 levels is observed as compared to the pre-industrial times (Gattuso et al., 2015). It has been reported that about one-third of the anthropogenically emitted CO_2 is sequestered in the oceans, resulting in ocean acidification, a condition wherein the pH of

the water decreases (Sabine et al., 2004; Gruber et al., 2019). A 0.1 unit decrease in the pH is currently observed in the global oceans. A few studies reported the impact of pH change on the photochemical and microbial degradation of organic matter (Timko et al., 2015; James et al., 2017). It is known that photochemical processes are mediated by pH and a study conducted by Timko et al. (2015) has shown large changes in photochemical degradation of OM at higher pH, whereas a decrease in degradation is expected at lower pH. Some studies have pointed out the increase in extracellular enzyme activities as a function of CO_2 suggesting increased microbial degradation (Teira et al., 2012; Piontek et al., 2013; James et al., 2017).

1.7. Ocean deoxygenation

Over the past 50 years, the number of oxygen minimum zones (OMZ) are increasing in the world ocean as a result of global warming (Keeling et al., 2010; Robinson, 2019), 15% of which is due to the decrease in oxygen solubility, while 85% is due to intensified stratification in the open ocean (Helm et al., 2011). Whereas, in the coastal waters the deoxygenation is mostly related to the respiration of organic matter (Diaz et al., 2019). Global models predicted a further decrease in dissolved oxygen by 1.5 to 4% by 2090 (Ciais et al., 2014). The effect of deoxygenation will be more amplified in the coastal waters as it is predicted due to the increased nutrient loadings compared to the current levels and hence enhanced respiration by microorganisms (Foley et al., 2005; Foley, 2017). This scenario will especially be important for Indian waters, which host the largest OMZ in the open ocean, apart from the coastal waters along the western continental shelf of India (WCSI) which experiences seasonal hypoxia during the late southwest monsoon (SWM). With an increase in global warming and tropical cyclones in the recent years, the effect of the organic matter loading on seasonal hypoxia will be important.

1.8. Background work in Indian waters

The pioneering work carried out on CDOM by Coble et al. (1998) in the western Arabian Sea (AS) during the SWM of 1995 showed a negative correlation between surface CDOM and temperature, reflecting that the upwelled waters are the source of CDOM. They also identified 3 distinctive water masses based on the excitation-emission matrix (EEM) fingerprints in the study region. Later, Del Castillo and Coble, (2000) studied the absorption and fluorescence properties of CDOM during the northeast (NE) and southwest

(SW) monsoon in the Arabian Sea of 1994-95 and found that the differences in the wind regimes were responsible for the seasonal variability of CDOM and fluorescent DOM (FDOM) in the study region.

There are several studies available on the CDOM and FDOM variation along the estuaries from the east coast of India (Das et al., 2016; Sarma et al., 2018; Chari et al., 2019; Sanyal et al., 2020; Chari et al., 2021), the coastal waters and along the shelf region in the Bay of Bengal (Chiranjeevulu et al., 2014; Chari et al., 2013a, 2016; Das et al., 2017; Pandi et al., 2021). In addition, experimental studies on the axenic cultures of phytoplankton were also conducted for the CDOM and FDOM production (Chari et al., 2013b). Studies related to the remote estimation of CDOM were also carried out along the east coast of India (Tiwari and Shanmugam, 2011; Shanmugam et al., 2016). In comparison, the studies on the CDOM variations along the west coast of India are quite limited. The estuarine and coastal waters of Goa were first studied for the CDOM variations by Menon et al. (2005; 2006a, b), and later Menon et al. (2011) reported the CDOM variability in the Mandovi and Zuari estuaries using *in-situ* and satellite data. In addition, Dias et al. (2017) studied the CDOM characteristics in the estuaries and the coastal waters of Goa but their study was limited to the spring-inter monsoon (SIM) season.

1.9. Why this study was undertaken?

The coastal and estuarine waters of Goa are very complex affected by many natural processes and anthropogenic influences. Several studies since long have been undertaken in these waters on the physical (Das et al., 1972; Sankaranarayanan and Jayaraman, 1972; Unnikrishnan et al., 1997; Shetye, 1999; Shetye et al., 2007; Unnikrishnan and Manoj, 2007; Manoj and Unnikrishnan, 2009), biogeochemical (Dehadrai, 1970; Dehadrai and Bhargava, 1972; Singbal, 1973; Bhargava and Dwivedi, 1976; Qasim and Sen Gupta, 1981; Matondkar et al., 2007; Ram et al., 2007; Ramaiah et al., 2007; Maya et al., 2011a; Parab et al., 2013; Kessarkar et al., 2013; Cowie et al., 2014; Bardhan et al., 2015; Kessarkar et al., 2015; Shynu et al., 2015; Rao and Chakraborty, 2016; Araujo et al., 2018; Pednekar et al., 2018, Fernandes et al., 2018) and bio-optical aspects (Sathyendranath and Varadachari, 1982; Suresh et al., 1998; Desa et al., 2001; Suresh et al., 2006a, b; Thayapurath et al., 2016; Menon et al., 2011; Tilstone et al., 2013; Talaulikar et al., 2015).

The Mandovi and the Zuari are the two main monsoonal estuaries of Goa, which originate from the Sahyadris. Goa receives heavy precipitation, land runoff from June to September, which brings about large changes in temperature, salinity, flow pattern, dissolved oxygen, and nutrients (Qasim and Sen gupta, 1981). The runoff is almost negligible during the other seasons. During the dry season, tides become the major driving force transporting and mixing the estuarine waters to the adjacent coastal waters (Shetye et al., 2007). There are mangroves along the banks of the Mandovi and Zuari estuaries, which harbor sediments rich in OM (Wafar, 1987). Many agricultural activities like rice cultivation, horticulture are practiced along the fertile coastal plain in the catchments of the Mandovi and Zuari estuaries. Khazan lands are also present along the estuaries. Goa is famous for mining iron and manganese ore and these mining rejects end up in these estuaries (De Souza, 1999). All these allochthonous inputs could be the probable sources of CDOM in these estuaries. The estuaries also support autochthonous production in terms of phytoplankton productivity, which varies with the season (Matondkar et al., 2007). The coastal waters are affected by the seasonal reversing currents with strong temperature inversions being observed due to the transport of low saline waters from the Bay of Bengal during winter (Prasanna Kumar et al., 2004). There is an increase in the number of hypoxic sites observed in the coastal waters of the world, and these 'dead zones' are spreading worldwide (Breitburg et al., 2018). Oxygen deficient conditions are reported along the western continental shelf of India (WCSI) with varying intensity (Naqvi et al., 2006), which has a large impact on the demersal fisheries and leads to a decline in the fish catch. These waters also experience phytoplankton bloom of varied species, which are seasonal and also episodic (Naqvi et al., 1998; Krishnakumari et al., 2002; Desa et al., 2005; Gomes et al., 2008; Pednekar, et al., 2012). Hence, the study of CDOM in these waters becomes very important.

The estuarine waters are dynamic and are affected by the land-use changes, the anthropogenic activities occurring in the estuaries and along its banks, the impact of climate change and the natural adversity arising from it. A number of studies have been carried out on the DOC and POC in these estuaries; however, the studies on CDOM are limited. The first report on CDOM studies was by Menon et al. (2005), and thereafter Menon et al. (2011) developed an algorithm for remote estimation of CDOM using the data collected during 2003-2004. The estuaries have undergone a great deal of transformation since 2005 with an increase in mining activities along its banks,

transportation of ore to the loading sites across the estuaries, sand extraction, pleasure cruises, Casinos, increase in urbanization, and industrialization along its banks, etc.

The proposed study will bridge the gap in understanding the spatial and temporal variability, probable sources and sinks of CDOM in the estuarine and coastal waters of Goa, and its characteristics during various phytoplankton blooms and hypoxic conditions.

In this study, a thorough investigation on the seasonality, over the years (2014-2018), has been undertaken and CDOM optical measurements are done both in the UV and visible region, along with the FDOM measurements which were missing in the previous studies from this region.

Objectives

- *Study the CDOM characteristics and their sources during all the seasons in the estuaries and during non-monsoon seasons in the coastal waters.*
- *Characterization of CDOM at varying levels of oxygen.*

The thesis is divided into 6 chapters as detailed below:

Chapter 1: Introduction

Chapter 2: Methodology

The characteristics of the study area, along with the sampling details are given in this chapter. A detailed overview of the methodology employed for sample collection, processing, and data analysis is given.

Chapter 3: Spatial and temporal variations of CDOM in the Mandovi and Zuari estuaries and the coastal waters of Goa (Objective 1)

This chapter mainly focuses on the spatial and temporal variability of the CDOM in the coastal and estuarine waters of Goa. The sources and sinks of CDOM based on the optical properties are discussed.

Chapter 4: Optical properties of CDOM during blooms in the coastal waters of Goa (Objective 1)

Cyanobacterial blooms of *Trichodesmium* are observed in the coastal waters of Goa during the SIM. The characteristics of CDOM during the blooms are discussed; also an attempt has been made to differentiate the stages of bloom based on the CDOM characteristics. Experimental results carried out on the bloom samples are also presented.

Chapter 5: Variations of CDOM during SWM and seasonal hypoxia along the western continental shelf of India (Objective 2)

During the SWM, seasonal hypoxia is observed along the WCSI. The result of CDOM variation during the early SWM is presented for the 4 transects of Kochi, Mangalore, Karwar, and Goa, whereas the Goa transect is studied in detail for the variation of oxygen and CDOM during the late SWM. Production of CDOM in the oxygen and OM controlled systems with time is also presented in this chapter.

Chapter 6: Summary and conclusion.

An overall summary of the research findings is presented in this chapter. The limitations of this research along with a brief overview of the future research openings (based on the work carried out in this study) are presented in detail.

Chapter 2

Materials and Methods

2. Materials and Methods

2.1 Study Area

Goa is situated on the west coast of India, along the Konkan coast encompassing a coastal stretch of 100 km between the Western Ghats and the Arabian Sea. Nine rivers rise in the ghats and flows towards the Arabian Sea through Goa. Of these, the Mandovi and Zuari are the most important rivers and occupy about 69% of the total geographical area of Goa. River Mandovi originates in the Parwaghat of Sahyadri hills in Karnataka state and meets the Arabian Sea after traversing a distance of 70 km through Aguada Bay near Panaji forming the Mandovi Estuary. While the river Zuari lies in the Digi Ghats of Sahyadri hills in the Karnataka state covering a distance of about 67 km and meeting the Arabian Sea through the Marmugoa Harbor forming the Zuari Estuary. The mouth region of the Mandovi Estuary is small and semi-circular with an area of ~4.36 km^2 and width of about 3.33 km, while the Zuari Estuary is comparatively wide, and funnel shape with an area of ~46.7 km^2 and width of 5 km (Rao et al., 2011). The Cumbarjua canal connects both the estuaries at a distance of ~15 km from the mouth. The depth of the estuary varies considerably and has an average depth of about 5m. Tides are mixed semidiurnal with a tidal range of ~2.3m during spring and 1.5m during neap tide (Manoj & Unnikrishnan, 2009; Shetye et al., 2007). Several tributaries are joining the Mandovi and Zuari estuaries of which the number joining the former is greater than the latter. Southwest monsoon (SWM) brings heavy rainfall and subsequent river runoff over this region; hence these estuaries are classified as "monsoonal estuaries" (Shetye et al., 2007; Vijit et al., 2009). The river runoff measured at the head of the Mandovi Estuary during SWM is ~258 m^3s^{-1}, whereas during non-monsoon it is ~6 m^3s^{-1} (Vijith et al., 2009). There is a dam in the upstream regions of the Zuari Estuary and the runoff measured at Sanguem and Kushavati tributaries during the monsoon is ~147 m^3s^{-1} while it decreases during the non-monsoon season to 7.3 m^3s^{-1}. The catchment area of Mandovi and Zuari estuaries are 1150 km^2 and 550 km^2, respectively which contribute to a large amount of land discharges especially during the SWM (Qasim and Sen Gupta, 1981). The banks of these estuaries are fringed with large patches of mangroves. Several open cast iron and manganese ore mines operate in the drainage basins of these estuaries, wherein 37 ore loading points are located in the Mandovi while 20 are in the Zuari Estuary. In recent years, these estuaries have been

exploited for various anthropogenic activities (Shynu et al., 2012; Veerasingam et al., 2015). Some of the anthropogenic activities along the bank and within the estuaries include the pleasure cruises, floating casinos, shipbuilding/repair yards, sand mining, small and large scale industries, fish processing units, fishing jetties, mine waste rejects, transportation of mineral ores by barges, discharge of treated municipal sewage, domestic waste discharge from the houses and commercial establishments, etc. (Shynu et al., 2015; Dias et al., 2017).

The coastal waters of Goa experience a seasonal reversal in wind patterns due to differential solar heating of the Indian Ocean and Eurasian landmasses resulting in the northeast (NE) and SW monsoon. Coastal upwelling is one of the prominent features observed along the west coast of India during the SWM. Upwelling induced primary production lead to seasonal hypoxia/anoxia along the west coast of India during the late SWM (Naqvi et al., 2000). Apart from this, transport of low-salinity water from the Bay of Bengal has been reported during the NEM (Prasanna Kumar et al., 2004). Various algal blooms reported in these waters (Naqvi et al., 1998; Krishnakumari et al., 2002; Desa et al., 2005; Gomes et al., 2008; Pednekar et al., 2012) are known to impact the biogeochemistry of the region.

2.2 Sampling

Water samples were collected at discrete depths at 6 stations in the Mandovi Estuary, 5 Stations in the Zuari Estuary, and 9 stations along the coastal waters (5 INCOIS and 4 CaTS) during all the seasons from 2014 to 2018 using a fishing trawler. Data was also collected in the Mandovi Estuary, Zuari Estuary, and Cumbarjua canal during the NEM of 2020-21. Details of the sampling stations are provided in Table 2.1. The stations were selected keeping in mind the various sources of CDOM in the Mandovi and Zuari estuaries from the mouth to the upstream regions. The coastal waters were sampled along 2 transects, one transect being the CaTS (Candolim time-series stations) while the INCOIS transect was from the mouth of the Mandovi Estuary to a distance of ~8 km. The CaTS transect was chosen since it has long been studied for various biogeochemical parameters since 1997, and present study would help in better understanding of the CDOM cycling in the known biogeochemical settings. The coastal waters of Goa are impacted by seasonal reversing currents, coastal hypoxia, phytoplankton blooms, etc. Therefore considering these phenomenons, the stations were selected. The observations in the study area were divided into 4 seasons; spring-inter monsoon

(SIM), southwest monsoon (SWM), fall inter monsoon (FIM), and northeast monsoon (NEM). The samples during 2014-2015 were collected monthly, while seasonal sampling was carried out during the consecutive years. A total number of 795 samples were collected during this study, out of which 146 samples were collected at the CaTS transect, 142 samples along the INCOIS transect, 288 samples in the Mandovi Estuary, 202 samples in the Zuari Estuary, and 17 samples in the Cumbarjua canal. Apart from this, 117 samples were collected along the 4 transects (Kochi, Mangalore, Karwar, and Goa) during SSD 052 cruise (June-July 2018), and 27 samples along the Goa transect during the SSD 057 cruise (September 2018) of *RV Sindhu Sadhana*.

Table 2.1: Details of the sampling stations from the study area.

Station no	**Latitude (°N)**	**Longitude (°E)**	**Max depth (m)**	**Distance from the coast (km)**
Coastal Waters				
CaTS transect				
Station 1	15.5198	73.7592	6	-0.56
Station 2	15.5203	73.7398	13	-2.54
Station 3	15.5197	73.71	15	-5.7
Station 4	15.5107	73.6494	28	-12.33
INCOIS transect				
Station 1	15.48064	73.79406	6	2.47
Station 2	15.46946	73.77449	11	0.03
Station 3	15.45743	73.75633	15	-2.334
Station 4	15.44653	73.73364	17	-5.042
Station 5	15.43326	73.71198	19	-7.795
Mandovi Estuary				
Station 1	15.49583	73.81563	6	5.341
Station 2	15.50273	73.83414	8	7.865
Station 3	15.5041	73.85956	4	10.556
Station 4	15.52013	73.9202	4	18.167

Station 5	15.52858	73.96967	8	26.979
Station 6	15.52189	73.98385	5	28.797
Zuari Estuary				
Station 1	15.42523	73.78745	10	1.142
Station 2	15.4162	73.85947	4	9.185
Station 3	15.41183	73.91065	6	14.65
Station 4	15.37475	73.95806	7	22.2
Station 5	15.34806	74.00473	9	28.414

Water samples were collected in 5L carboys which were previously rinsed with 10% HCl and later washed several times with Milli Q water. The water samples were analyzed for absorption by CDOM, detritus, phytoplankton, chlorophyll-*a*, and marker pigments (during a few trips), and TSM. Inherent and apparent optical properties were also measured at the study site using AC-9 meter and Radiometer, respectively.

2.3 Methodology

2.3.1 CDOM analysis

For CDOM analysis water samples were filtered immediately through a 0.2 micron nucleopore membrane filter. The membrane filter was first rinsed with Milli Q water (18.2 mΩ) followed by rinsing the filter paper with sample and then the sample was filtered and collected in 60 ml amber glass bottles for analysis. The filtration bottles were rinsed 3 times before sample collection; these samples were stored at 4ºC and analyzed within 24 hrs of collection.

CDOM absorption was measured using a spectrophotometer UV2600 (Shimadzu) in the spectrum mode using 10 cm path length quartz cells and Milli Q water as a reference in the spectral range of 200 to 850 nm. The spectrophotometer has a photometric precision of ± 0.002 absorbance which is comparable to an absorption coefficient of 0.046 m^{-1}.

Before scanning, the samples were kept in a water bath at room temperature (for an hour) to maintain the same temperature as the reference Milli Q water (Pegau et al., 1995). It is

presumed that CDOM absorption is near zero at longer wavelengths (~680-800 nm); however, this is not the case always. This could be due to the difference in temperature or salinity between the reference Milli Q water and sample (Pegau et al., 1995). The other reasons which could contribute to the absorption at a longer wavelength could be due to the scattering by particles that pass through 0.2 micron filter or the colloids, microbubbles, particulate contaminants from the air, lint on the optical window of the cuvettes, etc. (Mannino et al., 2019). Samples were corrected to remove any of the effects listed above by subtracting the values at wavelengths where absorbance tends to zero; in this case, it was 700 nm (Bricaud et al., 1981; Green and Blough, 1994; Loiselle et al., 2009; Li and Minor, 2015). Average values of 700 to 850 nm were subtracted from the entire spectrum. The raw absorbance values were then converted to absorption using equation 1

aCDOM (m^{-1}) = 2.303* A/l ---------- Equation (1)

where A is the absorbance value and l is the path length (0.1) in meters.

CDOM decreases exponentially with increasing wavelength and follows equation 2 (Bricaud et al., 1981; Kirk, 1994)

$$a_g(\lambda) = a_g(\lambda_0)e^{-S(\lambda-\lambda_0)} \quad \text{---------- Equation (2)}$$

where $a_g(\lambda_0)$ is the CDOM absorption at a reference wavelength and S is the spectral slope determining the steepness of the spectrum (Twardowski et al., 2004). The absorption coefficients at the wavelengths of 320, 350, 375, 412, and 440 nm (ag320, ag350, ag375, ag412, and ag440) were used in previous studies to represent the concentrations of CDOM (Kowalczuk et al., 2005; Yamashita and Tanoue, 2009; Para et al., 2010; Vantrepotte et al., 2015). The absorption by CDOM obtained at these wavelengths were significantly correlated and varied similarly between seasons (Fig. 2.1). In this study, a_g412 was used as the reference wavelength to represent the CDOM concentration for various reasons. It is always better to study CDOM at lower wavelengths in the UV region due to its high absorption and sensitivity as used in many studies (Blough et al., 1993; Battin, 1998; Del Castillo et al., 1999; Stedmon et al., 2000; Fichot and Benner, 2012). Since the present study could be of help in remote sensing applications, there was a need to select the reference wavelength in the blue region. The lowest available band in the ocean color satellites is 412 nm. However, many studies

prefer to use a_g440 for remote sensing studies due to atmospheric correction procedures. It is well known that there is a peak at 440 nm due to the absorption by accessory pigments in phytoplankton. When the contribution by phytoplankton at 440 is higher than CDOM, there will be an overestimation of CDOM derived from the satellite. Hence a_g412 was used as the reference wavelength in the present study. Also, recent studies (Vantepotre et al., 2015) have shown that a_g412 holds a very good correlation with DOC, and can be used to estimate DOC remotely.

The spectral slope has been used to differentiate the sources of DOM and track the changes in the composition of DOM (Carder et al., 1989; Blough and Green, 1995). Spectral slope coefficients were estimated in long-wavelength range of $S_{250\text{-}600}$ (nm^{-1}), and the narrow range of $S_{275\text{-}295}$ and $S_{350\text{-}400,}$ respectively. Spectral slope in the long-range was calculated by applying the non-linear regression following Twardowski et al. (2004), the R^2 for which was mostly greater than 0.98. However, slopes in the narrow wavelength ranges were calculated using a linear fit of the log-linearised spectrum. Helms et al. (2008) proposed the use of slope in the narrow wavelength ranges as they were much above the detection limit of the instrument and can be analyzed with high accuracy even in highly photobleached waters. They have shown that slope in the narrow wavelength range and slope ratio S_R ($S_{275\text{-}295}/S_{350\text{-}400}$) can be used as reliable proxies for average molecular weight and indicator of photobleaching.

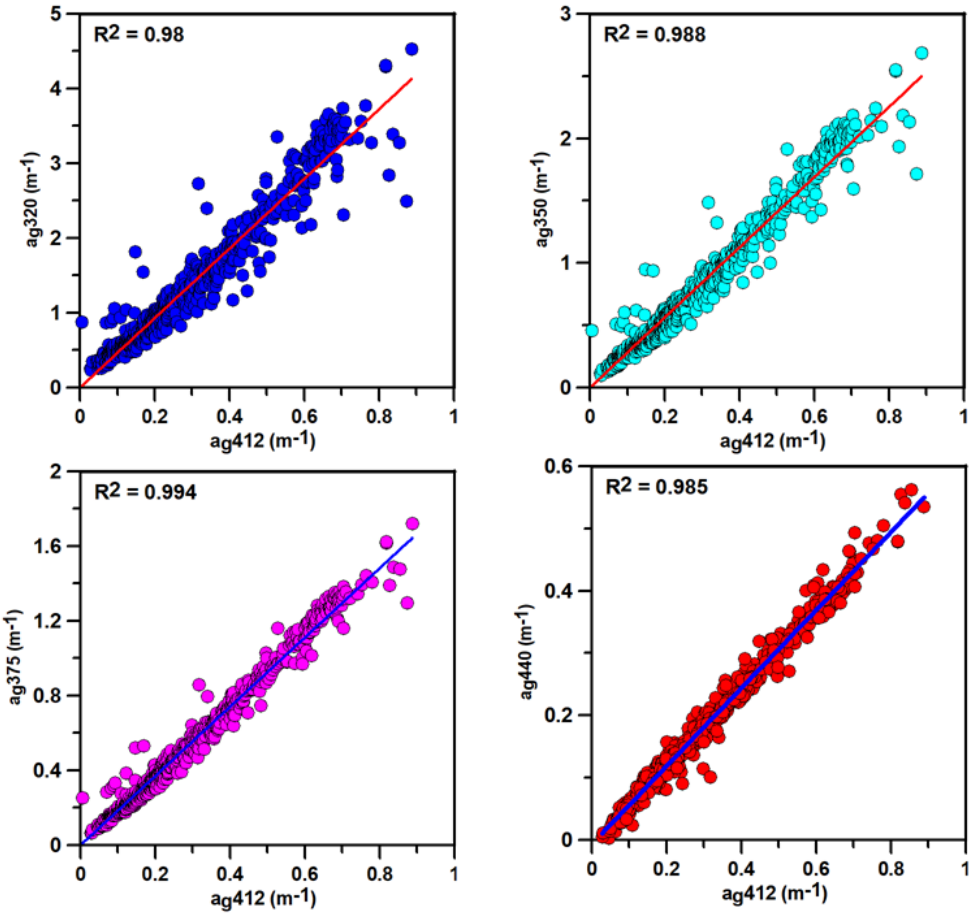

Figure 2.1: Correlation between CDOM absorption a_g (m^{-1}) at various reference wavelengths of 320, 350, 375, and 440 nm with 412 nm (a_g412).

2.3.2 FDOM analysis

CDOM fluorescence was determined using a spectrofluorometer (Cary Eclipse, Agilent). The excitation scanning range was from 200 to 450 nm and the emissions were recorded at 250 to 600 nm. Spectral readings were collected at 5 nm for excitation and 2 nm for emission at a scanning speed of 9600 nm min^{-1} and integration time of 0.0125 seconds. Milli Q water was taken as blank and the EEM of which was subtracted to eliminate Water Raman scatter peaks (McKnight et al., 2001; Stedmon et al., 2003; Zhang et al., 2010, 2011). The fluorescence estimations were corrected for excitation energy and emission detector response using the manufacturer's correction functions. Inner filter effect (IFE) poses a big issue in the measurements of EEM as a result of re-absorption of emitted light by the sample (Mcknight et

al., 2001). Larsson et al. (2007) showed that the sample fluorescence intensity can be reduced by 5% due to IFE. This issue of IFE was taken care of by using the CDOM absorbance of the sample, wherein the sample's absorbance spectrum was used to calculate a matrix of correction factors corresponding to the wavelength pair in the EEM. The instrument-measured fluorescence intensities are given in arbitrary units and then converted to Raman units (RU). This is done by taking the area under the Milli Q Raman Water peak which is then used to normalize the fluorescence intensities in sample EEM.

2.3.3 Absorption by optically active components in water

Apart from CDOM, there are other fractions in the water which are optically active and contribute to absorption in the water. For these analyses, water samples were filtered onto a 25mm, GF/F filter (0.7microns). The GF/F filter is an accepted material for particle collection (dead and alive) and hence all the particles which are present in the water and absorb light will be accounted for (Mitchell and Keifer, 1984). The volume of water filtered varied from 0.2 - 1L to maintain the optical density of samples between 0.05 and 0.4 that is ideal for path length amplification corrections (Mitchell et al., 2002). The filter paper was stored at -20ºC until analysis on the spectrophotometer. The sample analyses were performed within 24 hrs after collection. An Integration sphere attached to the UV2600 spectrophotometer (Shimadzu) was used in the analysis of particulate absorption. The filter paper was thawed in the dark before analysis followed by the spectral absorption of particulate matter (a_p) in the wavelength range of 250 to 850 nm at every 1 nm interval. After measurements, the same filter was subjected to methanol extraction for 30 min to extract soluble pigments. This filter was then rinsed with 0.2 micron filtered seawater to remove any traces of methanol from the filter. The filter was then scanned again for the determination of absorption by detritus (a_d) or de-pigmented particles. For blank determination, 0.2 micron filtered seawater was filtered onto a GF/F filter paper and the absorbance was measured. Phytoplankton pigment absorption (a_{ph}) was computed as the difference in particulate (ap) and detrital (ad) absorption after correcting for filter path length amplification factor (β) (Mitchell et al., 2002) following equation (3)

$$a_p(\lambda) = \frac{2.303 A_f}{\beta V_f}\left[\left(OD_{fp}(\lambda) - OD_{bf}(\lambda)\right) - OD_{null}\right]$$ ----------Equation (3)

Where $OD_{fp}(\lambda)$ is the measured optical density of the sample filter, $OD_{bf}(\lambda)$ is the optical density of a fully hydrated blank filter, and OD_{null} is a null wavelength residual correction (750 - 850 nm). V_f is the volume of water filtered and A_f is the clearance area of the filter.

2.3.4 Phytoplankton pigment analysis

For chlorophyll-*a* estimation, 0.5 to l L of water sample was filtered onto a 47mm GF/F (0.7micron) filter. The filter paper was then extracted in 10 mL of 90% acetone overnight at 4ºC and analyzed on the Turner fluorometer.

Phytoplankton pigments in the water samples were determined using High-performance liquid chromatography (HPLC). Samples were filtered on GF/F filters and were frozen at −20°C until analysis. The filters were extracted in 3 ml of 100% HPLC grade acetone (Merck) for 24 h at −20°C. The extract was then passed through a syringe filter (0.2 μm) to remove any cellular debris and later mixed with 0.5M ammonium acetate buffer (70:30 proportion). This was then placed directly into a temperature-controlled (4 °C) autosampler tray for HPLC analysis. The HPLC system was equipped with an Agilent 1100 pump together with an online degasser and a diode array detector. The column used was the Eclipse XDB C8 column (4.6 × 150 mm) connected via the guard column (Agilent Technologies). The column temperature was maintained at 60 °C. Elution was performed at a rate of 1.1 mL min^{-1} using a gradient program of 36 min with 5/95% and 95/5% of solvents B/A being the initial and final compositions of the eluent, where solvent B was methanol and solvent A was (70:30) methanol and 28 mM ammonium acetate (pH 7.2) (Roy et al., 2006). The eluting pigments were detected at 450 and 665 nm by the diode array detector. Calibration was carried out using standards procured from DHI, Denmark. All chemicals used were of HPLC grade (Merck).

2.3.5 Total suspended matter (TSM)

TSM was analyzed after filtering 0.5-1L of water onto a 0.45μm cellulose membrane filter which was pre-weighed and dried at 105ºC. After sample filtration, the filter membrane was rinsed 3 times with Milli Q water to remove traces of sea salt and the filter paper was then dried at 105ºC for 1hr. The filters were kept in desiccator to cool and then re-weighed. The

difference between the initial and the final weight and the volume of water filtered was used to quantify the TSM in the water.

TSM(mg/L)=Final weight of filter(mg)-Initial weight of filter(mg)/volume of water filtered(L)

2.3.6 Inherent and apparent optical measurements

The inherent *in-situ* spectral optical parameters of absorption and beam attenuation, was measured using an AC-9 spectrophotometer (WetLabs, USA). The instrument was calibrated before sampling using Milli Q water and the calibration coefficients were used to process the data. The apparent optical parameters in the water column were measured *in-situ* using a free-falling profiler and a hyperspectral radiometer (Satlantic Inc, Canada), which provides profiles of the upwelling radiance (L_u), downwelling irradiance (E_d), and surface solar irradiance (E_s) in the spectral range of 350-800 nm. Apart from this, it had auxiliary sensors for the measurements of conductivity, temperature, depth (CTD), fluorescence and backscatter sensors. The other associated optical parameters like diffuse attenuation coefficients (k_d), remote sensing reflectance (R_{rs}) were derived after processing the radiometer data using the software Prosoft. The penetration depth (Z_{90}), defined as the depth of penetration of light above which 90% of the diffusely reflected irradiance originates ($Z_{90} = 1/k_d$) was determined using K_d.

2.4 Statistical Analysis

Non-parametric test like the one-way analysis of variance (ANOVA) test was conducted to assess the differences in the mean values of the respective parameters at the sampling stations during different seasons at a 95% confidence level ($p<0.05$). The Pearson's correlation coefficient (r) was computed for various parameters to assess the relationship between the dependent and independent variables.

2.4.1 Principal Component Analysis (PCA)

PCA was used in this study to assess the relationship between DOM quality parameters between the estuaries and the coastal waters. PCA uses a mathematical algorithm to reduce the dimensionality of the data while explaining the maximum variance. Before the PCA analysis, DOM quality variables were normalized by calculating the log-linearized absolute values, subtracting the individual means, and dividing by their standard deviations. All the statistical analyses used in the study were performed in statistical package for the social sciences (SPSS).

2.4.2 Parallel Factor Analysis

To identify the sources of CDOM in this study, the Parallel Factor Analysis (PARAFAC) model was used on the EEMs. PARAFAC is a statistical model that uses the alternating least square algorithm (ALS) to decompose the EEM into the most representative fluorescence components from the complex DOM mixture. The model is generally written as follows:

$$X_{ijk} = \sum_{f=1}^{f} b_{if} c_{jf} d_{kf} + \in_{ijk}$$

$$i = 1,\ldots,I;\ j = 1,\ldots J;\ k = 1,\ldots,K$$

According to Stedmon et al. (2003), when applying the PARAFAC model to EEMs, X_{ijk} is the intensity of fluorescence for the i^{th} sample at emission wavelength j and excitation wavelength k; b_{if} is directly proportional to the concentration of the f^{th} component in sample i; c_{jf} is linearly related to the fluorescence quantum efficiency of the f^{th} component at emission wavelength j, d_{kf} is linearly proportional to the specific absorption coefficient at excitation wavelength k; f defines the number of components in the model, and a residual $\in_{ijk}$ represents the variability not accounted for by the model.

The analysis was performed in Matlab 2017 software using the DrEEM toolbox 0.20 (Murphy et al., 2013). Due to the SNR (signal-to-noise ratio), the EEM datasets were restricted to the excitation wavelength > 240 nm and emission wavelength <590 nm. Also, the Rayleigh scatter was removed before the PARAFAC modeling because the values do not describe the

DOM fluorophore in the area. To remove the Rayleigh scatter, the missing values (NaN-Not a number) were inserted in the regions ($Ex - 20 \leq Em \leq Ex+20$ and $2Ex - 20 \leq Em \leq 2Ex+20$; unit: nm) which are majorly influenced by the first and second-order scattering from the measured spectroscopic data (Hua et al., 2007; Stedmon and Bro, 2008). Samples with extreme leverages were identified and excluded from the model. The model was run with non-negativity constraints. Validation was performed by split-half analysis, analysis of residuals and loadings.

Chapter 3

Spatial and temporal variation of CDOM in the coastal and estuarine waters of Goa

Spatial and temporal variation of colored dissolved organic matter in the coastal and estuarine waters of Goa

3.1. Introduction

Dissolved organic matter (DOM) is one of the pivotal components of the marine ecosystem playing an important role in the cycling and availability of carbon in the aquatic environment. Colored DOM (CDOM) is a small fraction of the DOM pool which is optically active and hence can be detected using remote platforms. Apart from CDOM, detritus, phytoplankton, and water itself are the other optically active fractions and hence contribute to the absorption of light in water and influence the inherent and apparent optical properties of water.

Rivers and estuaries are important sources of DOM during its transport from the terrestrial ecosystem to the coastal seas. The coastal waters of Goa are affected by seasonal reversing currents with strong temperature inversions due to the transport of low-salinity water from the Bay of Bengal during the northeast monsoon (NEM) (Prasanna Kumar et al., 2004). Upwelling and associated primary production lead to seasonal hypoxia/anoxia along the west coast of India during the late SWM, which impacts demersal fisheries (Naqvi et al., 2000). This natural oxygen deficiency has intensified within the past few decades, which may be due to the enhanced nutrients loading and organic matter from land (Naqvi et al., 2000, 2006). However, recent measurements show a lack of a secular trend (Naqvi et al., 2009a). These waters also experience blooms of various algal species (diatoms, dinoflagellates, cyanobacteria), which are seasonal and episodic (Naqvi et al., 1998; Krishnakumari et al., 2002; Desa et al., 2005; Gomes et al., 2008; Pednekar et al., 2012), and affect the biogeochemistry of the region. The microbial remineralization of organic matter from the land would also lead to CDOM production.

The SWM causes high levels of allochthonous DOM transport from watersheds into estuaries and adjoining coastal waters. The Mandovi and Zuari estuaries, located on the west coast of India, are classified as monsoonal estuaries (Manoj and Unnikrishnan, 2009). During the SWM, both estuaries receive high levels of freshwater discharge, leading to stratification up to 12 km from the mouth. There is very little discharge from river runoff during the non-monsoon season. Therefore, the estuaries become an extension of the sea

and remain vertically well mixed (Shetye et al., 2007; Vijit et al., 2009). Thus, owing to the influences of both rivers and the sea, these estuaries receive autochthonous and allochthonous inputs from different sources, such as terrestrial, riverine discharge, mangrove leachate, and anthropogenic activities (Gonsalves et al., 2009).

3.2 Aim of the study

Though CDOM plays an important role in the carbon cycle, very few studies have been conducted in the estuaries and coastal waters of Goa. Menon et al. (2011) studied CDOM in the Mandovi and Zuari estuaries using the absorption at a reference wavelength (a_g440) and slope coefficient ($S_{400-550}$). They validated the *in-situ* derived CDOM using satellite data by applying an algorithm developed for the site. Recently, Dias et al. (2017) reported the CDOM characteristics in the Mandovi and Zuari estuaries and coastal waters of Goa; however, their study was restricted to the SIM season. Therefore, the aim of this study is to investigate the variability of the bio-optical properties of CDOM with changes in environmental conditions and to identify the major sources and sinks controlling the optical properties of these waters. The following hypotheses were tested: 1) the magnitude of CDOM absorption varies both spatially and temporally in the two estuaries and coastal waters of Goa and 2) with different sources and sinks of CDOM, the estuarine system could exhibit non-conservative mixing behavior.

3.3 Data collection and analysis

The measurements were carried out from the coastal waters of Goa and both the Mandovi and Zuari estuaries for four years (March 2014-December 2018) using fishing trawlers. During 2014-15 the samples were collected monthly, while in the consecutive years seasonal sampling at the study area was carried out (Fig. 3.1). Apart from the regular samplings, the Estuary was also sampled during the NEM of 2020-21 right from the upstream of both the estuaries covering the Cumbarjua canal which forms the conduit between the Mandovi and Zuari Estuary (Appendix 1.1). The Mandovi Estuary was sampled during the early NEM (November, 2020), while the Zuari estuary and the Cumbarjua canal were sampled during late NEM (February, 2021). Sampling was carried out at close interval with 24 stations in the Mandovi Estuary, 11 stations in the Zuari Estuary, and 9 stations in the Cumbarjua canal.

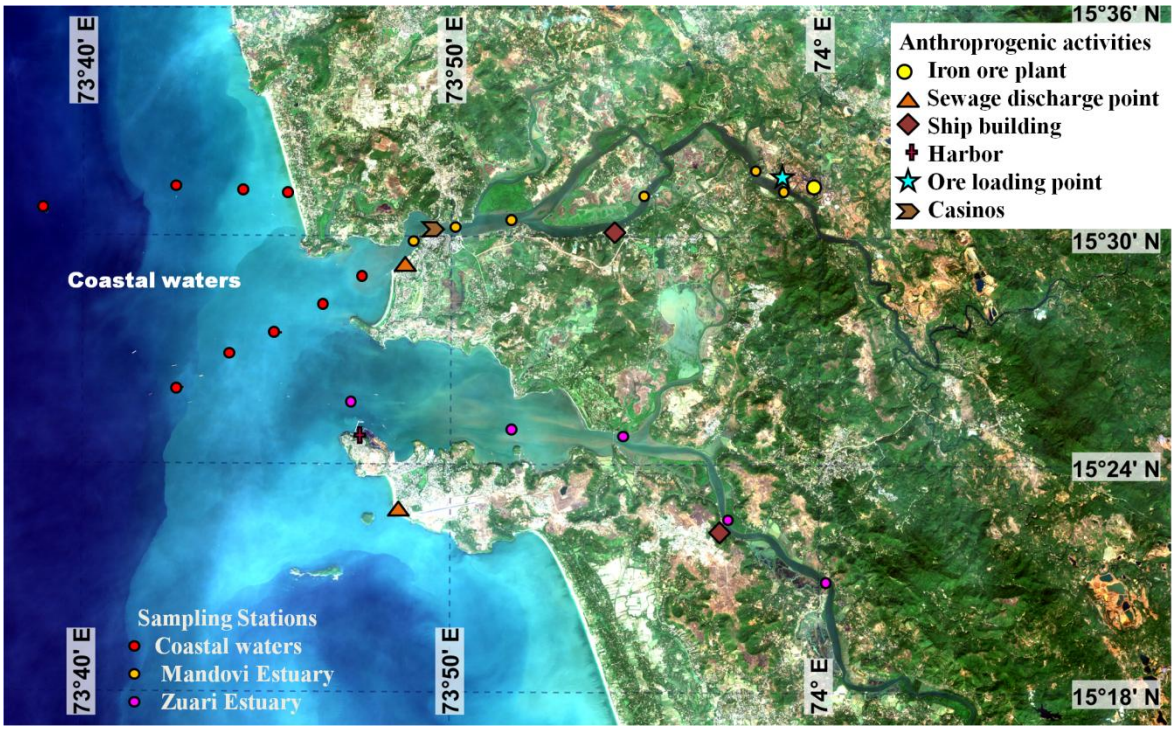

Figure 3.1: The study area indicating the regular sampling stations in the coastal waters of Goa and in the Mandovi and Zuari estuaries. It also depicts the anthropogenic activities occurring in the estuaries of Goa.

The water samples were collected in amber bottles, transported in ice, and were filtered within a few hours of collection following the standard SeaWiFS protocol (Mueller et al., 2003), and their CDOM and chlorophyll-*a* contents were analyzed. For CDOM analysis, a 0.2-µm nucleopore polycarbonate membrane was first rinsed with 100 mL of Milli-Q water followed by the sample. The filtered sample was then collected in amber glass bottles. The water samples were stored at 4°C until spectrophotometric analysis was conducted in the laboratory on the same day of collection. To analyze chlorophyll-*a*, 500 mL to 1 L of water was filtered through a 0.7-µm GF/F filter, which was then extracted in 10 mL of 90% acetone and analyzed using a Turner fluorometer (Knap et al., 1996). Particulate matter in water was concentrated on to a 25mm GF/F filter by filtering about 0.1 to 0.5 L water depending on the particle load for the estimation of absorption by detritus and phytoplankton. Spectral absorption of the detrital and phytoplankton fraction was then determined using an integrating sphere attached to Shimadzu UV2600 spectrophotometer. The details of analysis are provided in Chapter 2.

To ascertain the contribution of CDOM in rainwater, rainwater was collected on an event basis during 2015-16 into a glass flask using an HDPE funnel covered with a nylon mesh to prevent the entry of large particles. The flask was kept at a height above the ground on the terrace of CSIR-NIO to counter the contamination by droplet splashes. The entire assembly was washed with 10% HCl and rinsed several times with Milli Q water before collection to prevent contamination. This assembly was deployed for sampling as soon as the rain began and retrieved soon after the rain stopped. Samples were analysed and processed according to the methodology given, if the rainwater collected was above 50 mL. Daily average rainfall data for the Goa region was provided by the Indian Metrological Department, Mumbai.

The inherent *in-situ* optical parameters of absorption and scattering were measured using an AC-9 spectrophotometer (WetLabs, USA). The apparent optical parameters in the water column were measured *in-situ* using a free-falling profiler and a hyperspectral radiometer (Satlantic Inc, Canada).

The stability of the water column was determined for the coastal time series station (G5) using the Brunt Vaisala frequency (N) using the following equation

$$N\ (S^{-1}) = \sqrt{\frac{-g}{\rho} * \frac{d\rho}{dz}}$$

Where g is the gravity, ρ is the density and z is the depth.

3.4 Statistical analysis

A one-way analysis of variance (ANOVA) was conducted to assess the differences in the mean values of the respective parameters at the sampling stations during different seasons. The correlation coefficient (r) was computed for a_g412 vs. salinity and chlorophyll-*a*. Principal component analysis (PCA) was also performed on the DOM parameters to identify the sources of CDOM in these waters using the statistical package for the social sciences (SPSS).

3.5 Results

3.5.1 Physicochemical characteristics of the estuarine and coastal waters of Goa

The spatiotemporal variations in the physicochemical parameters were similar to those observed for these waters in previous work (Prasanna Kumar et al., 2004; Shetye et al., 2007; Maya et al., 2011b). The SWM plays an important role in the biological, physical, and chemical variations of the studied estuaries. The temperature and salinity variations in the coastal waters and the Mandovi and Zuari estuaries are presented in Table 3.1. The temperature was observed to be the highest during SIM and lowest during NEM. The temperature increased from the mouth to the upstream of both estuaries, while an inverse trend was observed for salinity. During the SWM, estuarine waters exhibited stratification, with cold, low-salinity water at the surface and warmer, more saline water at greater depths. Temperature inversions were seen in the coastal waters during the NEM. Chlorophyll-*a* was higher in the estuaries than that in the coastal waters (except during algal blooms during the SIM). In the estuaries and coastal waters, the highest chlorophyll-*a* concentration was observed during the SIM and NEM, respectively. Chlorophyll-*a* concentrations in the estuaries and coastal waters were low during the FIM season.

Table 3.1: Seasonal variation of environmental and CDOM characteristics for the Mandovi and Zuari estuaries and the coastal waters of Goa.

Para-meters	Sea-son	Mandovi Estuary			Zuari Estuary			Coastal waters		
		Mean	Min	Max	Mean	Min	Max	Mean	Min	Max
Temp (ºC)	SIM	30.54	28.34	33.22	31.79	29.55	33.22	30.54	28.43	32.12
	SWM	27.83	23.52	33.15	27.66	26.38	30.38	25.87	21.81	28.72
	FIM	30.50	30.21	31.16	29.15	25.94	32.22	27.26	21.42	31.58
	NEM	28.50	26.73	30.04	28.62	26.32	30.31	28.48	26.13	29.96
Salinity	SIM	28.60	19.91	35.55	29.03	16.86	35.35	35.23	34.21	35.94
	SWM	13.41	0.052	35.55	6.67	0.05	33.32	33.85	28.02	35.60
	FIM	19.32	0.95	32.34	23.78	2.31	34.95	34.17	32.03	35.29
	NEM	23.02	4.08	34.77	27.25	8.23	34.83	34.56	29.02	35.48
Chl a	SIM	5.28	0.18	16.14	5.24	0.71	14.12	1.21	0.2	5.19

(mgm^{-3})	SWM	3.70	0.09	14.45	6.22	2.98	13	No data		
	FIM	1.97	0.7	3.59	4.81	1.35	10.56	1.84	0.55	6.03
	NEM	4.01	0.33	9.71	3.25	0.02	9.13	2.44	0.27	14.67
$a_{ph}676$	SIM	0.102	0.042	0.203	0.096	0.020	0.207	0.032	0.009	0.098
(m^{-1})	SWM	0.059	0.002	0.198	0.063	0.027	0.136	No data		
	FIM	0.032	0.005	0.059	0.094	0.028	0.175	0.032	0.012	0.085
	NEM	0.067	0.025	0.138	0.0574	0.018	0.174	0.044	0.009	0.136
a_g412	SIM	0.478	0.164	0.761	0.517	0.069	0.908	0.166	0.038	1.455
(m^{-1})	SWM	0.385	0.128	0.842	0.586	0.182	1.458	1.074	0.062	6.627
	FIM	0.294	0.204	0.414	0.390	0.177	0.895	0.166	0.104	0.249
	NEM	0.353	0.175	0.696	0.452	0.084	1.527	0.153	0.049	0.333
$S_{250-600}$	SIM	0.0176	0.0162	0.0194	0.0180	0.017	0.0213	0.0209	0.0169	0.0295
(nm^{-1})	SWM	0.0154	0.0107	0.0203	0.0145	0.0112	0.0174	0.0121	0.0044	0.020
	FIM	0.0169	0.0148	0.0185	0.0161	0.0131	0.0187	0.0195	0.0168	0.022
	NEM	0.0171	0.0156	0.0198	0.0174	0.0135	0.0229	0.0203	0.017	0.027
$S_{275-295}$	SIM	0.0205	0.0184	0.0235	0.0209	0.019	0.027	0.0277	0.0225	0.0367
(nm^{-1})	SWM	0.0158	0.0096	0.0245	0.0142	0.0098	0.0201	0.0242	0.0053	0.0360
	FIM	0.0188	0.0143	0.0223	0.0178	0.0141	0.024	0.0244	0.0202	0.0286
	NEM	0.0194	0.0161	0.0235	0.0199	0.0152	0.0272	0.0267	0.021	0.0352
S_R	SIM	1.21	1.01	1.60	1.16	0.81	1.71	1.72	0.31	2.87
	SWM	1.05	0.57	1.94	0.91	0.66	1.27	2.05	0.98	4.53
	FIM	1.12	0.86	1.41	1.25	0.85	2.06	1.81	1.22	3.07
	NEM	1.20	0.92	1.63	1.23	0.94	1.94	1.75	1.13	2.55

3.5.2 Optical properties of CDOM in the coastal and estuarine waters of Goa

3.5.2.1 Variability of a_g412, spectral slope and slope ratio in the Mandovi and Zuari estuaries and the adjoining coastal waters

The ranges of the physicochemical and optical data measured in the two estuaries and coastal waters between 2014 and 2018 are presented in Table 3.1. Seasonal variability in CDOM absorption was observed in this study. As expected, a_g412 was much higher (0.439 m^{-1}) for estuarine waters than that in coastal waters (0.177 m^{-1}) during all seasons (Fig. 3.2). Spectral profiles of CDOM variations in the coastal and estuarine waters on a seasonal basis are given in Appendix 1.2. The magnitudes of the seasonal mean a_g412 exhibited marked differences in the estuarine (one-way ANOVA: $F = 5.777$, $p < 0.001$) and coastal waters ($F = 5.40343$, $p < 0.001$) during the four seasons. CDOM absorption (m^{-1}) was highest in the Mandovi and Zuari estuaries during the SIM (0.478 and 0.517) and SWM (0.385 and 0.586) seasons. Spatially, CDOM absorption increased from the mouth to the upstream of both estuaries during all seasons, suggesting a significant DOM source at the upstream of the estuaries ($p < 0.05$).

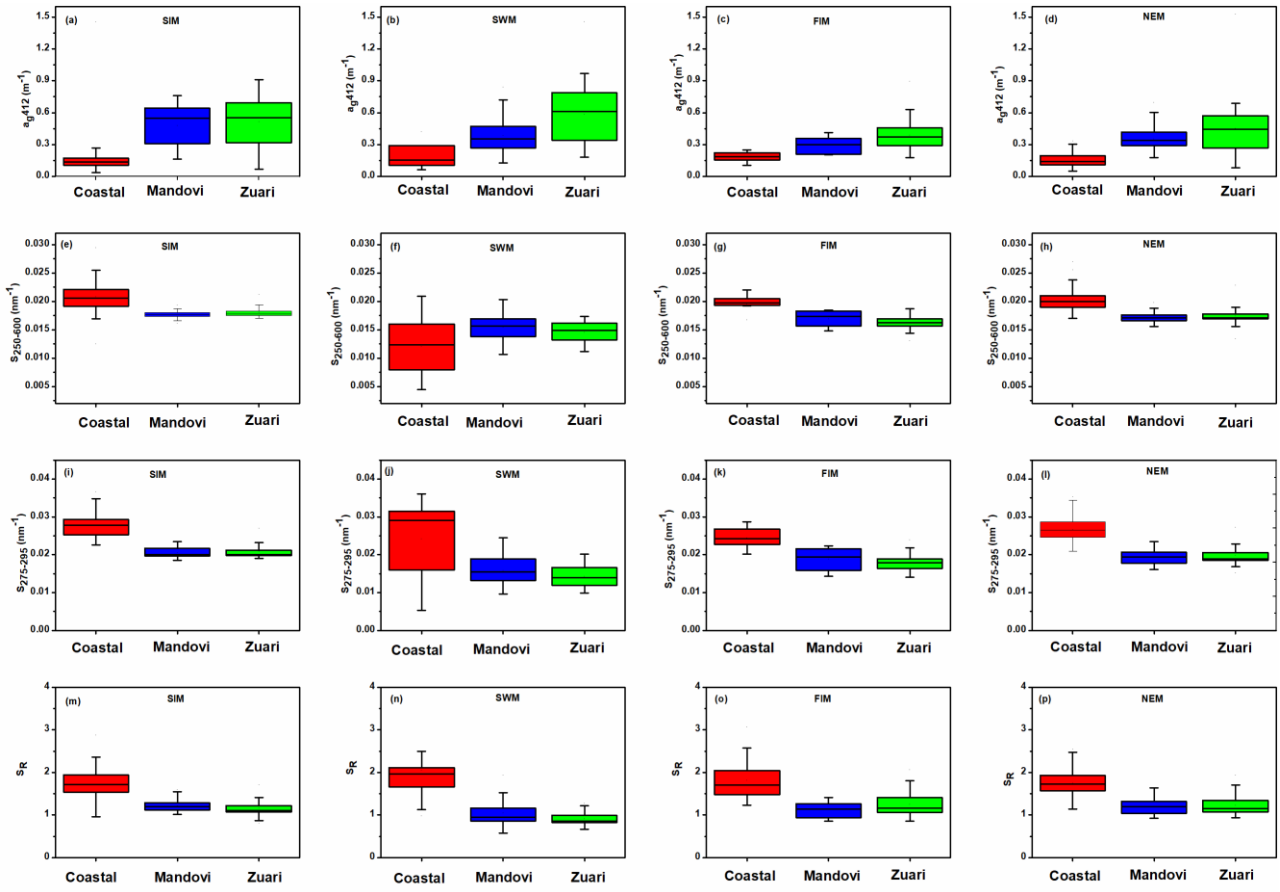

Figure 3.2: Seasonal variation of optical parameters in the coastal waters (red), Mandovi Estuary (blue) and the Zuari Estuary (green). a-d) a_g412 (m^{-1}); e-h) $S_{250-600}$ (nm^{-1}); i-l) $S_{275-295}$ (nm^{-1}) and m-p) S_R.

During the 2020-21 NEM sampling, the highest CDOM absorption was detected in the Cumbarjua canal (0.803 m^{-1}), followed by the Zuari Estuary (0.639 m^{-1}) and the least was observed in the Mandovi Estuary (0.323 m^{-1}). The CDOM absorption was 2 times lower in the Mandovi as compared to the Zuari Estuary (Fig. 3.3). Lower CDOM absorption was observed at the upstream of both the estuaries, while it increased towards the mid-stream region.

Figure 3.3a: Spatial variation of optical parameters of CDOM during the NEM (November 2020) in the Mandovi Estuary.

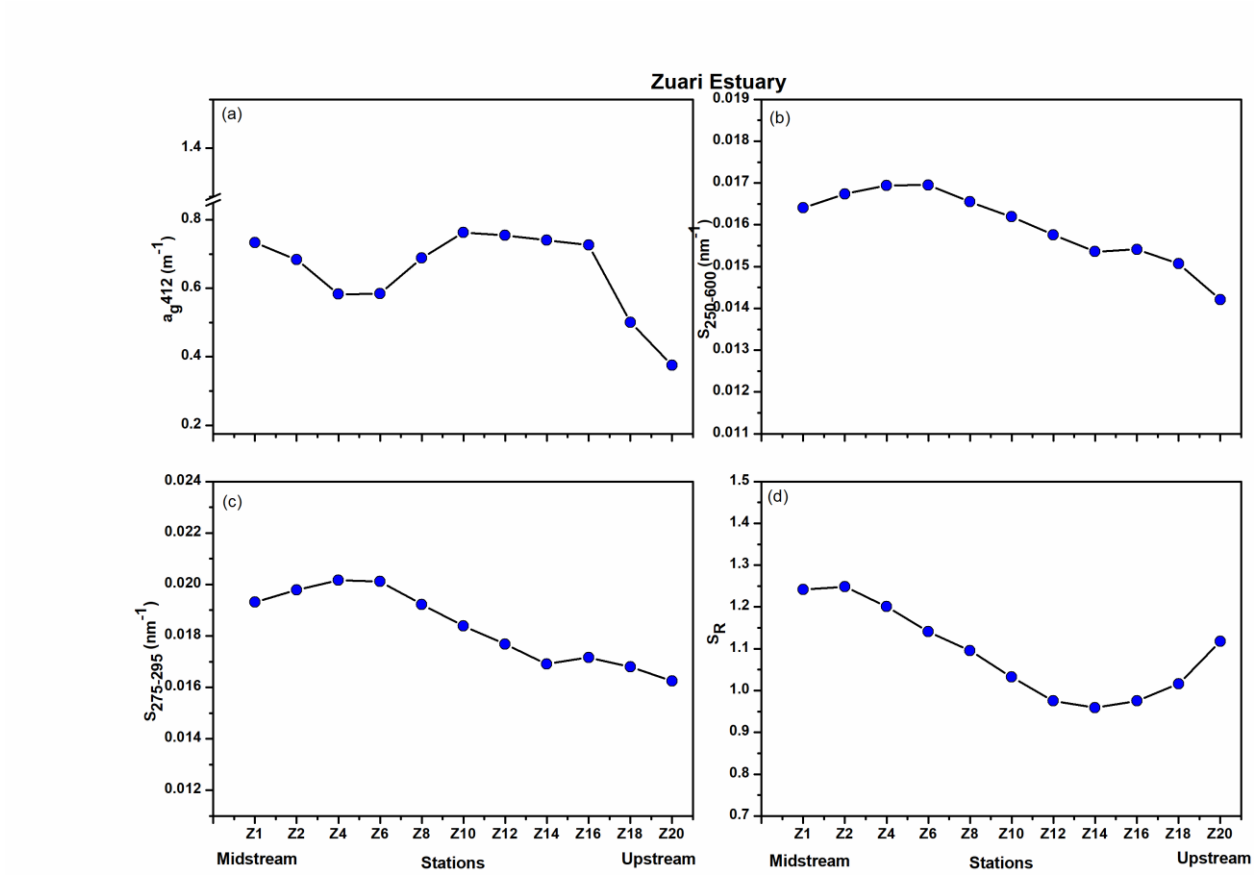

Figure 3.3b: Spatial variation of optical parameters of CDOM during the NEM (February, 2021) in the Zuari Estuary.

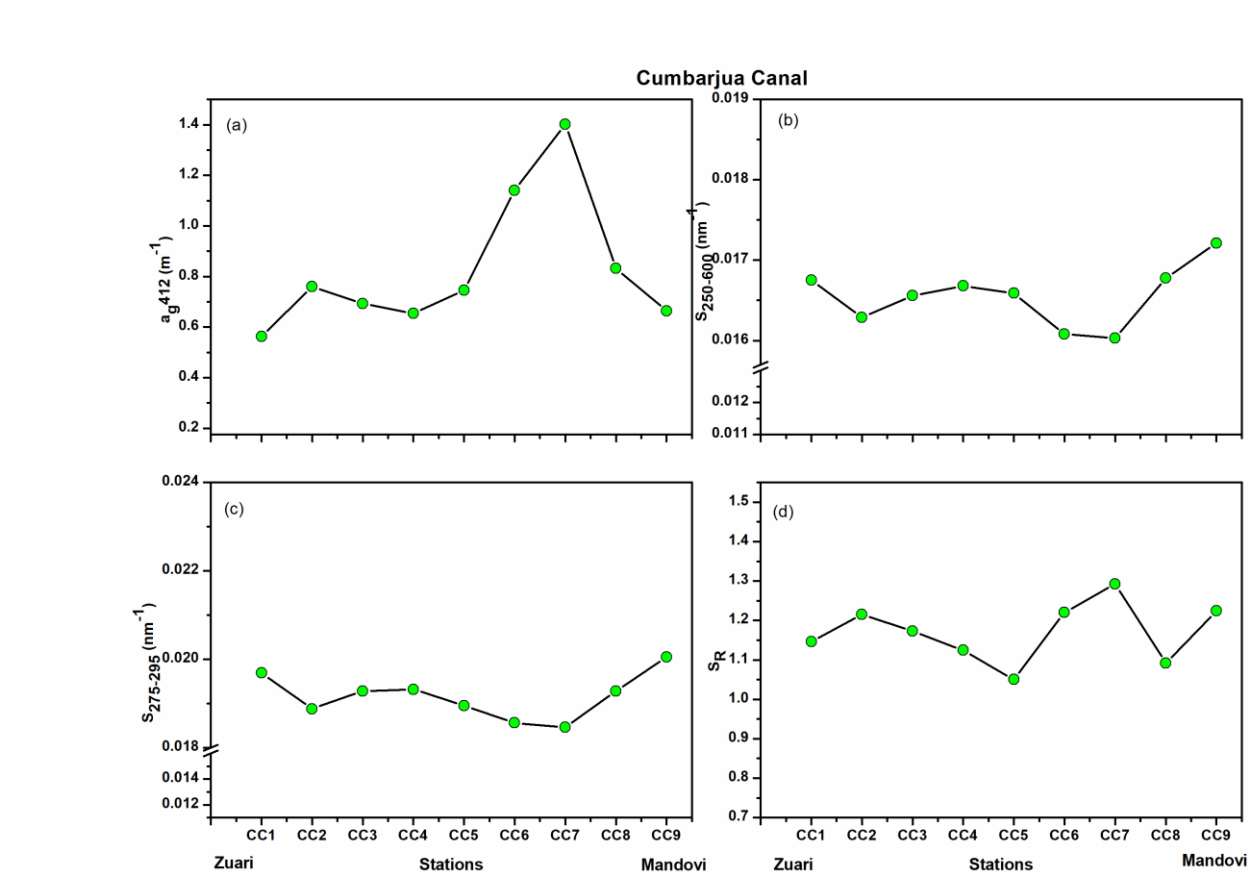

Figure 3.3c: Spatial variation of optical parameters of CDOM during the NEM (February, 2021) in the Cumbarjua canal.

In the coastal waters, the highest CDOM absorption was observed during the SWM followed by SIM and FIM (Fig. 3.2). The value of a_g412 decreased with increasing salinity, and higher values were observed close to the coast than the offshore waters. Extensive patches of *Trichodesmium* blooms were observed in the coastal waters during the SIM. The CDOM absorption spectra of these samples deviated from the normal exponential behavior and exhibited distinct peaks in the UV and blue regions, details of which are provided in chapter 4.

Significant seasonal variations in $S_{250-600}$, $S_{275-295}$, and the slope ratio S_R were observed in the coastal ($p < 0.05$) and estuarine waters ($p < 0.001$). In the coastal waters, $S_{250-600}$ was found to be high during the SIM, and low during the SWM season (Fig. 3.2; Table 3.1). $S_{275-295}$ was highest in the coastal waters during the SIM season, followed by NEM, and was lowest during the SWM and FIM seasons (Fig. 3.2). High values of S_R were observed

in the coastal waters and it increased towards the offshore. Large variability in spectral slopes was observed during SIM and NEM in the coastal waters (Fig. 3.2). Values of a_g412 were higher during March compared to April and May, whereas S values were lower during March compared to the other two months. A similar pattern of variation was observed during the NEM with lower values of a_g412 and higher S during November as compared to other months of NEM.

In both the estuaries, the lowest values of $S_{250-600}$ and $S_{275-295}$ were observed during the SWM with the increase in runoff from the catchments of the estuaries, while higher values were observed during the SIM period (Fig. 3.2). Seasonal variations in $S_{275-295}$ were marginal in the Mandovi Estuary, while large variations were observed in the Zuari Estuary (Table 3.1). S_R was highest during the SIM season and lowest during the SWM in both estuaries (Fig. 3.2). $S_{275-295}$ and S_R (indicators of molecular weight) increased towards the mouth of both estuaries from the upstream. Low-molecular-weight DOM was abundant near the mouths of the estuaries, while high-molecular-weight DOM was dominant in the upstream region, indicating the transformation and dilution of riverine DOM during its passage to the adjoining coastal waters (Figs 3.4 and 3.5). CDOM (a_g412) and $S_{275-295}$ showed a very good inverse relationship during SIM, NEM and FIM (Fig. 3.6), while the presence of multiple sources was evident during the SWM (Fig. 3.6).

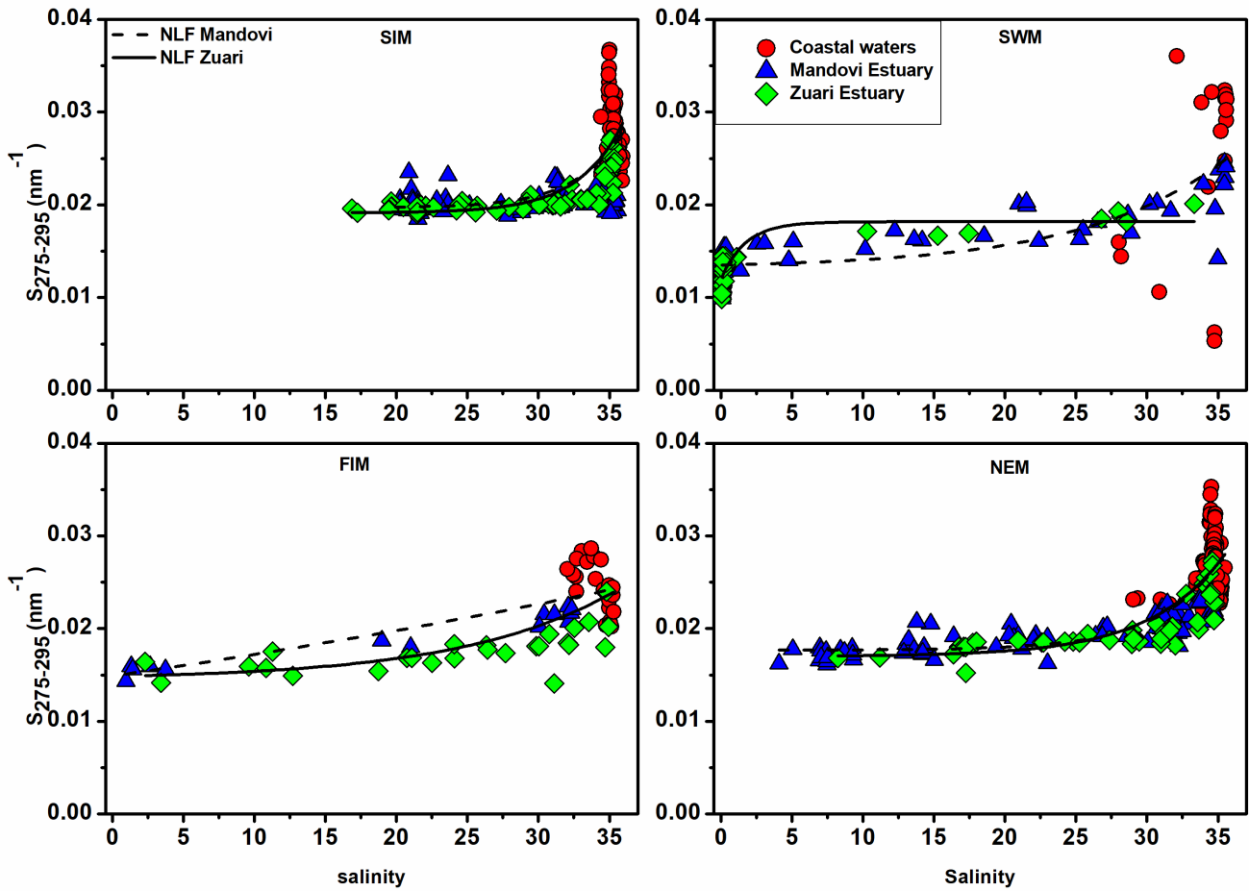

Figure 3.4: Variation of $S_{275-295}$ (nm^{-1}) with salinity in the Mandovi and Zuari estuaries, and the adjoining coastal waters. The black dotted line represents the nonlinear fit for Mandovi and the continuous line for Zuari Estuary.

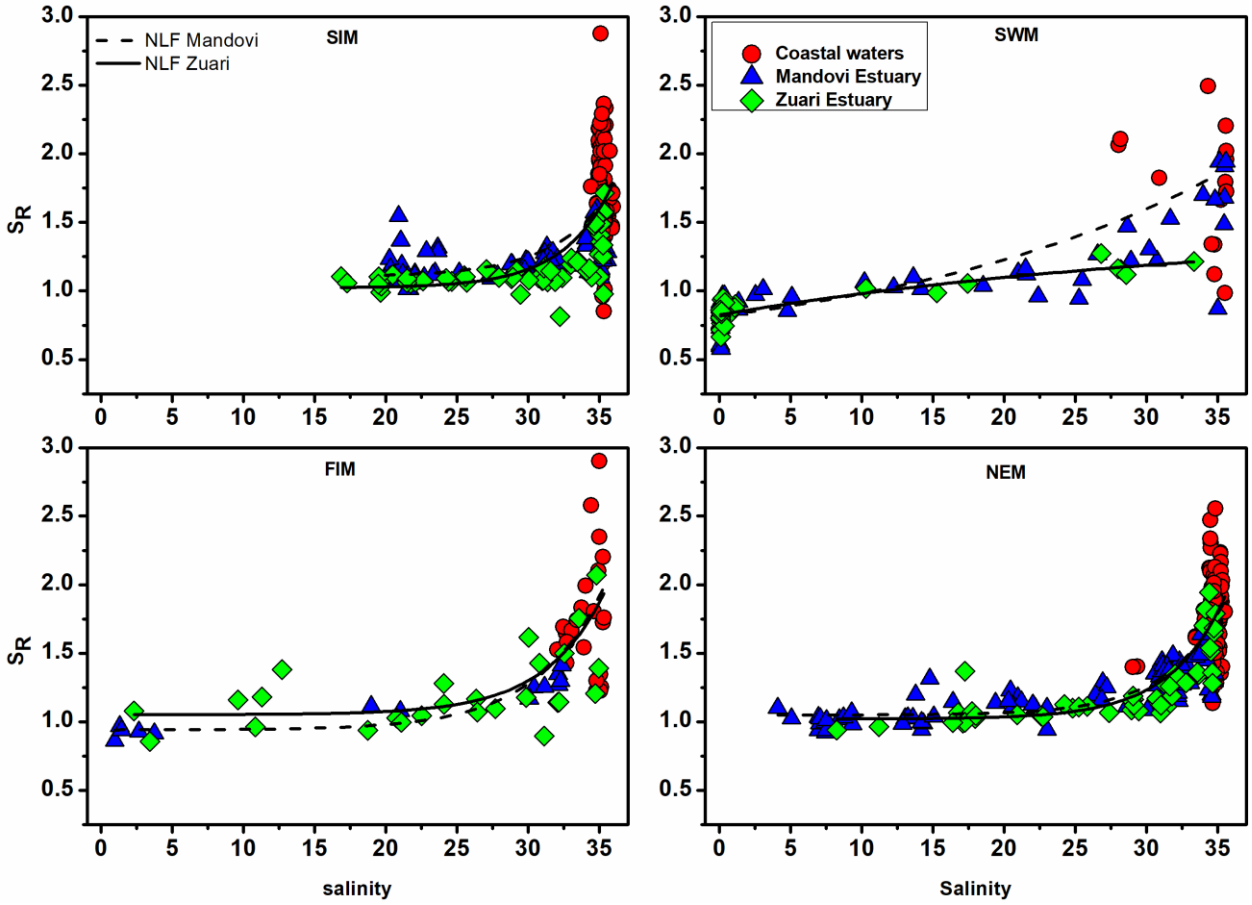

Figure 3.5: Variation of S_R with salinity in the Mandovi and Zuari estuaries, and the adjoining coastal waters. The black discontinuous line represents the nonlinear fit for Mandovi and the continuous line for Zuari Estuary.

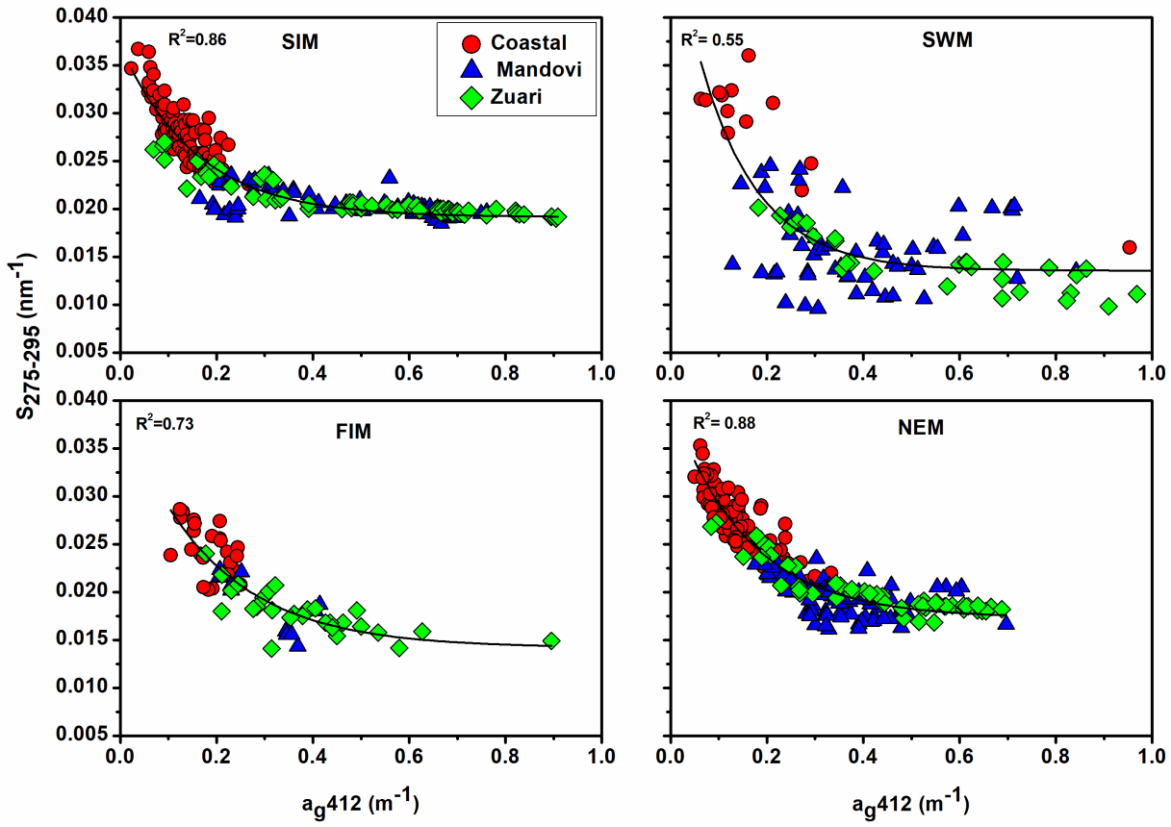

Figure 3.6: Variation of a_g412 (m^{-1}) with $S_{275-295}$ (nm^{-1}) in the estuaries and the adjoining coastal waters.

The spectral slope $S_{275-295}$ and S_R in the Mandovi Estuary during November, 2020 (NEM) was the lowest at the upstream ($S_{275-295}$ = 0.0135 nm^{-1}; S_R = 0.92) and increased towards the mouth ($S_{275-295}$ = 0.0198 nm^{-1}; S_R = 1.33). Zuari Estuary also showed similar trend in February 2021 with slope values increased from the upstream ($S_{275-295}$ = 0.0168 nm^{-1}; S_R = 1) towards the mouth ($S_{275-295}$ = 0.0195 nm^{-1}; S_R = 1.16). The Cumbarjua canal showed spectral slope characteristic of the mid-stream region of the estuary ($S_{275-295}$ = 0.0191 nm^{-1}; S_R = 1.16) (Fig. 3.3).

3.5.2.2 Variation of a_g412, spectral slopes, $S_{275-295}$, and S_R with salinity

The mixing curves of a_g412 for Mandovi and Zuari estuaries along with the adjoining coastal waters indicated a distinct non-conservative behavior of CDOM (except during FIM) (Fig. 3.7). A mixing diagram was constructed by joining the high and low-salinity end members, and the values above and below the theoretical dilution line are attributed to sources and sinks, respectively (Stedmon et al. 2003). In this study in general, the a_g412 values were below the mixing line at very low (< 2) salinities during the SWM, and at high (> 33) salinities during SIM and NEM in both the estuaries and coastal waters (Fig. 3.7). However, additions were observed at salinities between 3 and 32, as indicated by the values above the mixing line. During the FIM, conservative mixing of CDOM was observed in the Zuari Estuary while a quasi-conservative mixing was observed in the Mandovi Estuary (Fig. 3.7).

The spectral slopes and slope ratio ($S_{250-600}$, $S_{275-295}$, and S_R) exhibited a characteristic pattern with salinity, with an almost constant value ($S_{275-295}$ = 0.019 nm^{-1}, S_R = 1.14) within a salinity range of 3 – 32, while a decrease in S and S_R ($S_{275-295}$ = 0.0098 – 0.016 nm^{-1} and S_R = 0.5 – 1) was observed at the upstream of the estuaries (salinity range; 0 – 3) during the SWM. However, at high salinities (>32), S and S_R exhibited a large variability ($S_{275-295}$ = 0.0142 – 0.036 nm^{-1} and S_R = 1 – 4.5) (Figs 3.4 and 3.5). This suggests that there were variations in the quality of CDOM in both the estuaries and the coastal waters ($p < 0.001$). In general $S_{275-295}$ and S_R increased with salinity due to the mixing of terrestrial and marine DOM.

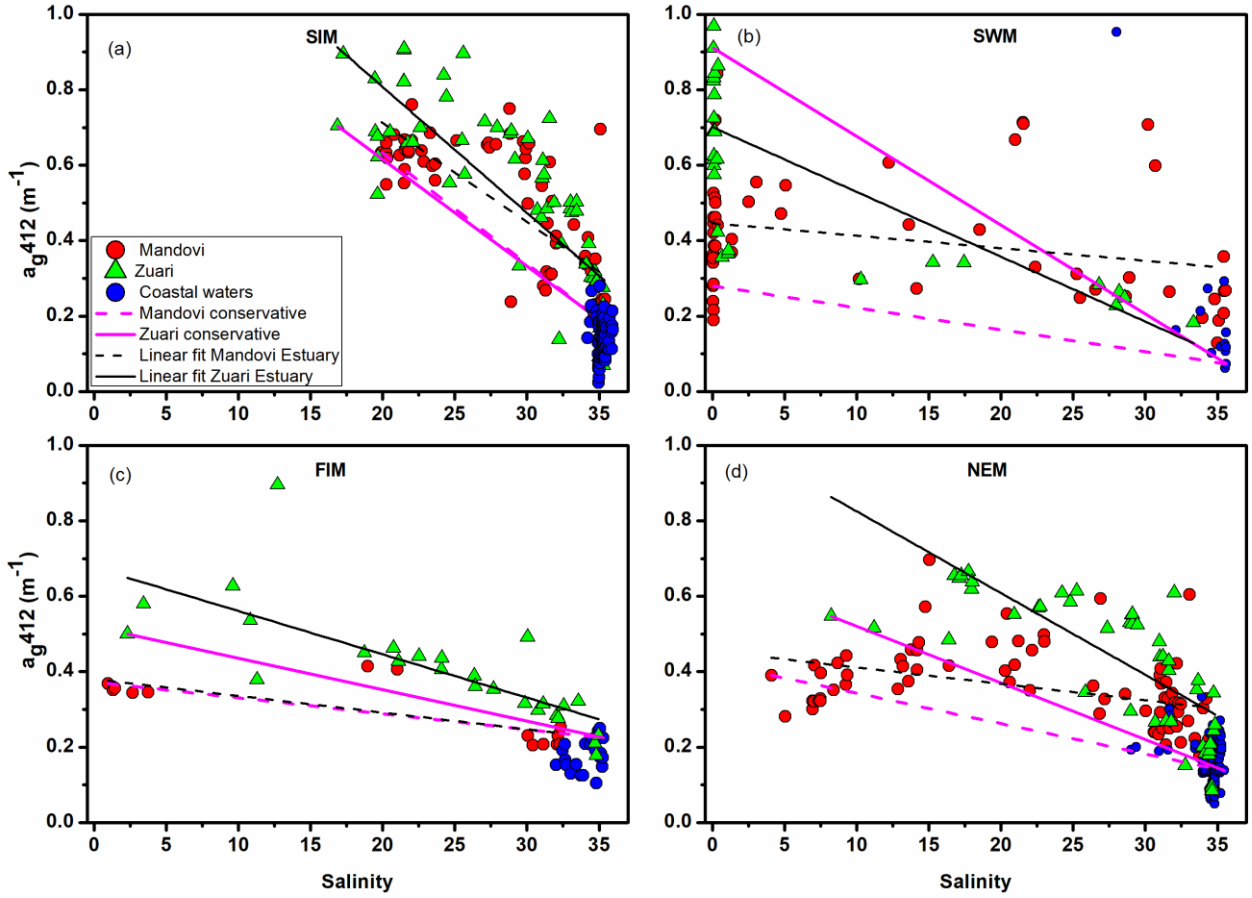

Figure 3.7: The conservative mixing diagram showing the variations of a_g412 (m^{-1}) with salinity in the Mandovi and Zuari estuaries, and the adjoining coastal waters. The Magenta continuous line represents the theoretical dilution line (joins the lowest and highest salinity end members) for Zuari and the dotted line for the Mandovi Estuary. The black continuous line represents the linear fit for Zuari and the dotted line represents the Mandovi Estuary.

3.5.2.3 Variations of the optically active fractions, CDOM, detritus, and phytoplankton in the coastal and estuarine waters of Goa

The contribution of CDOM to the total absorption (in the blue region) was found to be dominant during all the seasons (SWM sampling was not done for absorption by phytoplankton and detritus) in the coastal waters. CDOM contribution was highest during the SIM followed by FIM and NEM seasons (Fig. 3.8a). Among the phytoplankton and detrital absorption, they have equal contribution during the NEM, but the latter dominates during the FIM.

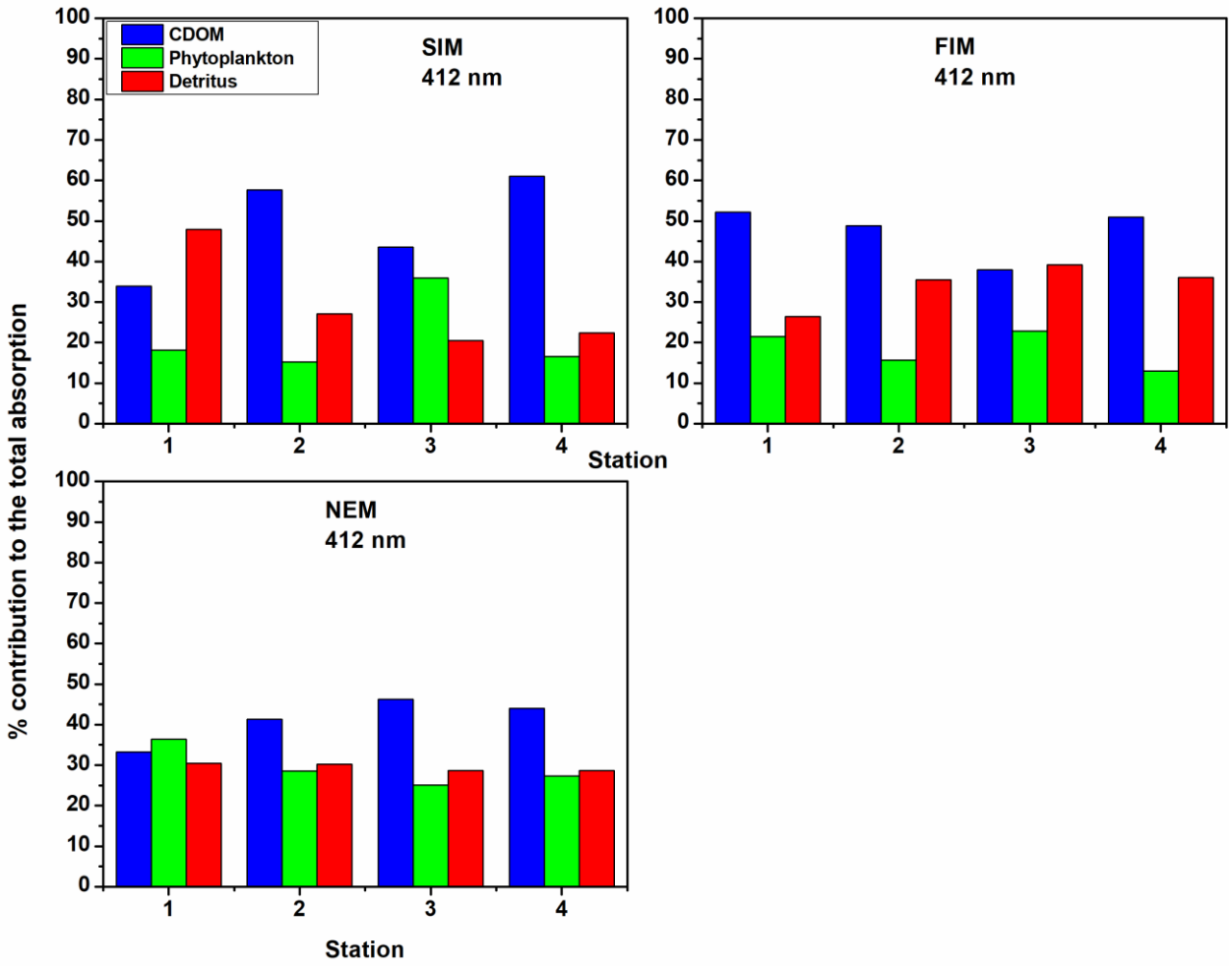

Figure 3.8a: Contribution of the optically active fractions to the total absorption in the coastal waters in the blue region.

In the estuaries, the detrital fraction was dominant during the SWM and FIM seasons. During the SIM, CDOM and detritus contribute equally to the total absorption towards the upstream of the estuary while towards the mouth the detrital fraction dominates (Fig. 3.8b and c). On the other hand, CDOM and detritus contribute equally towards the mouth while at the upstream stations the detrital fraction dominates during the NEM (Figs 3.8b and c).

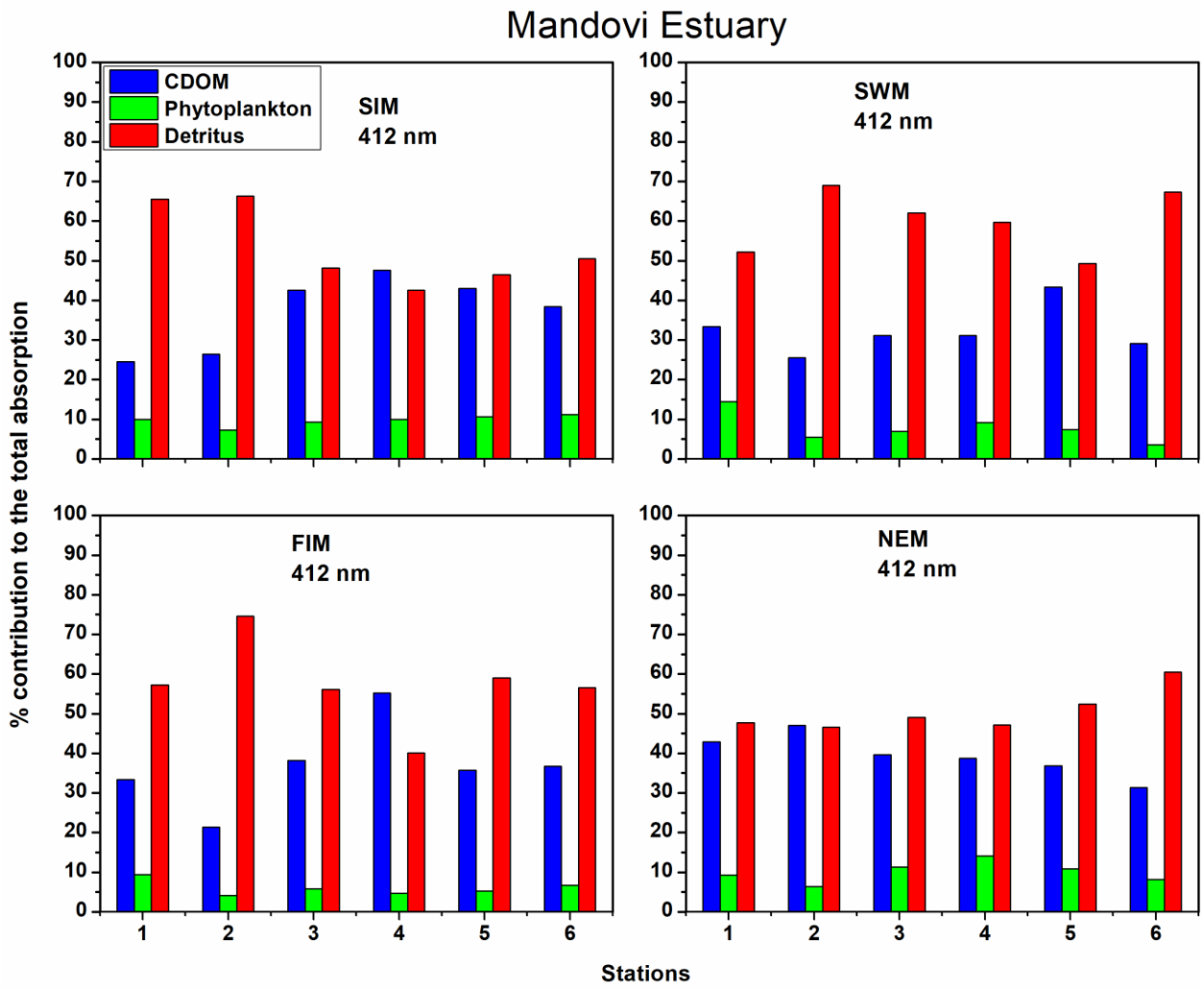

Figure 3.8b: Contribution of the optically active fractions to the total absorption in the Mandovi Estuary in the blue region.

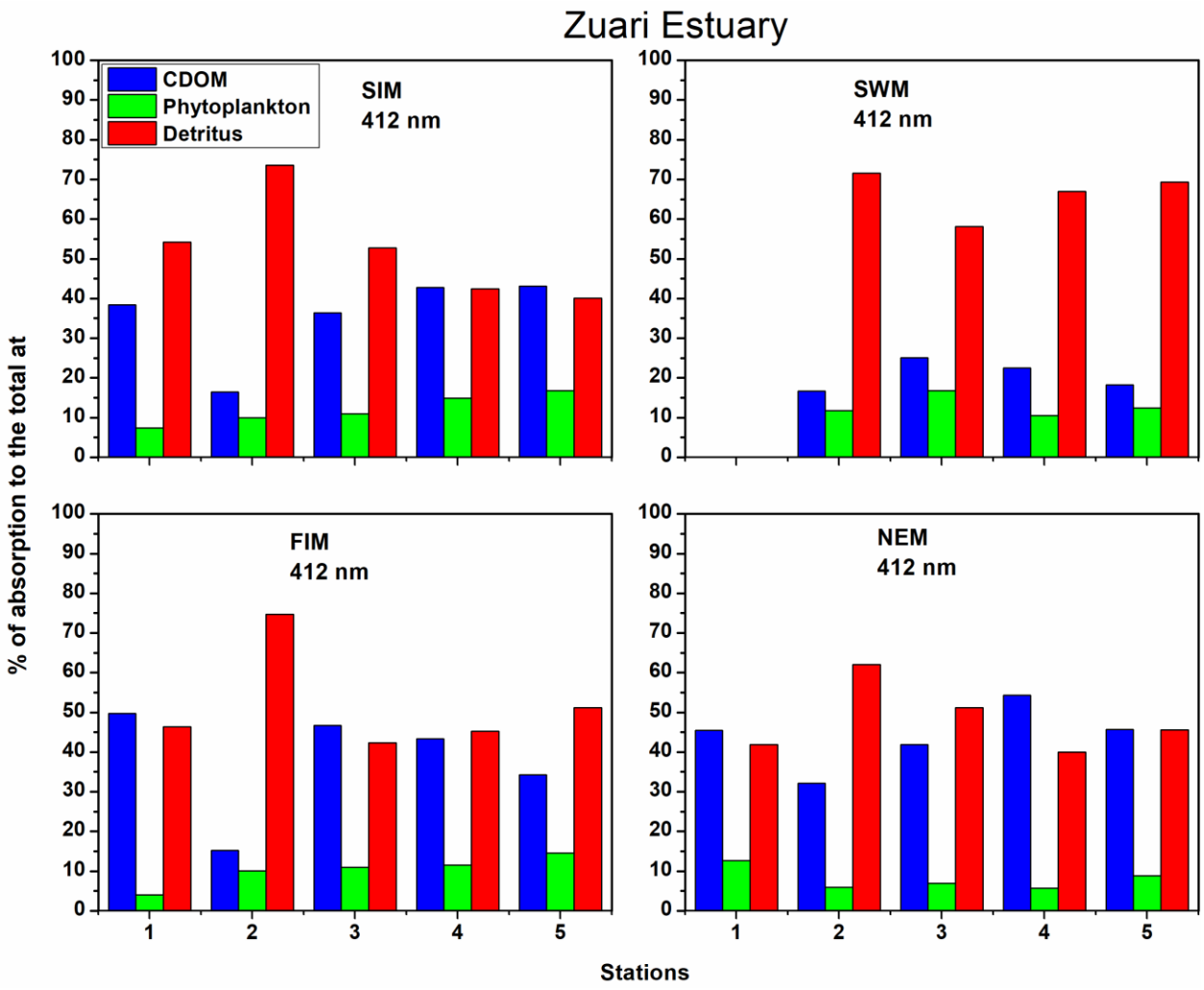

Figure 3.8c: Contribution of the optically active fractions to the total absorption in the Zuari Estuary in the blue region.

3.5.3 Variations of in-situ inherent and apparent optical properties

The optical complexity of the water could be observed from the $R_{rs}(\lambda)$, with its typical shape in the coastal and estuarine waters (Fig. 3.9a). The $R_{rs}(\lambda)$ spectra of the coastal waters had a peak at around 550 nm, whereas a shift to a longer wavelength (580 nm) was observed for the estuarine waters. Very low values in the blue and the red region of the $R_{rs}(\lambda)$ spectra indicated the attenuation of light due to absorption in water. During the SWM the $R_{rs}(\lambda)$ was observed to be the highest in the estuarine waters due to the scattering effect (Fig. 3.9a).

The surface solar irradiance, E_s at the sampling stations was the highest during the SIM and lowest during the SWM (Fig. 3.9b). The average value of E_s (at noon) over the spectral range of 350-800 nm during SIM was 511.67 Wm^{-2} whereas the lowest value (317.72 Wm^{-2}) was observed during the SWM.

The diffuse attenuation coefficient, K_d (m^{-1}) was the lowest and the penetration of light, Z_{90} (m) was the highest during the SIM and vice versa during the NEM in the coastal waters. In the estuaries, maximum light penetration occurred during the FIM (1.82 m) and NEM (1.76 m) while, lowest during the SWM (1.14 m) and SIM (1.25 m) (Figs 3.9c and 3.9d). A shift in the spectral light quality was observed with blue-green (500 nm) penetrating the deepest in the coastal waters during SIM to greenish-red (570 nm) in the estuarine waters (Fig. 3.9c).

The absorption and scattering measured from AC-9 were observed to be the highest in the estuarine waters and lowest in the coastal waters during all the seasons. In the coastal waters, the highest absorption was observed during the FIM (Fig. 3.9e). The total absorption was highest during the SWM followed by SIM in the estuarine waters (Fig. 3.9e). A very good correlation was observed between the measured CDOM absorption (a_g412) and *in-situ* a412 ($r = 0.72$). The average particulate backscattering coefficient at 700 nm, $b_{bp}700$ (m^{-1}) in the estuaries during the SWM was 0.344 m^{-1} compared to 0.112, 0.095 and, 0.165 m^{-1} during SIM, FIM, and NEM, respectively. The $b_{bp}700$ was observed to be the highest in both the estuaries during the SWM than the non-monsoon season (Fig. 3.9f).

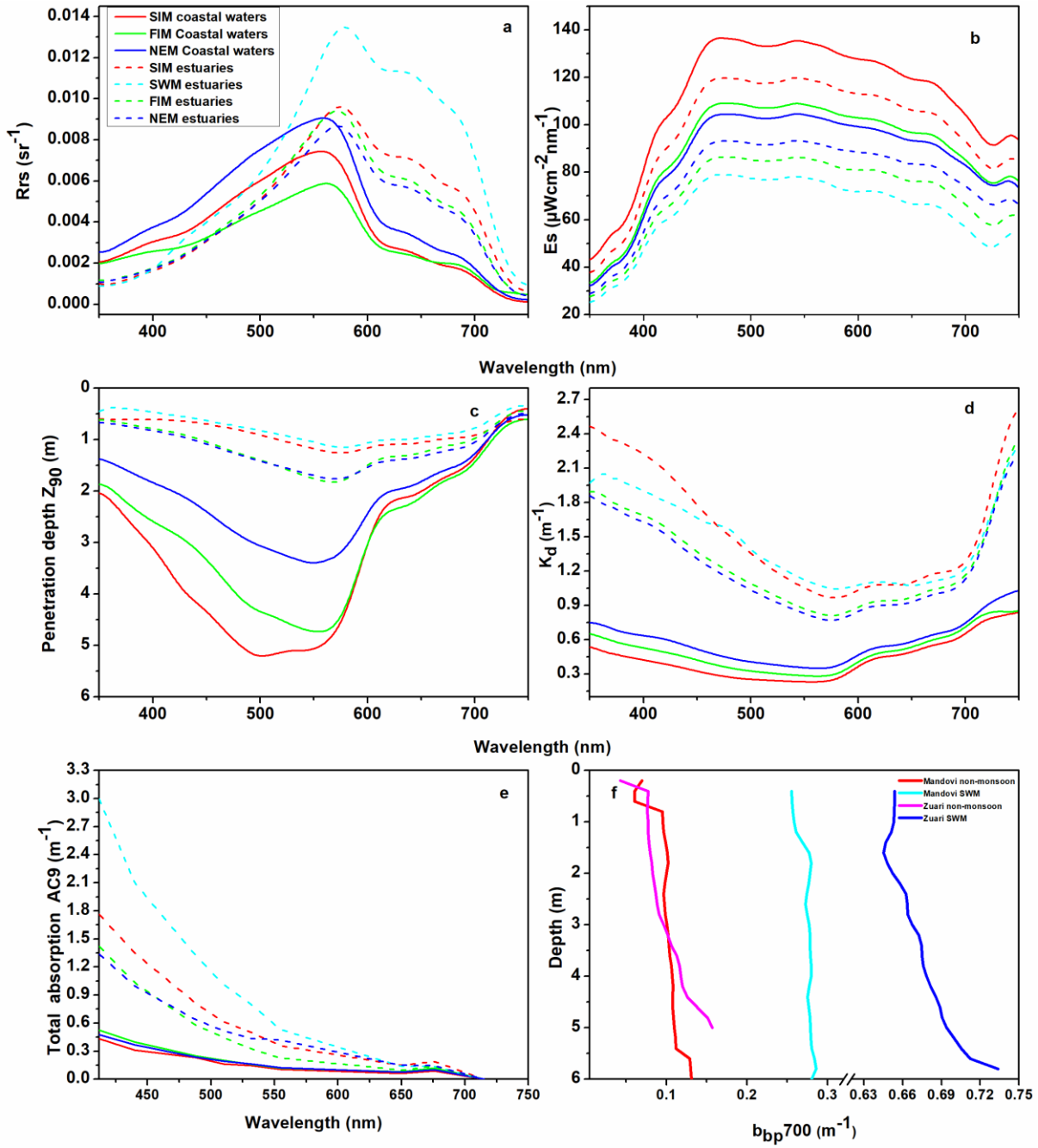

Figure 3.9: Seasonal variation of *in-situ* optical parameters in the coastal and estuarine waters. Since Mandovi and Zuari estuaries showed similar variations, the mean value is plotted in figures a – e. The dotted line represents the estuary while the continuous line represents the coastal waters. a) Spectral (350 – 750 nm) variation of Rrs (sr^{-1}); b) Spectral variation of surface solar irradiance, E_s ($\mu Wcm^{-2}nm^{-1}$); c) Spectral variation of light penetration depth, Z_{90} (m); d) Spectral variation of light attenuation in water, k_d (m^{-1}); e) Variation of total absorption in water obtained at 9 wavelengths (412, 440, 488, 510, 555,

650, 676 and 715 nm) from the profiles of AC9; f) The vertical profile at a mid-stream station showing the scattering in water indicated by the particulate backscatter at 700 nm ($b_{bp}700$) during the SWM and non-monsoon seasons in the Mandovi and Zuari estuaries. Please note that there is a break in the X-axis for figure f. The figure clearly shows that the scattering is much higher in the Zuari as compared to the Mandovi Estuary.

3.6. Discussion

High CDOM absorption (a_g412) was observed during the SIM and SWM seasons in both the Mandovi and Zuari estuaries and the coastal waters. However, these two seasons exhibited contrasting characteristics with basically dry weather, high solar irradiance, and no discharge in the former, whereas heavy rainfall, high discharge, and low solar irradiance in the latter.

3.6.1 Variations of CDOM optical properties in the Mandovi and Zuari estuaries during the non-monsoon (SIM and NEM) seasons

During the SIM, sea surface temperature and salinity were found to be the highest and tides are the sole driving force for mixing and circulation in the estuaries during the non-monsoon season (Shetye et al., 2007; Manoj and Unnikrishnan, 2009). In addition, river discharge in the estuaries is the lowest during this season (Shetye et al., 2007; Manoj and Unnikrishnan, 2009). Hence, the contribution of CDOM in the estuaries from riverine inputs would be insignificant in comparison to that during the SWM and FIM seasons, when river discharges were higher. Phytoplankton is a major source of CDOM in coastal and estuarine waters; however, their contributions to the total CDOM may vary on a regional basis. During the SIM, high CDOM absorption in these estuaries could be attributed to *in-situ* production and the degradation of phytoplankton (Zhang et al., 2009; Loginova et al., 2016), as indicated by the good correlation between CDOM absorption and chlorophyll-*a* (Mandovi Estuary r = 0.95; Zuari Estuary r = 0.93; Fig. 3.10). This was also substantiated by a good correlation between absorption by phytoplankton ($a_{ph}676$) and a_g412 (r = 0.84). The longer residence time of water (~50 days) during non-monsoon season (Shetye et al., 2007) would have favored the accumulation of phytoplankton. The inverse relationship observed between CDOM absorption and $S_{275\text{-}295}$ in the coastal and estuarine waters also supports the autochthonous production (Fig. 3.6) and accumulation of

marine organics in the estuaries. Mangroves are another potential source of CDOM in these estuaries, and they cover a relatively smaller area in the Zuari Estuary (735 ha) than in the Mandovi Estuary (1107 ha) (Shynu et al., 2015). The leachate from mangrove leaves and stems is a significant source of CDOM (Shank et al., 2010). Anthropogenic activities peak during the SIM, which significantly contributes to the CDOM. The petroleum hydrocarbons from river transport systems, such as barges, ferryboats, and trawlers, could also form another source of CDOM (Coble, 2007; Chiranjeevulu et al., 2014). Sand mining activities in the Mandovi Estuary during non-monsoon season disturb the benthic layers, resulting in the release of organic matter, leading to CDOM production. Domestic and treated municipality sewage is discharged into these estuaries, which could also serve as a source of CDOM (Baker, 2001; Coble, 2007; Guo et al., 2010).

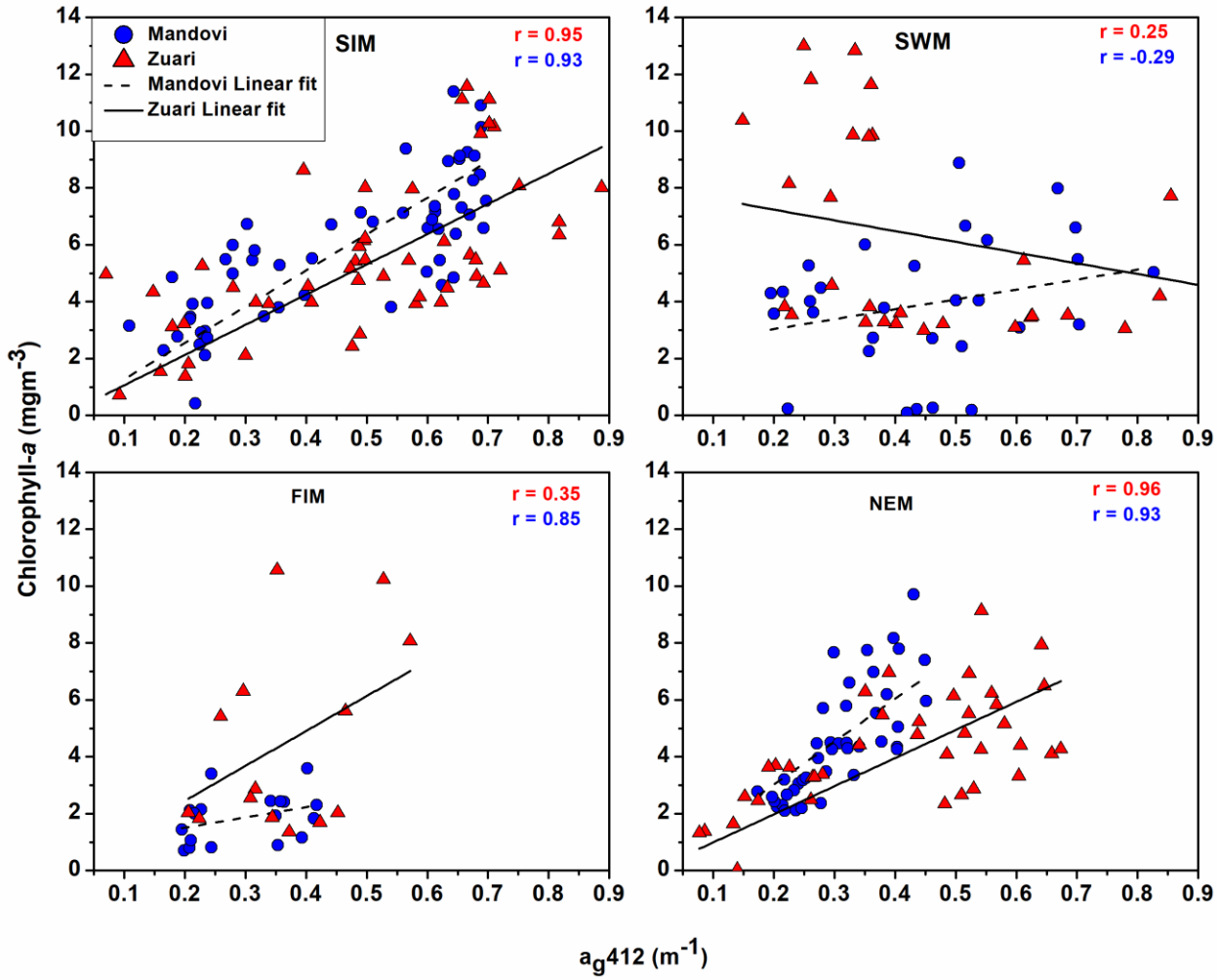

Figure 3.10: Correlation between CDOM absorption (a_g412) and chlorophyll-*a* during the SIM, SWM, FIM and NEM in the Mandovi (blue) and Zuari (red) estuaries.

The slopes ($S_{250-600}$ and $S_{275-295}$) and slope ratio (S_R) were highest during the SIM in both estuaries (Fig. 3.2), indicating that CDOM was modified by photochemical transformation (DelVecchio and Blough, 2002; Helms et al., 2008; Yamashita et al., 2013). The residence or flushing times of the Mandovi and Zuari estuaries were found to be approximately 50 days during the non-monsoon season (Shetye et al., 2007). A longer residence time of water will cause favorable condition for prolonged microbial and photochemical degradation of organic matter and the generation of CDOM (Mari et al., 2007; Peierls et al., 2012). Overall, during the SIM season, CDOM is largely driven by *in-situ* production and anthropogenic processes in both the estuaries of Goa.

During the NEM, the temperature decreases while the salinity gradually increases. Circulation is largely influenced by tides, which is manifested in the distribution patterns of CDOM (Johnson et al., 2001; Kowalczuk et al., 2003). During the NEM, CDOM was probably contributed by autochthonous production in both the estuaries, as indicated by the good correlation between CDOM and chlorophyll-*a* (Mandovi Estuary r = 0.96, Zuari Estuary r = 0.93; Fig. 3.10), and $a_{ph}676$ (r = 0.81). This was also observed from the inverse relationship of CDOM with S (Fig. 3.6). Contribution from other sources was also evident during this season as seen from the additions observed during the mixing behavior (Fig. 3.7d) and also from the lower slopes (0.017 nm^{-1}) of CDOM absorption (a_g412; between 0.2 and 0.4 m^{-1}) in the Mandovi Estuary (Fig. 3.6). The sources of CDOM during the SIM and NEM were presumed to be similar. However, the autochthonous CDOM in both estuaries seem to undergo rapid photochemical and microbial degradation, as indicated by the high $S_{250-600}$, $S_{275-295}$, and S_R values.

Our observations in the Mandovi and Zuari estuaries and, the Cumbarjua canal during the NEM of 2020-21 showed maximum CDOM absorption in the Cumbarjua canal especially at the stations CC6 and CC7 with distinguishably lower spectral slopes (Fig. 3.3c). This indicates an additional source of organic matter at these locations. There are Khazan lands (which are low-lying areas that are fringed with mangroves and are designed as topo-hydro-engineered agro-aqua cultural ecosystems) in the proximity of these stations and also a water treatment plant of the Agrochemical Industry is situated close to CC7. The seeping of water from the treatment plant or inputs from the Khazan lands must be contributing to the observed high CDOM in this region. Moreover, the slope ratio was

higher at the CC7 station, which indicates low molecular weight organic matter, probably coming from the Agrochemical Industry (Fig. 3.3c). Apart from this, the Mandovi Estuary exhibited lower absorption than the Zuari Estuary (Figs 3.3a and 3.3b), although the values were within the range observed during the previous years of NEM. The reason behind this could be sampling time as the observations in Mandovi were carried out during November, whereas Zuari was sampled in February. A gradual decrease in CDOM absorption was observed from the upstream of the Mandovi Estuary (Ganjem) up to the station M12 followed by a gradual increase in absorption in the mid-stream region. Several point sources such as floating platforms and fish processing units seem to be present at the banks of the estuary leading to an increase in CDOM absorption at certain stations. The station M6 in the mid-stream region is situated at the confluence of the Mandovi Estuary and Cumbarjua canal also showed high absorption of CDOM. A gradual increase in spectral slope and slope ratio is observed from the head of the estuary to the mouth region, which shows the transformation of organic matter during its passage through the estuary (Fig. 3.3a). The spectral slopes and slope ratio (<0.8) are very low towards the upstream which points to the terrestrial nature of DOM at the upstream (Fig. 3.3a).

CDOM absorption was high in the Zuari Estuary for the upstream stations (from Z16) to Z10 in the mid-stream region while lower values were recorded at the upstream stations Z18 and Z20 (Fig. 3.3b). The sharp increase in CDOM absorption at the upstream region is observed at the proximity of the mouth of Kushavati River, a major tributary to the Zuari Estuary. Further, the recent reports by the River Rejuvenation Committee, (2019) showed that the stretch of the Zuari Estuary between Curchorem and Marcaim Jetty is polluted with high values of Fecal Coliform and attributed these to the discharge of domestic sewage directly into the river or the storm river drains to the estuary. Stations Z16 to Z1 fall within this stretch of polluted river where high values of CDOM were reported in the recent observation.

3.6.2. Variations of CDOM optical properties in the Mandovi and Zuari estuaries during the monsoon season

CDOM was also higher during the SWM in both the estuaries. Mandovi and Zuari are monsoonal estuaries, as their biogeochemistry is mostly controlled by the freshwater influx received during the SWM (Vijith et al., 2009; Vijith and Shetye, 2012). During the SWM,

strong south-westerly winds bring about heavy rainfall and subsequent river discharge in these estuaries from June to September. The runoff in the Mandovi Estuary (258 $m^3 s^{-1}$) is much higher than that of the Zuari Estuary (147 $m^3 s^{-1}$) (Rao et al., 2015). The discharge rates in the Mandovi and Zuari estuaries during the SWM were 175 and 125 $m^3 s^{-1}$, respectively. The large influx of freshwater from the rivers joining these estuaries decreases the temperature and salinity of estuarine water (Shetye et al., 2007). The rainfall over the Goa region during the SWM is substantial at approximately ~2200 mm. There is also considerable daily variability in the rainfall patterns, and runoff would be particularly high during the active phase of the SWM. Hence, the high CDOM during the SWM would largely be controlled by rainfall (freshwater dilution) and subsequent river runoff from the watersheds of the two estuaries (Table 3.1). A high CDOM during the high inflow of water into the estuaries has also been reported in previous studies (Medeiros et al., 2015 and Aulló-Maestro et al., 2017). $S_{250-600}$, $S_{275-295}$, and S_R were lowest during the SWM season (Fig. 3.2), indicating that the high terrestrial inputs and soil organic matter from the watershed are sources of CDOM (Green and Blough, 1994; DelVecchio and Subramaniam, 2004).

The watersheds of these estuaries contain mines, agricultural land, and Khazan lands. However, the contribution from mangrove leaf litter would be the lowest during this season because of a period of new growth due to the increased supply of nutrients by freshwater inflow (Wafar et al., 1997). Agricultural inputs would be high due to the cultivation of crops and the use of fertilizers (Nikolaou et al., 2008; Fellman et al., 2010; Heinz et al., 2015).

The detrital fraction was high during monsoon and contributed to CDOM production, as indicated by the good correlation between a_d440 and a_g412 (r = 0.86). However, the *in-situ* contribution of phytoplankton appear to be insignificant, as indicated by the poor correlation of CDOM with chlorophyll-*a* (Mandovi Estuary r = 0.25; Zuari Estuary r = -0.29; Fig. 3.10). Despite the increased nutrients in the estuary from land runoff, increased discharge rates and faster flushing time do not allow the accumulation of phytoplankton during the SWM (Rennella and Quiros, 2006; Peierls et al., 2012). The presence of multiple sources of CDOM in the estuaries was also evident from the wide variation of $S_{275-295}$ with CDOM absorption (Fig. 3.6b). Absorption was slightly higher in the Zuari

Estuary than that in the Mandovi Estuary during the SWM (Fig. 3.2). This could be due to the higher runoff, faster flushing, and greater dilution by the larger number of tributaries in the Mandovi Estuary when compared to that of the Zuari. The drainage basin of Zuari Estuary is largely located in coastal plains whereas the catchment of Mandovi Estuary is in elevated and mountainous regions with narrow coastal plain downstream. As the Zuari Estuary flows through the coastal plains, CDOM is dominated by highly aromatic soil organic matter. This was indicated by the lower values of $S_{275\text{-}295}$ and S_R in the Zuari than those in the Mandovi Estuary, indicating the predominance of DOM with higher molecular weight in the former. Shynu et al. (2015) reported lower particulate organic carbon to particulate nitrogen ratios (8.7 – 10.1) in the Zuari Estuary than those in the Mandovi Estuary (12.2 – 14.6) due to the predominance of soil organic matter during the SWM. In addition, the detrital fraction was also higher in Zuari Estuary than in Mandovi during the SWM.

During the SWM, the cloudy sky during most of the day and the high turbidity of the water column would lower the UV-photic zone (Kowalczuk et al., 2003). The $S_{275\text{-}295}$ was low during this season indicating a low level of photochemical transformation. The high inputs of DOM, lower residence time, and lower solar irradiance would have hindered photobleaching. Hence, photobleaching is not a major CDOM-removal process during this season. Microbial degradation would be one of the sinks of CDOM as observed by high a_g412 and lower spectral slope, $S_{250\text{-}600,}$ and $S_{275\text{-}295}$. Contrary to the widely accepted notion that terrestrial CDOM is largely resistant to microbial degradation, recent studies have proved the microbial degradation of terrestrial CDOM and potential CO_2 outgassing (Fasching et al., 2014). The a_g412 and $S_{275\text{-}295}$ values deviated from the conservative mixing line in the upstream regions with low salinity (Figs. 3.6 and 3.7). The flocculation or sorption of CDOM would have occurred due to the high particle load (Shynu et al., 2012) indicated by the particulate backscatter $b_{bp}700$ and lower salinities during the SWM. Hence, the hydrodynamic conditions in the estuaries determine the sources of DOM during the SWM.

The FIM season is characterized by a steady increase in temperature, a decrease in the level of freshwater, and a corresponding increase in salinity. The upstream regions are still influenced by freshwater, and some rainfall was observed during this period. The

absorption of CDOM during this period was lowest in the Mandovi Estuary, while higher CDOM was observed in the Zuari Estuary (Fig. 3.2). A plausible reason for the low CDOM in the former could be due to the low primary production as indicated by low chlorophyll-*a*, and poor correlation with CDOM (r = 0.35). The high absorption by CDOM in the Zuari Estuary is likely due to autochthonous sources indicated by the good correlation between CDOM and chlorophyll-*a* (r = 0.85) and higher abundance of zooplankton. Studies conducted by other researchers in the Zuari Estuary observed a peak in zooplankton biomass during this season (Gauns et al., 2015; Bardhan et al., 2015). Based on an experimental study, Steinberg et al. (2004) concluded that the fecal pellets and excretion of metabolites by zooplankton or the exudation of mucus and other extracellular secretions result in CDOM production. High solar irradiance, clear skies, and longer residence times during the FIM season might favor photobleaching or the degradation of CDOM, resulting in higher losses. The rapid degradation of photo-labile and terrestrially derived allochthonous carbon could be another reason for the low CDOM; this was also corroborated by the higher values of $S_{250\text{-}600}$ and $S_{275\text{-}295}$ in the Mandovi Estuary than those in the Zuari Estuary (Fig. 3.2). $S_{275\text{-}295}$ increased towards the mouth of the Mandovi Estuary, suggesting a transformation of DOM and the influences of marine organic matter (Fig. 3.4). The bacterial population was also found to be higher in the Mandovi Estuary than in the Zuari Estuary (Rodrigues et al., 2011). The respiration and remineralization of organic matter would have resulted in decreased CDOM. All these factors indicate the rapid degradation of allochthonous carbon at a faster pace in the Mandovi Estuary than in the Zuari Estuary. Towards the upstream of the Mandovi Estuary, the slope values were still lower, indicating that the CDOM was of terrestrial origin. The Zuari Estuary exhibited low and constant $S_{250\text{-}600}$ values with salinity, indicating the influence of fresh CDOM, which is also indicated by the lower $S_{275\text{-}295}$ and S_R values that reflect the predominance of high-molecular-weight DOM (Figs 3.4 and 3.5).

Overall, CDOM exhibited significant seasonal variations in the Mandovi Estuary, with a four-fold decrease in the FIM and NEM seasons from its level in the SIM and SWM seasons, but such inter-seasonal variations were not observed in the Zuari Estuary. Biogeochemical processes control the variability of CDOM in the estuaries during the non-monsoon season, whereas physical processes are responsible for the observed variations in CDOM during the monsoon season.

3.6.3 Contribution of CDOM from rainfall over the Goa region

Rainwater would be another source of CDOM during the SWM, though its contributions could be marginal in the estuaries. Globally, rainwater deposits 90 and 340 Tg of DOC per year to the sea and land respectively (Willey et al., 2000), which is an important source of organic carbon to the marine and terrestrial environments. Considering this, an attempt was made to study the CDOM in rainwater for this region during the SWM. Rain affects the CDOM of these waters either directly or indirectly. The mean value of rainwater CDOM (0.113 m^{-1}) was 5 times lower than the CDOM absorption in the estuaries (0.570 m^{-1}) during the SWM. The spectral variations of CDOM in rainwater (measured for the first time over this region) are given in Appendix 1.2h. CDOM absorption in the rainwater exhibited an increase after a break, which could be attributed to the buildup of aerosols in the atmosphere during this period. The $S_{275-295}$ value of rainwater increased drastically towards the end of the SWM season. The levels of aerosols (atmospheric fallout of fly ashes with polyaromatic hydrocarbons from ore processing, industrial activities, and motor vehicle exhausts) were found to be high over the Goa region during the SIM season (Suresh et al., 1996; Satheesh and Srinivasan, 2002), and rainfall likely transports these aerosols into the estuaries during the SWM. Detailed fluorescence analysis clearly showed the presence of humic- and protein-like substances in the rainwater samples (Keiber et al., 2006; Fu et al., 2015; Chen et al., 2016; Bao et al., 2018). In addition, Fu et al. (2015) reported that biomass-burning, fossil fuel combustion, and primary biological aerosols were the main sources of fluorescent organics in the Arctic region. Goa has a large area covering agricultural activities and the biomass is generally burnt to prepare the fields for cultivation before the rains. It has also been shown that the mineral dust from the Middle-East finds its way to the Goa region during storms (Ramaswamy et al., 2017). We speculate that all these factors plausibly contribute to the CDOM in rainwater.

Apart from the small contributions of CDOM directly from the rainwater to the estuaries, monsoons indirectly enhance the CDOM of these waters. A significant positive correlation ($r = 0.813$) was observed between daily average rainfall over the Goa region and CDOM absorption in the study region (Mandovi and Zuari estuaries) (Appendix 1.3). The increased rainfall will result in a greater runoff from the catchments into the estuaries and coastal waters that flush terrestrial CDOM, resulting in an increase in CDOM absorption.

However, this will significantly influence the availability of light in the water column. The effect of dilution of CDOM by the increase in rainfall was not significant in this study.

3.6.4. Variations of CDOM optical properties in the coastal waters during the monsoon seasons

Maximum CDOM absorption was observed during the SWM season in the coastal waters, owing to the high land driven runoff received during the monsoon (Fig. 3.2). This has also been supported by the low spectral slope values, high CDOM absorption, low $S_{R,}$ and salinity values in the coastal waters which further circumstantiate the terrestrial nature of DOM (Fig. 3.2). The stability of the water column was observed to be the maximum during the SWM and FIM at the coastal station G5 (Appendix 1.4a). The high stability favours the accumulation of DOM from the terrestrial origin with low spectral slopes in the stratified layer (Appendix 1.4b). A detailed discussion of CDOM during the SWM is provided in chapter 5.

During the FIM season, the temperature in the coastal waters was remarkably high. The influence of freshwater on the coastal waters was still evident during the FIM season owing to the low salinity (Table 3.1). In addition to the Mandovi and Zuari estuaries, other small rivers flow into the Arabian Sea. The high CDOM absorption during the FIM season was due to the export of terrigenous organic matter from the catchment areas of the rivers and estuaries to the adjoining coastal waters during SWM. The terrestrial origin of CDOM was indicated by its optical properties, with low $S_{275\text{-}295}$ and S_R values (Fig. 3.2), indicating the predominance of high-molecular-weight DOM. Detritus absorption (a_d440) and a_g412 exhibited a good correlation (r = 0.64), which further supported the contribution of terrigenous DOM to CDOM production during this season. However, the *in-situ* production of CDOM by phytoplankton was insignificant, as indicated by the poor correlation between CDOM and chlorophyll-*a* (r = 0.37; Fig. 3.11). The removal of CDOM by photodegradation was also insignificant, as indicated by the low values of $S_{275\text{-}295}$ and S_R (Fig. 3.2), despite the availability of sunlight. The terrestrial pool of CDOM from the estuaries was conservatively diluted during its mixing with the adjoining coastal waters (Fig. 3.7).

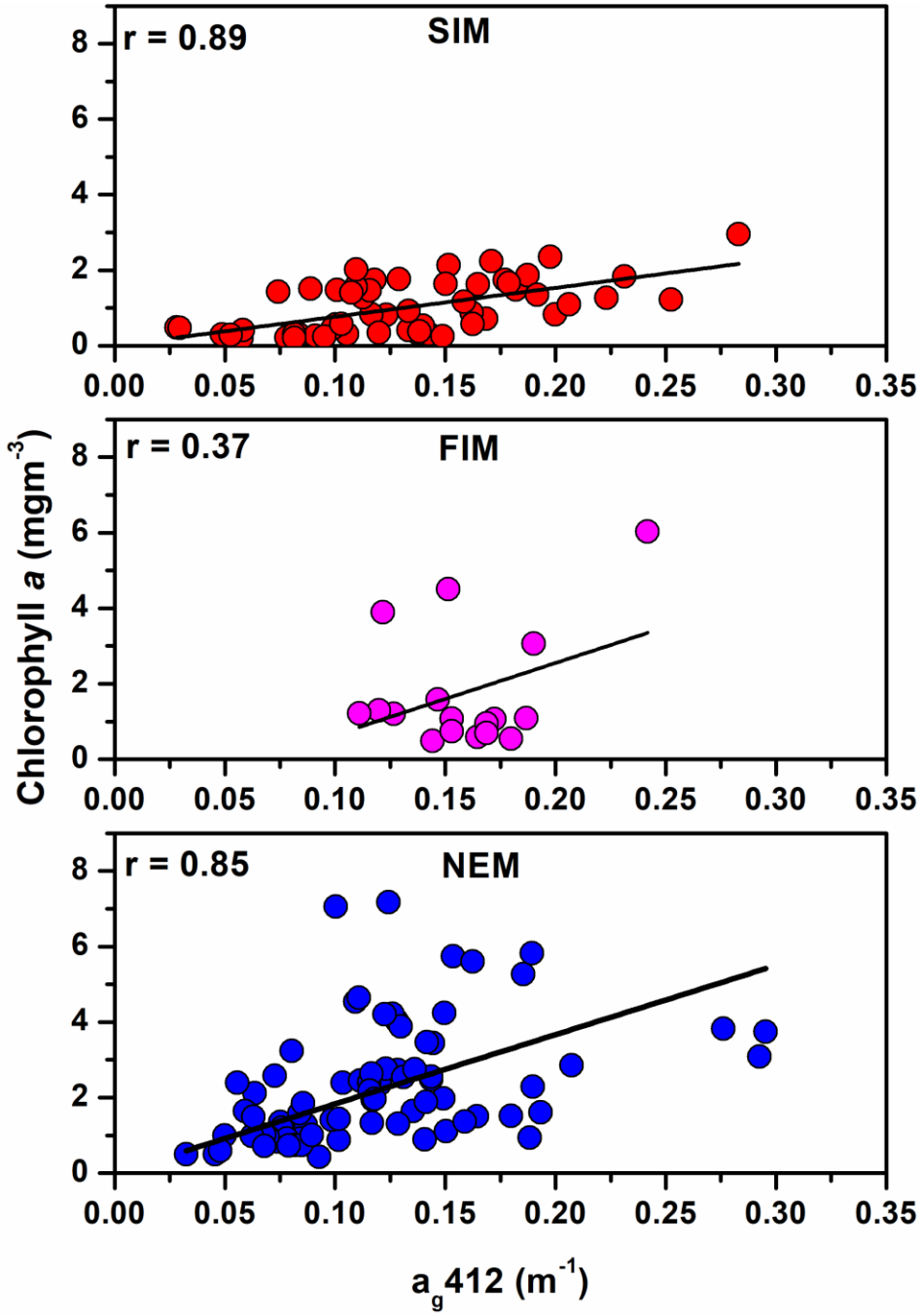

Figure 3.11: Correlation between CDOM absorption (a_g412) and chlorophyll-*a* during the SIM, FIM and NEM in the coastal waters. Please note that the chlorophyll-*a* concentration during *Trichodesmium* bloom was very high and hence these points were not considered here.

3.6.5. Variations of CDOM optical properties in the coastal waters during the non-monsoon seasons

High CDOM absorption was also observed during the SIM season. Solar irradiance, temperature, and salinity were also high during this period. One of the prominent sources of CDOM in the coastal waters was the large *Trichodesmium* bloom observed in the study area; the senescence of the bloom would increase the CDOM pool. The CDOM during the *Trichodesmium* bloom is discussed in chapter 4. Autochthonous production could be the primary source of CDOM, as indicated by the good correlation between CDOM and chlorophyll-*a* (r = 0.89; Fig. 3.11), and $a_{ph}676$ (r = 0.82). However, the chlorophyll-*a* concentration during the bloom was very high and hence these points were not considered in Fig. 3.11. The a_g412 and $S_{275-295}$ relationship (Fig. 3.6) also points out to the autochthonous source. The high $S_{275-295}$ and S_R values corresponding to low CDOM absorption support *in-situ* production (Fig. 3.6). The observed large variability in the spectral slopes ($S_{250-600}$ and $S_{275-295}$) could be explained by the intra seasonal variations in a_g412 and salinity. High a_g412 and low slope during March could be due to the autochthonous production followed by photo-degradation and bacterial utilization of CDOM (Nelson et al., 2004; Fichot and Benner, 2012; Yamashita et al., 2013). The increase in $S_{275-295}$ was observed during the latter months of April - May (except bloom) indicating efficient photobleaching. S_R values were highest in the coastal waters during SIM, demonstrating the predominance of low-molecular-weight CDOM (Fig. 3.2). CDOM removal by photobleaching and microbial degradation exceeded the high level of autochthonous production in the coastal waters during the SIM period. Despite high photobleaching during SIM, absorption of light in the coastal waters was dominated mostly by CDOM (50%) followed by detritus (29%) and least by phytoplankton in the blue region.

CDOM absorption was the lowest during the NEM, when there was no external input of freshwater to the coastal region, and it decreased offshore. The contribution of CDOM from the estuaries was low during this season. In general, during the NEM, *in-situ* production of CDOM by the degradation of phytoplankton was a major source of CDOM, as indicated by the good correlation between CDOM and chlorophyll-*a* (r = 0.85; Fig. 3.11) and $a_{ph}676$ (r = 0.69). This was also observed from the a_g412 and $S_{275-295}$ relationship (Fig. 3.6). The transformation of DOM by photochemical degradation was indicated by the

high values of $S_{275-295}$ and S_R with salinity (Figs 3.4 and 3.5). Large variability in S observed during the NEM was due to low a_g412 and high S values observed during November which could be attributed to the photochemical degradation of terrestrial DOM (Vodacek et al., 1997; Moran et al., 2000) received during the SWM.

3.6.6. Characterization of waters based on the optical properties of CDOM

Principal component analysis has been used to characterize the estuarine and coastal waters based on the optical properties of DOM (a_g412, $S_{275-295}$, $S_{250-600}$, $S_{350-400,}$ and S_R). A two component model explained 69% of the variability in the data, of which component 1 explained 42% variability. $S_{275-295}$ (0.9), S_R (0.86) were positively related while a_g412 (-0.64) was negatively related to component 1. Component 2 was explained equally (0.79) by the spectral slope $S_{250-600}$ and $S_{350-400}$ and accounted for 27% of the variability in the data (Fig. 3.12). Since S_R and $S_{275-295}$ are indicators of molecular weight of DOM and photobleaching, component 1 describes the variability of DOM in terms of its molecular weight, while component 2 can be attributed to the source of DOM. It was observed that the coastal waters had positive PC1 and PC2 scores, while the estuarine waters had negative PC1 and PC2 scores. Further, the samples during the SIM and NEM were clustered together indicating a common source, which can be attributed to autochthonous based on the explanation given in section 2.2 (Fig. 3.12). While the samples during monsoon (SWM and FIM) clustered together in the coastal and estuarine waters indicating the terrestrial nature of DOM during this season (Fig. 3.12). Thus, PCA successfully helped in differentiating the coastal and estuarine waters of Goa based on the DOM indices and has the potential of identifying and characterizing the sources of DOM.

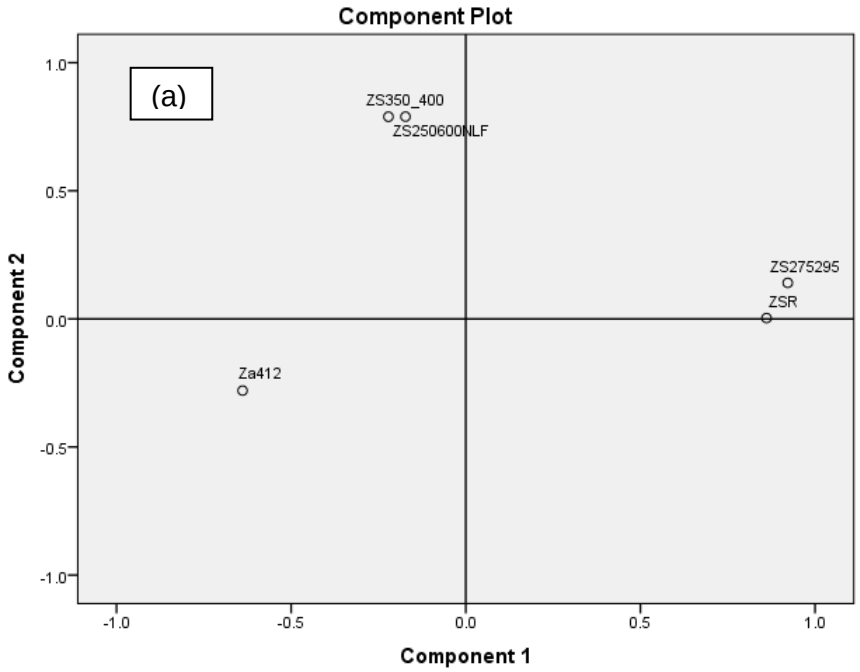

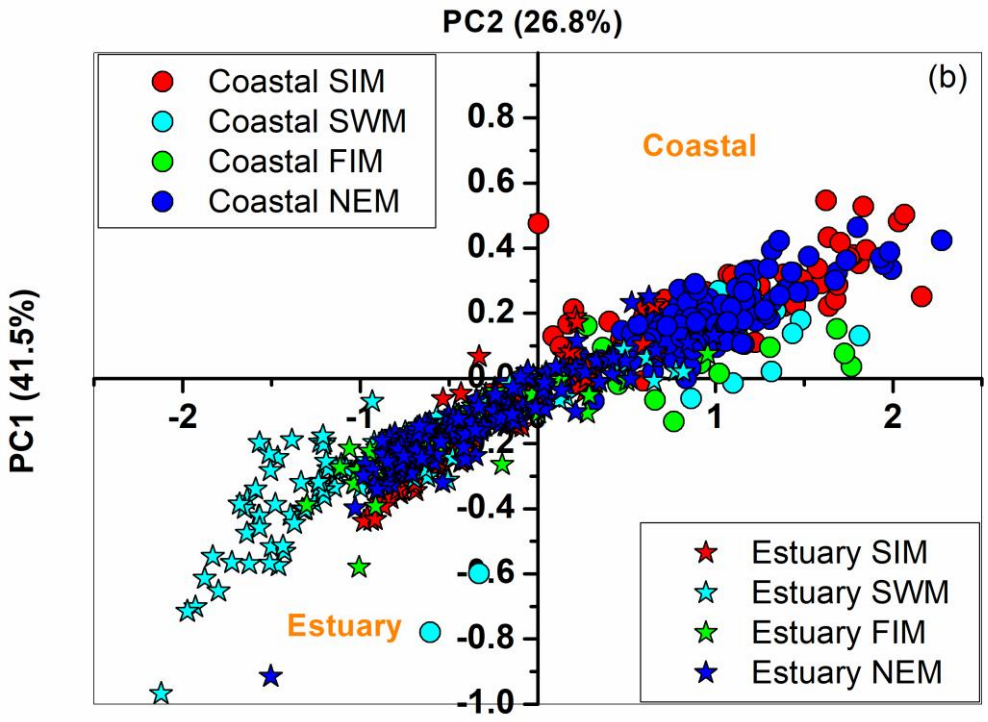

Figure 3.12 (a): The component plot of the CDOM variables used in the PCA analysis and, (b) the individual sample scores. The coastal waters are represented with circles, while the estuarine waters are depicted with stars.

3.6.7. Influence of the optically active substances on the modulation of underwater light in the coastal and estuarine waters of Goa

In the estuaries maximum underwater light penetration occurred towards a relatively longer wavelength of 570 nm as compared to the coastal waters (Fig. 3.9c). The absorption by detritus (50%) and CDOM (40%) was high in these estuaries during the non-monsoon seasons, while detritus (70%) dominated the absorption during SWM (Fig. 3.8b and c). Hence the contribution of colored detrital matter (CDM = CDOM+ detritus) will shift the penetration of light towards a longer wavelength. Also, the dominance in the detritus was observed in the estuary from upstream to mouth during the NEM and SIM. This dominance by detritus could be attributed to the estuarine turbidity maxima (ETM) observed at the mouth of the estuary during SIM and in the upstream during NEM (Kessarkar et al., 2009). The absorption by CDOM and detritus contributes significantly to the total light absorption in the coastal and estuarine waters of Goa. CDM also influences the shape of $R_{rs}(\lambda)$ spectra. Since $R_{rs}(\lambda)$ is a function of the ratio of $b_b(\lambda)$ and $a(\lambda)$, the dominance of $b_b(\lambda)$ or $a(\lambda)$ controls the shape of the $R_{rs}(\lambda)$. Contribution from $a(\lambda)$ was much higher than $b_b(\lambda)$ in the estuaries during non-monsoon seasons, however, $b_b(\lambda)$ dominates during SWM. Hence the R_{rs} peak was also observed around the wavelength of maximum light penetration (580 nm; Fig. 3.9a and c). The highest $R_{rs}(\lambda)$ during the SWM in the estuaries was due to the dominance of $b_b(\lambda)$ over $a(\lambda)$ (Fig. 3.9a).

Underwater light penetration showed a shift towards 540 nm in the coastal waters due to the combined effect of CDOM (~43 %), and detritus (~32 %) during the FIM and NEM. The effect of $b_b(\lambda)$ is low as compared to $a(\lambda)$ in the coastal waters, and hence the peak in $R_{rs}(\lambda)$ was observed at around 550 nm (Fig. 3.9a).

The observed results and statistical analyses support our hypothesis that the magnitude of CDOM absorption varies both spatially and temporally in the two estuaries and coastal waters of Goa.

3.6.8. CDOM mixing behavior

The mixing patterns of the Mandovi and Zuari estuaries varied seasonally, with a prominent non-conservative mixing behavior. A land-to-sea decreasing trend of CDOM was observed during all the seasons indicating a definite terrestrial influence. An apparent loss of CDOM was observed during the period of high freshwater inflow (majorly terrestrially derived) in the Zuari Estuary at very low salinity (Fig. 3.7b). The terrigenous and highly aromatic nature of DOM in this low salinity region was also supported by its typical optical properties with very low $S_{275\text{-}295}$ and S_R values (Figs. 3.4b and 3.5b). The scattering of particles given by the backscatter b_{bp} 700(m^{-1}) was higher during the SWM, indicating higher amounts of suspended sediments than those during the non-monsoon seasons. Hence, the loss of CDOM could be attributed to the adsorptive removal by suspended sediments and flocculation when the aromatic content and molecular weight of CDOM (S_R) was high (Fig. 3.5b) (Uher et al., 2001; Asmala et al., 2014). Wachenfeldt and Tranvik (2008) reported that allochthonous DOM (with the humic matter as a major constituent) is a precursor for flocculation in the water column of a Swedish boreal lake. The photobleaching of DOM might be insignificant during the SWM, as solar radiation was lowest due to the high cloud cover and high turbidity of the water column. In contrast, the Mandovi Estuary exhibited apparent additions of CDOM, even during the high-inflow period of the SWM (Fig. 3.7b). A higher number of tributaries join the Mandovi Estuary, and more CDOM could be exported from these tributaries and their watersheds. Different pools of CDOM were also evident from the a_g412 and $S_{275\text{-}295}$ relationship (Fig. 3.6b). In the Mandovi Estuary, removal due to flocculation seems to be insignificant in comparison to the additions of CDOM. During the FIM season, conservative behavior of CDOM was observed in the Zuari Estuary with a very good correlation with salinity ($r = -0.90$), while the Mandovi Estuary exhibited quasi-conservative mixing behavior with additions in the mid-stream region (Fig. 3.7c). This indicates that the terrigenous source of CDOM in the upstream is significantly diluted during its passage through the estuary during the FIM.

Apparent additions of CDOM were observed in both estuaries during the SIM and NEM seasons (Figs 3.7a and 3.7d), when freshwater inflow was insignificant. Similar results were found in previous studies of other estuarine and coastal waters (Doering et al., 1994; Rochelle-Newall and Fisher, 2002; Chen et al., 2015). This indicates that there are sources

of CDOM other than the inputs received upstream of the estuary. CDOM input from the watersheds was almost negligible during these seasons. *In-situ* production could be a source of CDOM, as indicated by the good correlation of CDOM and chlorophyll-*a* ($r > 0.9$) during the SIM and NEM seasons. The inverse relationship between a_g412 and $S_{275-295}$ observed in this study shows the influence of marine sources in the estuary (Figs 3.6a and 3.6d). The maximum deviation from the theoretical mixing line occurs in the mid-salinity areas, close to the urbanized regions. This region also contains large patches of mangroves and is prone to anthropogenic activities, such as pleasure cruises, shipbuilding, treated sewage discharge, and so on. The deviation from the mixing line is greater in the Mandovi Estuary than that in the Zuari. Furthermore, more anthropogenic activities occur in the Mandovi Estuary. Hence, our study clearly indicates the presence of a continuous source of CDOM in the mid-stream region of Mandovi Estuary, which was also evident from the values deviating from the a_g412 and $S_{275-295}$ relationship. This was more pronounced during the NEM in the Mandovi Estuary (Fig. 3.6d). In the coastal waters, most of the a_g412 values fell below the mixing line (Fig. 3.7), indicating the removal of CDOM, which can be attributed to photobleaching. This was also observed from the $S_{275-295}$ and S_R values which increased drastically in the coastal waters indicating the transformation of DOM by the process of photobleaching (Figs 3.4 and 3.5). The results obtained support our hypothesis of non-conservative mixing behavior in the estuarine waters.

3.7. Conclusion

In this study, the spatio-temporal variability of CDOM in the estuaries and adjoining coastal waters of Goa was explored. High CDOM was observed in the Mandovi and Zuari estuaries during the SIM and SWM seasons. *In-situ* production and inputs from mangroves and anthropogenic activities contributed to the high CDOM during the SIM season. Meanwhile, a high influx of terrestrial organic matter from the watersheds of the estuaries resulted in high CDOM during the SWM. The environmental forcing of the SWM plays an important role in regulating CDOM by controlling the inflow from the watersheds and the flushing rate in the estuaries. However, tidal circulation significantly controls the spatial distribution of CDOM during the non-monsoon seasons.

In the coastal waters, high CDOM was observed during the SWM followed by SIM and FIM seasons. Terrestrial organic matter from the riverine runoff is the major allochthonous

source during the SWM, while *Trichodesmium* bloom acts as a major autochthonous source of CDOM in the coastal waters during the SIM season. Photobleaching was found to be the dominant sink of CDOM during the non-monsoon season, resulting in deeper penetration of UV light in the coastal waters.

The photochemical transformation of DOM was also evident in the estuaries during the SIM season, which was enhanced by the longer residence time of water. However, CDOM removal by flocculation and adsorption at low salinities was observed in the estuaries during the SWM. The $S_{250\text{-}600}$, $S_{275\text{-}295}$, and S_R in these waters indicated the transformation of DOM during its passage from the upstream of the estuaries (high molecular weight with greater aromatic content) to the adjoining coastal waters (low molecular weight and low in aromatic content). Non-conservative mixing behavior of CDOM was observed in the waters of Goa during all seasons, with large additions in the mid-stream regions and removal by flocculation and adsorption at low salinities in the estuaries and by photobleaching in the coastal waters. SWM plays an important role in the CDOM bio-optical properties in these waters. Our results clearly showed the influence of rainfall and allochthonous input (through anthropogenic activities) in controlling the CDOM variability in the estuaries. The influence of CDOM in modulating the spectral quality of underwater light was also observed in the coastal and estuarine waters of Goa. The present study is important to understand the biogeochemical processes in these waters in addition to ocean color remote sensing applications.

Chapter 4

Optical properties of CDOM during phytoplankton blooms in the coastal waters of Goa

Optical properties of CDOM during phytoplankton blooms in the coastal waters of Goa

4.1. Introduction

Phytoplankton blooms are an important driver in maintaining the marine food web by supplying copious amounts of organic matter, thus playing a key role in the biogeochemical cycling of elements (Behrenfeld and Boss, 2014; Baetge et al., 2021). Autochthonous production arising from phytoplankton exudation, cell lysis, passive leakage, and sloppy feeding by grazers, etc. (Nagata, 2000; Van den Meersche et al., 2004) are the major contributors to the DOM pool in coastal waters. The accumulation of DOM during phytoplankton bloom has been reported in both field and laboratory experiments (Suksomjit et al., 2009; Zhang et al., 2009; Romera-Castillo et al., 2010).

Bloom-forming phytoplankton have been reported in the coastal waters of Goa (D'silva et al., 2012) among which *Trichodesmium*, a marine diazotrophic cyanobacteria prevalent during sping-inter monsoon (SIM), is repeatedly observed (Devassy et al., 1978; Desa et al., 2005; Parab et al., 2006, 2012; Basu et al., 2011; Ahmed et al., 2017). *Trichodesmium* bloom is known for its sporadic appearance in warm surface waters as yellow-brown slicks, commonly known as sea sawdust (Qasim, 1972; Capone et al., 1997). These blooms fix large amounts of atmospheric nitrogen into the photic zone and hence play a substantial role in the nitrogen cycle (Carpenter and Capone, 1992; Capone et al., 1997; Gandhi et al., 2011). *Trichodesmium* is also known to produce microcystin, a hepatotoxin (Klisch and Hader, 2008; Sivonen and Borner, 2008). In the SIM season the bloom of green *Noctiluca* was found to coincide with the *Trichodesmium* bloom in the coastal waters off Goa. Green *Noctiluca* are not known to produce organic toxins, but are still categorized as harmful due to their association with massive fish mortalities attributed to toxic levels of ammonia (Okaichi, 1976).

Extensive work on *Trichodesmium* had begun as early as the 1970s along the west coast of India. Devassy et al. (1978) studied *Trichodesmium's* occurrence in the coastal waters of Goa and the Arabian Sea (AS) along with other phytoplankton and nutrients. Apart from *in-situ* observations, detection of *Trichodesmium* blooms using ocean color sensors has also been undertaken in the AS by Desa et al. (2005). The relationship between halocarbons and phytoplankton pigments during a *Trichodesmium* bloom has been studied

earlier by Roy et al. (2011). Besides, the rates of primary productivity and nitrogen fixation during *Trichodesmium* blooms were estimated in the AS (Parab et al., 2012; Ahmed et al., 2017). However, these studies did not focus on the CDOM characteristics during the *Trichodesmium* bloom.

The *Trichodesmium* bloom builds up large pools of organic carbon and nitrogen in the coastal waters (Bar-Zeev et al., 2013). Monitoring these blooms will improve our understanding on the fate of biogeochemically important elements. Several bio-optical algorithms have been developed to detect *Trichodesmium* blooms from satellite sensors (Mckinna, 2015 and references therein). *In-situ* observations and monitoring will help fine-tune these algorithms for improvement and provide a platform for validating ocean color-derived variables. Ocean color is one of the crucial components of essential biodiversity variables under, class 'Species traits', to observe seasonal and inter-annual changes, including bloom timing and duration (Groom et al., 2019).

4.2. Aim of the study

Phytoplankton blooms account for a notable fraction of annual production in many marine and freshwater systems, and contribute to benthic and pelagic production, in turn regulating the biogeochemical cycles. Many studies point to the significant production of DOC during the phytoplankton bloom (Norrman et al., 1995; Wetz and Wheeler, 2007; Spilling et al., 2014). Many phytoplankton blooms have been reported along the west coast of India (D'Silva et al., 2012), of which *Trichodesmium* has often been reported since 1970. However, in recent years, green *Noctiluca* have also been observed in the waters of Goa. *Trichodesmium* plays a crucial role in global biogeochemical cycles by actively fixing atmospheric nitrogen (Capone et al., 1997). *Trichodesmium* has been distinguished as an important contributor of new nitrogen in tropical and sub-tropical waters (Karl et al., 1997; Capone et al., 2005). The occurrence of green *Noctiluca* blooms in Indian waters has also been reported following the enhanced phytoplankton production due to upwelling or winter convective mixing (Sahayak et al., 2005; Padmakumar et al., 2010). Green *Noctiluca*, a bioluminescent heterotrophic dinoflagellate bloom, harbors a photosynthetic symbiont — *Protoeuglena noctilucae* (Wang et al., 2016). Generally *Noctiluca* is heterotrophic, whereas the green *Noctiluca* from the Arabian Sea is reported to be a mixotroph (Goes and Gomes, 2016) since it can sustain itself either through carbon fixation by its green autotrophic endosymbiont (*Protoeuglena noctilucae*) or via ingestion

of exogenous prey (heterotrophic). To understand the CDOM production during phytoplankton blooms in the coastal waters of Goa, the following specific objectives were proposed in this study:

- Demonstrate the spectral and fluorescent characteristics of CDOM during *Trichodesmium* blooms along the coastal waters of Goa
- Understand the CDOM production/ degradation based on experiments using bloom samples collected from the coastal AS.

4.3. Methodology

4.3.1. Water column sampling

The coastal waters of Goa were monitored at regular stations during 2014 to 2018, but the focus of this study was to understand the CDOM characteristics during *Trichodesmium* blooms, which are usually observed in these waters during SIM. Measurements were carried out during April - May in the coastal waters of Goa (Fig. 4.1) with the help of a fishing trawler. *Trichodesmium* blooms under favorable environmental conditions form surface mats, which is visible to the naked eye (Fig. 4.2). The occurrence of the surface bloom was sporadic, and the presence of surface mats was designated as bloom stations, while the stations where such aggregations were absent are referred to as non-bloom stations. Table 4.1 provides the details of sampling along with the stages of bloom. A bloom sample from the sea surface was collected using a bucket. Seawater samples were collected using Niskin sampler (at discrete depths) and were filtered and analyzed for CDOM, phytoplankton pigments, and absorption by phytoplankton.

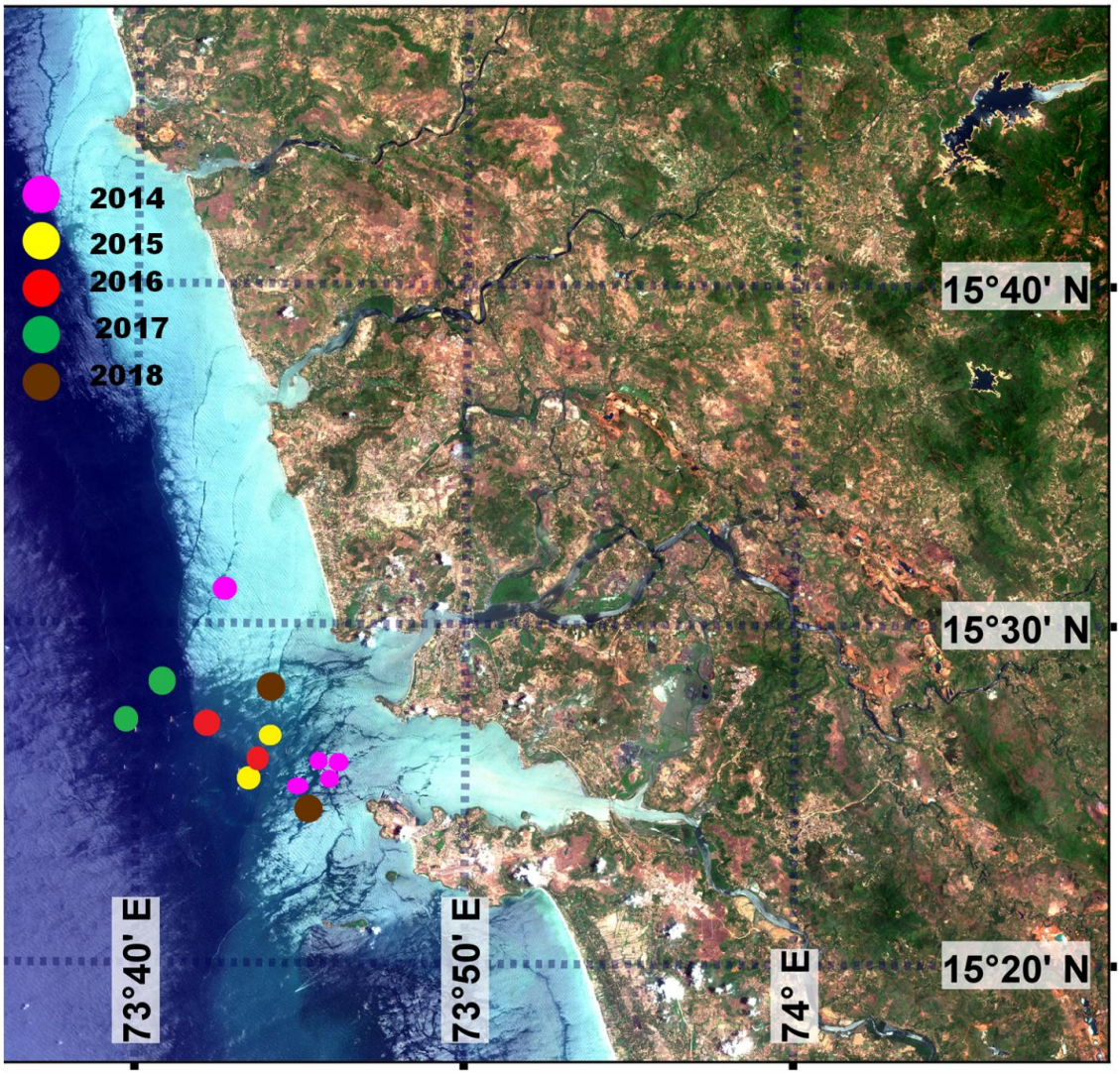

Figure 4.1: The Sentinel-2 satellite image of the study area indicating the sampling stations during the SIM of 2014-2018,where *Trichodesmium* blooms were observed in the coastal waters of Goa.

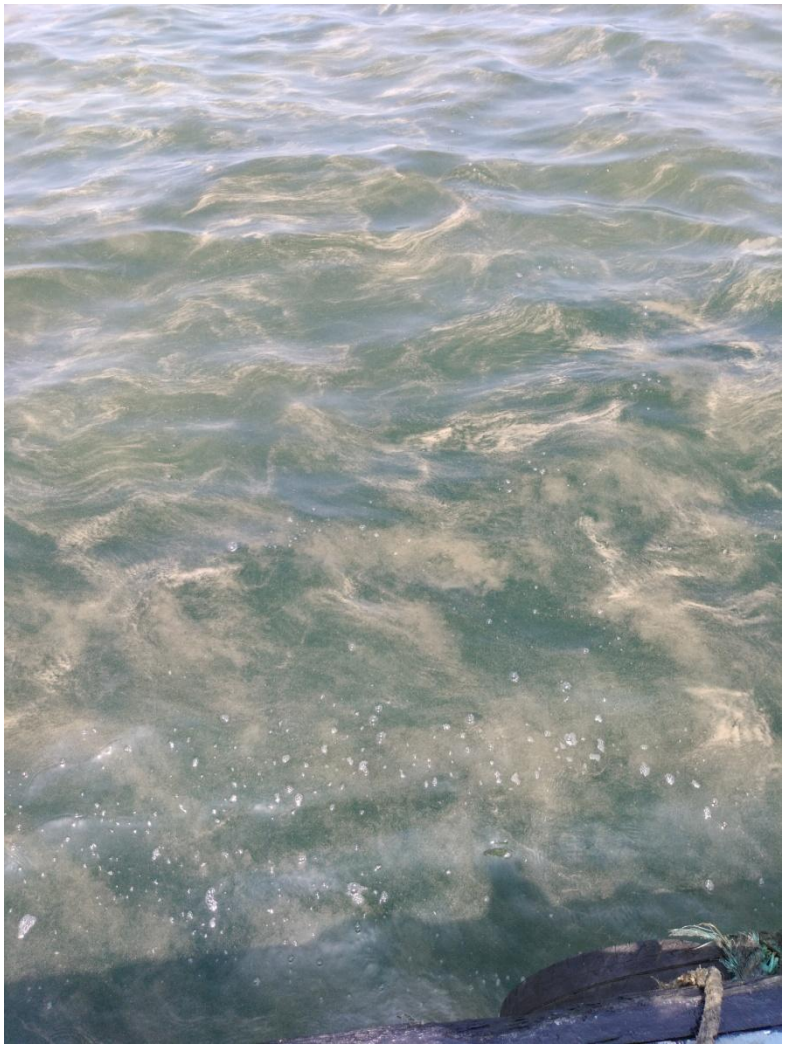

Figure 4.2: An image of the *Trichodesmium* bloom observed in the coastal waters during the sampling.

Table 4.1: Biological and chemical parameters observed at the bloom and reference stations during 2014-2018. Only surface samples are presented in the table.

Date	Lat °N/ Long °E	Station	*Tricho-desmium* counts (trichomes/l)	Chl *a* (µg/l)	Pheopigments (µg/l)	Zeaxanthin (µg/l)	Peaks identified in CDOM	a_g412 (m^{-1})	Probable stage of bloom
25th April 2014	15.43187/ 73.76219	A	111840	70.499	10.734	-	497,542, UV region	5.772	Senescence phase
25th April 2014	15.43083/ 73.76558	B	80000	1935	1188.2	-	495,547,614, UV region	8.180	Senescence phase
25th April 2014	15.42662/ 73.76407	C	87840	3359	10138	-	497,545,614 ,UV region	30.939	Senescence phase
25th April 2014	15.42043/ 73.75071	D	176000	3089	214.2	-	497, 545, 614, UV region	8.891	Senescence phase
25th April 2014	15.42896/ 73.74368	E	-	0.711	0.415	-	326, 360	0.175	Non-bloom station
30th April 2014	15.51970/ 73.70972	3	88000	247.197	99.546	-	330,364	1.354	Growth phase
30th April 2014	15.50991/ 73.65008	4	4400	0.308	0.0534	-	No peaks	0.092	Non-bloom station
18th May	15.44653/ 73.73358	4	148	2.63	-	0.072	314	0.145	Growth phase

2015									
18th May 2015	15.42807/ 73.72401	A	892361	3533	374.22	677.7	265,329,366 ,495,547, 614	6.381	Senescence phase
18th May 2015	15.47918/ 73.79319	1	-	3.9	-	-	No peaks	0.193	Non-bloom station
31st May 2016	15.43245/ 73.72644	A	1710000	596.52	-	17.19 8	314,362,498 ,548,618	22.98 3	Senescence phase
31st May 2016	15.45422/ 73.7007	B	-	2.26		0.706	324	0.092	Growth phase
9th May 2017	15.47453/ 73.67883	A	-	3.87	-	-	330, 360	1.466	Growth phase
9th May 2017	15.45409/ 73.66177	B	-	39.64	-	-	330,364,497	7.648	Senescence phase
9th May 2017	15.45968/ 73.71832	C	-	0.17	-	-	No peaks	0.169	Non-bloom station
8th May 2018	15.46994/ 73.73687	A	-	44.43	-	-	329,363	4.328	Growth phase
8th May 2018	15.409016 /73.75335	B	19,200	29.58	-	-	360	9.087	Growth phase
8th May 2018	15.37909/ 73.76486	C	-	0.27	-	-	No peaks	0.124	Non-bloom station

4.3.2. Spectral CDOM absorption

For CDOM analysis, the water sample was filtered through a 0.2μm nucleopore membrane filter and stored in an amber color glass bottle at 4˚C until analysis in the laboratory (Mitchell et al., 2000; Tilestone et al., 2002). Absorbance measurements were carried out after bringing the refrigerated samples to room temperature (Zaneveld and Pegau, 1993), and all samples were analyzed on the same day of collection. Spectral characteristics of CDOM were determined on a dual beam UV2600 spectrophotometer (Shimadzu) using a cuvette of 10 cm path length. The bloom samples which showed saturation during analysis using a 10 cm cuvette were reanalysed using 1cm cuvettes. The spectral CDOM absorption $a_g(\lambda)$ (m^{-1}) was estimated using the following equation from the corrected absorbance data.

$$a_g(\lambda) = \frac{2.303 * A(\lambda)}{l}$$

Where A(λ) is the absorbance at a specific wavelength and *l* is the pathlength of cuvette (m).

4.3.3. Fluorescence measurements of CDOM

The excitation emission matrix of CDOM was measured using a spectrofluorometer (Cary Elipse, Varian) with a xenon lamp. The scanning range used for excitation was 200 to 450 nm, whereas 250 to 600 nm was used for emission with a slit width of 5 nm each. Readings were taken at 5 nm intervals for excitation and 2 nm intervals for emission, using a scanning speed of 9600 nm min^{-1}. The EEMs of a Milli Q water (blank) was subtracted to eliminate the Raman scatter peaks of water (McKnight et al., 2001; Stedmon et al., 2003; Zhang et al., 2010, 2011). The fluorescence estimations were corrected for excitation energy and emission detector response using the manufacturer's correction functions. The bloom samples were highly concentrated and hence the samples were diluted using Milli Q water. The absorbance spectrum of samples was used to calculate a matrix of correction factors corresponding to each wavelength pair in the EEM to correct for inner filter effect correction. Finally, the area under the Milli Q water Raman peak (λ_{ex} = 350 nm, λ_{em} = 365 to 450 nm) was used to normalize the fluorescence intensities in all sample EEMs (Lawaetz and Stedmon, 2009).

PARAFAC was applied to a dataset of 85 EEMs using MATLAB software (2017), including the DrEEM toolbox 0.20 (Murphy et al., 2013). The model was restricted to the excitation wavelength >240 nm and emission wavelength < 590 nm to avoid noise. The

model was run with non-negativity constraints. Validation was performed by split-half analysis and analysis of residuals and loadings. Two samples with high leverages were excluded from the model.

4.3.4. Analyses of chlorophyll-a, phytoplankton pigments and phytoplankton absorption

For chlorophyll-*a* estimation, 0.05 to 1 L of seawater was filtered on a GF/F (0.7 µm) filter depending on the bloom density. The filter was later extracted in 90 % acetone overnight at 4˚C and chlorophyll-*a* concentration was measured on a fluorometer (Turner Trilogy). Pheopigments were estimated by measuring the extract's fluorescence before and after acidification with 1.2M HCl following the JGOFs protocol (Knap et al., 1996). High performance liquid chromatography (HPLC) was used to determine the phytoplankton pigments in the water samples. Water samples were filtered on GF/F filters and were frozen at -20ºC until analysis. The filters were extracted in 3 ml of 100% HPLC grade acetone (Merck) for 24 hrs at -20˚C. Water samples were also analysed for phytoplankton pigment absorption by quantitative filter technique using an integrating sphere attached to a Shimadzu UV2600 spectrophotometer. Water samples preserved with 1% lugol's iodine solution were used for phytoplankton enumeration and identified using the standard taxonomic key (Tomas and Haste, 1997). The details of methodology used is provided in chapter 2.

4.3.5. CDOM photodegradation- Experimental setup

In order to understand the production/degradation of CDOM during *Trichodesmium* bloom, two photodegradation experiments were performed under natural sunlight, one with *Trichodesmium* cells and on another occasion with 0.7 micron (GF/F) filtered samples. In the first experiment, surface water from the *Trichodesmium* bloom site was directly incubated (without filtration) in a glass flask, kept in a water bath under natural solar radiation, on the terrace of the CSIR-National Institute of Oceanography (NIO), Goa. During the night, samples were stored in the dark at room temperature. This experiment was carried out for a period of 11 days, and the sample was withdrawn for CDOM analysis at regular intervals. The same water sample, incubated in the dark in a glass flask and covered with multiple layers of aluminium foil, was considered as the 'control'.

In the second experiment, the surface sample of *Trichodesmium* bloom was filtered through GF/F filter, and the filtrate was immediately transferred into a number of 40 ml

glass tubes without headspace. These glass tubes were then placed in a shallow plastic tray containing water and were incubated on the terrace of CSIR-NIO, Goa. The daily average exposure to solar radiation was ~10 hours, and the samples were incubated for 12 days (one tube was analyzed on a daily basis). Since the cell density of *Trichodesmium* was high, it was difficult to filter a large volume of water through a 0.2 micron membrane filter. Hence we used GF/F (0.7 micron) filtered water for the degradation experiment (Reche et al., 1999; Gueguen et al., 2014). Since the filtration was done through 0.7µm, the filtrate might contain picoplankton and bacteria. To compare the difference between CDOM absorption on a GF/F and 0.2 micron (nucleopore polycarbonate membrane) filtered samples, we used both as 'controls'. This would also help to understand the influence of bacteria on the modification of DOM. The 'controls' were wrapped with multiple layers of aluminium foil and incubated in the same water bath until the end of the experiment. The samples were monitored for changes in CDOM absorption and fluorescence on a daily basis. Since the glass tube was used for incubation, it would allow only UV A and PAR light (Reche et al., 1998) and might result in some under-estimation. However, these experiments will help to understand the influence of solar light on CDOM production and degradation during blooms.

4.4. Results

4.4.1. *Environmental conditions during the Trichodesmium bloom*

Trichodesmium blooms were observed as extensive surface patches of discolored water during April and May (2014-2018) in the coastal waters of Goa (Fig. 4.1 and 4.2). The sea surface temperature (SST) ranged between 30.8 and 31.8˚C, and the salinity varied from 35 - 36. The light penetration in the water column was found to be high, with a secchi depth of ~ 6 m. The chlorophyll-*a* at the surface was found to be very high (30 - 3533 µg/l) at the bloom stations, while it was very low (0.168 – 3.9 µg/l) at the non-bloom stations. The concentration of pheopigments was also found to be very high (10.73 – 1188.2 mgm^{-3}) at the bloom stations during 2014-15 (Table 4.1); however, these were not measured in the successive years. Bloom samples during 2015-16 were analyzed by HPLC to determine the phytoplankton pigment concentration. Phytoplankton pigments are known as diagnostic markers of various groups. The presence of zeaxanthin pigment is indicative of *Trichodesmium* (cyanobacteria), while fucoxanthin generally represents the diatoms. A very high concentration of zeaxanthin, total carotene and chlorophyll-*a* were observed for

the bloom samples, whereas fucoxanthin was the dominant pigment at the non-bloom stations. Zeaxanthin concentration was found to be very high (17 - 677.7 µg/l) at the bloom stations, while its concentration was very low (0.2 - 0.8 µg/l) at the non-bloom stations.

4.4.2. Spectral characteristics of the absorption during the Trichodesmium blooms

The surface water collected during the bloom had a natural light pink color. CDOM absorption at a reference wavelength (a_g412) was found to be very high (1.35 - 32.23 m^{-1}) during the *Trichodesmium* blooms compared to the samples from non-bloom stations (0.1 - 0.2 m^{-1}). Unlike the usual exponential decreasing behavior of CDOM, distinct features were observed in the absorption spectra (both in the UV and visible range) for the bloom samples. The peaks in the visible range were more prominent while using a 10 cm path length cuvette for measurements (Fig. 4.3a). The spectra of CDOM absorption during bloom were decomposed, assuming Gaussian distribution (Table 4.1). A very dominant peak was also noticed in the UV range, which was saturated when analyzed using 10 cm path length cuvette. When analyzed on a 1 cm cuvette, the same sample showed the peak in the UV range at 330 nm with a shoulder at 360 nm (Fig. 4.3b) due to mycosporine-like amino acids (MAA). The peaks in the visible wavelength range due to phycobiliprotein pigments were 495 - 497 nm, 542 - 547 nm, and 614 - 618 nm corresponding to absorption by phycourobilin (PUB), phycoerythrobilin (PEB) and, phycocyanin (PC) respectively (Fig. 4.3a). During our field measurements in 2018, a mixed bloom of *Noctiluca* (10,504 cells/l) and *Trichodesmium* (19,200 trichomes/l) was observed at one of the stations (station B). The spectral CDOM absorption of this mixed bloom differed from the *Trichodesmium* absorption. The notable difference during 2018 when *Trichodesmium* was dominant showed a peak at ~330 nm with a shoulder at ~360 nm and a peak at ~495 nm. In contrast, in the case of a mixed bloom of *Trichodesmium* and *Noctiluca,* the absorption peak in the UV range was at 360 nm, and the peak at 495 nm was absent. In 2016 during the *Trichodesmium* bloom, the UV range peak was observed at 314 nm and shoulder at 362 nm (Table 4.1). The phytoplankton absorption spectra during the *Trichodesmium* blooms also showed peaks at similar wavelengths (330, 360, 490, 565 nm) as in the CDOM absorption, in addition to the usual peaks in the phytoplankton absorption spectra (440, 676 nm) but were of lower magnitude as compared to the CDOM spectra (Fig. 4.4). Here we attempted to differentiate the stages of bloom into the growth and senescence phase. During the growth phase the CDOM absorption is low, there is no leaching of

phycobiliprotein pigments into the water, and the corresponding chlorophyll-*a* is also low. On the other hand, the senescence phase is marked by very high CDOM absorption, leaching of phycobiliprotein pigments, and high chlorophyll-*a*. CDOM production (a_g412) during the bloom was observed to be the highest during 2014 (30.939 m^{-1}) and in 2016 (22.983 m^{-1}), followed by other years during the study. Absorption due to phycobiliproteins (a_g547) in the CDOM spectra was also high during 2014 (74.816 m^{-1}) and 2016 (17.381 m^{-1}). It also coincided with high chlorophyll-*a* (>500 µg/l) and pheopigments during these years (Table 4.1). This suggests that the bloom was in the senescence phase. Comparatively low CDOM (< 9 m^{-1}) and chlorophyll-*a* (< 45 mgm^{-3}) were observed during 2017 (station A) and 2018 at the bloom sites. CDOM absorption peaks due to phycobiliproteins were not observed during these years. This suggests that the bloom was in the growing stage. However, the peaks due to MAA were prominent in the CDOM absorption of bloom samples during all the years. The CDOM spectra at the non-bloom stations and at the subsurface waters of bloom stations had no peaks and decreased exponentially as expected (Fig. 4.3c).

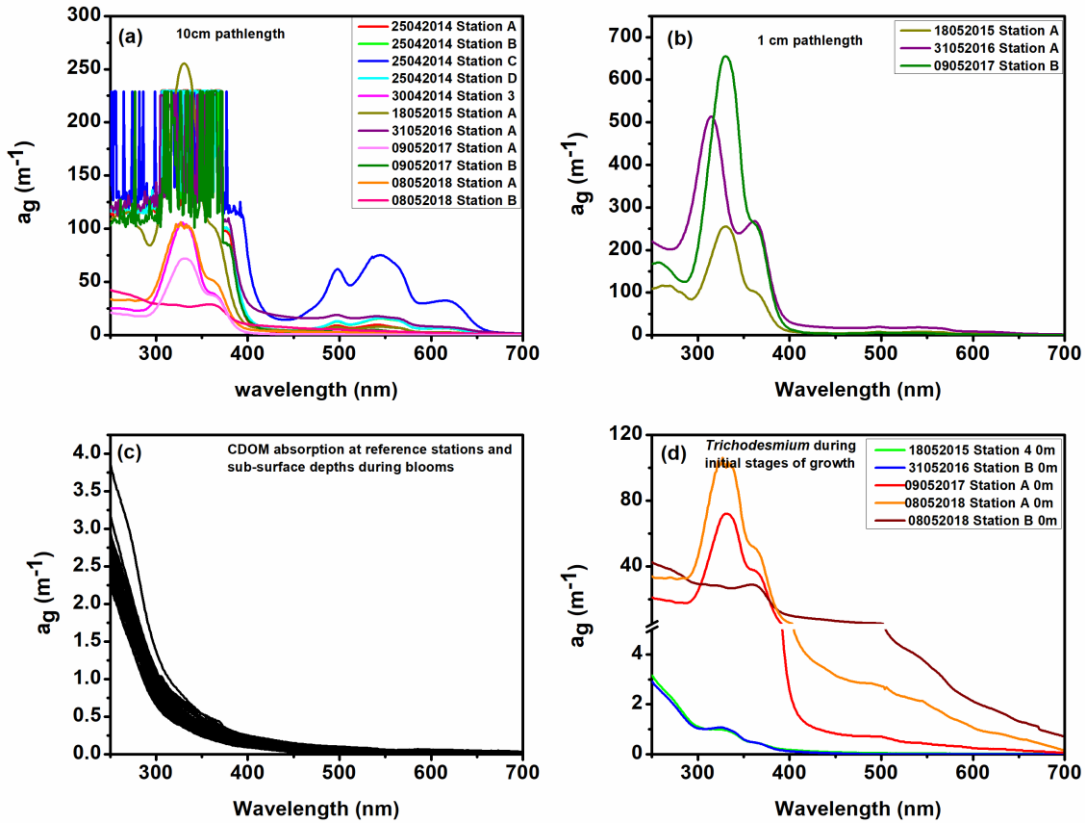

Figure 4.3: Spectral absorption by CDOM (a_g m^{-1}) during *Trichodesmium* blooms (2014 – 2018). (a) CDOM absorption measured using a 10 cm cell (b) using 1cm cell (c)

CDOM absorption at non-bloom stations and sub-surface depths (d) CDOM absorption during initial stages of growth during *Trichodesmium* bloom (please note that there is a break in the Y-axis).

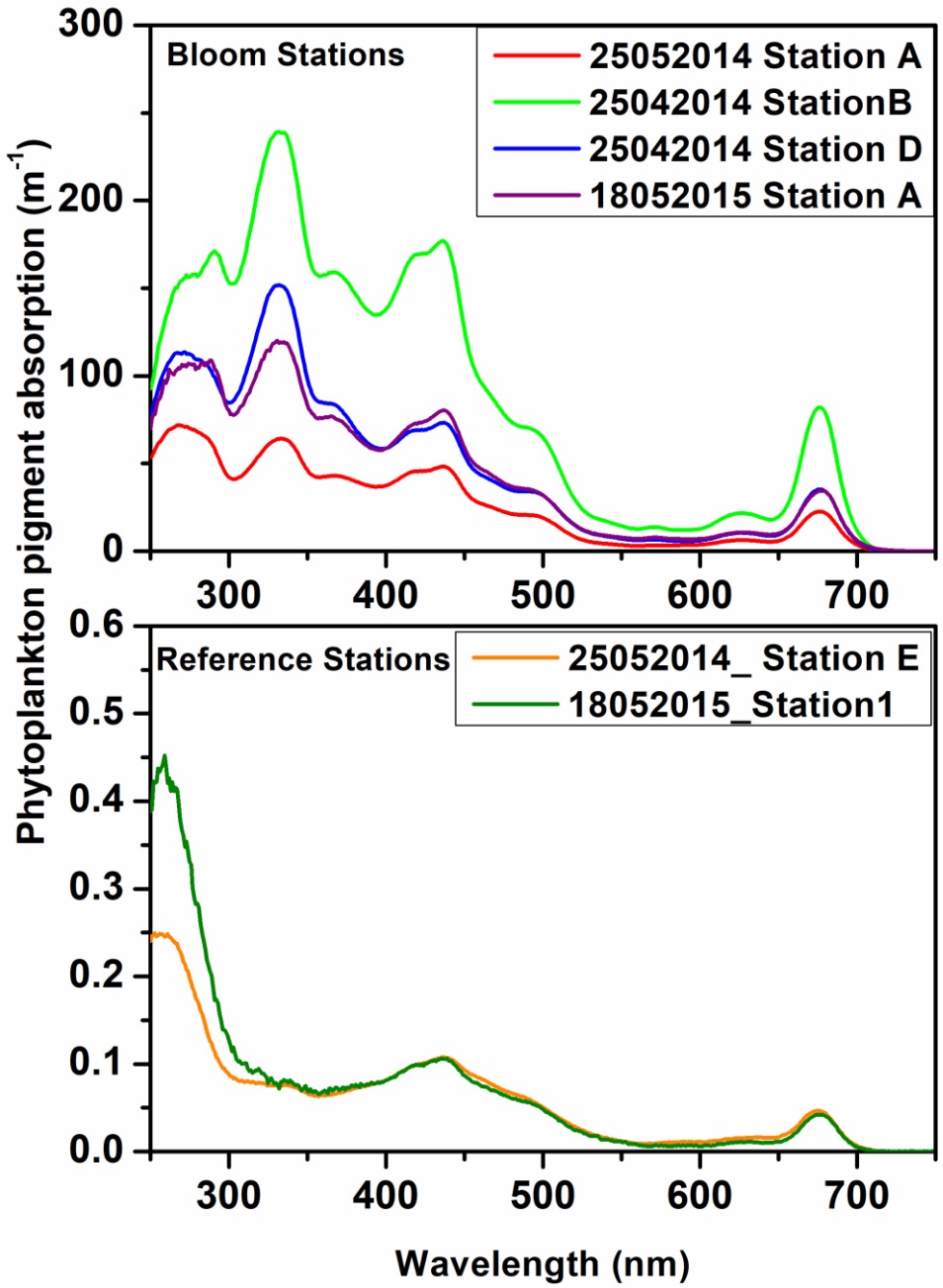

Figure 4.4: Spectral phytoplankton pigment absorption (a_{ph} m^{-1}) during *Trichodesmium* blooms (top), and at non-bloom stations (Reference station; bottom).

4.4.3. Fluorescence characteristics of Trichodesmium blooms

In all the surface samples collected during the bloom EEMs had fluorescence peaks, 1 in the protein-like and 2 in the humic-like regions, as previously identified using the traditional peak picking method (Coble, 1996). In the protein-like region, peak 1 (T) corresponds to tryptophan (Ex/Em: 270 - 280/ 320 - 340 nm) whereas in the humic-like region peak 2 (A) corresponds to Ex/Em of 250 - 260/ 440 - 480 nm and peak 3 (C1) corresponds to 360 - 370/460 nm (Fig. 4.5).

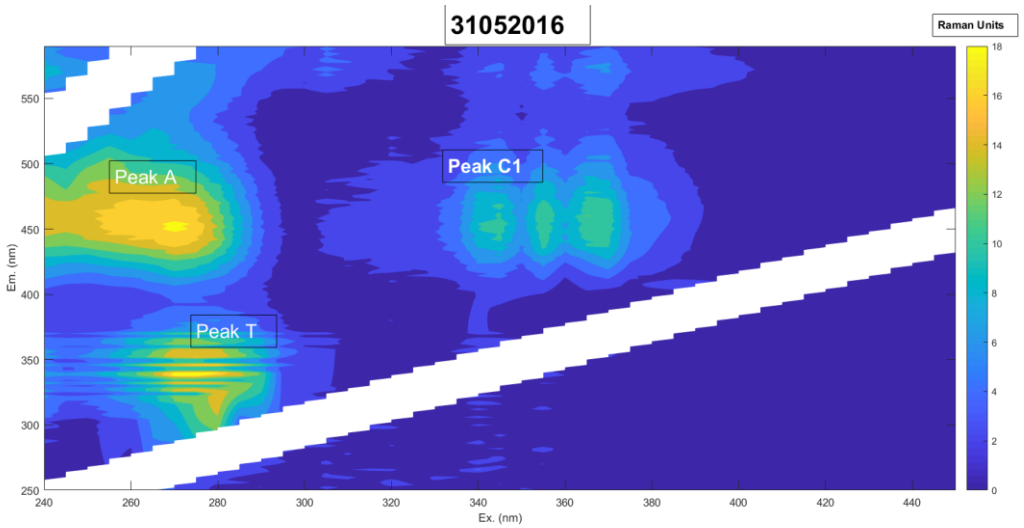

Figure 4.5: CDOM fluorescence EEM and peaks identified using peak picking during *Trichodesmium* bloom on 31st May 2016 at station A.

The PARAFAC model identified three components in the samples during *Trichodesmium* bloom and also in *Trichodesmium* degradation experiments (Fig. 4.6). Table 4.2 shows the fluorescence properties, potential source of each component, and comparison with previous studies. The component 1 (C1) had two excitations and one emission peak (Ex/Em: 260, 360/460), and corresponds to a humic-like fluorophore, peak C (Coble, 1996; Yamashita et al., 2010; Stedmon et al., 2011). A recent study by Zhao et al. (2017), showed that picocyanobacteria produce a fluorescent component spectrally similar to C1 in our study, and attributed it to the degradation product of tetrapyrroles. The component 2 (C2) resembled protein-like amino acid, tryptophan, (Ex/Em: 275/315) reflecting recent biological production; whereas component 3 (C3) was humic-like (Ex/Em: 305/420) with a resemblance to the terrestrial origin.

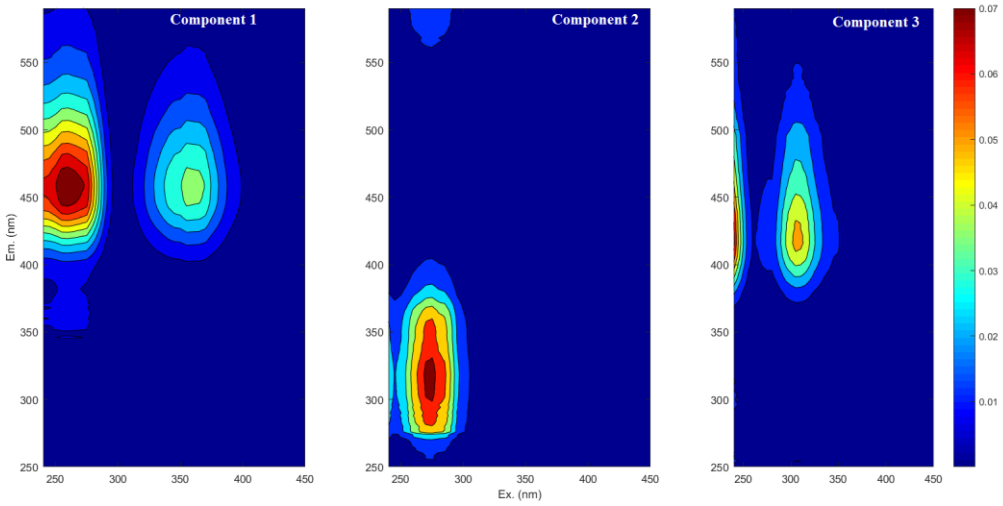

Figure 4.6: Components of CDOM fluorescence (Raman units) identified using PARAFAC.

Table 4.2: CDOM spectral fluorescence characteristics of excitation and emission maxima identified by PARAFAC and their comparison with previous studies.

Component	**Ex_{max}/Em_{max}**	**Comparison with previous studies**	**Possible source**
Component 1 (C1)	260 (360)/460	255(360)/450[a,b]	Humic-like, Peak C degradation product of tetrapyrrole
Component 2 (C2)	275/315	275/306(338)[c] 270-280/320-350[d]	Protein-like Tryptophan
Component 3 (C3)	<250(305)/420	290-310/370-420[e,f]	Marine humic-like substance (biological degradation) Peak M

[a] Stedmon et al., (2011).

[b] Zhao et al., (2017).

[c] Stedmon and Markager, (2005)

[d] Yamashita and Tanoue, (2003)

[e] Coble, (1996)

[f] Coble et al., (1998)

4.4.4. Degradation of Trichodesmium blooms

To understand the production/degradation of phytoplankton-derived autochthonous CDOM, surface samples of *Trichodesmium* bloom were exposed to natural solar radiation without filtration. The absorption of CDOM was documented at three wavelengths (330, 412 and 547 nm) (Fig. 4.7). In addition to 412 nm (the reference wavelength normally used to study the CDOM absorption), the absorption at 330 and 547 nm were chosen as peaks were observed at these wavelengths during the bloom period. The highest absorption in CDOM was observed due to MAA, which has increased almost two fold (781.04m^{-1}) from the initial reading (345.54 m^{-1}) during the first 2 days of the experiment. Continued exposure to solar radiation resulted in a decrease in CDOM absorption in the UV region from the initial value, with a shift in λ_{max} to 300 nm and a shoulder at 350 nm during the seventh day of the experiment (Fig. 4.7a). The peaks due to phycobiliproteins in CDOM spectra disappeared within two days of solar light exposure (Fig. 4.7b). CDOM absorption in the visible region of 400 - 500 nm showed a decrease in absorption during the initial two days, followed by a gradual increase from the 4^{th} to the 11^{th} day (Fig. 4.7d). The absorption beyond 500 nm showed a gradual decline throughout the experiment. The peak corresponding to MAA was present until the end of the experiment, while the peaks in the visible range disappeared immediately.

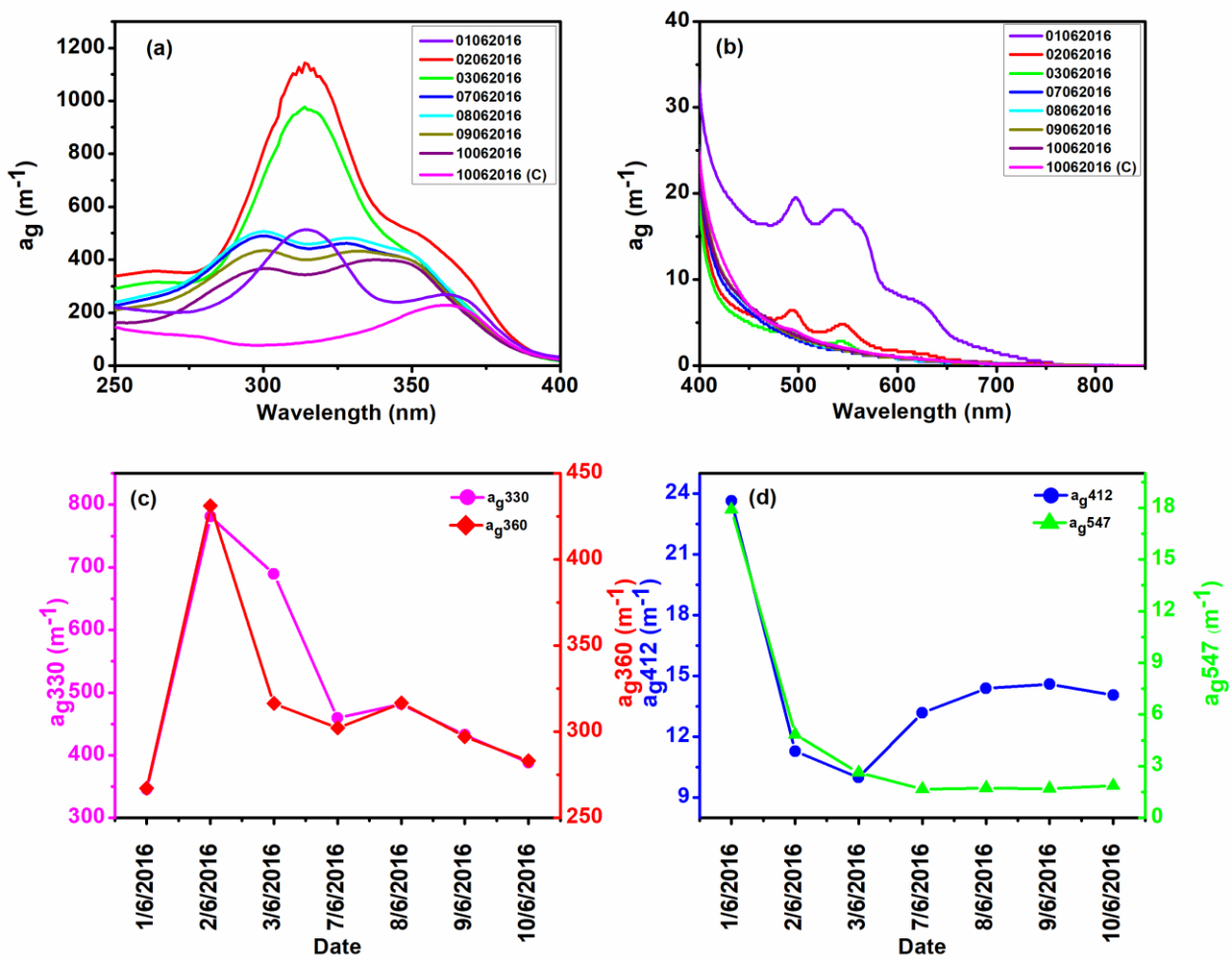

Figure 4.7: CDOM absorption during the photodegradation experiment carried out in 2016 (1-10 June). (a) Changes in CDOM spectra over a period of 10 days in the UV range; (b) in the visible range; (c) Changes in CDOM absorption at the reference wavelength a_g330 (m^{-1}) and a_g360 (m^{-1}); (d) at the reference wavelength a_g412 (m^{-1}) and a_g547 (m^{-1}).

The 'control', which had the same bloom sample but which was incubated in the dark, exhibited a decrease in CDOM absorption (a_g330 decreased from the initial 345.54 to 305.57 m^{-1}) and a shift in the peak due to MAA (λ_{max} to ~300 nm) after one day of incubation (Fig. 4.8). The shoulder due to MAA (λ_{max} to ~360 nm) was intact but showed an increase in absorption from 267.2 m^{-1} (initial) to 368.6 m^{-1} on the second day of the experiment (Fig. 4.8). The dissociated peak due to MAA (300 nm) disappeared after 7 days of dark incubation, while the shoulder still persisted till the end of the experiment. A small decrease in absorption (360 nm, 228 m^{-1}) at the shoulder region from the initial was observed at the end of the experiment on the 11th day. CDOM absorption decreased in the visible region from the initial value till the end of the experiment. The peaks due to

phycobiliproteins were evident in the 'control' for a longer period, as compared to the flask exposed to light, and disappeared towards the end of the experiment.

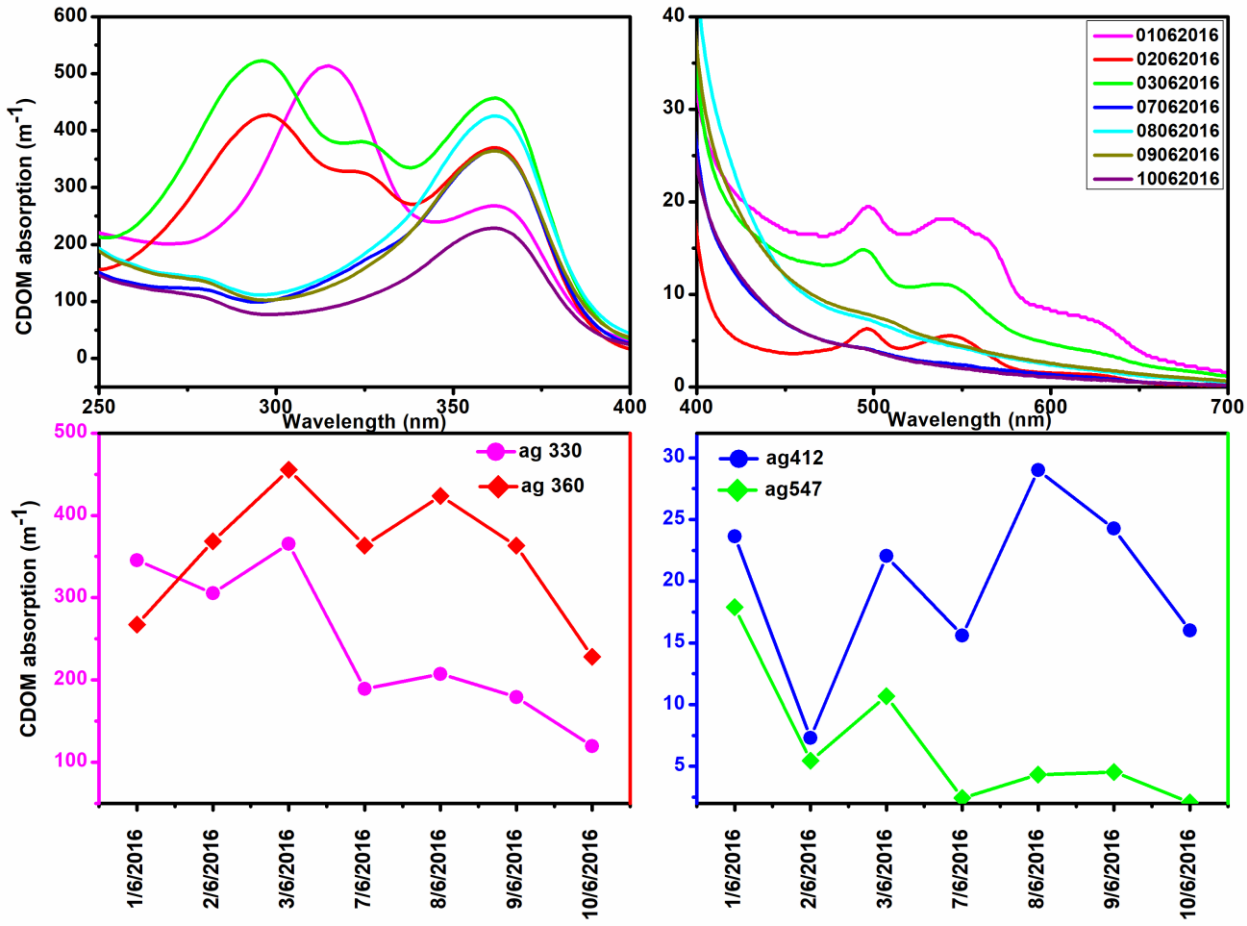

Figure 4.8: CDOM absorption in the 'control' (incubated in the dark) during the photodegradation experiment carried out in 2016 (1-10 June). (a) Changes in CDOM spectra over a period of 10 days in the UV range; (b) in the visible range; (c) Changes in CDOM absorption at the reference wavelength a_g330 (m^{-1}) and a_g360 (m^{-1}); (d) at the reference wavelength a_g412 (m^{-1}) and a_g547 (m^{-1}).

Another experiment was carried out in 2018 to understand the fate of CDOM produced during blooms. Surface water samples from the *Trichodesmium* bloom station were filtered through 0.7µm, and the filtrate was exposed to natural solar radiation. The CDOM produced during the *Trichodesmium* bloom decreased gradually over 13 days (Fig. 4.9). The peak due to MAA (λ_{max} 330) disappeared, while the shoulder (λ_{max} 360) was still evident after a day of solar light exposure (Fig. 4.9b). Subsequently, the CDOM absorption in the UV region decreased exponentially over time, whereas a rapid and faster decrease was observed in the 400 - 500 nm region (a_g412). A steady decline was observed in the

visible region of 500 - 600 nm (a_g547) (Fig. 4.9c and 4.9d). Although the 0.7 micron filtered 'control' showed higher absorption than the 0.2 micron filtered 'control', the spectral shape was comparable (Fig. 4.9a). Both these controls did not show much change in the visible region of CDOM absorption. The peak due to MAA (at 330 nm) had disappeared in both the controls, whereas the peak at 360 nm was intact, however with a small decrease from the initial value towards the end of the experiment (Fig. 4.9a).

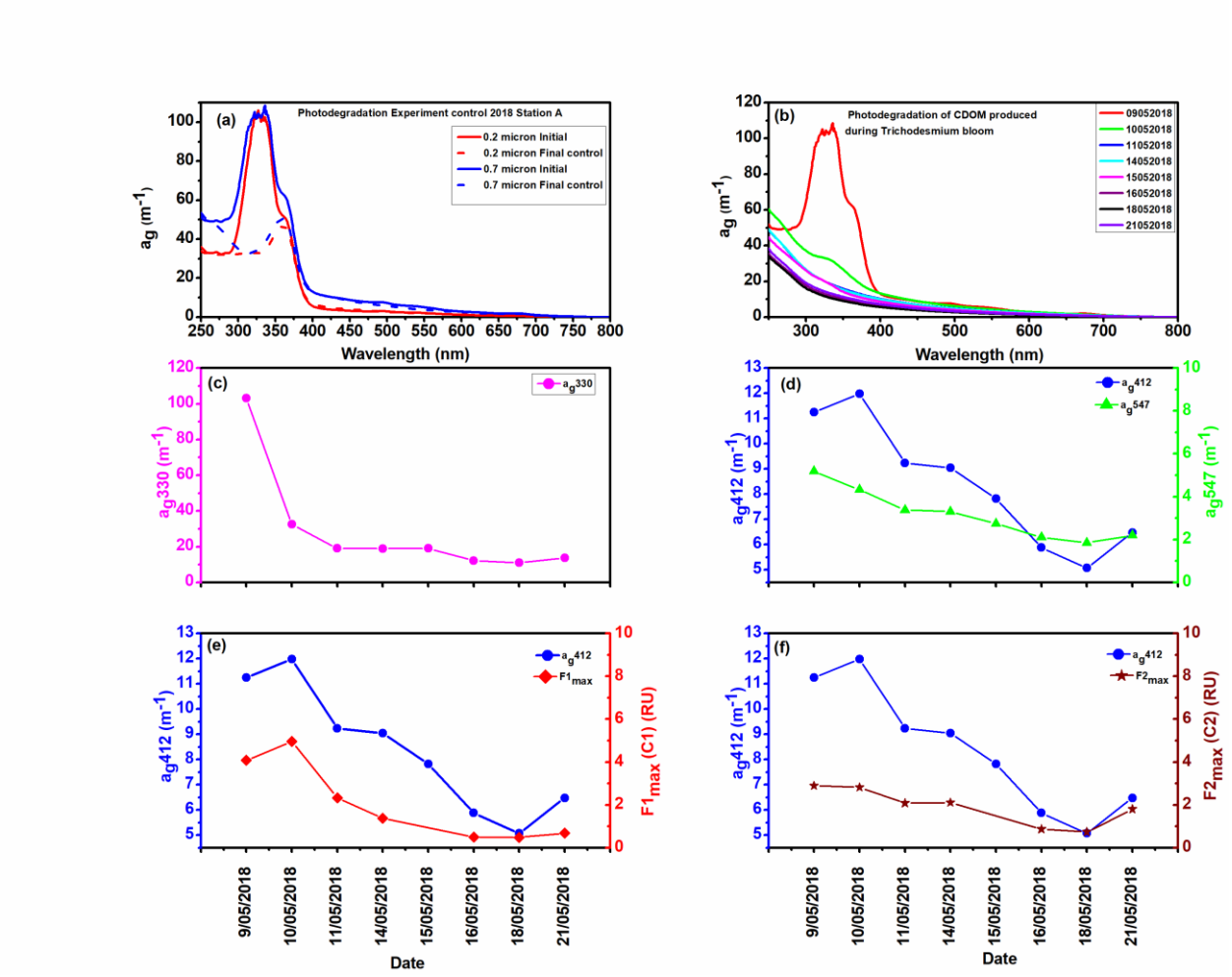

Figure 4.9: CDOM absorption (0.7 micron filtered) during the photodegradation experiment carried out in 2018 (9 - 21 May). (a) Spectral profile of CDOM absorption for 0.2 and 0.7 micron filtered 'controls'; (b) Changes in CDOM spectra over a period of 12 days; (c) Changes in CDOM absorption at the reference wavelength a_g330 (m^{-1}); (d) at the reference wavelength a_g412 (m^{-1}) and a_g547 (m^{-1}); (e) Comparison of a_g412 (m^{-1}) and $F1_{max}$ (PARAFAC); (f) Comparison of a_g412 (m^{-1}) and $F2_{max}$ (PARAFAC).

4.5. Discussion

Trichodesmium blooms occur in the coastal waters of Goa during SIM when the solar insolation is the highest (average PAR ~528.46 Wm^{-2}) over this region (Suresh et al., 1996). The coastal waters of Goa showed oligotrophic conditions during this time, which also experience high SST and salinity. The chlorophyll-*a* concentrations at the bloom sites were found to be very high, however, with a large inter-annual variability based on the intensity of the bloom. Such high concentrations of chlorophyll-*a* in these waters during *Trichodesmium* blooms were earleir reported by Parab and Matondkar, (2012). These blooms have been reported in the northern Indian Ocean since the 1970s and were attributed to the highly stratified waters with nitrogen limitation, and calm water conditions favoring the formation of surface mats during the SIM and early SWM (Qasim, 1972, Devassy, 1978, Capone et al., 1997; Subramaniam et al., 1999; Jyothibabu et al., 2003, Parab et al., 2006; D'Silva et al., 2012). A recent study by Jyothibabu et al. (2017) showed that warm core eddies favor the formation of *Trichodesmium* blooms. It has been ascertained that phosphorus and iron are responsible for restricting the growth and N_2 fixation of most of the marine nitrogen-fixers (Deutsch et al., 2001, 2007; Webb et al., 2001; Kustka et al., 2003; Shi et al., 2007; Whittaker et al., 2011). Various mechanisms of nutrient scavenging by *Trichodesmium* are detailed in Bergman et al. (2013). The Asian continent, with major deserts in the Middle East, and Central and East Asia, is the world's second largest dust source. The mineral dust rich in iron seems to be transported to the west coast of India following the dust storms in the Middle East and Sahara during spring and summer seasons (Mahowald et al., 2005 and the references therein; Tanaka and Chiba, 2006). Recently, a study by Basu et al. (2019) has shown that *Trichodesmium* and associated bacteria have mutualistic interactions for the utilization of iron from dust, where bacteria promote dust dissolution by producing Fe-complexing molecules (siderophores) and hence provide physical settings for dissolution and uptake. This could be another reason for the occurrence of *Trichodesmium* blooms during the SIM in the Arabian Sea.

4.5.1. Optical properties of CDOM under bloom conditions

Trichodesmium blooms were observed as surface mats in the present study. This stage of bloom has been previously reported as collapsing/decaying phase of the bloom, and therefore consists of only a few viable trichomes (Chen et al., 1996; Bell et al., 2005; Jyothibabu et al., 2017). The data presented here is collected when surface mats of

Trichodesmium were observed. The absorption by CDOM during the bloom was found to be characteristically different, and the spectrum deviated from normal exponential behavior in both the UV and visible regions (Figs 4.3a and 4.3c). The extremely high CDOM absorption observed in the present study may be due to the collection of water samples using a bucket, which led to the aggregation of *Trichodesmium* cells. A prominent absorption in the UV region of the spectra peaked at 330 nm with a shoulder at 360 nm ($a_g330 \sim 600\ m^{-1}$) could be due to MAAs, asterina 330 (λ_{max} at 330 nm) and palythene (λ_{max} at 360 nm) (Dupouy et al., 2008, Coble, 2007). MAA is water-soluble and is produced by the phytoplankton to provide protection from the harmful, damaging UV light in the water. The most significant capacity of MAAs is photoprotection (Rastogi and Sinha, 2009; Richa et al., 2011), and they are commonly depicted as "microbial sunscreens". These compounds secure the cell because of their capacity to scatter harmful UVR into the surrounding environment without forming reactive photoproducts (Conde et al., 2004; Oren and Gunde-Cimerman, 2007). *Trichodesmium* has gas vesicles to regulate buoyancy (Van Baalen and Brown, 1969) and help form surface slicks. Since *Trichodesmium* needs to survive at the surface under intense solar radiation (particularly the UV light), it has evolved a self-defense mechanism by producing the MAAs that serve as sunscreens. The presence of MAAs in CDOM was observed during all the years when *Trichodesmium* surface mats were present. Though the peak of MAA shifted between years (314 - 330 nm), the shoulder due to palythene (~ 360 nm) was always observed (Table 4.1). Apart from the UV region, peaks were also present in the visible region of the spectra. *Trichodesmium* are known to produce phycobiliproteins, brilliant colored water-soluble pigments covalently joined by open chain tetrapyrroles (Neveux et al., 2006). These are intracellular compounds, akin to sheath pigments commonly found in cyanobacteria (Subramaniam et al., 1999). The breakage of the cell wall of *Trichodesmium* releases these compounds into the water, giving it a pinkish tinge, as observed in the present study.

Being water soluble, the phycobiliproteins contribute to the CDOM absorption. The absorption peaks due to these pigments were observed in the CDOM spectra during the senescence stage of the bloom, and showed inter-annual variation depending on the intensity of the bloom. CDOM spectra of samples collected at four stations on 25th April 2014, showed high absorption by phycobiliproteins and high concentrations of chlorophyll-*a* and pheopigments (Fig. 4.3). This indicates that *Trichodesmium* was in the

senescence stage and hence phycobilins were leached into the water, as also observed by the pink color of the water at the bloom site. A surface sample collected from another location on the same day (Station E, non-bloom station) had a peak in the UV region in the CDOM spectra. CDOM, chlorophyll-*a* and pheopigments were low at this station (Table 4.1). Since MAA is not photosensitive, the strong signals of MAA from the bloom vicinity area may not be diluted quickly and hence were detected. Such features were also observed by Steinberg et al. (2004) in their study. The sub-surface waters (13.4 m) of bloom station B had a considerably high count of *Trichodesmium* cells along with high chlorophyll-*a* (10 µg/l); yet the CDOM spectra did not show any signature of either MAA or phyobiliproteins (Table 4.1). This indicates that the *Trichodesmium* was in a growing phase and produced MAA only during the formation of surface mats to combat high solar irradiance (Fig. 3d). During our subsequent sampling on 30th April 2014, the surface bloom was observed at another station in the coastal waters (Table 4.1). CDOM spectra showed absorption due to MAA but peaks due to phycobiliproteins were absent in the samples. The chlorophyll-*a* concentration and *Trichodesmium* counts were low at this station, indicating that the bloom was still in the growing phase. However, blooms observed in the consecutive years (2015 and 2016) showed leaching of phycobiliproteins and MAA in the CDOM spectra, indicating the bloom's senescing phase. During 2017 (station A) and 2018, the CDOM spectra had absorption peaks due to MAA only. The chlorophyll-*a* was comparatively low during these years, which indicates that *Trichodesmium* was in the growth phase at the time of sampling.

Our study indicates that MAAs are released into the water only during surface blooms and are absent in the sub-surface waters even if *Trichodesmium* is abundant. Another noteworthy observation was the presence of phycobiliproteins in the CDOM only during the senescence phase of the bloom. Hence absorption by phycobiliproteins in CDOM can help in understanding the stages of the *Trichodesmium* bloom. Attempts could be made from such observations, for use in remote sensing, to identify the bloom stages from ocean color satellites. Our study clearly shows that the CDOM concentration increases many fold during *Trichodesmium* bloom. These peaks were observed only during bloom conditions and were absent when *Trichodesmium* cells were in low abundance. With recent advances in ocean color remote sensing, efforts are made to include bands in the UV region on the satellite sensors (Groom et al., 2019). Since MAA absorbs very strongly in the UV region, especially the absorption due to palythene (λ_{max} 360 nm), this can be used in the remote

sensing of phytoplankton-like *Trichodesmium* blooms with greater accuracy. MAA adds a considerable amount to CDOM during bloom, and could also improve the quantification of DOC using remote methods.

Trichodesmium bloom samples showed significant CDOM fluorescence peaks at ~ 275/320-340 (Ex/Em), which are due to a protein-like material corresponding to Tryptophan (Peak T; Fig. 4.5) (Coble et al., 1998; Yamashita and Tanoue, 2003; Suksomjit et al., 2009). Romera-Castillo et al. (2010) also reported a similar peak in phytoplankton cultures of *Chaetoceros*, *Skeletonema*, *Prorocentrum*, and *Micromonas*. Phytoplankton is known to discharge extracellular nitrogenous compounds such as proteins, peptides, amino acids, and carbohydrates such as polysaccharides (Myklestad, 1995). A portion of these substances with proteinaceous aromatic structures was most likely identified as peak T. Tryptophan-like fluorescence is frequently used as the characteristic of the state (free or combined amino acids) or degree of amino acid degradation. DOM with increased tryptophan-like fluorescence has been ascribed to intact proteins or less degraded peptide material (Mayer et al., 1999; Yamashita and Tanoue, 2004). Peaks observed at 250 - 260/440 - 460 nm (Ex/Em) (peak A) and 360 - 370/460 nm (Ex/Em) (peak C1) were in the humic-like fluorescence region (Fig. 4.5) (Coble, 2007). During pre-monsoon, there is no influence of terrestrial runoff to the coastal waters, and the CDOM coming from the estuaries undergo photobleaching due to longer residence time (Dias et al., 2020a). The humic-like fluorescence observed during bloom could be directly linked to the autochthonous production and microbial transformation. Our field study highlights that phytoplankton does produce humic-like fluorescence, which was previously known to originate from the terrestrial environment. Other studies also reported humic-like DOM fluorescence in axenic culture experiments (Fukuzaki et al., 2014; Kinsey et al., 2018).

The PARAFAC model provided a more robust understanding of the CDOM production/degradation during the bloom and identified three components (Fig. 4.6). The C1 seems to arise from the degradation of the tetrapyrrole structure, arising from either phycobilins or chlorophyll pigment. This component had identical fluorescent characteristics to C1 reported by Zhao et al. (2017), which was attributed to the degradation product of tetrapyrrole from picocyanobacteria. *Trichodesmium* produces phycobilins (which are highly water-soluble) and chlorophyll pigment, both of which have a tetrapyrrole structure. Pure phycocyanobilin produces this component on exposure to solar irradiation, and the presence of pyrrolic ring was confirmed by ultrahigh resolution

mass spectrometry and nuclear magnetic resonance spectrometry (Zhao et al., 2017). Owing to the high water solubility of phycocyanobilins, it is more likely that cyanobacteria produce this C1 fluorescence on the degradation of the tetrapyrrole structure from phycocyanobilins. The other source of tetrapyrrole could be chlorophyll pigments. Degradation of chlorophyll produces intermediate fluorescent chlorophyll catabolites (FCCs), which shows fluorescence in the blue region peaking at 450 nm (Dartnell et al., 2011). Blue shifting in the emission maxima from the active chlorophyll-*a* (680 nm) to FCCs (450 nm) is probably due to the changes in the molecular structure (loss of aromatic rings or reduction in conjugated bonds) (Coble, 1996). Even though the Ex/Em peaks of FCCs correspond well with our C1, it is unlikely that chlorophyll-*a* would contribute to this fluorescence, since they are not readily water-soluble and FCCs are not very stable. Though phycocyanobilins could be the significant source of this component, detailed study is required to confirm the exact origin.

C2, resembled Tryptophan fluorescence (Fig. 4.6) which is an indicator of recent biological production, as evident from high concentrations of CDOM, chlorophyll-*a*, and dominant pigment zeaxanthin during the *Trichodesmium* bloom. C3 (with a peak at 250 (305)/420), identified as a humic-like component, was found to shift towards the longer Ex/Em wavelengths (Fig. 4.6). This component was found to be similar to peak M designated by Coble, (1996) as marine humic-like. Romera-Castillo et al. (2010) detected peak M in culture filtrates of four algal species. In addition, Fukuzaki et al. (2014) reported peak M in FDOM produced by *Heterocapsa cicularisquama*. Peak M is mainly produced by microbial reprocessing of the plankton-derived organic matter. Additionally, bacteria are known to be associated with *Trichodesmium* blooms (Sellnar, 1992; Steinberg et al., 2004; Basu et al., 2011). Though bacterial counts were not available in the present study, we can ascertain that the microbial reworking on the *Trichodesmium* colonies would lead to this marine humic-like component.

Fluorescence index (FI), the proportion of emission at 470 and 520 nm at excitation of 370 nm, has been utilized to recognize DOM derived from terrestrial sources (degraded plant and soil organic matter; lower values) versus microbial sources (extracellular release and leachate from bacteria and algae; higher values) (McKnight et al., 2001; Cory et al., 2007, 2010). FI values normally range between 1.2 and 1.8 in marine waters (Jaffe et al., 2008; Cory et al., 2010; Carpenter et al., 2013; Helms et al., 2013; Fleck et al., 2014). During *Trichodesmium* bloom, the FI value was found to be higher (~ 3) than the values observed

for marine waters. Such high FI values were also observed by Korak et al. (2015) in leachates of intracellular organic matter of cyanobacteria (> 2). As suggested by Hansen et al. (2016), higher FI values can be used as an indicator of DOM derived from phytoplankton production in the water column, as also seen in the present study.

4.5.2. Photodegradation of CDOM

In the first experiment, when the unfiltered bloom sample (including DOM, trichomes, and bacteria) was exposed to natural sunlight, a significant increase in MAA (λ_{max}~314 nm; almost two fold) was seen during the initial 2 days of the experiment (Fig. 4.7a and 4.7c). This increase could be attributed to the production of MAA by *Trichodesmium* to combat the high intensity of solar radiation. After two days, a gradual decrease in MAA was observed, which could be due to the mortality of *Trichodesmium* cells and the degradation of available MAA in the medium. The degradation of MAA occurred at a faster pace, and the formation of its photo-products was evident from a shift in the λ_{max} to 300 nm, while the MAA palythene (λ_{max} 360 nm) underwent degradation at a much slower pace. The presence of photosensitizers in natural seawater aids in the photodegradation of MAA (Whitehead and Hedges, 2005).

CDOM absorption in the visible region (400 - 500 nm) showed a decrease in absorption during the initial two days, followed by a gradual increase, clearly seen in the values of reference wavelength a_g412 (Figs 4.7b and 4.7d). This initial decrease in absorption was also evident in the 'control'. The decrease in absorption is likely due to the combined effect of photo- and biodegradation of the labile DOM. *Trichodesmium* must have undergone genetically controlled programmed cell death (PCD) due to the stress of light and nutrient limitation (Berman-Frank et al., 2007; Bar-Zeev et al., 2013). Bar-Zeev et al. (2013) observed that the mortality of *Trichodesmium* through PCD is morphologically and physiologically distinct from necrotic death and triggers a quick sinking of biomass. The sinking of *Trichodesmium* in the flasks was observed in the present study. Sinking is either because of accompanying interior cell debasement, vacuole loss, or because of excess release of transparent exopolymeric particles (TEP) (Berman-Frank et al., 2007; Bar-Zeev et al., 2013). The release of TEP and intra-cellular degradation, followed by bacterial remineralization of labile DOM, would have contributed to an increase in CDOM (a_g412) from the 4^{th} to 11^{th} day of the experiment. However, nearly constant a_g412 from the 9^{th} to 11^{th} day of the experiment suggests the production of recalcitrant DOM (Fig.

4.7d). The CDOM in the wavelength range of 500 - 700 nm showed a steady decrease from the initial value throughout the experiment. The peak at a_g547 observed in the CDOM spectra due to phycoerythrin decreases throughout the experiment, and the loss of pink color of the water indicates that phycoerythrin is highly photoreactive and undergoes bleaching (Fig. 4.7d). The changes seen in the 'control' in the first experiment will be totally autochthonous (microbially derived) and will not be mediated by photodegradation. It is clear from the shift in the peak position and decrease in MAA peak that it is microbially labile and degrades, hence a shift in the peak position of MAA is observed, which is also seen in the experimental flask (Fig. 4.8). The shoulder due to MAA palythene seems to be stable to photo- and microbial degradation. The presence of phycobiliproteins in the 'control' for a longer time as compared to the experimental flask indicates that they are highly photosensitive and degrade at a faster pace in the presence of sunlight than the bacteria. An increase in CDOM absorption in both the 'experimental' and 'control' flasks over the initial value shows that CDOM is produced by both bacterial and photodegrdation. The higher CDOM absorption in the visible range in the 'control', rather than the experimental sample, shows that the bacterial degradation of photobleached DOM occurs at a faster pace. Similar observations were also observed by Moran et al. (2000) in their study.

In the second experiment, wherein CDOM from *Trichodesmium* bloom was exposed to natural solar radiations, a_g330 decreased drastically (Fig. 4.9b and 4.9c). The a_g412 showed a gradual decrease until the 10^{th} day of the experiment (Fig. 4.9d). Since phytoplankton cells were removed by filtration, the labile CDOM present in the filtrate undergoes degradation under solar radiation. On the 11^{th} day, an increase in a_g412 was observed which could be attributed to the rise in the tryptophan (Fig. 4.9f). The a_g412 was found to correlate with C1 and C2 fluorescent components identified from the PARAFAC (Figs 4.9e and 4.9f). This clearly indicates that the degradation product of tetrapyrrole and tryptophan are responsible for the increase in a_g412 observed in the present study. The 0.2 and 0.7 micron filtered 'controls' showed nearly similar spectra, which indicate that the bacteria had minimal effect, and the changes recorded in the experiment are mainly due to photodegradation. The disappearance of the peak at 330 nm in the 'control' indicates that asterina is labile and undergoes degradation while the peak at 360 nm due to palythene is more stable. Similar results were also observed by Coba et al. (2019) when different MAAs were exposed to a range of temperatures and pH values. Our experiments clearly

indicate that the MAAs are photoprotective and undergo slow degradation, whereas the CDOM in the visible region undergoes degradation at a much faster pace. Hence MAA, especially palythene, can be used as an index for remote sensing of bloom forming phytoplankton like *Trichodesmium*, due to high absorption and photo stability as seen from the experimental results.

Both the experiments clearly show that the CDOM decreases initially, followed by an increase as a result of photodegradation. In the first experiment (unfiltered), the rise in CDOM is observed within seven days and may attributed to the combined effect of photo- and biodegradation. In the second experiment, wherein the filtered samples were exposed to photodegradation, an increase in CDOM was observed towards the end of the experiment (12 days). This shows that biodegradation was limited, and we assume that the bacteria were mostly eliminated during filtration, though 0.7 micron filters were used. It is well documented that bacteria are attached to the trichomes (Borstad, 1978; Paerly et al., 1989) and are easily removed during filtration. This is also supported by the fact that 0.2 and 0.7 micron filtered 'controls' didn't show much change in the visible region until the end of the experiment. Hence, based on both experiments (filtered and unfiltered), it is concluded that bacteria play an important role in the degradation of organic matter along with photodegradation.

4.6. Conclusion

Based on field data during bloom and degradation experiments, this study presents the spectral and fluorescence characteristics of CDOM produced during *Trichodesmium* blooms in the coastal waters of Goa. *Trichodesmium* has a unique CDOM absorption with peaks due to MAA in the UV region and phycobiliproteins in the visible region. *Trichodesmium* was found to produce one protein-like (tryptophan) and two humic-like fluorescence. The field study highlights that phytoplankton do produce humic-like fluorescence, which was previously known to originate from the terrestrial environment. The FI values observed in the present study were found to be much higher (~ 3) than the typical values noted for natural waters (1.2 - 1.8). Phycobiliproteins produced by *Trichodesmium* seem to be highly photosensitive and undergo immediate degradation on exposure to solar radiation, as seen by the disappearance of pink color within one day of photo exposure. However, the decrease in CDOM absorption on exposure to solar radiation was followed by an increase towards the end of the experiment. This increase in

CDOM absorption was found to be correlated with the tryptophan-like protein component, as traced from PARAFAC. The experimental study proves that bacteria play an important role in the degradation of organic matter along with photodegradation. It is concluded that *Trichodesmium* blooms build up large pools of CDOM and play an important role in the DOM cycling of coastal waters.

Chapter 5

Variations of CDOM during the south west monsoon and seasonal hypoxia along the WCSI of India

Variations of CDOM during the southwest monsoon and seasonal hypoxia along the western continental shelf of India

5.1. Introduction

The Indian summer monsoon or southwest monsoon (SWM) is a typical feature of the tropics and prevails over India from June to September anually. This occurs due to the differential heating between the land and the ocean (Halley, 1686; Webster et al., 1998) and accounts for 70- 90% of the yearly precipitation over India (Shukla and Haung, 2016). The seasonal reversal of winds blowing along the shores of the Indian Ocean brings heavy rainfall to the Indian subcontinent, feeding the numerous small and medium rivers that flow through the coastal plain and join the Arabian Sea (AS). Large spatial and temporal variability has been observed in the Indian summer monsoon rainfall (Hrudya et al., 2021).

The south-westerly winds blowing over the Indian subcontinent drives offshore Ekman transport, which successively brings about upwelling along the western and the eastern AS, thus making the AS a unique basin of study. The coastal upwelling brings high-salinity, high-nutrient, and low-oxygen waters to the surface, which supports primary production and hence organic carbon production (Prasanna Kumar et al., 2001). Narvekar et al. (2021) has shown that the upwelling in the eastern AS is affected by the strength of stratification as a result of freshwater flux received from the runoff and precipitation.

The nothern AS is well known for being the most prominent and intense perennial oxygen minimum zone (OMZ) in the world, wherein oxygen concentrations less than 2µM are reported at a mid-water depth of 100 to 1,000 m in the water column (Sen Gupta and Naqvi, 1984; Naqvi et al., 2006). In addition to this, the western continental shelf of India (WCSI) is also known to host the world's largest natural seasonal hypoxic zone covering an area of 1,80,000 km^2 (Naqvi et al., 2000). Variability in terms of duration and intensity of the seasonal oxygen deficiency has been reported earlier (Naqvi et al., 2009a). Even though it possesses less than 2% of the world's ocean area, the AS is liable for up to 40% of global water column denitrification, a cycle that diminishes the oceanic inventory of bioavailable nitrogen (essential for phytoplankton growth) and releases N_2O a major greenhouse gas (Codispoti et al., 2001; Bange et al., 2005; Naqvi et al., 2006). It is well established that OMZs influence marine biogeochemical cycles such as the global carbon and nutrient cycles (Bange et al., 2005; Naqvi et al., 2006).

Carbon dynamics is closely associated with dissolved oxygen (DO) and therefore the advancement of hypoxia (Bianchi et al., 2010), as DO is being consumed both in the surface and bottom waters due to photochemical and heterotrophic oxidation of DOM (Green et al., 2006; Diaz and Rosenberg, 2008). Moreover, DOM assumes a significant role in the fate and transport of numerous organic contaminants and heavy metals (McCarthy and Zachara, 1989; Santschi et al., 1998). Along these lines, information regarding sources, abundance, chemical composition, and cycling pathways of DOM is imperative for a better understanding of ecosystem health in aquatic environments.

5.2. Aim of the study

The WCSI is one of the unique basins which is affected by seasonal reversing currents, leading to coastal upwelling. This region also receives a large terrestrial influx from the perennial rivers along the west coast. Moreover, this region hosts the world's largest hypoxic zones in recent times. The influx of freshwater received during the SWM leads to a strong stratification of the water column. The coastal upwelled waters being low in oxygen would deteriorate further due to nutrient-fuelled primary production and very low mixing. Episodic seasonal anoxia along the coastal waters of Goa has also been reported during the late SWM (Naqvi et al., 2006).

The study of CDOM variability is the first of its kind along the WCSI during the SWM. Earlier the study on the optical properties of CDOM was conducted by Coble et al. (1998) during the SWM along the Gulf of Oman and central AS (56 – 66ºE). A negative correlation for surface CDOM samples was observed with temperature suggesting upwelling as a source of CDOM. Also, three water masses with distinct fluorescence were identified in their study. Del Castillo and Coble (2000) studied the seasonal variability of CDOM during the NEM and SWM in the AS (56 – 66ºE) and attributed the differences in the wind regimes between the monsoons for the distribution of CDOM. Recently, a study carried out by Minu et al. (2020) along the coastal waters of Kochi reported the terrigenous nature of CDOM during the SWM, *in-situ* production during the pre-monsoon, and autochthonous-allochthonous origin during the post-monsoon. Thus this region becomes an ideal place to study the variations of CDOM under the given biogeochemical settings. Keeping the importance of the region in mind, it was decided to study the behavior of CDOM during hypoxic conditions observed along the WCSI. Hence the following specific objectives were proposed:

- Study the spatial variability of CDOM and FDOM during the SWM along the WCSI.
- Characterize the CDOM at varying levels of oxygen.
- Study the influence of seasonal hypoxia on the CDOM in the coastal waters of Goa.
- Estimate the production of CDOM under varying levels of oxygen and organic matter based on lab experiments.

5.3. Methodology

Sampling was done along the WCSI at four transects (Kochi, Mangalore, Karwar, and Goa) during the early SWM (June – July) of 2018 onboard *RV Sindhu Sadhana* (SSD 052 cruise). In addition, sampling was also carried out during the late SWM (September) along the Goa transect in 2018 (SSD 057). Previously the Goa transect was sampled during the late SWM (September to October) in 2016 when the coastal waters experienced seasonal hypoxia. The sampling details are given in Table 5.1 and the station locations are shown in Figure 5.1.

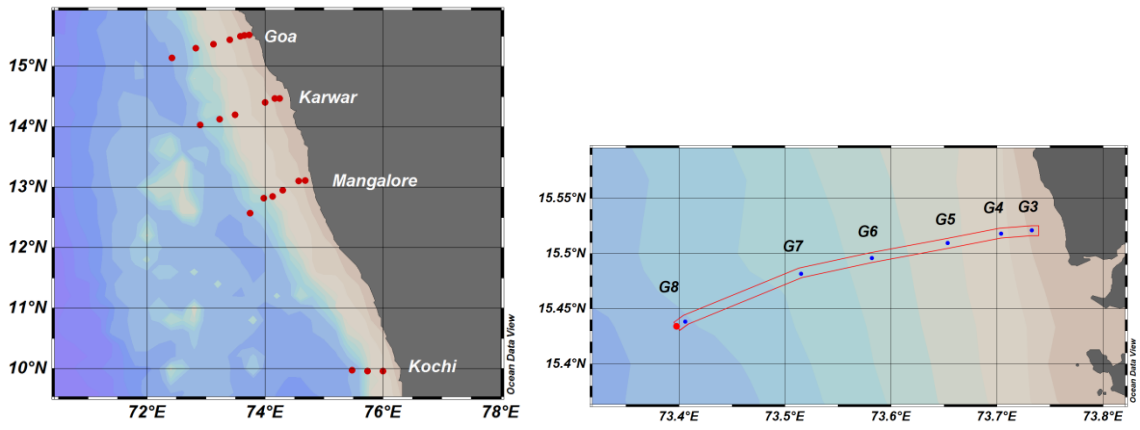

Figure 5.1: Study area showing the four transects (left) along the WCSI, where sampling was carried out during June-July 2018 (SSD 052 cruise), and the Goa transect (right), where sampling was done during September 2018 (SSD 057 cruise). The Goa transect was also sampled between September and October 2016.

Table 5.1: Details of sampling carried out during 2016-2018

Transects sampled	**Cruise/boat**	**Sampling dates**	**Stations covered**
Goa	Mechanized boat	1st September 2016	2 (G5, G6)
Goa	SSD 026	8th October 2016	1 (G5)
Goa	SSK 093	31st October-1st November 2016	4 (G3- G6)
Kochi Mangalore Karwar Goa	SSD 052	29th June 2018 01st July 2018 02-03rd July 2018 04 -05 July 2018	3 (KOTS2- KOTS6) 6 (M1 – M12) 6 (K2 - K13) 7 (G3 - G14)
Goa	SSD 057	20th September 2018	6 (G3 - G8)

5.3.1. Experimental setup

Apart from the *in-situ* study, an experiment was also conducted to understand the behavior of DOM under varying levels of oxygen and organic matter in the laboratory. For this, the bottom water from the CaTS (G5) location was collected on 31st July 2018 onboard *RV Sindhu Sadhana*. For the experimental setup, we used amber-colored glass bottles (4 bottles of 4 L capacity and labeled as A, B, C, and D.) to curtail the effect of light on DOM alteration. Two bottles (A & B) were filled with 0.2 micron filtered water keeping little headspace, whereas the remaining two bottles (C & D) were enriched with organic matter. The residue collected on the 0.2 micron filters was resuspended in the water before filling the bottles C and D. One bottle of each set (A & C) was kept in a closed system using an airtight cap connected with a tube having a Luer lock. The headspace of these bottles was purged with N_2 gas to remove any traces of oxygen. The other two bottles (B & D) were kept saturated with oxygen by using an aerator. The experimental setup is depicted in Figure 5.2. All four bottles were monitored for changes in DO and CDOM for 30 days. Every day, an aliquot of 50 mL was withdrawn from these bottles with glass syringes attached to Luer locks. Before sampling, the glass syringes were flushed with N_2 gas to eliminate contamination by atmospheric oxygen. The headspace in the bottles was replaced with N_2 gas by connecting nitrogen bags to the bottles during sample collection.

Bottle A: 0.2 micron filtered water, oxygen-limited

Bottle B: 0.2 micron filtered water, aerated

Bottle C: Sample enriched with organic matter, oxygen-limited

Bottle D: Sample enriched with organic matter, aerated

Figure 5.2: Experimental setup used in the laboratory, two bottles were oxygen-limited by purging of N_2 gas in the headspace (left), and two bottles were aerated using an aerator (right).

5.3.2. CDOM analysis

The water samples were collected and filtered onboard for CDOM absorption and fluorescence using a 0.2 micron nucleopore membrane filter following standard protocols and stored in an amber colored glass bottle at 4˚C until analysis (Mitchell et al., 2002; Tilstone et al., 2002). The details of analysis are given in chapter 2. The FDOM data (148 EEMs) were further subjected to PARAFAC analysis using MATLAB software (2017), including the DrEEM toolbox 0.20 (Murphy et al., 2013). PARAFAC modeling was restricted to the excitation wavelength >240 nm and emission wavelength < 590 nm to avoid the noise. The model was run with non-negativity constraints. Validation was performed by split-half analysis and analysis of residuals and loadings.

5.3.3. Dissolved oxygen analysis

Samples for dissolved oxygen were fixed immediately upon collection and analyzed following Winkler's titration method (Grasshoff, 1983) for the field samples. During the laboratory experiment, the sample for DO analysis was collected in 10 mL glass syringes and fixed using Winkler reagents, followed by analysis using a spectrophotometer at 456 nm as detailed in Pratihary et al. (2014). Dissolved oxygen (µM) is calculated using the following the equation

$$DO = (Abs_{456} - Blank_{456})*476$$

5.4. Results

5.4.1. Spatial variation of physicochemical parameters along the WCSI during the early SWM of 2018

The surface inshore waters along the WCSI were characterized by low temperatures (28ºC), low salinity (32), and higher oxygen concentration (4.5 mL/L) as compared to the offshore waters (Fig. 5.3). The sea surface temperature (SST) and salinity increased, while the dissolved oxygen decreased from the coast to the offshore along the four transects. Signatures of upwelled waters with low temperature, high salinity, and low DO were observed on the southwest coast of India (10ºN). A prominent decrease in sea surface salinity (SSS) and increase in DO was observed towards the north (15ºN) along the coast.

Along the Kochi transect, the SST increased from the coast (28ºC) to the offshore (28.22ºC), while SSS also showed a similar trend, with values ranging from 33 to 33.7 from the coast to the offshore. A cap of high saline waters (35) was restricted at the depth of 20 to 40 m in the water column. The surface waters along the transect were oxic while the sub-surface waters were hypoxic. The low oxygenated waters (1.8 mL/L) were seen close to the coast (KOTS 2) and the DO in the sub-surface waters decreased offshore (Fig. 5.4).

The SST and SSS increased from the coast to the offshore varying from 27.7ºC to 28.7ºC and 30.7 to 33.9, respectively, at the Mangalore transect. The presence of high saline (35.3) water mass at the sub-surface (30-60 m depth) was also seen at this transect. The surface waters were oxic while hypoxic conditions were seen in the bottom waters from the coast to the offshore (Fig. 5.5).

The station close to the coast of the Karwar transect had an SST of 27.8ºC which increased offshore to about 28.8ºC, while SSS showed large spatial variations varying from 29.1

close to the coast to 34.1 towards the offshore. The bottom inshore waters were hypoxic while the waters experienced suboxic conditions offshore (Fig. 5.6).

The Goa transect recorded the highest temperatures (28.15ºC) and lowest salinity (28) in the surface waters near the coast which increased towards offshore (29ºC and 34.8, respectively). The near-shore waters were oxic while hypoxic-suboxic conditions were seen in the sub-surface depths towards offshore (Fig. 5.7).

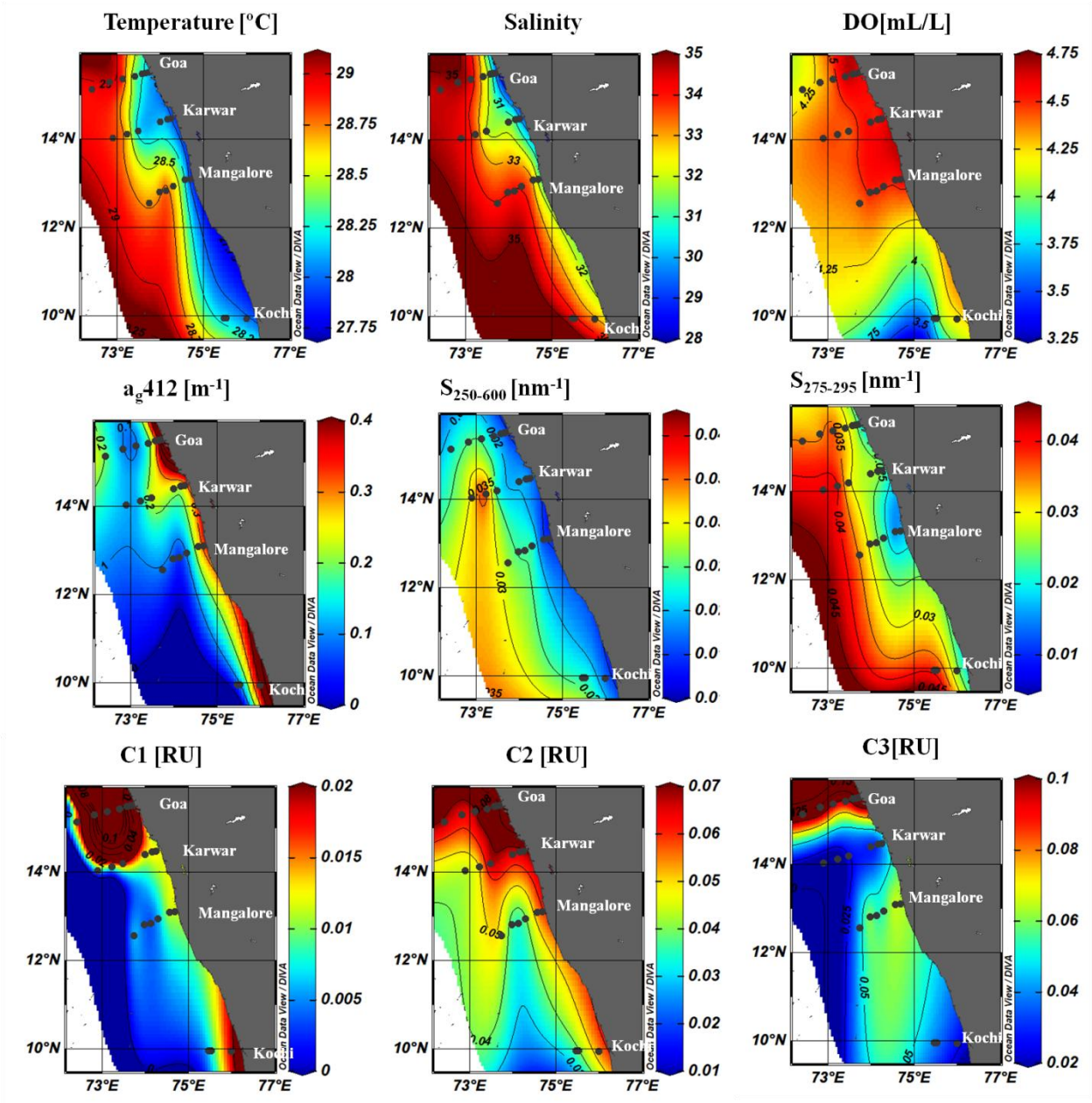

Figure 5.3: Spatial variation of physicochemical parameters and CDOM characteristics in the surface waters of WCSI (Kochi, Mangalore, Karwar, and Goa) during the SWM (June-July) of 2018.

5.4.2. Spatial variation of CDOM characteristics along the WCSI during the early SWM of 2018

The CDOM absorption (a_g412) at the surface waters varied from 0.0035 to 0.953 m^{-1}, and the values increased towards the north (15˚N; Fig. 5.3). All transects showed very high CDOM absorption (m^{-1}) near the coast and decreased offshore. Spatially there was a significant difference in CDOM absorption with $p < 0.01$. The spectral slopes $S_{250-600}$ and $S_{275-295}$ were low near the coast, while these increased offshore (Fig. 5.3). Based on PARAFAC, three fluorescent DOM components were identified along the WCSI (Appendix 1.5). Components 1 (C1) and 2 (C2) were humic-like with emissions in the longer wavelength, while component 3 (C3) was protein-like with excitation and emission in the UV region. These components were matched with the previously reported components in the Openfluor database (Murphy et al., 2014). C2 and C3 were matched with more than 21 components with a Tucker's coefficient of 0.95, while component 1 matched with only two components at a Tucker's coefficient of 0.9. C1 and C2 had two excitation and one emission maxima, <250 (420)/480 nm, <250 (320)/410 nm, respectively. C1 was a mixture of traditional humic-like A+C (Coble, 1996), while C2 has been identified as humics produced in the marine environment (Stedmon et al., 2011). C3 was protein-like and was associated with productivity, consisting of free and protein-bound amino acids, and was linked to autochthonous production of CDOM. The distribution of all the three FDOM components was high along the Goa transect as compared to other transects (Fig. 5.3).

In general, CDOM absorption increased with depth and was high at the nearshore stations during the SWM season. High CDOM absorption was seen at the coastal station off Kochi, which increases towards the bottom with low spectral slope values (Fig. 5.4). C1 was high in the surface waters at the nearshore station while it increased in the sub-surface waters at the offshore stations. C2 was high near the shore, while C3 showed a maximum in the offshore bottom waters along the Kochi transect (Fig. 5.4).

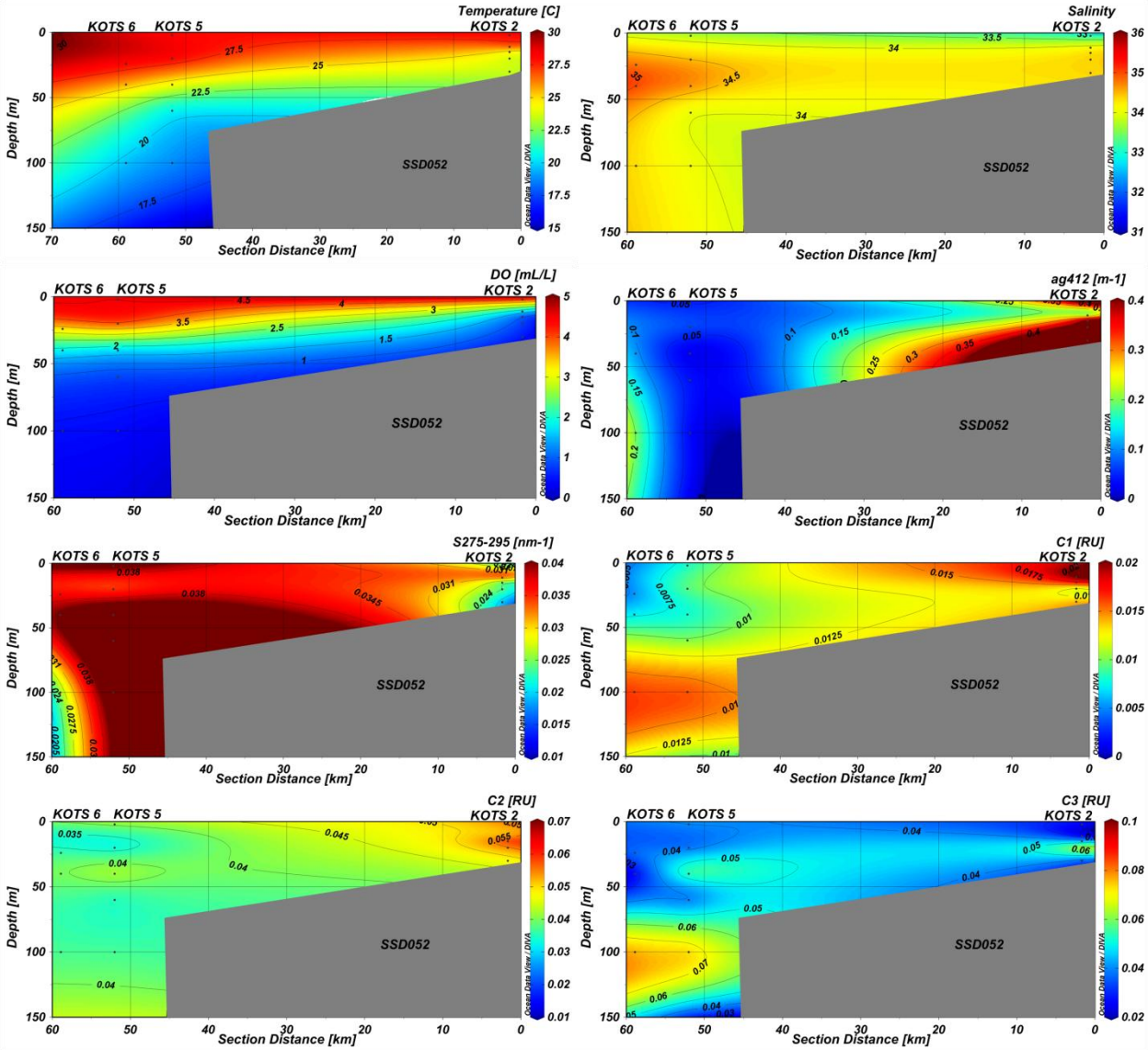

Figure 5.4: Spatial variation of physicochemical parameters and CDOM absorption (a_g412, m^{-1}), spectral slopes ($S_{275-295}$ nm^{-1}), and FDOM (C1, C2, and C3) along the Kochi transect during the SWM (June 2018).

Along the Mangalore transect, CDOM increases with depth in the coastal waters except for station 3. *Trichodesmium* bloom was noticed at this station, which is characterized by high CDOM absorption and peaks in the UV region of CDOM spectra in the surface waters. In the offshore waters, CDOM absorption was high at the sub-surface depths (Fig. 5.5). FDOM components C1, C2, and C3 increase with depth with maxima in the bottom waters near the shore, while an increase was observed in the sub-surface waters in the offshore region.

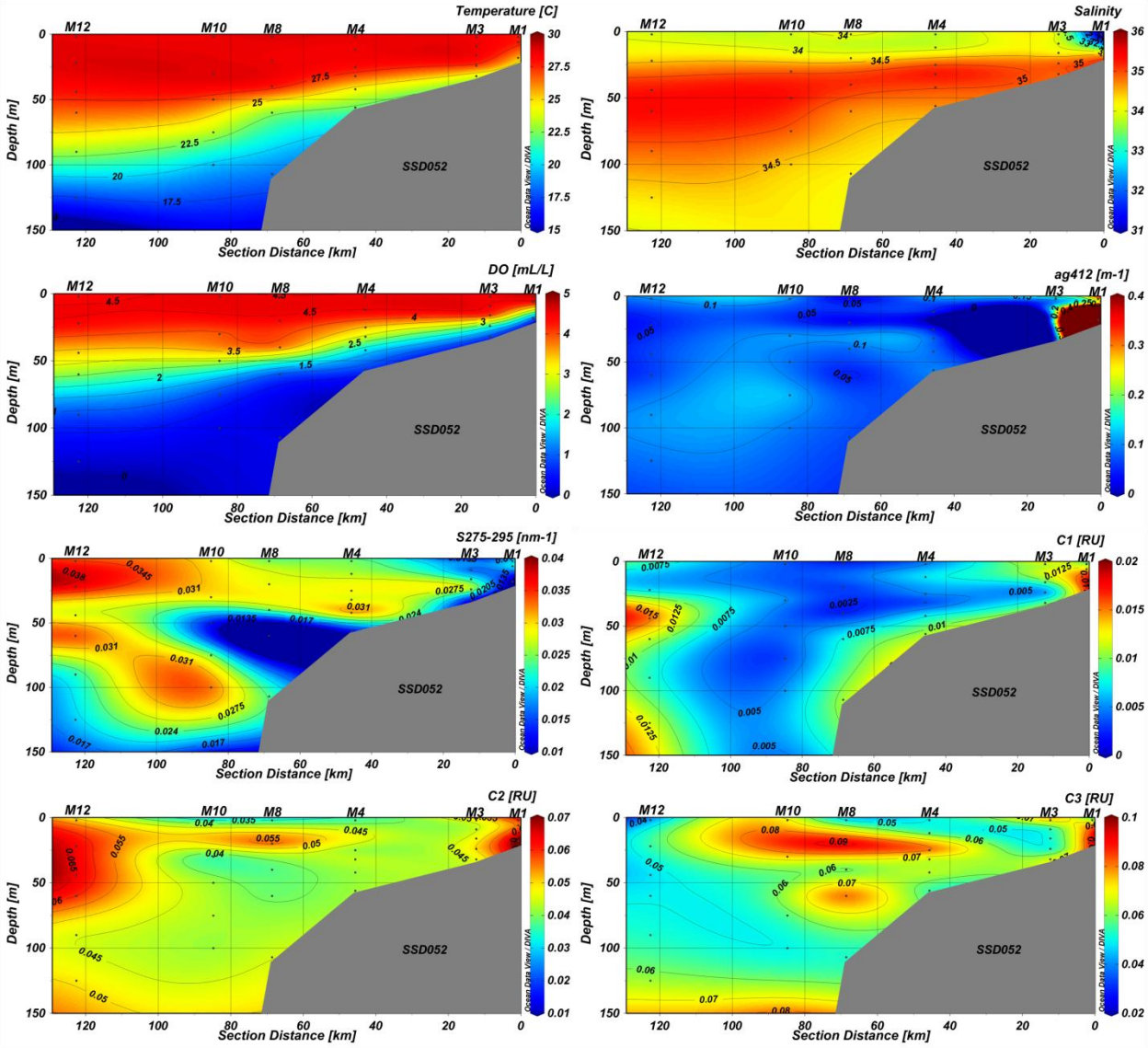

Figure 5.5: Spatial variation of physicochemical parameters and CDOM absorption (a_g412, m^{-1}), spectral slopes ($S_{275-295}$ nm^{-1}), and FDOM (C1, C2, and C3) along the Mangalore transect during the SWM (July 2018).

At the Karwar transect, an increase in CDOM absorption with depth was observed along the coastal and shelf region. High CDOM absorption (2.7589 m^{-1}) was observed in the bottom waters of the nearshore station, which decreased offshore (0.1543 m^{-1}; Fig. 5.6). The spectral slopes $S_{250-600}$ and $S_{275-295}$ were high at the surface and decreased with depth. Lower spectral slope values were observed close to the coast, and it increased offshore (Fig. 5.6). DO decreased with depth with hypoxic waters at the bottom near the coast, whereas suboxic waters were seen offshore (Fig. 5.6). The FDOM components C1 and C2 were high at the inshore stations and decreased offshore, as expected.

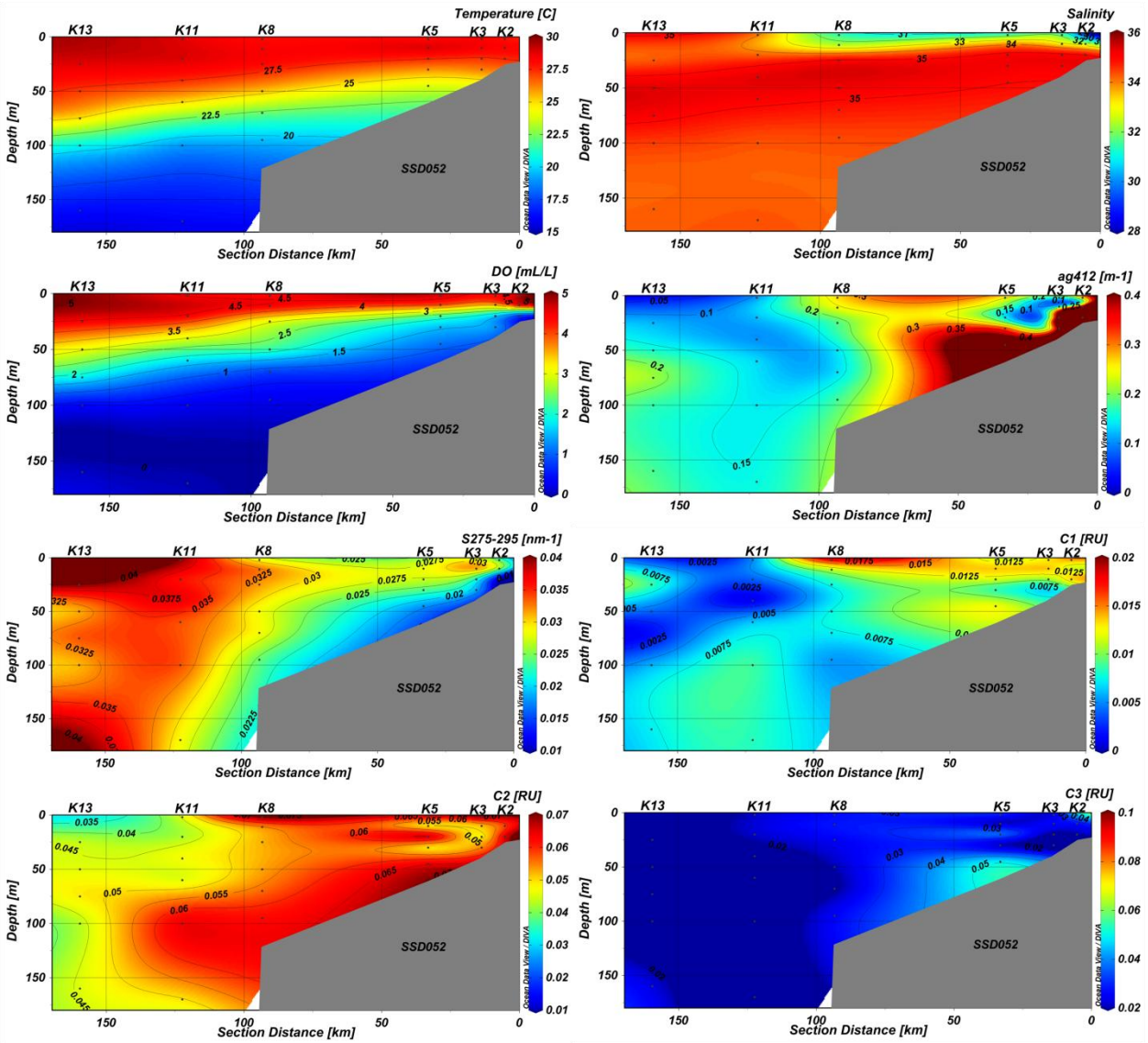

Figure 5.6: Spatial variation of physicochemical parameters, CDOM absorption (a_g412, m^{-1}), spectral slopes ($S_{275-295}$ nm^{-1}), and FDOM (C1, C2, and C3) along the Karwar transect during the SWM (July 2018).

During the SWM of 2018, CDOM absorption increased with depth with the highest values recorded in the bottom waters of nearshore stations, and the maximum was observed along the Goa transect (5.3285 m^{-1}) (Fig. 5.7). The nearshore coastal waters were oxic (> 3 mL/L), characterized by high CDOM absorption, low spectral slope during the onset of SWM. The slope $S_{250-600}$ and $S_{275-295}$ decreased with depth, with the lowest slopes observed in the bottom waters (Fig. 5.7). CDOM absorption was high at the surface and also at the oxycline (100 - 200 m) at the offshore station G14. The spectral slope was low at this depth, which increases towards greater depth. Fluorescence maxima (1.94 RU) of component C1 (humic-like) was observed in the sub-surface waters close to the

thermocline and oxycline along the shelf off Goa. Low fluorescence of C1 was observed in the inshore waters. In the offshore waters, C2 was high in the sub-surface waters, with the maxima observed in the OMZ region. C3 was moderately high in the surface waters along the coast, while maxima were observed in the sub-surface waters along the shelf and the open ocean (Fig. 5.7).

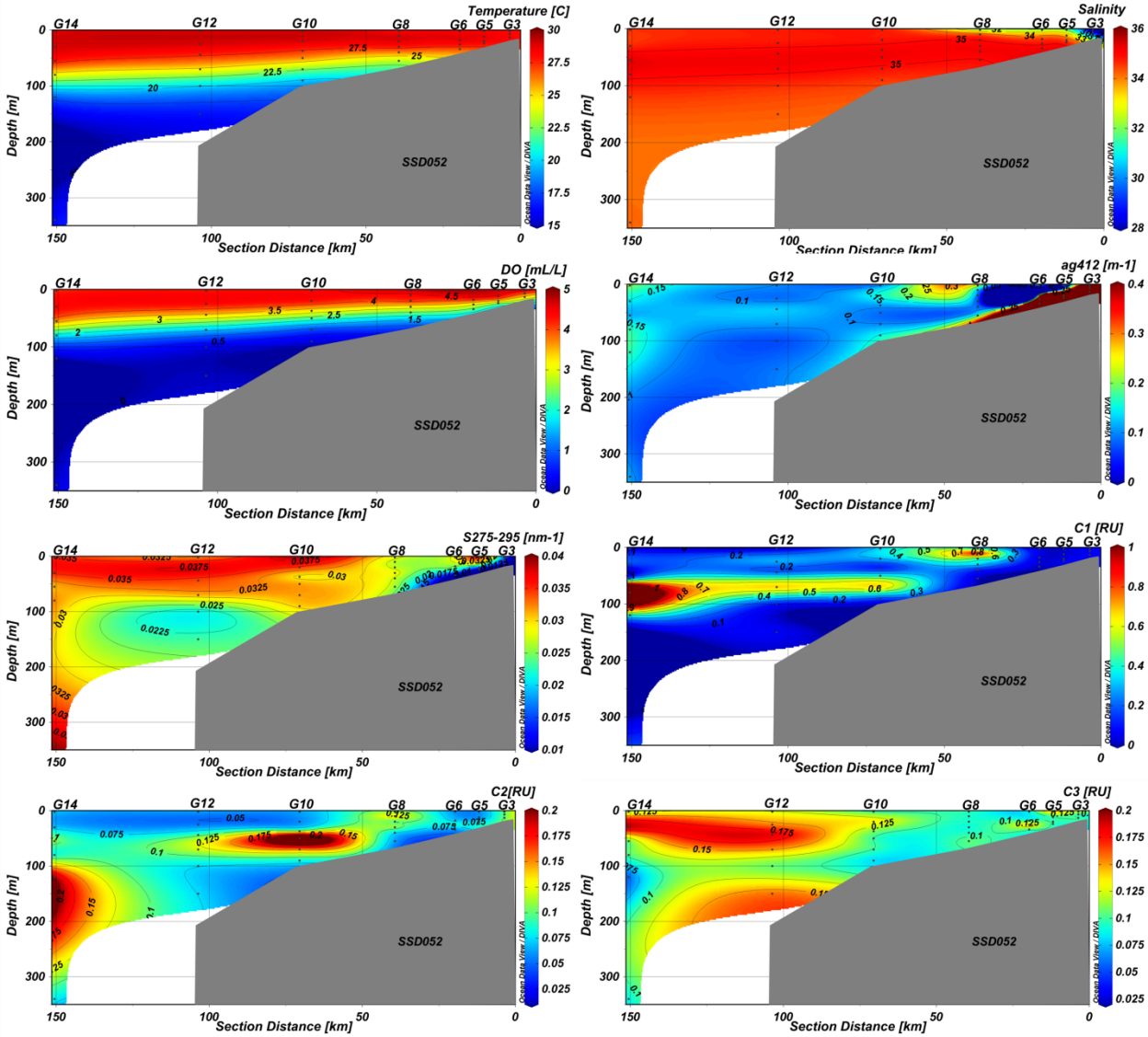

Figure 5.7: Spatial variation of physicochemical parameters, CDOM absorption (a_g412, m^{-1}), spectral slopes ($S_{275-295}$ nm^{-1}), and FDOM (C1, C2, and C3) along the Goa transect during the SWM (July 2018).

5.4.3. Variation of CDOM during seasonal hypoxia

5.4.3.1. Spatial variation of physical parameters across the Goa transect during the late SWM of 2018

Off Goa transect (stations G3 to G8) was again sampled in September (late SWM) 2018 for various biogeochemical parameters. The surface waters were warmer during the late SWM as compared to July, and temperature increased offshore. Large temperature variation was observed from the surface to the bottom, ranging from 24.99ºC to 22.74ºC at the nearshore station (G3), while temperature varied from 28.15ºC at the surface to 20.29ºC in the bottom waters at station G8. Low saline waters were present at the surface (35.48 – 34.69). A cap of high saline water (35.75) was present in the sub-surface (20 – 40 m) waters at the offshore stations (G6 to G8). The surface waters were well-oxygenated, and the DO at the surface increased offshore (3.06 to 5.23 mL/L). A sharp decline in DO was observed with depth from oxic to hypoxic waters at the sub-surface throughout the transect. Signatures of coastal upwelling were observed during this period with low temperatures, high salinity, and low DO in the sub-surface waters (Fig. 5.8).

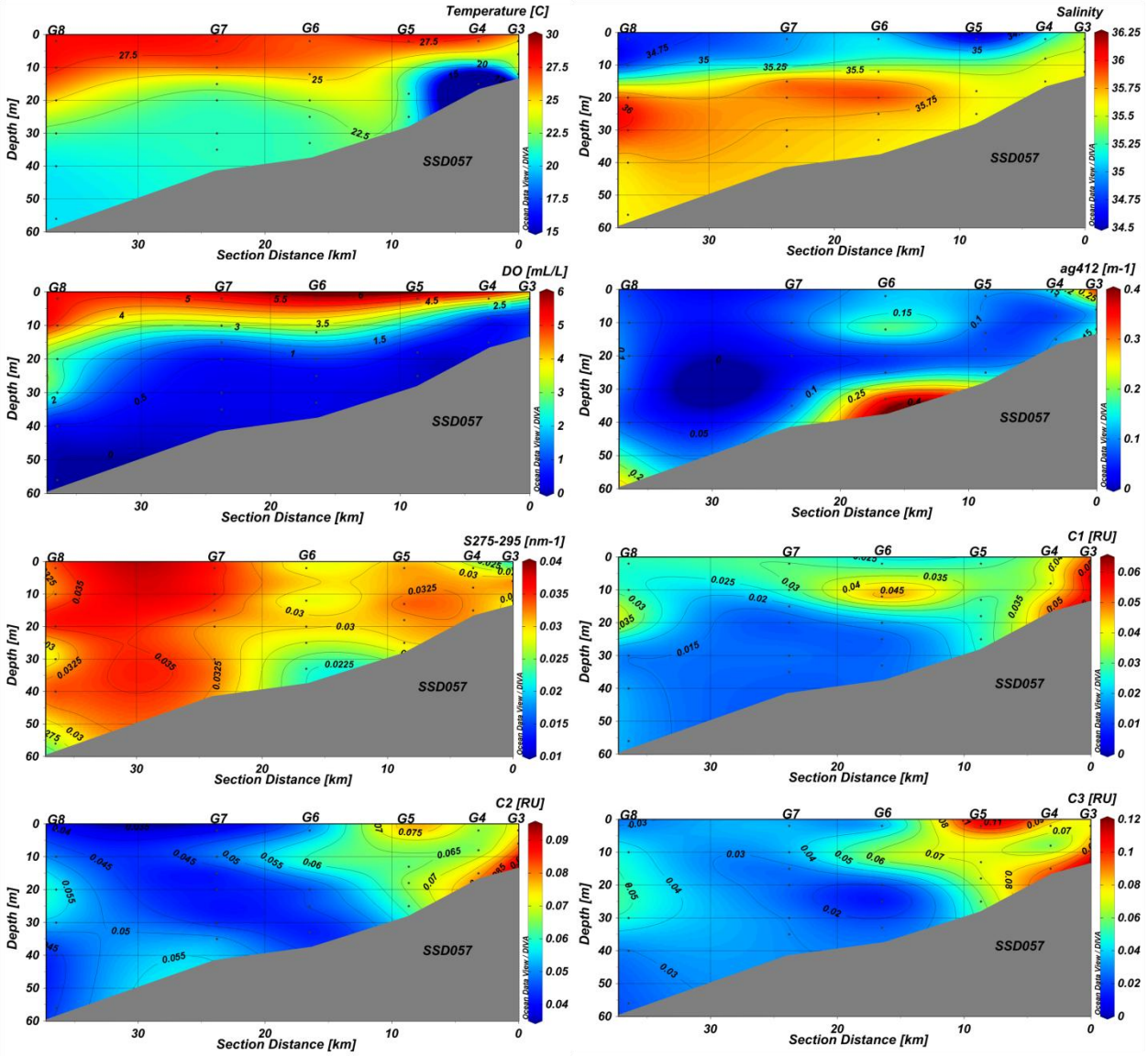

Figure 5.8: Spatial variation of physicochemical parameters, CDOM absorption (a_g412, m^{-1}), spectral slopes ($S_{275-295}$ nm^{-1}), and FDOM (C1, C2, and C3) along the Goa transect during the late SWM (September 2018).

5.4.2.2. CDOM variation across the Goa transect during the late SWM of 2018

The CDOM in the surface waters decreased, while $S_{275-295}$ increased from July to September 2018 (Figs. 5.7 and 5.8). The surface CDOM absorption decreased from 0.953 m^{-1} during July to 0.291 m^{-1} during September at the nearshore station (G3), while at the offshore station (G8) it decreased from 0.230 m^{-1} to 0.064 m^{-1}. A similar significant decrease in CDOM at the bottom waters was also observed from July to September. The spectral slope $S_{275-295}$ was low (0.0247 nm^{-1}) at the nearshore stations and increased offshore (0.0339 nm^{-1}). The Spectral slope $S_{275-295}$ increased with depth at the near-shore

stations, while it decreased with depth at the offshore station. The spectral slope $S_{250-600}$ was high at the surface and decreased with depth along this transect. $S_{250-600}$ did not show any drastic variations from July to September at the surface waters of the Goa transect. The spectral slope $S_{250-600}$ did not show any variation with depth at the near-shore station, while it increased in the bottom waters from July to September. The fluorescent DOM, C1 was high in the nearshore waters and was present within 20m in the offshore waters (Fig. 5.8). C2 and C3 were also high in the nearshore bottom waters, while very low FDOM was observed in the surface offshore waters. Build-up of C3 was observed in the sub-surface waters at the offshore region.

5.4.2.3. CDOM variation at the coastal time series station G5

Monthly sampling of biogeochemical parameters is being carried out at the CaTS station G-5 (off Goa) since 1997 (Naqvi et al., 2000). CDOM absorption was the highest during the SWM as compared to other seasons (Dias et al., 2020a) at this station. Observations during 2016 at G-5 indicate that the surface waters were well oxygenated during late SWM (Figs. 5.9 and 5.10). Temperature decreased from 27.15ºC (September) to 25.46ºC (October), while a reverse trend was observed for salinity (Fig. 5.10). Another notable observation was the progressive increase in CDOM absorption (a_g412) from September to October in the surface (0.0975 to 0.2217 m^{-1}) and bottom waters (0.0852 to 0.2435 m^{-1}) (Fig. 5.10). The spectral slope $S_{250-600}$ did not show any significant change in the surface and bottom waters (0.0215 - 0.0213 nm^{-1}), during September 2016. However, a significant decrease in spectral slope was observed during October both at the surface (0.0195 nm^{-1}) and bottom (0.0171 nm^{-1}). On the other hand, an increase in $S_{250-600}$ was observed during the end of October in the bottom waters (0.0204 nm^{-1}), while no such change was observed in the surface waters (0.0198 nm^{-1}). The $S_{275-295}$ was low in the bottom waters and decreased from September (0.0250 nm^{-1}) to October (0.0246 nm^{-1}).

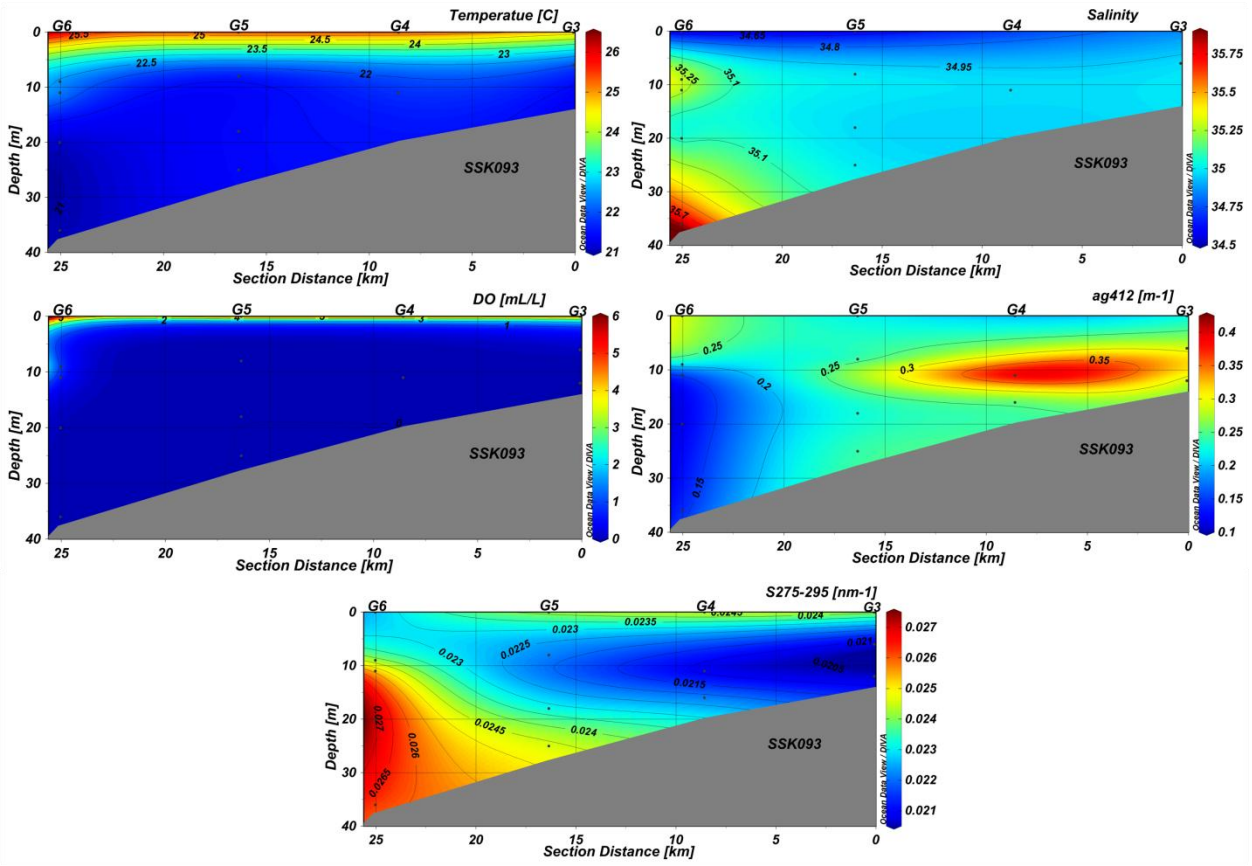

Figure 5.9: Spatial variation of physicochemical parameters, CDOM absorption, and spectral slope along the Goa transect during the late SWM (October 2016).

CDOM absorption was higher at the nearshore station, while it decreased offshore. A gradual decrease of DO was also seen from hypoxic during September (0.109 mL/L) to anoxic by the end of October (Fig. 5.10). An increase of CDOM in the bottom waters was seen during September of 2016 and 2018 (Figs 5.8, 5.9, and 5.10). In most of the cases, the bottom CDOM values were higher than the surface suggesting a linkage between low oxygen conditions and higher CDOM absorption. High CDOM in the bottom waters was associated with hypoxic, suboxic, or anoxic conditions. A weak positive correlation was observed with a_g412 and apparent oxygen utilization (AOU) ($R^2 = 0.55$) (Fig. 5.11a). Also, C1 showed a good positive correlation with AOU ($R^2 = 0.64$) (Fig. 5.11b).

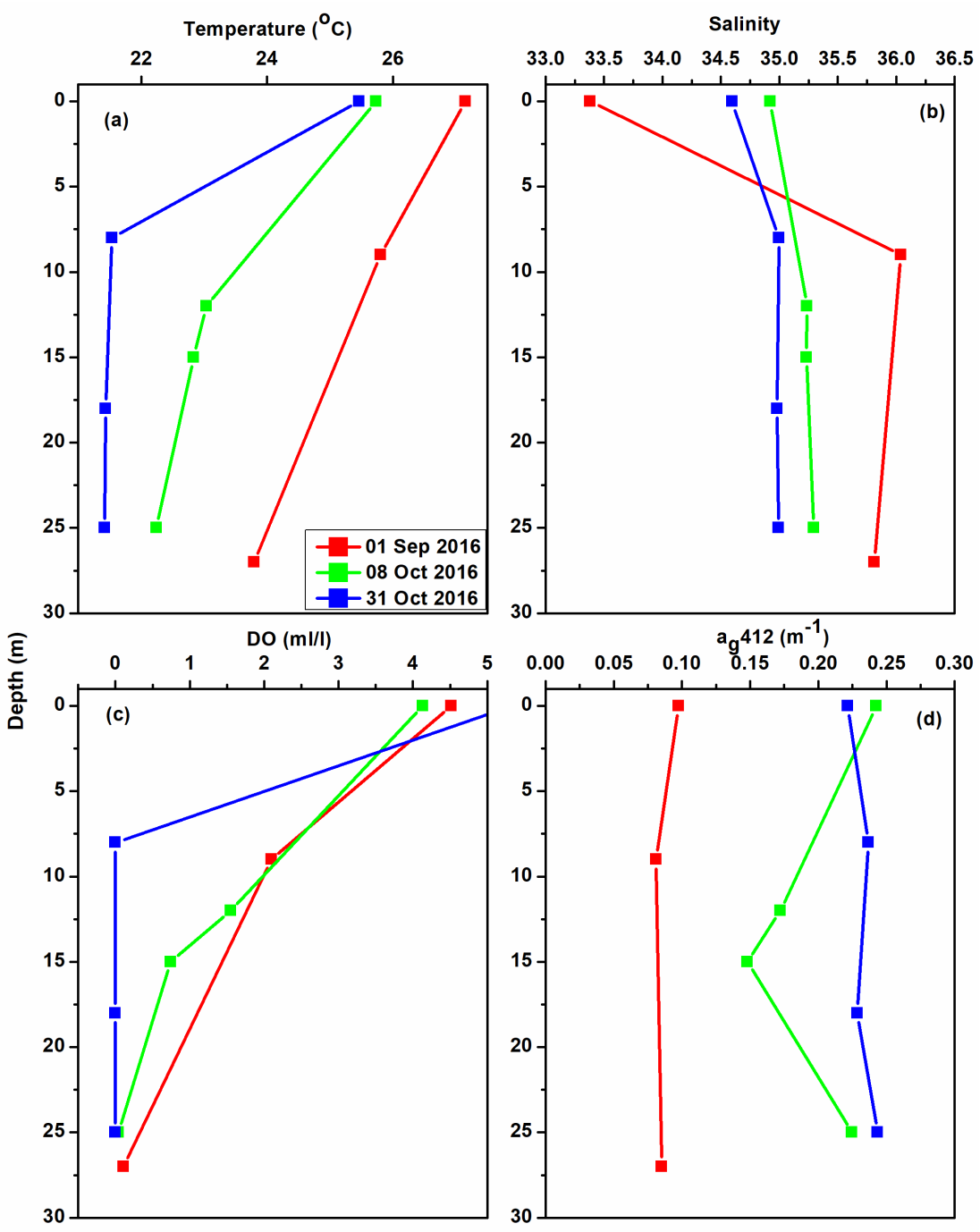

Figure 5.10: Vertical profiles of temperature, salinity, DO, and CDOM absorption (a_g412 m^{-1}) at the coastal time-series station (G5) during the seasonal hypoxia (September-October) 2016.

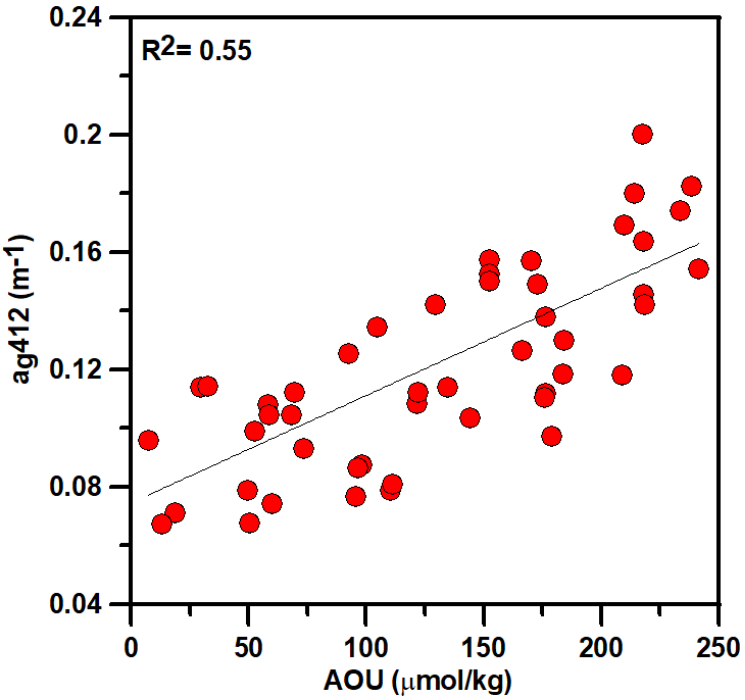

Figure 5.11a: Correlation between AOU (µmol/kg) and CDOM absorption (a_g412 m^{-1}).

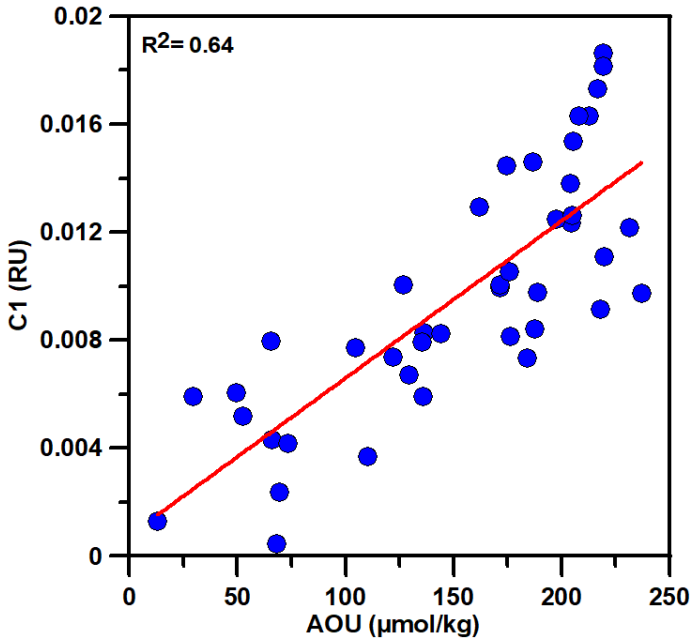

Figure 5.11b: Correlation between AOU and C1 (humic-like) FDOM.

5.4.4 Characterization of CDOM during the SWM and seasonal hypoxia: Statistical approach

Principal component analysis (PCA) was used to classify waters at varying levels of oxygen during the SWM. PCA was performed on 10 variables (temperature, salinity, DO, AOU, a_g412, spectral slopes at varying ranges ($S_{250-600}$, $S_{275-295}$, $S_{350-400}$, $S_{280-400}$) and S_R) collected during the SWM. This analysis extracted three components, which explained 76.5% of the variability in the data set (PC1 - 33.4%, PC2 - 25.4%, and PC3 - 17.7%). The results are presented in terms of component plots and sample score plots in Figure 5.12. Temperature (-0.84 component score), DO (-0.83) and ag412 (-0.57) were negatively correlated, while AOU (0.85), salinity (0.71) and $S_{280-400}$ (0.51) were positively correlated to PC1. PC2 was explained by the a_g412 which was negatively correlated (-0.7), while the spectral slopes $S_{250-600}$ (0.65), $S_{275-295}$ (0.58), and DO (0.5) were positively correlated. PC3 was positively related to the slope ratio S_R (0.92) and negatively to $S_{350-400}$ (-0.77). The low oxygenated samples were clustered together with a positive PC1 score and negative PC2 score, while the oxygenated samples were with negative PC1 score and positive PC2 score (Fig. 5.12b).

The samples were also separated on the basis of oxygen into five groups, anoxic (0 mL/l), suboxic (<0.1 >0 mL/L), hypoxic (<1.4 >0.1 mL/L), oxic (< 3.5 >1.4 mL/L) and oxic (>3.5mL/L). Two data points were not considered in this analysis from the oxic category due to the high CDOM absorption from the nearshore stations probably arising from the bottom resuspension. Very high CDOM absorption is evident in the low oxygenated waters with low spectral slopes in this study (Fig. 5.13). One-way ANOVA was also performed on the grouped samples and each group was significantly different from the other based on the CDOM absorption and spectral slopes ($p<0.05$). The statistical details are provided in Table 5.2.

Table 5.2: Statistics of the optical parameters of CDOM at varying levels of oxygen along the Goa transect in 2016 and 2018.

Oxygen concentration (mL/L)	**Mean a_g412 (m^{-1})**	**Mean $S_{250-600}$ (nm^{-1})**	**Mean $S_{275-295}$ (nm^{-1})**
Anoxic, 0	0.262	0.0184	0.0174
Suboxic, <0.1>0	0.167	0.0197	0.0242
Hypoxic ,<1.4>0.1	0.119	0.0168	0.0284
Oxic,<3.5>1.4	0.131	0.0181	0.0262
Oxic, >3.5	0.183	0.0200	0.0278
F value	2.564	2.640	3.624
P value	0.044	0.039	0.009

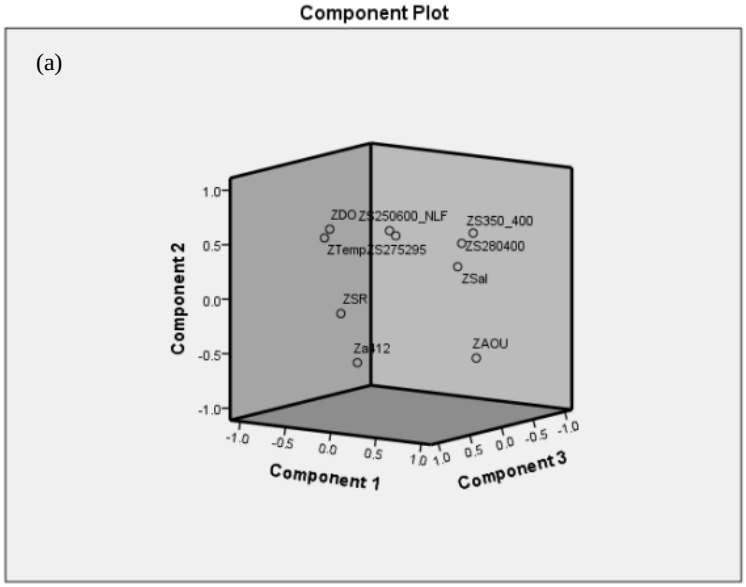

Figure 5.12: (a) The correlation plot of components used in the PCA analysis

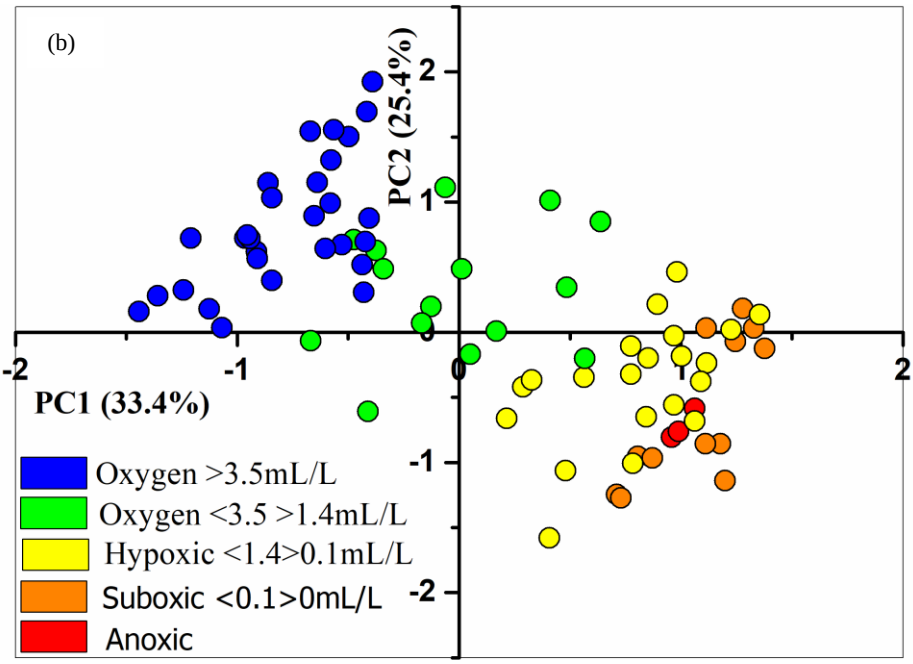

Figure 5.12: (b) the scores of the samples for the first two principal components, PC1 and PC2. The color represents the oxygen concentration of the samples.

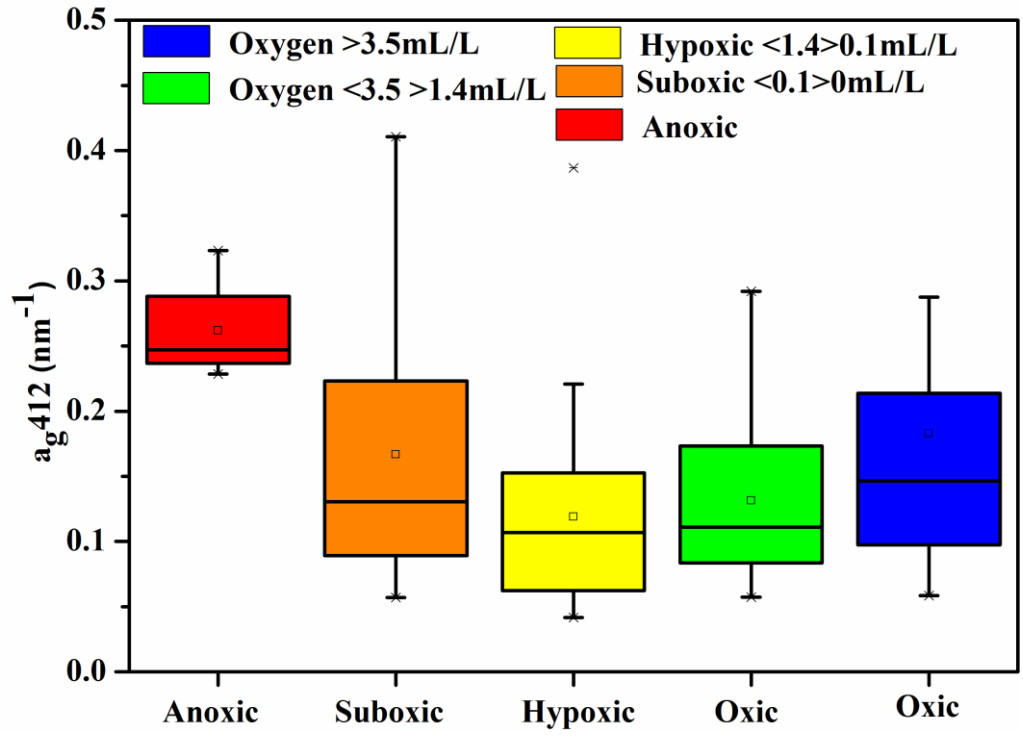

Figure 5.13: Variation of CDOM absorption at different oxygen levels.

5.4.5. Experimental set up under controlled conditions

To understand the CDOM production at varying oxygen levels, an experiment was conducted in amber-colored glass bottles with and without additional organic matter. Bottle A, which had only dissolved organic matter (0.2µ filtered water), did not show much variation in DO concentration (Fig. 5.14). The trend was a decrease in CDOM concentration initially for 21 days (from 0.2608 to 0.1360 m^{-1}) followed by a gradual increase in the latter part of the experiment (up to 0.2221 m^{-1}) though not very significant. The aerated bottle B (0.2µm filtered water) showed an initial CDOM absorption of 0.2608 m^{-1} and did not show much variation throughout the experiment (Fig. 5.14). The bottle C, which was enriched in organic matter and maintained under low oxygen condition, experienced a gradual decrease in DO over time (3.9 to 0.8 mL/L), while the CDOM was nearly constant initially (t_0 = 0.1431 m^{-1}) and increased after 20 days (t_{final} =0.2805 m^{-1}) when the DO was low. The bottle D, which was enriched in organic matter and kept in aerated condition, showed an increase in CDOM absorption over time (t_0= 0.1431m^{-1} and t_{final} = 0.29688 m^{-1}) (Fig. 5.14).

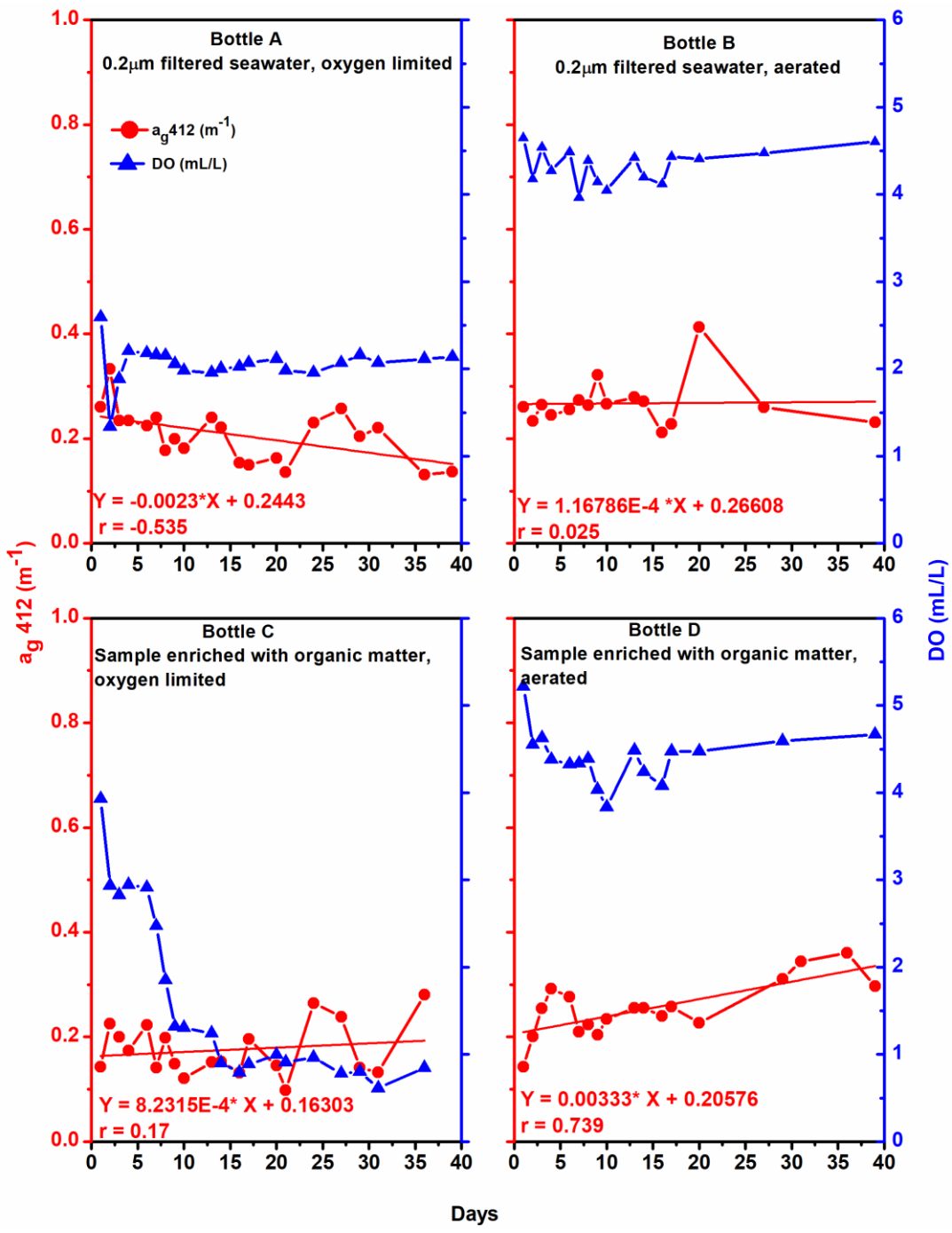

Figure 5.14: Variation of CDOM absorption (ag412 m^{-1}; red) and DO (mL/L; blue) with days during the experiment carried out in the laboratory.

5.5. Discussion

5.5.1 Spatial variability of CDOM along the WCSI during the early SWM

The onset of SWM results in open ocean upwelling beginning from the southern tip of the west coast of India, propagating northwards with time (Madhuprathap et al., 2001; Smitha et al., 2008). During our sampling, signatures of upwelling were observed along the southwest coast of India (10ºN) with low temperature, and low DO in the bottom waters along with high saline waters at the surface (Fig. 5.3). These waters were associated with high CDOM absorption. The moisture-laden strong southwesterly winds blowing over the Indian sub-continent result in heavy precipitation in this region from June to September. Most of the rainfall over the AS occurs during SWM, exceeding 300 cm y^{-1} (Naqvi et al., 2009b). As a result, the AS receives maximum runoff during this period from the perennial rivers and estuaries along the west coast of India. Maximum rainfall and river discharge is reported along the southern coast of India during the SWM months of June and July (Narvekar et al., 2021). This is manifested by the observed low values of salinity at the nearshore stations in our study and was more prominent towards the Karwar and Goa transects (Fig. 5.3). The temperature and salinity were found to increase offshore. The surface DO concentration increased from the south (off Kochi) to the north (off Goa; Fig. 5.3), and the low DO along the Kochi transect could be due to the coastal upwelling.

The CDOM absorption showed a fairly strong negative correlation with salinity ($r = 0.78$, $p < 0.01$), and temperature ($r = 0.5$, $p < 0.05$) in the surface waters along the WCSI during July 2018. A negative correlation was also observed between C2 and salinity ($r = 0.62$, $p < 0.01$); however C1 and C3 didn't show any relation. The negative correlation between salinity and CDOM indicates the conservative mixing of CDOM in the surface waters. Also, based on the sea level anomaly a cold core eddy was located in the study area (between 8º and 15ºN) close to the coast during this time. The negative correlation between temperature and CDOM also points that this cold core eddy could be a probable source in the distribution of surface CDOM in the study region. A negative correlation between FDOM and temperature was observed by Coble et al. (1998) in their study in the AS and attributed it to the upwelling observed during the SWM. Such a correlation between FDOM and temperature was not seen in our study.

In general, high CDOM absorption with low spectral slopes indicates the terrestrial nature of organic matter along the WCSI. This is due to the high runoff received from the perennial rivers along the coast, which is also observed from the low salinity along the

coast. The signatures of humic-like FDOM, arising from the land runoff (terrestrial origin), was also high along the WCSI with the maximum along the coast of Goa (Fig. 5.3) which coincided with higher precipitation and lowest salinity observed during our sampling. A prominent increase in CDOM was observed in the bottom waters of coastal station at all transects, with the maximum at the Goa transect (Figs 5.4 to 5.7). A decreasing trend of the spectral slopes $S_{250\text{-}600}$ and $S_{275\text{-}295}$ was observed in the bottom waters (Figs 5.4 to 5.7). Resuspension of sediments has been considered an important source of DOM to the bottom waters (Boss et al., 2001; Lubben et al., 2009). The burrowing activities of benthos in the oxic bottom waters lead to the resuspension of sediments and hence, the observed high CDOM absorption. The surface offshore waters showed lower CDOM absorption with high spectral slopes at all four transects. The effect of land runoff was not observed at the offshore stations during the early SWM and hence, this could be attributed to the photodegradation of DOM which results in a decrease in CDOM absorption and an increase in spectral slopes in the offshore waters (Figs 5.4 to 5.7).

During the early SWM, signatures of upwelling were seen at the Kochi transect during our sampling. Upwelling-driven high primary productivity and phytoplankton blooms in the Arabian Sea have been reported during the SWM (Prasanna Kumar et al., 2001; Wiggert et al., 2005). An increase in the protein-like fluorescence (C3) in the sub-surface offshore waters of the Kochi transect could be attributed to upwelling-induced autochthonous production. The satellite images obtained for the sampling day also showed high chlorophyll-*a* along the southern tip of India (8-10°N; Fig. 5.15a) suggesting C3 to an autochthonous source.

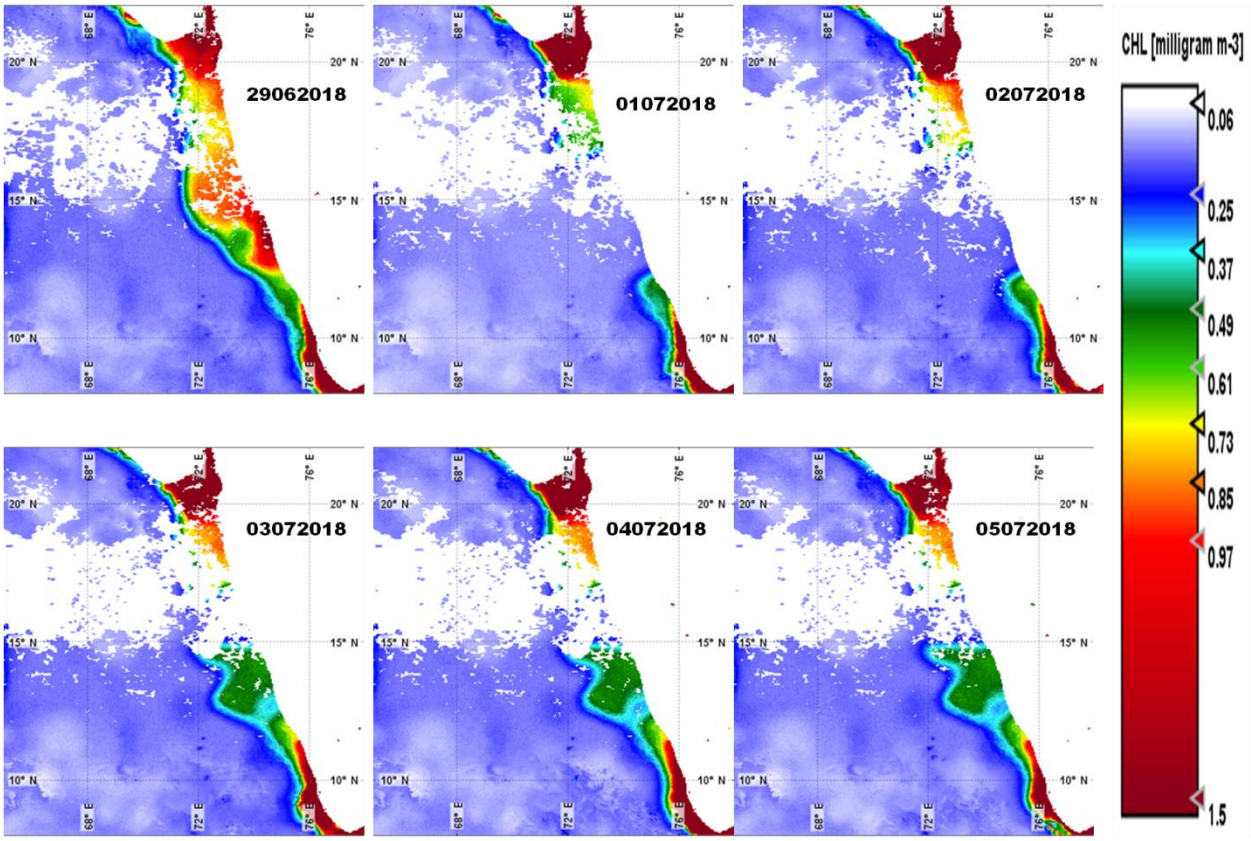

Figure 5.15a: Satellite derived chlorophyll-*a* during sampling period (29th June – 5th July 2018) along the WCSI.

The surface bloom of *Trichodesmium spp* was also observed during our sampling at the M3 station of the Mangalore transect. Blooms of *Trichodesmium* have been reported during the SIM along the west coast of India (Dsilva e al., 2012; Ahmed et al., 2017; Dias et al., 2020b). The CDOM spectra collected from the bloom site had unique absorption with peaks in the UV region due to mycosporine-like amino acids. The CDOM absorption during *Trichodesmium* blooms are detailed in chapter 4. Previous studies on *Trichodesmium* blooms have shown the accumulation of DOM. The increase in the FDOM components with depth at the nearshore stations could be attributed to the production of protein-like and humic-like components reported during *Trichodesmium* blooms. The microbial remineralization of sinking dead cells during the bloom might have resulted in the observed maxima of humic-like components in the sub-surface waters along the transect. The high protein-like fluorescence in the surface and sub-surface waters is probably due to the autochthonous production of DOM.

High surface and bottom CDOM absorption was observed at the nearshore stations of the Karwar transect. Apart from this, high surface (K8) and sub-surface (K13) CDOM

observed in the offshore waters were associated with high humic-like FDOM (C1 and C2) and spectral slopes (Fig. 5.6). This humic-like fluorescence is associated with marine DOM. Very low recent autochthonous production was seen from the low C3 FDOM values along this transect.

The highest values of CDOM and FDOM were recorded along the Goa transect (Fig. 5.7) especially at the nearshore stations with low spectral slopes indicating the high aromaticity of the organic matter. The Goa coast received heavy rainfall during the sampling period, and the resultant land runoff could be one of the reasons for high CDOM and FDOM along this transect. Hypoxic- suboxic waters were seen in the sub-surface depths along the shelf off Goa. CDOM absorption was high at the surface and also at the oxycline (100 - 200 m) at the offshore station G14. The spectral slope was low at this depth which increased towards greater depth.

Humic-like C1 fluorescence showed the maxima in the low oxygenated waters (coinciding with the thermocline and oxycline (Fig. 5.7) suggesting that C1 is produced as a result of aerobic microbial remineralization of particulate organic matter (Hayase and Shinozuka, 1995; Yamashita et al., 2007; Yamashita and Tanoue, 2008; Swan et al., 2009; Nelson et al., 2010; Jørgensen et al., 2011; Tanaka et al., 2014; Catalá et al., 2015; Kim and Kim, 2015). Statistical correlation between humic-like DOM and apparent oxygen utilization (AOU) was used to account for the microbial production (production of FDOM H) in the Pacific and the Indian Ocean (Hayase and Shinozuka, 1995; Yamashita and Tanoue, 2008; Swan et al., 2009; Nelson et al., 2010; Jørgensen et al., 2011; Kim and Kim, 2015). A positive correlation has been observed between C1 and AOU (which is the measure of oxygen utilization by microbes) in the present study (Fig. 5.11a), indicating microbial remineralization as the source of humic-like DOM in the deep waters. Yamashita and Tanoue, (2008) reported that *in-situ* humic-like FDOM production in the deep Pacific Ocean is much larger than the riverine flux. Coble et al. (1998) also observed FDOM maxima in the midwater samples associated with low oxygen, and concluded that AS midwaters have elevated FDOM compared to other areas of the ocean (away from river inflow). The increase in marine humic-like C2 with depth observed in the waters off Goa could be a result of photodegradation at the surface and *in-situ* production by microbial metabolism at deeper waters (Nelson and Siegel, 2013). Similar results have also been observed by Fujita et al. (2010) and Takata et al. (2005) in the East Sea. An increase of

humic-like FDOM components with depth has previously been reported for open ocean waters (Catala et al., 2015 and references therein).

5.5.2. CDOM variation across the Goa transect during the late SWM of 2018

Upwelling was observed along the Goa coast during the late SWM sampling (September) with low temperature, high salinity and low DO waters at the sub-surface. The up-sloping of 24ºC isotherm (an indicator of upwelling; Narvekar et al., 2021) was observed in the present study at the nearshore station, which depicts the presence of upwelled waters along the transect. A cap of low saline waters from the runoff and heavy precipitation during this season prevents the upwelled water from reaching the surface. A high amount of terrestrial CDOM received from the freshwater flux during the SWM is photolabile and undergoes rapid degradation in the presence of sunlight (Omori et al., 2010, 2011), hence low CDOM absorption with high spectral slopes was observed at the surface. Photobleaching of DOM results in an increase in the spectral slopes (Helms et al., 2008), which was observed in the present study along the offshore waters (Fig. 5.8). The negative correlation of temperature with CDOM absorption and FDOM (C1) for the surface waters clearly shows the influence of upwelled waters in the distribution of CDOM and humic-like FDOM. We also hypothesize that one of the reasons for high humic-like component C1 at the nearshore stations is from the advection of humic rich upwelled sub-surface waters (Siegel et al., 2002). C1, C2, and C3 were high at the nearshore stations and decreased offshore (Fig. 5.8). High C3 could be due to high primary productivity due to the presence of nutrient-rich upwelled waters near the coast. This is also observed from the high chlorophyll-*a* during the study period from the satellite image (Fig. 5.15b).

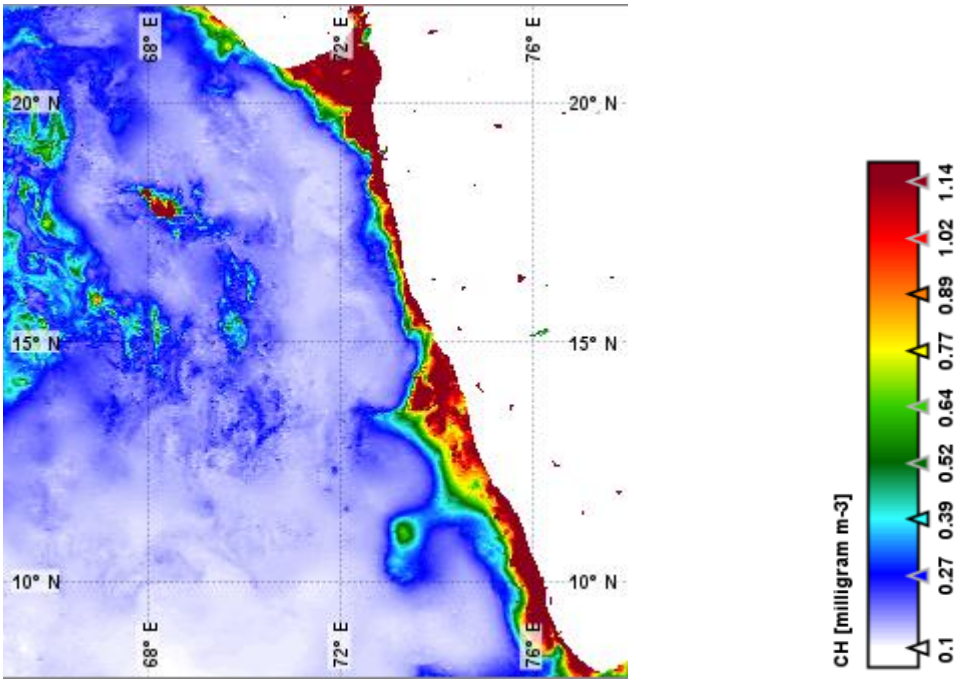

Figure 5.15b: Satellite derived chlorophyll-*a* along the WCSI during the sampling period (20th September 2018).

High CDOM absorption in the bottom waters of station G-6 is probably from the benthic flux. The strong thermocline prevents the exchange of dissolved oxygen, and microbial respiration further reduces the oxygen level in the sub-surface waters, as seen in our study. Few studies reported the release of iron-bound organic matter due to reductive dissolution of Fe(III) to Fe(II) from the sediments to the water column under anoxic conditions (Skoog et al., 1996; Skoog and Arias-Esquivel, 2009; Peter et al., 2016). During the seasonal hypoxia/suboxia, the anoxic sediments would lead to the release of iron oxide-bound and phosphorous-bound organic matter to the overlying water column (Maloney et al., 2005, Scholz et al., 2014; Watson et al., 2018). The iron content in the waters and the sediments off Goa were reported to be high (Naik et al., 2017). This could be another plausible reason for high CDOM absorption in the bottom waters during this period.

5.5.3. CDOM variation at the coastal time series station G5, off Goa

The strong halocline during the late SWM from the freshwater inputs prevents the mixing of the sub-surface upwelled water, which already has low oxygen. Due to biological respiration and microbial remineralization, the oxygen level in the water column deteriorates further. This progressive decrease in DO is observed in our study from September to October (Fig. 5.10). High autochthonous production might have led to high CDOM absorption in the surface waters, which was also supported by a high protein-like component in the surface waters. The upwelled waters from the sub-surface seem to be enriched with humic-like DOM, and the progressive increase of CDOM during October is probably from the benthic flux. In our study, high CDOM absorption was associated with low values of $S_{250\text{-}600}$, indicating high molecular weight DOM in the bottom waters. Mining of iron and manganese ores is an important industry in Goa, and the ore is being transported to various destinations via waterways. High concentrations of iron in sediments have been reported in the Goan estuaries (Kamat and Sankaranarayanan, 1975; Naik et al., 2017). During the SWM, there are chances of this iron being transported from the banks of the estuaries to the adjoining coastal waters. Earlier, Kritzberg et al. (2014) has shown that iron can be transported to open waters by its association with DOM. Co-precipitation of DOM and iron oxides is a well-perceived fact (Skoog et al., 1996; Lalonde et al., 2012; Riedel et al., 2013). Lalonde et al. (2012) observed that iron oxides and DOM precipitates biologically available fractions, especially protein-like DOM, more preferably.

Trichodesmium and *Noctiluca* blooms have been observed during the SIM along the coastal waters of Goa (Dias et al., 2020b). The degradation of blooms supplies a copious amount of organic matter to the sediments. This sedimented organic matter is probably released back to the bottom waters during seasonal hypoxia. Hence, the build-up of CDOM was observed when the bottom waters experienced low oxygen condition (Figs 5.7, 5.8, and 5.9).

5.5.4 Relationship between biogeochemical variables and optical parameters

A significant but weak positive relationship between salinity and spectral slopes $S_{250\text{-}600}$ ($r = 0.37$, $p<0.01$) and $S_{275\text{-}295}$ ($r = 0.39$, $p<0.01$) was observed in the oxygenated waters (DO >1.4 mL/L), whereas such a relationship was not observed in the low oxygenated waters (DO <1.4 mL/L). It is evident from figure 5.16 that at very high salinity and with increase in distance from the coast (> 60 km), the spectral slope values are very high indicating the

transformed DOM by the process of photobleaching as reported earlier (Vodacek et al., 1997; Del Castillo et al., 1999). However, the values of spectral slope are lower even at high salinity but close to the coast (<60 km), indicating the terrestrial nature of DOM (Fig. 5.16). A significant weak positive relationship between temperature and CDOM absorption ($r = 0.26$, $p<0.05$) is also noticed in the low oxygenated waters, implying high CDOM in the upwelled waters.

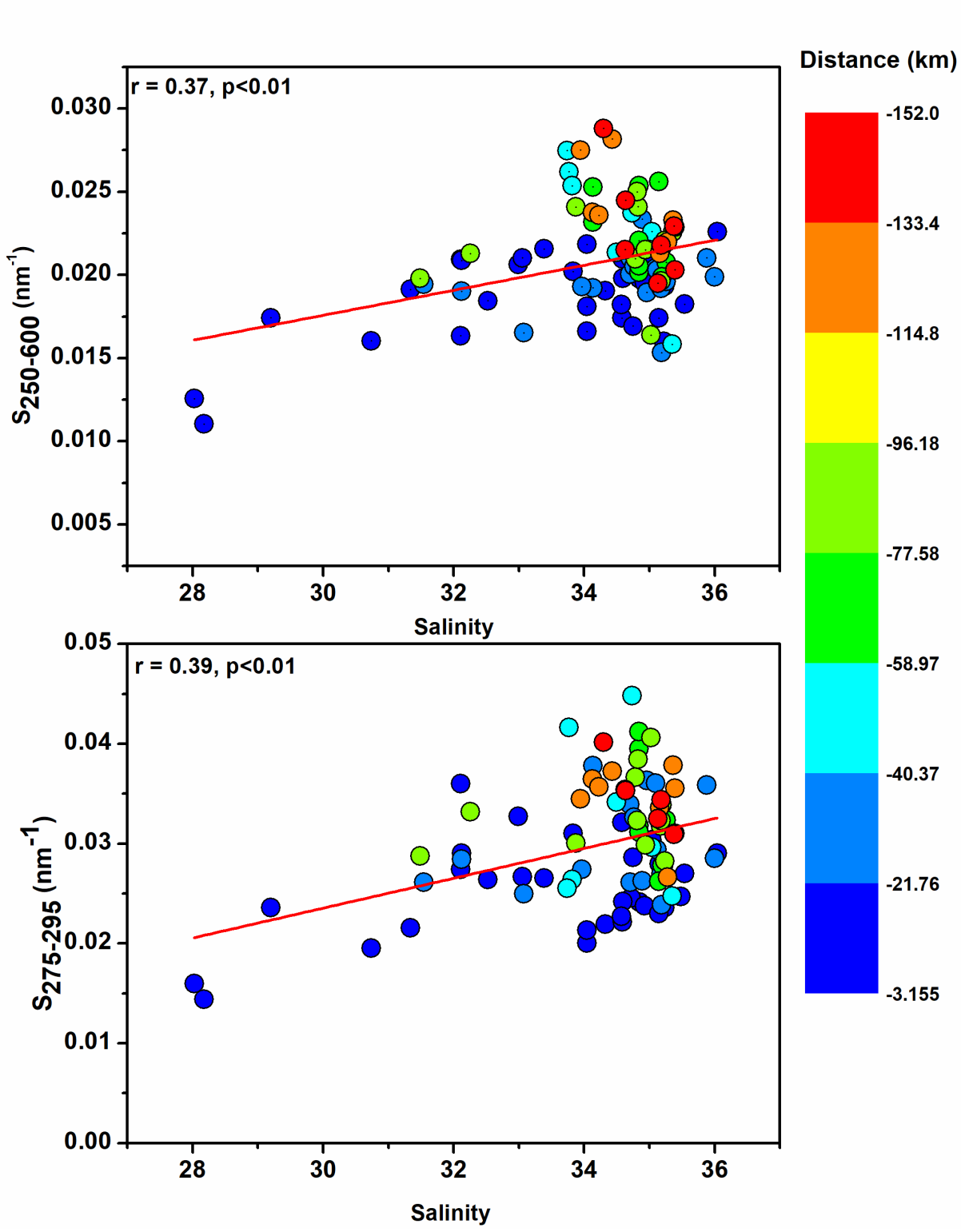

Figure 5.16: The relationship between salinity and spectral slopes $S_{250\text{-}600}$ and $S_{275\text{-}295}$ in the oxygenated waters. The z axis signifies the distance from the coast.

A significant negative correlation was observed between CDOM absorption (a_g412) and spectral slopes $S_{250\text{-}600}$ (r = -0.57 oxygen rich and r = -0.543 in oxygen poor waters,

$p<0.01$; Fig. 5.17a), $S_{275-295}$ ($r = -0.552$ oxygen rich and $r = -0.582$ oxygen poor, $p<0.01$, Fig. 5.17b) and $S_{350-400}$ ($r = -0.42$ oxygen rich and $r = 0.36$ oxygen poor, $p<0.01$, Fig. 5.17c), wherein spectral slope decreases with increase in CDOM absorption. A notable observation in the present study is a significant difference in the relation between spectral slope and a_g412 specifically in the broad spectral range $S_{250-600}$ for oxygenated (>1.4 mL/L, $r = -0.57$) and low oxygen (<1.4 mL/L, $r = -0.54$) waters (Fig. 5.17a). A similar relationship is also observed between $S_{275-295}$ and a_g412 (Fig. 5.17b). Experimental studies carried out by Moran et al. (2000) and Helms et al. (2008) revealed that microbial activities result in a decrease in spectral slope, while the vice-versa is observed for the effect of photobleaching. Also, a significant negative correlation was observed between AOU and spectral slope $S_{250-600}$ ($r = -0.40$, $p<0.01$) along the WCSI (Fig. 5.17d) in the present study, indicating the new production of CDOM via microbial remineralisation processes, which results in decrease in spectral slope. Similar results were also reported by Swan et al. (2009) in the Pacific below 300m. A significant difference in the spectral slope $S_{250-600}$ is observed between the anoxic, suboxic, hypoxic and oxygenated waters (ANOVA, $F= 6.846$, $p<0.01$). This result indicate that the source of CDOM in oxygenated waters and that in low oxygenated waters is different and $S_{250-600}$ can be used to differentiate the origin of DOM. A good correlation is also observed between $S_{250-600}$ and $S_{275-295}$ specifically in the oxygenated waters ($r= 0.7$) while this relationship is weak and poor in low oxygenated waters ($r = 0.3$). This indicates that $S_{275-295}$ is a very good tracer for terrestrial signatures (lignin), as reported earlier by Fichot and Benner, (2012). Previous studies reported that terrestrial material absorption is dominated by lignin, which absorbs below 300 nm (Mcknight and Aiken, 1998; Spencer et al., 2008).

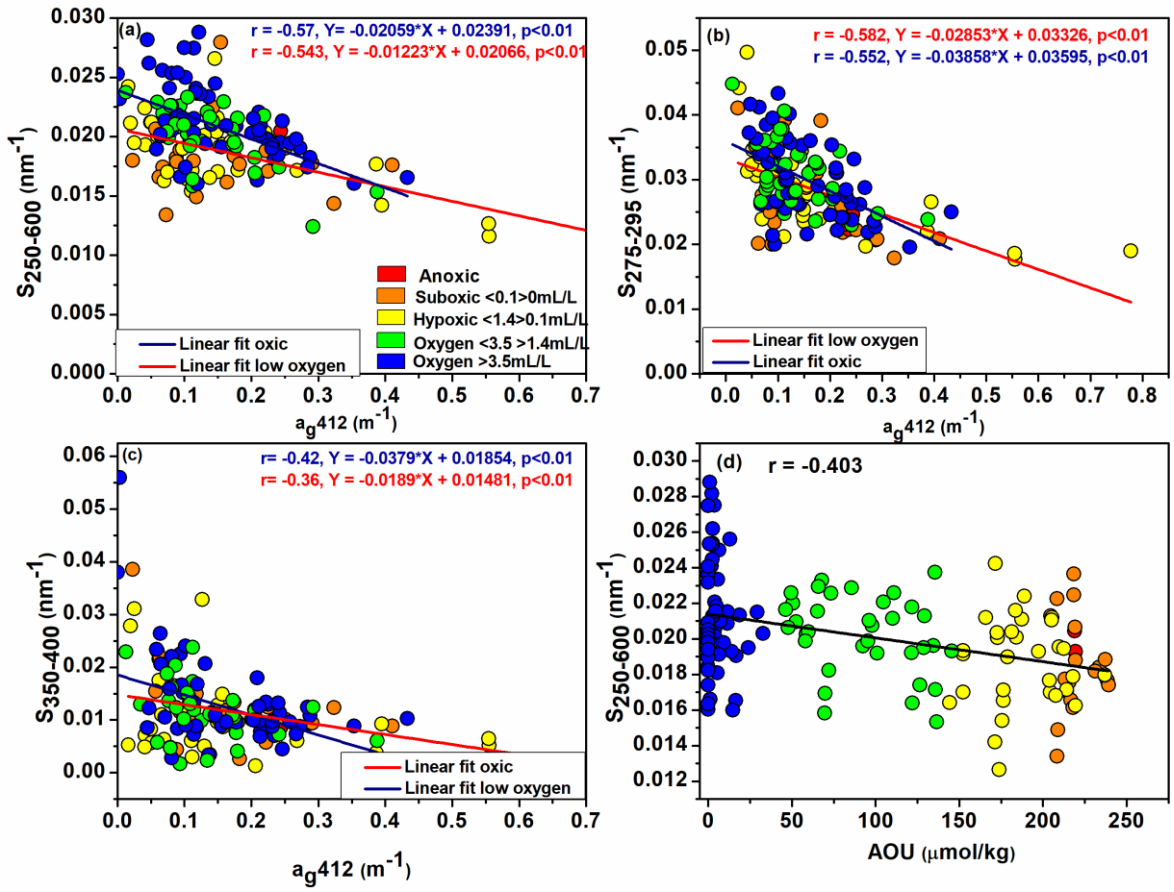

Figure 5.17: The relationship between a_g412 (m^{-1}) and spectral slopes a) $S_{250-600}$, b) $S_{275-295}$ and c) $S_{350-400}$. d) Correlation between AOU and spectral slope $S_{250-600}$ (nm^{-1}). The colors represent varying levels of oxygen.

5.5.5. Characterization of CDOM

The principal component analysis was used to investigate the link between the CDOM variables and the physicochemial parameters. Figure 5.12 clearly shows the distribution of samples based on the CDOM variables and DO. The samples with low oxygen concentration are having positive PC1 values and negative PC2 values, while vice versa is observed for the oxygenated samples. Since PC2 is described by the CDOM absorption and spectral slopes of CDOM, component 2 can be used to characterize the source of CDOM, while PC1 separates the samples based on the physical parameters. Figure 5.13 clearly shows that maximum CDOM absorption occurs in low oxygenated (anoxic and suboxic) waters as compared to well oxygenated waters. The statistical details of these are given in table 5.2. Two values of CDOM absorption were not considered in the analysis as the values were very high. These were from the bottom waters of G3 and G5 (off Goa transect during July 2018) when the oxygen level was <3.5mL/L. The high CDOM

absorption may be attributed to the bottom resuspension. The oxic waters showed a moderately lower spectral slope $S_{250-600}$ (0.018 nm^{-1}) characteristic of a terrestrial source of OM, while the hypoxic waters had the least spectral slopes (0.016 nm^{-1}) which can be attributed to the release of soil organic matter. The suboxic and anoxic waters had the highest $S_{250-600}$ indicating the transformation of the OM due to microbial respiration, wherein the oxygen is utilized for the degradation, thereby leading to a decrease of oxygen in the water. This can be ascertained from the good correlation between CDOM and AOU (Fig. 5.11). The $S_{275-295}$ also seems to be the lowest in the suboxic and anoxic waters, suggesting the dominance of low molecular weight DOM, brought about by microbial transformations.

5.5.6. Insights from the laboratory experiments

The experiment carried out in the laboratory sheds some light on the CDOM production in low oxygenated waters. Nearly constant DO values in bottle A suggest no utilization of oxygen as the water was filtered (0.2µm) and organic matter was limited (Fig. 5.14). In general, a gradual decrease in CDOM absorption is evident with time from the linear regression model (r = - 0.5) in bottle A. While bottle B under aerated condition didn't show much variation, and a slight decrease in CDOM absorption was observed towards the end of the experiment, the change in CDOM over time was marginal with a very poor correlation (r = 0.02; Fig. 5.14). Chin et al. (1998) determined that transparent exopolymeric particles (TEP) are formed from filtered precursors (<0.2µm) under laboratory conditions and can cause aggregation of DOM and is a probable sink of CDOM. We hypothesize that the decrease in CDOM observed in bottle A in the closed environment is probably due to the flocculation of CDOM by TEP. This removal is not observed in bottle B throughout the experiment and may be due to the continuous aeration of the bottle, which would have kept the DOM in suspension. On the other hand, a decrease in DO in bottle C from day 1 indicated that microbial respiration consumes the DO and probably the labile organic matter for metabolism, and hence no change in the CDOM absorption was detected during the initial phase of the experiment. As the DO started decreasing, there was an increase in CDOM absorption, which indicates that CDOM starts building up when there is sufficient organic matter and DO is low. This increase in CDOM absorption is very marginal with a very weak positive linear relation over time (r = 0.17) with a very small slope value of the linear regression line (8.23×10^{-4}) indicating a small change over time. The bottles being amber-colored and kept in the dark,

the effect of photodegradation would have been negligible. Microbes seem to be the major player for CDOM production in this condition. Our experiment shows that there is a link between CDOM production by microbes during low oxygen conditions, as also seen in the coastal waters of Goa during our sampling. Bottle D showed a moderate increase in CDOM till the end of the experiment, as also observed from the linear regression line (r = 0.73). This increase was probably due to the presence of additional organic matter along with microorganisms and sufficient oxygen in the system. This experiment clearly shows that organic matter is required for the production of CDOM, and the production will occur at a faster pace in the presence of oxygen (Fig. 5.14).

5.6. Conclusions

In the present study, the CDOM variation along the WCSI during the SWM and seasonal hypoxia was examined. High CDOM absorption with low spectral slopes and high humic-like fluorescence (C1) was observed at the nearshore stations during the SWM, which could be attributed to the riverine flux of terrestrial organic matter. The sub-surface waters were hypoxic- suboxic at most of the transects. Humic-like fluorescence C1 was found to be maximum near the coast (terrestrial origin) and also at the offshore stations at deeper depths may be due to microbial action. C1 fluorescence was also high in the low oxygenated waters off Goa during July, possibly due to microbial origin. A good correlation was observed between C1 and AOU and between CDOM and AOU, which shows that CDOM is mainly produced during microbial remineralization. Accumulation of CDOM in the bottom waters during the seasonal hypoxia along the Goa transect is probably due to the benthic flux (release of iron-oxides bound organic matter to the overlying water column). A significant difference in the composition of CDOM (specifically, $S_{250\text{-}600}$) was observed between the oxygen-rich and low oxygenated waters, and hence it can be used to differentiate the source of CDOM. Based on CDOM and oxygen characteristics, the waters were classified using PCA. Our laboratory experiment also shed light on CDOM production and utilization of oxygen when there is enough organic matter in the system; the production occurs in both oxygenated and O_2 limited environments, but it occurs at a much slower pace in the latter.

Chapter 6

Summary, Future Work, and Recommendations

Summary, Future Work, and Recommendations

6.1. Summary

The coastal waters are interlinked to several ecosystems like the estuaries, rivers, wetlands, etc., and hence form an important conduit for the transport of terrestrial organic carbon to the ocean. Additionally, the estuaries and the coastal waters are the storehouses for the largest reservoir of carbon on earth arising from either terrestrial or marine inputs. In this study, the seasonal variations of CDOM, an optically active fraction of DOM were studied for the coastal and estuarine waters of Goa. Spatial and temporal variations in CDOM absorption were evident with changing environmental conditions, and the highest CDOM absorption was recorded during the SWM and SIM in the estuarine and coastal waters. A significant difference in the quality and quantity of CDOM (absorption and spectral slope) were also observed seasonally and spatially ($p<0.05$) for these waters with the estuarine waters showing two-fold higher CDOM absorption than the coastal waters. Terrigenous DOM contributed to high CDOM during the SWM when the freshwater inflow from the watersheds of the estuaries was high, while autochthonous sources, inputs from mangroves, and anthropogenic activities contributed to high CDOM during the SIM. The longer residence time of water during the non-monsoon season favors the accumulation of phytoplankton in the estuary, contributing significantly as a source of CDOM. Physical processes in the estuaries control the CDOM variations during the monsoon, while biogeochemical processes are responsible for the observed CDOM variability during the non-monsoon season. The PCA analysis helped in differentiating the sources of DOM based on the CDOM absorption and the spectral slopes for the coastal and estuarine waters. The coastal waters had positive PC1 and PC2 scores, while the estuarine waters had negative PC1 and PC2 scores. The samples during non-monsoon clustered together indicating the dominant autochthonous source, while samples during monsoon clustered together indicating the terrestrial nature of DOM. A prominent non-conservative mixing behavior of CDOM was observed in the coastal and estuarine waters of Goa with a land to sea decreasing trend indicating a definite terrestrial influence. Large additions of CDOM were observed in the mid-salinity regions of the estuary, which showed the maximum deviations from the theoretical mixing line. These regions lie very close to the most urbanized regions and have large patches of mangroves and are prone to anthropogenic activities such as pleasure cruises, shipbuilding, treated sewage discharge, fish processing

units, etc. During FIM conservative mixing was observed in the estuaries. The apparent loss of CDOM was observed at very low salinities in the estuaries and very high salinities in the coastal waters during the SWM and non-monsoon seasons, respectively. The loss of CDOM at low salinities is attributed to the adsorptive removal by sediments and flocculation owing to the high aromatic content of DOM. The removal in the coastal waters at very high salinities during the non-monsoon season is attributed to photobleaching, which was the utmost during the SIM with high spectral slope ($S_{275-295}$) values and S_R, resulting in the penetration of UV light to greater depths which were evident from the K_d350 values. It is observed from the present study that CDOM modulates the spectral quality of underwater light, with the maximum light penetration occurring at 570 nm in the estuaries which are dominated by CDOM and detritus, while the maximum light penetration occurs at 540 nm in the coastal waters dominated by CDOM. In short, the coastal and estuarine waters are dynamic having a distinct seasonality in CDOM variations with the environmental forcing playing an important role in driving its composition.

One of the important sources of CDOM is the autochthonous production resulting from phytoplankton exudation, cell lysis, passive leakage, and sloppy feeding (Nagata, 2000; Van den Meersche et al., 2004) during the non-monsoon season in the waters of Goa. A thorough study from 2014 - 2018 has been undertaken on the CDOM produced during the phytoplankton blooms, especially *Trichodesmium* which was observed seasonally during the SIM in the coastal waters. CDOM absorption follows the exponential decreasing model without any peaks due to the presence of a complex mixture of compounds in CDOM with superimposed absorption spectra. Unlike the usually known fact, CDOM produced during the *Trichodesmium* bloom had distinct absorption peaks in the UV (330 nm and shoulder at 360 nm) due to Mycosporine-like amino acids, and in the visible regions due to phycobiliproteins (495-497 phycourobilin; 542-547 phycoerythrobilin; 614-618 phycocyanin). Mycosporine-like amino acids are produced by *Trichodesmium* and released in the water to protect themselves from the harmful UV radiations, while phycobiliproteins are water-soluble diagnostic pigments present in cyanobacteria. The surface bloom regions were characterized with high CDOM absorption as compared to the non-bloom station. In this study, an attempt has been made to differentiate the stages of bloom into growth and senescence phases. CDOM absorption was low and there was no leaching of phycobiliprotein pigments in water during the growth phase, while the senescence phase was marked with high CDOM absorption and leaching of phycobiliproteins in the water.

From earlier studies, it is clear that the growth of the *Trichodesmium* takes place in the sub-surface waters and a thick surface mat is formed mostly during the declining phase (Capone et al., 1998; Bell et al., 2005; Mohanty et al., 2010; Jyothibabu et al., 2017). FDOM studies revealed the presence of 2 humic-like, and 1 protein-like, fluorescence in the bloom samples. The presence of humic-like substances in DOM produced by phytoplankton is also evident in this study which was previously assumed to originate from terrestrial source. This further corroborates that humic-like fluorescence observed during bloom could be directly linked to autochthonous production and microbial transformation. The humic-like component (C1) observed in this study was linked to the degradation product of tetrapyrroles, and the other (C2) was similar to the marine humic-like component. The protein-like component resembled tryptophan-like amino acid and is an indicator of recent autochthonous production. The fluorescence index (FI) which is an indicator of freshly produced DOM was very high (~ 3) at the *Trichodesmium* bloom stations compared with the typical range of 1.2 – 1.8 observed for the non-bloom region. Experimental studies were conducted on the bloom water samples to understand the CDOM degradation over time when exposed to solar radiation. The results of the experimental studies shed light on the important role of photo- and bacterial- degradation for the decomposition of organic matter. The present study showed that *Trichodesmium* blooms build up large pools of organic carbon and play an important role in the DOM cycling of the coastal waters.

The Arabian Sea is known to host one of the world's largest and most intense perennial OMZ in the world. In addition, the WCSI experience natural oxygen deficiency following the seasonal upwelling during the late SWM. Though seasonal hypoxia of varying intensity is observed in the coastal waters of Goa and along the WCSI, there are no reports on the CDOM variation and its composition during this season. Hence, the WCSI was sampled during the beginning of upwelling in July 2018, and the coastal waters along the Goa transect were monitored during the late SWM of 2016 and 2018. During the early SWM high CDOM with low spectral slopes was observed at the nearshore stations along the WCSI indicating the terrestrial nature of DOM from the land runoff. An increase in CDOM was observed towards the bottom and coincided with hypoxic or sub-oxic conditions. Three FDOM components were identified, and two of which were humic-like with long wavelength emissions, while the third one was protein-like. The humic-like (C1) component had maximum fluorescence in the sub-surface low oxygenated waters off Goa,

suggesting that C1 is produced as a result of aerobic microbial remineralization of particulate organic matter. Also, a positive correlation between C1 and apparent oxygen utilization (AOU) was observed in the sub-surface waters along the WCSI, indicating the role of microbial respiration for CDOM production. A good correlation was also observed between CDOM and AOU, indicating the *in-situ* production of CDOM.

Seasonal upwelling was evident along the Goa transect as seen from the 24ºC isotherm during the late SWM (September) and the sub-surface upwelled waters were hypoxic and rich in humic-like DOM. The CaTS time-series station, G5 witnessed a gradual decrease in oxygen concentration (from hypoxic to anoxic) along with an increase in CDOM until October. During suboxic and especially anoxic condition, high CDOM absorption with low spectral slopes was observed and the difference was statistically significant ($p<0.05$) from the oxygenated waters. The increase in CDOM in the bottom low oxygenated waters is attributed to the benthic flux, and release of phosphorus and iron bound organic matter from the sediments to the overlying water column. PCA classified the waters based on the physico-chemical and CDOM characteristics, with oxygenated waters having negative PC1 and positive PC2 scores, and vice versa for low oxygenated samples. In addition, an experiment was also conducted to study the CDOM at varying levels of oxygen and organic matter. Laboratory experiments conducted shed light on the production of CDOM in low oxygenated waters with sufficient organic matter. This study gives insight into the cycling of DOM under varying oxygen conditions prevailing in these waters.

The present study generated the baseline data of CDOM for the coastal and estuarine waters of Goa, and hence the impact of any natural and anthropogenic effects on the CDOM variation in this region can be assessed. In a recent study carried out by Dias et al. (2021) in the Mandovi Estuary, a decrease in CDOM absorption was reported in the mid-stream regions of the estuary during the COVID-19 imposed lockdown. The observation during May 2020 in the estuary was compared with the previous data and the decrease in CDOM was attributed to the reduction in the anthropogenic activities during the lockdown.

6.2. Limitations

Some of the limitations of the present study are listed below.

The sampling undertaken during present study was coarse with regards to time, space and depth. A better understanding of the CDOM could have been possible if the measurements

were carried out more often with more stations and at fine depth intervals. The sampling stations were selected based on the results of the earlier studies carried out in these waters. With the availability of high resolution (10 m) Sentinel -2 satellite data in the estuaries, various micro features such as pockets of very high CDOM are evident. The satellite images will help in a better understanding of the CDOM in these estuaries.

Measuring *in-situ* depth profiles of CDOM spectra at fine depth intervals will provide a lot more information which can be achieved using filters on the *in-situ* absorption measuring instruments with reflecting tube methods such as AC-9 and ACS (WeTLabs) (Dall'Olmo et al., 2017) and Point Source Integrating Cavity Absorption Meters (PSICAM) (Röttgers and Doerffer, 2007). Presently, the method adopted for the measurements of EEM spectra is based on the analysis of water samples using spectrofluorometers in the laboratory. Storage and handling of water samples are critical issues. Recently, instruments like the Underwater mass spectrometry (UMS) have been developed to measure EEM spectra *in-situ* in their natural environments (Carstea et al., 2020; Zielinski et al., 2018) with better capabilities and measuring more parameters including dissolved atmospheric gases, hydrocarbons, and organic compounds (Chua et al., 2016). However, the *in-situ* instruments need to improve on the limit of detection, sensitivity, signal-to-noise ratio (SNR), calibrations, minimizing various errors from external environmental factors such as biofouling, particles, bubbles, temperature, pH, and others.

6.3. Future work

It is proposed to use multiple methods including traditional techniques using a spectrophotometer and spectral fluorometer, and the recent methods using stable isotopes, ultra high resolution mass spectrometry, Fourier transform ion cyclotron resonance mass spectrometry (FT ICR-MS), nuclear magnetic resonance (NMR) to extract more accurate information on the abundance, chemical structure, composition, and sources of CDOM (Zhang et al., 2021).

It is hypothesized in the present study that the benthic flux and release of iron and phosphorous bound organic matter during anoxic condition are the probable sources of CDOM in the low oxygenated waters, which needs to be addressed in detail.

In recent years Earth system models are used for climate projections studies, which mostly rely on the chlorophyll *a* concentration as the dominant absorption in water (Morel et al., 1989; Manizza et al., 2005). From the present study carried out on the contribution of

optically active substances to the total absorption, it is evident that CDOM and colored detrital matter (CDM) dominate the absorption of light in the coastal and estuarine waters, respectively; and hence both need to be incorporated in the models for better predictions, especially in the coastal and estuarine waters.

European space agency satellite, Sentinel-2 gives very good resolution up to 10m and is very useful in mapping the estuarine waters. NASA's PACE (Plankton Aerosol Cloud and Ocean Ecosystem) satellite which is supposed to be launched in 2023 will have bands ranging from UV to visible. This will be the first ocean color sensor with bands in the UV range to study the CDOM. With the advancement in ocean color satellites, there is a need for refinement of existing ocean color algorithms to derive various ocean color products with great accuracy. There is a need for a robust algorithm to derive the spectral absorption of CDOM for all the water types.

A very good relationship between CDOM and DOC are reported in the coastal waters (Vodacek et al., 1997; Ferrari, 2000; Fichot and Bernner, 2011 and 2012; Brezonik et al., 2015; Massicotte et al., 2017; Song et al., 2017; Griffin et al., 2018; Cao et al., 2018), however this needs to be investigated for the study region. Though CDOM has been used to derive DOC and TOC at a regional level, a universal algorithm for all water types needs to be developed (Li and Hur, 2017).

Studies on linkages of CDOM with different physical (radiant heating, upwelling), biological (grazing, phytoplankton functional type, phytoplankton size class), and chemical (chemical composition of CDOM, interaction with metals) settings need to be carried out.

Appendix

Appendix 1.1: (a) The sampling locations in the Mandovi (magenta), Zuari estuaries (red), and the Cumbarjua canal (black) during the NEM of 2020-21, (b) represents the enlarged view of the sampling locations in the Mandovi Estuary, (c) represents the enlarged view of the sampling locations in the Cumbarjua Canal, and (d) represents the enlarged view of the sampling locations in the Zuari Estuary.

Appendix 1.2: Spectral profiles of CDOM variations in the coastal (a - c) and estuarine waters (d - g) on a seasonal basis. Spectral profiles of rain water samples collected during 2015-16 are shown in h. The thick red line for the coastal and rainwater spectra indicates the average of all the values. The Mandovi Estuary is represented in green, while the Zuari Estuary in blue and the average of the spectra are shown in magenta and red colour respectively. Please note that the Y-axis for coastal and estaurine samples are different.

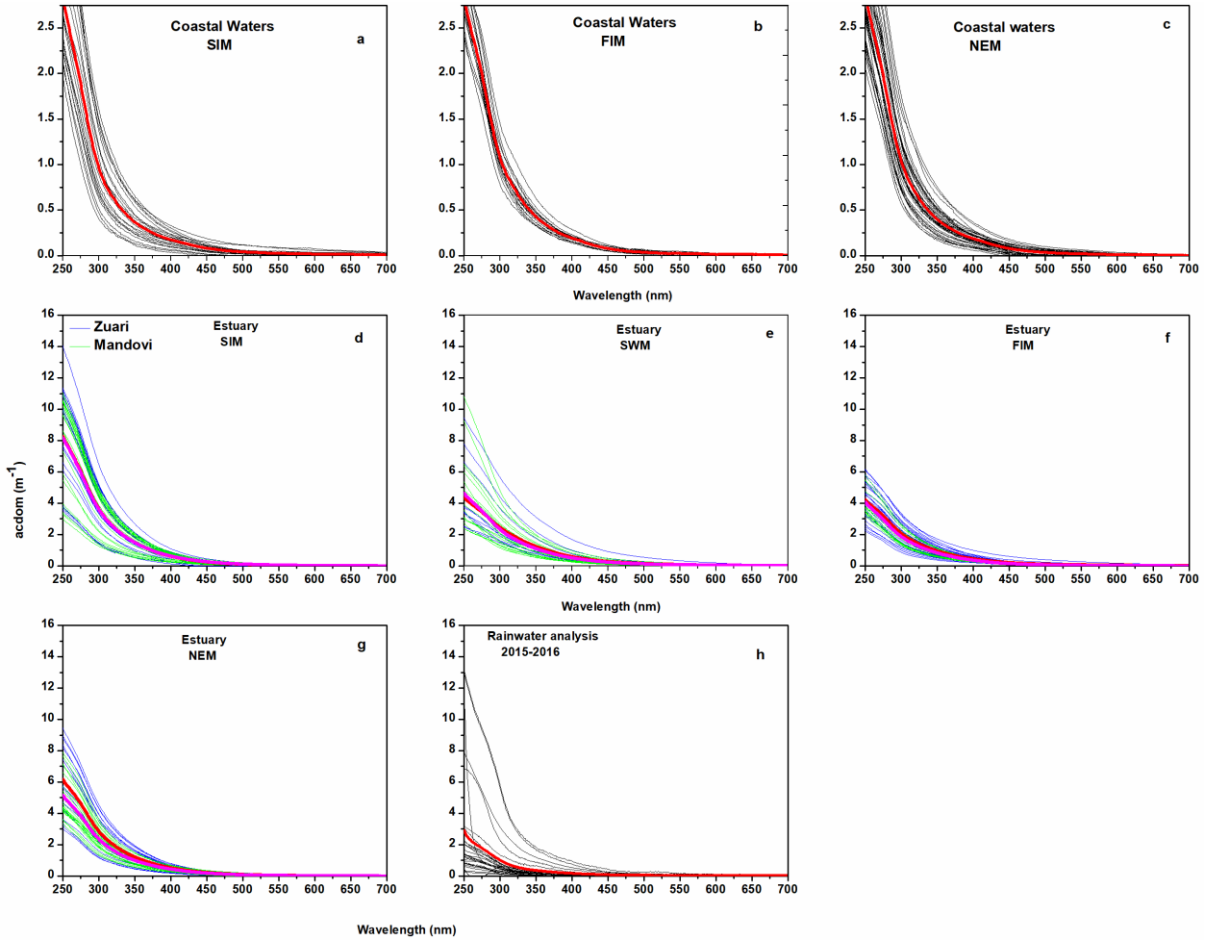

Appendix 1.3: Relationship between daily average rainfall (mm) over the Goa region and CDOM absorption a_g412 (m^{-1}) in the Mandovi and Zuari estuaries.

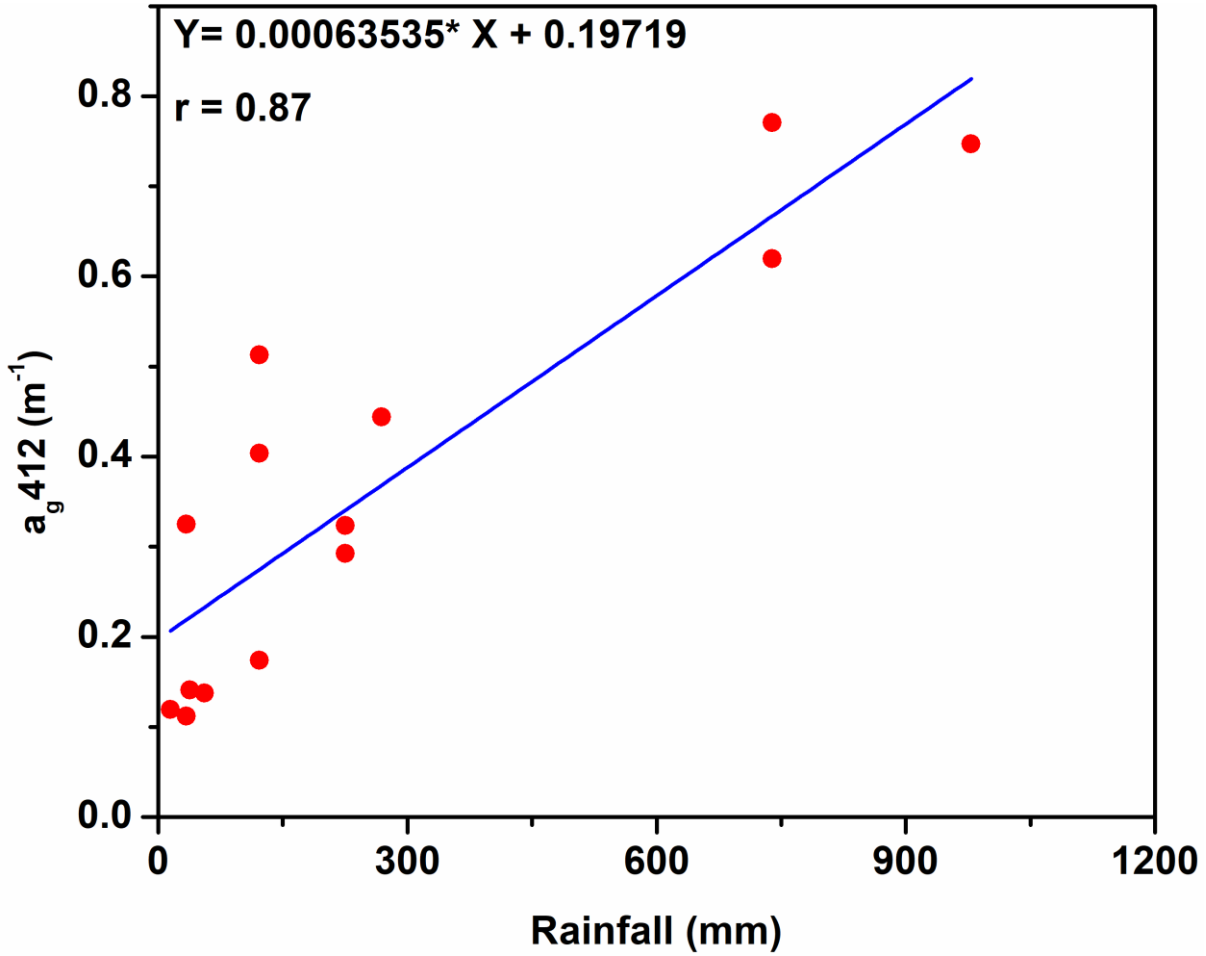

Appendix 1.4: Temporal variation of Brunt Vaisala frequency N (s^{-1}) at the coastal station, G5 overlaid with (a) CDOM absorption (a_g412 m^{-1}) and (b) ($S_{250-600}$ nm^{-1}). The X-axis represents Julian days.

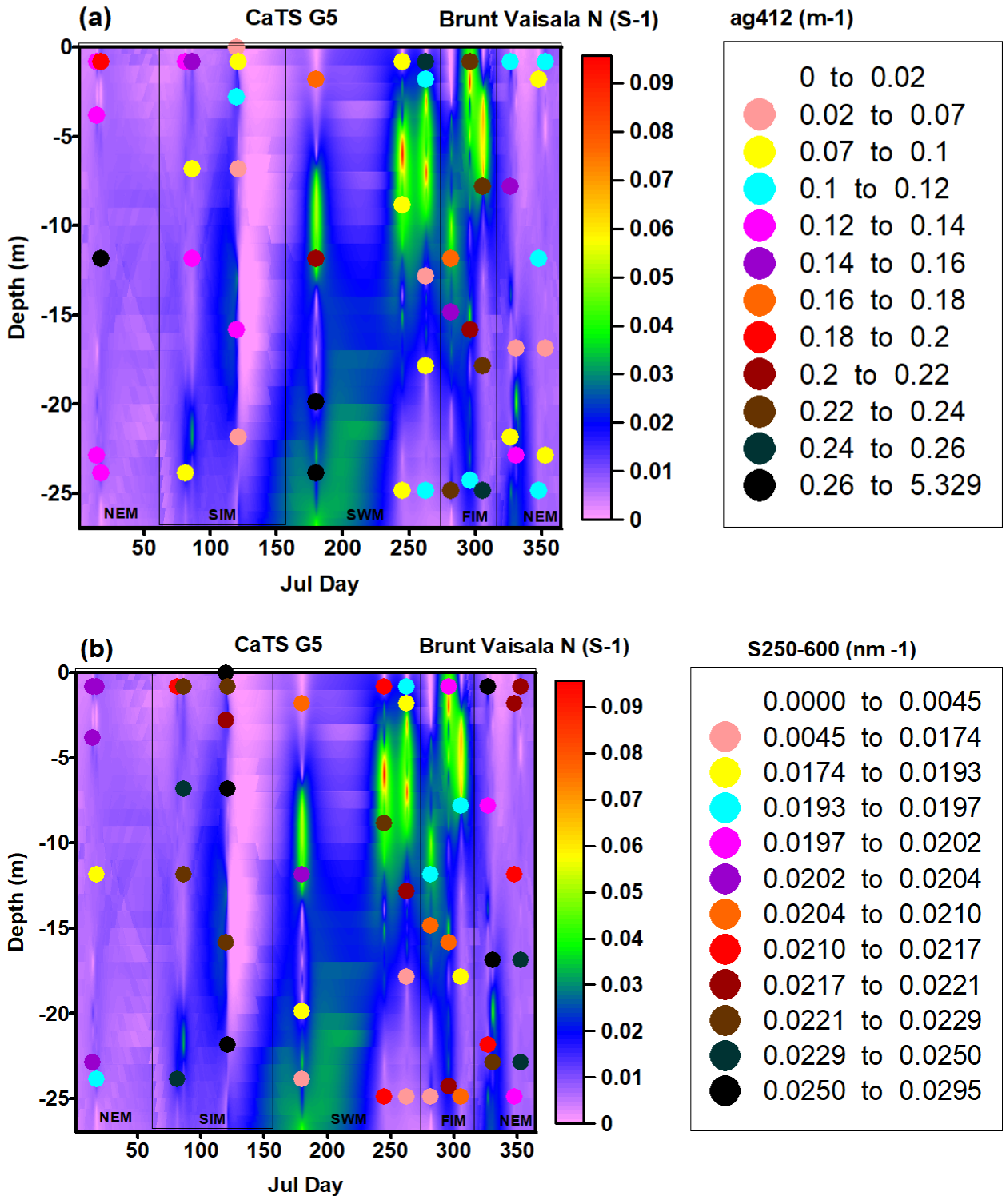

Appendix 1.5: Components of CDOM fluorescence (Raman units) identified using PARAFAC during the SWM along the WCSI.

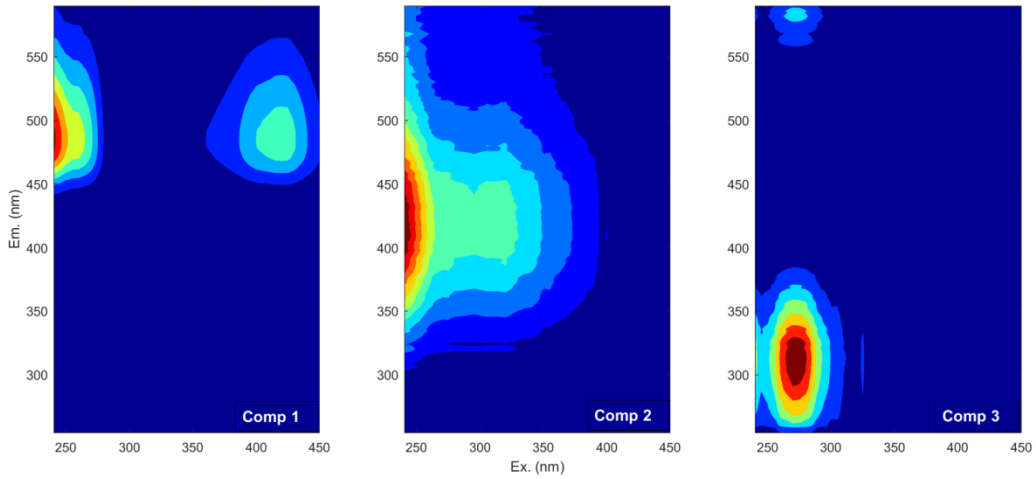

References

References

Ahmed, A., Gauns, M., Kurian, S., Bardhan, P., Pratihary, A., Naik, H., ... & Naqvi, S. W. A. (2017). Nitrogen fixation rates in the eastern Arabian Sea. *Estuarine, Coastal and Shelf Science*, *191*, 74-83.

Araujo, J., Naqvi, S. W. A., Naik, H., & Naik, R. (2018). Biogeochemistry of methane in a tropical monsoonal estuarine system along the west coast of India. *Estuarine, Coastal and Shelf Science*, *207*, 435-443.

Asmala, E., Bowers, D. G., Autio, R., Kaartokallio, H., and Thomas, D. N. (2014). Qualitative changes of riverine dissolved organic matter at low salinities due to flocculation. *Journal of Geophysical Research: Biogeosciences*, 119(10), 1919-1933.

Aulló-Maestro, Hunter, M. E., P., Spyrako,s E., Mercatoris, P., Kovacs, A. W., Horváth, H., Preston, T., Présing, M., Palenzuela, J. T., and Tyler, A. (2017). Spatio-seasonal variability of chromophoric dissolved organic matter absorption and responses to photobleaching in a large shallow temperate lake. *Biogeosciences*, 14(5), 1215.

Baetge, N., Behrenfeld, M. J., Fox, J., Halsey, K. H., Mojica, K. D., Novoa, A., ... & Carlson, C. A. (2021). The Seasonal Flux and Fate of Dissolved Organic Carbon Through Bacterioplankton in the Western North Atlantic. *Frontiers in Microbiology*, *12*, 669883.

Baker, A. (2001). Fluorescence excitation− emission matrix characterization of some sewage-impacted rivers. *Environmental science & technology*, 35(5), 948-953.

Bange, H. W., Naqvi, S. W. A., & Codispoti, L. A. (2005). The nitrogen cycle in the Arabian Sea. *Progress in Oceanography*, *65*(2-4), 145-158.

Bao, H., Yi, Y., Wang, C., Spencer, R. G., Deng, X., & Guo, W. (2018). Dissolved organic matter in coastal rainwater: Concentration, bioavailability and depositional flux to seawater in southeastern China. *Marine Chemistry*, *205*, 48-55.

Bardhan, P., Karapurkar, S. G., Shenoy, D. M., Kurian, S., Sarkar, A., Maya, M. V., ... & Naqvi, S. W. A. (2015). Carbon and nitrogen isotopic composition of suspended particulate organic matter in Zuari Estuary, west coast of India. *Journal of Marine Systems*, *141*, 90-97.

Bar-Zeev, E., Avishay, I., Bidle, K. D., & Berman-Frank, I. (2013). Programmed cell death in the marine cyanobacterium *Trichodesmium* mediates carbon and nitrogen export. *The ISME journal*, *7*(12), 2340.

Basu, S., Gledhill, M., de Beer, D., Matondkar, S. P., & Shaked, Y. (2019). Colonies of marine cyanobacteria Trichodesmium interact with associated bacteria to acquire iron from dust. *Communications biology*, *2*(1), 1-8.

Basu, S., Matondkar, S. P., & Furtado, I. (2011). Enumeration of bacteria from a *Trichodesmium* spp. bloom of the Eastern Arabian Sea: elucidation of their possible role in biogeochemistry. *Journal of applied phycology*, *23*(2), 309-319.

Battin, T. J. (1998). Dissolved organic matter and its optical properties in a blackwater tributary of the upper Orinoco river, Venezuela. *Organic Geochemistry*, *28*(9-10), 561-569.

Beal, L. M., Vialard, J., Roxy, M. K., Li, J., Andres, M., Annamalai, H., ... & Parvathi, V. (2020). A road map to IndOOS-2: Better observations of the rapidly warming Indian Ocean. *Bulletin of the American Meteorological Society*, *101*(11), E1891-E1913.

Behrenfeld, M. J., & Boss, E. S. (2014). Resurrecting the ecological underpinnings of ocean plankton blooms. *Annual review of marine science*, *6*, 167-194.

Bell, P. R., Uwins, P. J., Elmetri, I., Phillips, J. A., Fu, F. X., & Yago, A. J. (2005). Laboratory culture studies of *Trichodesmium* isolated from the great Barrier Reef Lagoon, Australia. *Hydrobiologia*, *532*(1-3), 9-21.

Bergman, B., Sandh, G., Lin, S., Larsson, J., & Carpenter, E. J. (2013). Trichodesmium–a widespread marine cyanobacterium with unusual nitrogen fixation properties. *FEMS microbiology reviews*, *37*(3), 286-302.

Berman-Frank, I., Quigg, A., Finkel, Z. V., Irwin, A. J., & Haramaty, L. (2007). Nitrogen-fixation strategies and Fe requirements in cyanobacteria. *Limnology and Oceanography*, *52*(5), 2260-2269.

Bhargava, R. M. S., & Dwivedi, S. N. (1976). Seasonal distribution of phytoplankton pigments in the estuarine system of Goa. *Indian Journal of Marine Science*, *5*, 87-90.

Bianchi, T. S., DiMarco, S. F., Cowan Jr, J. H., Hetland, R. D., Chapman, P., Day, J. W., & Allison, M. A. (2010). The science of hypoxia in the Northern Gulf of Mexico: a review. *Science of the Total Environment*, *408*(7), 1471-1484.

Blough, N. V., & Green, S. A. (1995). Spectroscopic characterization and remote sensing of non-living organic matter. In R.G. Zepp and Ch. Sonntag (Ed.), *The role of non-living organic matter in the earth's carbon cycle* (pp. 23-45). John Wiley & Sons.

Blough, N. V., Zafiriou, O. C., & Bonilla, J. (1993). Optical absorption spectra of waters from the Orinoco River outflow: Terrestrial input of colored organic matter to the Caribbean. *Journal of Geophysical Research: Oceans*, *98*(C2), 2271-2278.

Bojinski, S., Verstraete, M., Peterson, T. C., Richter, C., Simmons, A., & Zemp, M. (2014). The concept of essential climate variables in support of climate research, applications, and policy. *Bulletin of the American Meteorological Society*, *95*(9), 1431-1443.

Borges, A. V., Delille, B., & Frankignoulle, M. (2005). Budgeting sinks and sources of CO2 in the coastal ocean: Diversity of ecosystems counts. *Geophysical research letters*, *32*(14).

Borstad, L. E. (1978). *A Qualitative and Quantitative Examination of Bacteria Associated with Trichodesmium:(Cyanobacteria) Species Near Barbados* (Doctoral dissertation, McGill University).

Boss, E., Pegau, W. S., Gardner, W. D., Zaneveld, J. R. V., Barnard, A. H., Twardowski, M. S., ... & Dickey, T. D. (2001). Spectral particulate attenuation and particle size distribution in the bottom boundary layer of a continental shelf. *Journal of Geophysical Research: Oceans*, *106*(C5), 9509-9516.

Boucher, O., Randall, D., Artaxo, P., Bretherton, C., Feingold, G., Forster, P., et al. (2013). Clouds and Aerosols. In T. F. Stocker, & more (Eds.), *Climate Change 2013: The Physical Science Basis. Contribution of Working Group I to the Fifth Assessment Report of the Intergovernmental Panel on Climate Change* (pp. 571-657). Cambridge: Cambridge University Press.

Breitburg, D., Levin, L. A., Oschlies, A., Grégoire, M., Chavez, F. P., Conley, D. J., ... & Zhang, J. (2018). Declining oxygen in the global ocean and coastal waters. *Science*, *359*(6371).

Brezonik, P. L., Olmanson, L. G., Finlay, J. C., & Bauer, M. E. (2015). Factors affecting the measurement of CDOM by remote sensing of optically complex inland waters. *Remote Sensing of Environment*, *157*, 199-215.

Bricaud, A., Morel, A., & Prieur, L. (1981). Absorption by dissolved organic matter of the sea (yellow substance) in the UV and visible domains 1. *Limnology and oceanography*, *26*(1), 43-53.

Burdige, D. J., & Komada, T. (2015). Sediment pore waters. In D. A. Hansen and C. A. Carlson (Ed.), *Biogeochemistry of marine dissolved organic matter* (pp. 535-577). Academic Press.

Burdige, D. J., & Gardner, K. G. (1998). Molecular weight distribution of dissolved organic carbon in marine sediment pore waters. *Marine Chemistry*, *62*(1-2), 45-64.

Caldeira, K., & Wickett, M. E. (2003). Anthropogenic carbon and ocean pH. *Nature*, *425*(6956), 365-365.

Cao, F., Tzortziou, M., Hu, C., Mannino, A., Fichot, C. G., Del Vecchio, R., ... & Novak, M. (2018). Remote sensing retrievals of colored dissolved organic matter and dissolved organic carbon dynamics in North American estuaries and their margins. *Remote sensing of Environment*, *205*, 151-165.

Capone, D. G., Burns, J. A., Montoya, J. P., Subramaniam, A., Mahaffey, C., Gunderson, T., ... & Carpenter, E. J. (2005). Nitrogen fixation by Trichodesmium spp.: An important source of new nitrogen to the tropical and subtropical North Atlantic Ocean. *Global Biogeochemical Cycles*, *19*(2).

Capone, D. G., Subramaniam, A., Montoya, J. P., Voss, M., Humborg, C., Johansen, A. M., ... & Carpenter, E. J. (1998). An extensive bloom of the N2-fixing cyanobacterium Trichodesmium erythraeum in the central Arabian Sea. *Marine Ecology Progress Series*, *172*, 281-292.

Capone, D. G., Zehr, J. P., Paerl, H. W., Bergman, B., & Carpenter, E. J. (1997). *Trichodesmium*, a globally significant marine cyanobacterium. *Science*, *276*(5316), 1221-1229.

Carder, K. L., Steward, R. G., Harvey, G. R., & Ortner, P. B. (1989). Marine humic and fulvic acids: Their effects on remote sensing of ocean chlorophyll. *Limnology and oceanography*, *34*(1), 68-81.

Carlson, C. A., & Hansell, D. A. (2015). DOM sources, sinks, reactivity, and budgets. *Biogeochemistry of marine dissolved organic matter*, 65-126.

Carpenter, K. D., Kraus, T., Goldman, J., Saracen, J. F., Downing, B., & Bergamaschi, B. (2013). *Sources and characteristics of organic matter in the Clackamas River, Oregon, related to the formation of disinfection by-products in treated drinking water*: U.S. Geological Survey Scientific Investigations Report 2013–5001.

Carpenter, E. J., & Capone, D. G. (1992). Nitrogen fixation in *Trichodesmium* blooms. In E.J Carpenter and D.G. Capone (Ed.), *Marine pelagic cyanobacteria: Trichodesmium and other diazotrophs* (pp. 211-217). Springer, Dordrecht.

Carstea, E. M., Popa, C. L., Baker, A., & Bridgeman, J. (2020). In situ fluorescence measurements of dissolved organic matter: a review. *Science of the Total Environment*, *699*, 134361.

Catalá, T. S., Reche, I., Fuentes-Lema, A., Romera-Castillo, C., Nieto-Cid, M., Ortega-Retuerta, E., ... & Alvarez-Salgado, X. A. (2015). Turnover time of fluorescent dissolved organic matter in the dark global ocean. *Nature communications*, *6*(1), 1-9.

Chari, N. V. H. K., Venkateswararao, C., & Shyamala, P. (2021). Comparison of the absorption characteristics of coloured dissolved organic matter between river and wave dominated distributaries of Godavari estuary, India. *Journal of Earth System Science*, *130*(2), 1-11.

Chari, N. V. H. K., Pandi, S. R., Kanuri, V. V., & Basuri, C. K. (2019). Structural variation of coloured dissolved organic matter during summer and winter seasons in a tropical estuary: A case study. *Marine pollution bulletin*, *149*, 110563.

Chari, N. V. H. K., Sarma, N. S., Rao, P. S., Chiranjeevulu, G., Kiran, R., Murty, K. N., & Venkatesh, P. (2016). Fluorescent dissolved organic matter dynamics in the coastal waters off the Central East Indian Coast (Bay of Bengal). *Environ Ecol Res*, *4*, 13-20.

Chari, N. V. H. K., Rao, P. S., & Sarma, N. S. (2013a). Fluorescent dissolved organic matter in the continental shelf waters of western Bay of Bengal. *Journal of Earth System Science*, *122*(5), 1325-1334.

Chari, N. V. H. K., Keerthi, S., Sarma, N. S., Pandi, S. R., Chiranjeevulu, G., Kiran, R., & Koduru, U. (2013b). Fluorescence and absorption characteristics of dissolved organic matter excreted by phytoplankton species of western Bay of Bengal under axenic laboratory condition. *Journal of experimental marine biology and ecology*, *445*, 148-155.

Chen, Q., Miyazaki, Y., Kawamura, K., Matsumoto, K., Coburn, S., Volkamer, R., ... & Ramasamy, S. (2016). Characterization of chromophoric water-soluble organic matter in urban, forest, and marine aerosols by HR-ToF-AMS analysis and excitation–emission matrix spectroscopy. *Environmental science & technology*, *50*(19), 10351-10360.

Chen, Z., P. H. Doering, M. Ashton, and B. A. Orlando. (2015). Mixing behavior of colored dissolved organic matter and its potential ecological implication in the Caloosahatchee River estuary, Florida. *Estuaries and coasts*, 38(5), 1706-1718.

Chen, Y. B., Zehr, J. P., & Mellon, M. (1996). Growth and nitrogen fixation of the diazotrophic filamentous nonheterocystous cyanobacterium *Trichodesmium* sp. Ims 101 in defined media: evidence for a circadian rhythm 1. *Journal of Phycology*, *32*(6), 916-923.

Chin, W. C., Orellana, M. V., & Verdugo, P. (1998). Spontaneous assembly of marine dissolved organic matter into polymer gels. *Nature*, *391*(6667), 568-572.

Chiranjeevulu, G., Murty, K. N., Sarma, N. S., Kiran, R., Chari, N. V. H. K., Pandi, S. R., ... & Rao, K. N. (2014). Colored dissolved organic matter signature and phytoplankton

response in a coastal ecosystem during mesoscale cyclonic (cold core) eddy. *Marine environmental research*, *98*, 49-59.

Chua, E. J., Savidge, W., Short, R. T., Cardenas-Valencia, A. M., & Fulweiler, R. W. (2016). A review of the emerging field of underwater mass spectrometry. *Frontiers in Marine Science*, *3*, 209.

Ciais, P., Sabine, C., Bala, G., Bopp, L., Brovkin, V., Canadell, J., ... & Thornton, P. (2014). Carbon and other biogeochemical cycles. In T. F. Stocker, D. Qin, G-K. Plattner (Ed.), *Climate change 2013: the physical science basis. Contribution of Working Group I to the Fifth Assessment Report of the Intergovernmental Panel on Climate Change* (pp. 465-570). Cambridge University Press.

Coba, F., Aguilera, J., Korbee, N., de Gálvez, M. V., Herrera-Ceballos, E., Álvarez-Gómez, F., & Figueroa, F. L. (2019). UVA and UVB photoprotective capabilities of topical formulations containing mycosporine-like amino acids (MAAs) through different biological effective protection factors (BEPFs). *Marine drugs*, *17*(1), 55.

Coble, P. G. (2007). Marine optical biogeochemistry: the chemistry of ocean color. *Chemical reviews*, *107*(2), 402-418.

Coble, P. G., Del Castillo, C. E., & Avril, B. (1998). Distribution and optical properties of CDOM in the Arabian Sea during the 1995 Southwest Monsoon. *Deep Sea Research Part II: Topical Studies in Oceanography*, *45*(10-11), 2195-2223.

Coble, P. G. (1996). Characterization of marine and terrestrial DOM in seawater using excitation-emission matrix spectroscopy. *Marine chemistry*, *51*(4), 325-346.

Codispoti, L. A., Brandes, J. A., Christensen, J. P., Devol, A. H., Naqvi, S. W. A., Paerl, H. W., & Yoshinari, T. (2001). The oceanic fixed nitrogen and nitrous oxide budgets: Moving targets as we enter the anthropocene?. *Scientia Marina*, *65*(S2), 85-105.

Conde, F. R., Churio, M. S., & Previtali, C. M. (2004). The deactivation pathways of the excited-states of the mycosporine-like amino acids shinorine and porphyra-334 in aqueous solution. *Photochemical & Photobiological Sciences*, *3*(10), 960-967.

Cory, R. M., Miller, M. P., McKnight, D. M., Guerard, J. J., & Miller, P. L. (2010). Effect of instrument-specific response on the analysis of fulvic acid fluorescence spectra. *Limnology and Oceanography: Methods*, *8*(2), 67-78.

Cory, R. M., McKnight, D. M., Chin, Y. P., Miller, P., & Jaros, C. L. (2007). Chemical characteristics of fulvic acids from Arctic surface waters: Microbial contributions and photochemical transformations. *Journal of Geophysical Research: Biogeosciences*, *112*(G4).

Cowie, G., Mowbray, S., Kurian, S., Sarkar, A., White, C., Anderson, A., ... & Kitazato, H. (2014). Comparative organic geochemistry of Indian margin (Arabian Sea) sediments: estuary to continental slope. *Biogeosciences*, *11*(23), 6683-6696.

D'Silva, M. S., Anil, A. C., Naik, R. K., & D'Costa, P. M. (2012). Algal blooms: a perspective from the coasts of India. *Natural hazards*, *63*(2), 1225-1253.

Dall'Olmo, G., Brewin, R. J., Nencioli, F., Organelli, E., Lefering, I., McKee, D., ... & Tilstone, G. (2017). Determination of the absorption coefficient of chromophoric dissolved organic matter from underway spectrophotometry. *Optics express*, *25*(24), A1079-A1095.

Dartnell, L. R., Storrie-Lombardi, M. C., Mullineaux, C. W., Ruban, A. V., Wright, G., Griffiths, A. D., ... & Ward, J. M. (2011). Degradation of cyanobacterial biosignatures by ionizing radiation. *Astrobiology*, *11*(10), 997-1016.

Das, P. K., Murty, C. S., & Varadacha, V. V. R. (1972). Flow characteristics of Combarjua canal connecting Mandovi and Zuari estuaries. *Indian Journal of Marine Science*, *1*, 95-102.

Das, S., Hazra, S., Giri, S., Das, I., Chanda, A., Akhand, A., & Maity, S. (2017). Light absorption characteristics of chromophoric dissolved organic matter (CDOM) in the coastal waters of northern Bay of Bengal during winter season. *Indian Journal of Marine Science*, *46*(05), 884-892.

Das, S., Hazra, S., Lotlikar, A. A., Das, I., Giri, S., Chanda, A., ... & Kumar, T. S. (2016). Delineating the relationship between chromophoric dissolved organic matter (CDOM) variability and biogeochemical parameters in a shallow continental shelf. *The Egyptian Journal of Aquatic Research*, *42*(3), 241-248.

De Sousa, S. N. (1999). Effect of mining rejects on the nutrient chemistry of Mandovi estuary, Goa. *Indian Journal of Marine Science*, *28*, 355-359.

DeGrandpre, M. D., Vodacek, A., Nelson, R. K., Bruce, E. J., & Blough, N. V. (1996). Seasonal seawater optical properties of the US Middle Atlantic Bight. *Journal of Geophysical Research: Oceans*, *101*(C10), 22727-22736.

Dehadrai, P. V., & Bhargava, R. M. S. (1972). Seasonal organic production in relation to environmental features in Mandovi & Zuari estuaries, Goa. *Indian Journal of Marine Science*, *1*, 52-56.

Dehadrai, P. V. (1970, August). Changes in the environmental features of the Zuari and Mandovi estuaries in relation to tides. In *Proceedings of the Indian Academy of Sciences-Section B* (Vol. 72, No. 2, pp. 68-80). Springer India.

Del Castillo, C. E., & Coble, P. G. (2000). Seasonal variability of the colored dissolved organic matter during the 1994–95 NE and SW monsoons in the Arabian Sea. *Deep Sea Research Part II: Topical Studies in Oceanography*, *47*(7-8), 1563-1579.

Del Castillo, C. E., Coble, P. G., Morell, J. M., Lopez, J. M., & Corredor, J. E. (1999). Analysis of the optical properties of the Orinoco River plume by absorption and fluorescence spectroscopy. *Marine Chemistry*, *66*(1-2), 35-51.

Del Vecchio, R., and Subramaniam, A. (2004). Influence of the Amazon River on the surface optical properties of the western tropical North Atlantic Ocean. *Journal of Geophysical Research: Oceans*, 109, C11001.

Del Vecchio, R., & Blough, N. V. (2002). Photobleaching of chromophoric dissolved organic matter in natural waters: kinetics and modeling. *Marine chemistry*, *78*(4), 231-253.

Desa, E. S., Suresh, T., Matondkar, S. G. P., Desa, E., Goes, J., Mascarenhas, A. A. M. Q., ... & Fernandes, C. E. G. (2005). Detection of *Trichodesmium* bloom patches along the eastern Arabian Sea by IRS-P4/OCM ocean color sensor and by in-situ measurements. *Indian Journal of Marine Sciences, 34*(4), 374-386.

Desa, E. S., Suresh, T., Matondkar, S. P., & Desa, E. (2001). Sea truth validation of sea WiFS ocean colour sensor in the coastal waters of the eastern Arabian Sea. *Current Science, 80*(7), 854-860.

Deutsch, C., Sarmiento, J. L., Sigman, D. M., Gruber, N., & Dunne, J. P. (2007). Spatial coupling of nitrogen inputs and losses in the ocean. *Nature*, *445*(7124), 163-167.

Deutsch, C., Gruber, N., Key, R. M., Sarmiento, J. L., & Ganachaud, A. (2001). Denitrification and N2 fixation in the Pacific Ocean. *Global Biogeochemical Cycles*, *15*(2), 483-506.

Devassy, V. P., Bhattathiri, P. M. A., & Qasim, S. Z. (1978). *Trichodesmium* phenomenon. *Indian Journal of Marine Sciences*, *7*(3), 168-186.

Dias, A., Kurian, S., Thayapurath, S., & Pratihary, A. K. (2021). Variations of Colored Dissolved Organic Matter in the Mandovi Estuary, Goa, During Spring Inter-Monsoon: A Comparison With COVID-19 Outbreak Imposed Lockdown Period. *Frontiers in Marine Science*, *8*, 638583.

Dias, A., Kurian, S., & Thayapurath, S. (2020a). Influence of environmental parameters on bio-optical characteristics of colored dissolved organic matter in a complex tropical coastal and estuarine region. *Estuarine, Coastal and Shelf Science*, *242*, 106864.

Dias, A., Kurian, S., & Thayapurath, S. (2020b). Optical characteristics of colored dissolved organic matter during blooms of *Trichodesmium* in the coastal waters off Goa. *Environmental Monitoring and Assessment, 192*(8), 1-18.

Dias, A. B., Suresh, T., Sahay, A., and Chauhan, P. (2017). Contrasting characteristics of colored dissolved organic matter of the coastal and estuarine waters of Goa during summer. *Indian Journal of Marine Sciences*, 46(05), 860-870.

Diaz, R. J., Rosenberg, R., and Sturdivant, K. (2019). Hypoxia in estuaries and semi-enclosed seas. In D. Laffoley and J. M. Baxter (Ed.), *Ocean Deoxygenation: Everyone's Problem - Causes, Impacts, Consequences and Solutions* (pp. 85-102), IUCN Global Marine and Polar Programme, Switzerland.

Diaz, R. J., & Rosenberg, R. (2008). Spreading dead zones and consequences for marine ecosystems. *Science*, *321*(5891), 926-929.

Doering, P. H., Oviatt, C. A., McKenna, J. H., and Reed, L. W. (1994). Mixing behavior of dissolved organic carbon and its potential biological significance in the Pawcatuck River Estuary. *Estuaries*, 17(3), 521-536.

Dupouy, C., Neveux, J., Dirberg, G., Rottgers, R., Tenório, M. M. B., & Ouillon, S. (2008). Bio-optical properties of the marine cyanobacteria *Trichodesmium* spp. *Journal of Applied Remote Sensing*, *2*(1), 023503.

Dutkiewicz, S., Hickman, A. E., Jahn, O., Henson, S., Beaulieu, C., & Monier, E. (2019). Ocean colour signature of climate change. *Nature communications*, *10*(1), 1-13.

Fasching, C., Behounek, B., Singer, G. A., & Battin, T. J. (2014). Microbial degradation of terrigenous dissolved organic matter and potential consequences for carbon cycling in brown-water streams. *Scientific reports*, *4*, 4981.

Fellman, J. B., Hood, E., and Spencer, R. G. M. (2010). Fluorescence spectroscopy opens new windows into dissolved organic matter dynamics in freshwater ecosystems: A review. *Limnology and Oceanography*, 55(6), 2452-2462.

Fernandes, L. L., Kessarkar, P. M., Suja, S., Ray, D., & Bhat, M. (2018). Seasonal variations in the water quality of six tropical micro-and mesotidal estuaries along the central west coast of India. *Marine and Freshwater Research*, *69*(9), 1418-1431.

Ferrari, G. M. (2000). The relationship between chromophoric dissolved organic matter and dissolved organic carbon in the European Atlantic coastal area and in the West Mediterranean Sea (Gulf of Lions). *Marine Chemistry*, *70*(4), 339-357.

Fichot, C. G., & Benner, R. (2012). The spectral slope coefficient of chromophoric dissolved organic matter (S275–295) as a tracer of terrigenous dissolved organic carbon in river-influenced ocean margins. *Limnology and Oceanography*, *57*(5), 1453-1466.

Fichot, C. G., & Benner, R. (2011). A novel method to estimate DOC concentrations from CDOM absorption coefficients in coastal waters. *Geophysical research letters*, *38*(3), L03610.

Fleck, J. A., Gill, G., Bergamaschi, B. A., Kraus, T. E., Downing, B. D., & Alpers, C. N. (2014). Concurrent photolytic degradation of aqueous methylmercury and dissolved organic matter. *Science of the Total Environment*, *484*, 263-275.

Foley, J. (2017). Living by the lessons of the planet. *Science*, *356*(6335), 251-252.

Foley, J. A , DeFries, R., Asner, G. P., Barford, C., Bonan, G., Carpenter, S. R., Chapin, F. S., Coe, M. T., Daily, G. C., Gibbs, H. K., Helkowski, J. H., Holloway, T., Howard, E. A., Kucharik, C. J., Monfreda, C., Patz, J, A., Prentice, I. C., Ramankutty, N., and Snyder, P. K. (2005) Global Consequences of Land Use. *Science*, *309*, 570-574.

Fu, P., Kawamura, K., Chen, J., Qin, M., Ren, L., Sun, Y., ... & Yamashita, Y. (2015). Fluorescent water-soluble organic aerosols in the High Arctic atmosphere. *Scientific reports*, *5*, 9845.

Fujita, S., Kuma, K., Ishikawa, S., Nishimura, S., Nakayama, Y., Ushizaka, S., ... & Aramaki, T. (2010). Iron distributions in the water column of the Japan Basin and Yamato Basin (Japan Sea). *Journal of Geophysical Research: Oceans*, *115*(C12).

Fukuzaki, K., Imai, I., Fukushima, K., Ishii, K. I., Sawayama, S., & Yoshioka, T. (2014). Fluorescent characteristics of dissolved organic matter produced by bloom-forming coastal phytoplankton. *Journal of Plankton Research*, *36*(3), 685-694.

Gandhi, N., Singh, A., Prakash, S., Ramesh, R., Raman, M., Sheshshayee, M. S., & Shetye, S. (2011). First direct measurements of N2 fixation during a *Trichodesmium* bloom in the eastern Arabian Sea. *Global Biogeochemical Cycles*, *25*(4), GB4014.

Gattuso, J. P., Magnan, A., Billé, R., Cheung, W. W., Howes, E. L., Joos, F., ... & Turley, C. (2015). Contrasting futures for ocean and society from different anthropogenic CO2 emissions scenarios. *Science*, *349*(6243), 1-35.

Gattuso, J. P., Frankignoulle, M., & Wollast, R. (1998). Carbon and carbonate metabolism in coastal aquatic ecosystems. *Annual Review of Ecology and Systematics*, *29*(1), 405-434.

Gauns, M., Mochemadkar, S., Patil, S., Pratihary, A., Naqvi, S. W. A., and Madhupratap, M. (2015). Seasonal variations in abundance, biomass and grazing rates of

microzooplankton in a tropical monsoonal estuary. *Journal of oceanography*, 71(4), 345-359.

Gnanaseelan, C., Roxy, M. K., & Deshpande, A. (2017). Variability and trends of sea surface temperature and circulation in the Indian Ocean. In *Observed climate variability and change over the Indian Region* (pp. 165-179). Springer, Singapore.

Goes, J. I., & Gomes, H. D. R. (2016). An ecosystem in transition: the emergence of mixotrophy in the Arabian Sea. In *Aquatic Microbial Ecology and Biogeochemistry: A Dual Perspective* (pp. 155-170). Springer.

Gomes, H., Goes, J. I., Matondkar, S.G. P., Parab, S. G., Al-Azri, A. R.N., and Thoppil, P. G. (2008). Blooms of Noctiluca miliaris in the Arabian Sea—An in situ and satellite study. *Deep Sea Research Part I: Oceanographic Research Papers*, 55(6), 751-765.

Gonsalves, M. J., Nair, S., Loka Bharathi, P.A., and Chandramohan, D. (2009). Abundance and production of particle-associated bacteria and their role in a mangrove-dominated estuary. *Aquatic Microbial Ecology*, 57(2), 151-159.

Grasshoff, K. (1983). Determination of oxygen. *Methods of seawater analysis*, 61-72.

Green, R. E., Bianchi, T. S., Dagg, M. J., Walker, N. D., & Breed, G. A. (2006). An organic carbon budget for the Mississippi River turbidity plume and plume contributions to air-sea CO 2 fluxes and bottom water hypoxia. *Estuaries and Coasts*, *29*(4), 579-597.

Green, S. A., and Blough, N. V. (1994). Optical absorption and fluorescence properties of chromophoric dissolved organic matter in natural waters. *Limnology and Oceanography*, 39(8), 1903-1916.

Griffin, C. G., McClelland, J. W., Frey, K. E., Fiske, G., & Holmes, R. M. (2018). Quantifying CDOM and DOC in major Arctic rivers during ice-free conditions using Landsat TM and ETM+ data. *Remote Sensing of Environment*, *209*, 395-409.

Groom, S. B., Sathyendranath, S., Ban, Y., Bernard, S., Brewin, B., Brotas, V., ... & Ciavatta, S. (2019). Satellite ocean colour: current status and future perspective. *Frontiers in Marine Science*, *6*, 485.

Gruber, N., Clement, D., Carter, B. R., Feely, R. A., Van Heuven, S., Hoppema, M., ... & Wanninkhof, R. (2019). The oceanic sink for anthropogenic CO2 from 1994 to 2007. *Science*, *363*(6432), 1193-1199.

Guéguen, C., Cuss, C. W., Cassels, C. J., & Carmack, E. C. (2014). Absorption and fluorescence of dissolved organic matter in the waters of the Canadian Arctic Archipelago, Baffin Bay, and the Labrador Sea. *Journal of Geophysical Research: Oceans*, *119*(3), 2034-2047.

Guo, W., Xu, J., Wang, J., Wen, Y., Zhuo, J., and Yan, Y. (2010). Characterization of dissolved organic matter in urban sewage using excitation emission matrix fluorescence spectroscopy and parallel factor analysis. *Journal of Environmental Sciences*, 22(11), 1728-1734.

Halley, E. (1686). An historical account of the trade winds, and monsoons, observable in the seas between and near the Tropicks, with an attempt to assign the physical cause of the said winds. *Philosophical Transactions of the Royal Society of London*, *16*(183), 153-168.

Hansell, D. A., Carlson, C. A., & Suzuki, Y. (2002). Dissolved organic carbon export with North Pacific Intermediate Water formation. *Global Biogeochemical Cycles*, *16*(1), 7-1.

Hansen, A. M., Kraus, T. E., Pellerin, B. A., Fleck, J. A., Downing, B. D., & Bergamaschi, B. A. (2016). Optical properties of dissolved organic matter (DOM): Effects of biological and photolytic degradation. *Limnology and Oceanography*, *61*(3), 1015-1032.

Hayase, K., & Shinozuka, N. (1995). Vertical distribution of fluorescent organic matter along with AOU and nutrients in the equatorial Central Pacific. *Marine Chemistry*, *48*(3-4), 283-290.

Hedges, J. I. (2002). Why dissolved organics matter?. In D. Hansell and C. Carlson (Ed.), *Biogeochemistry of marine dissolved organic matter* (pp. 1-33), New York, NY: Academic Press.

Hedges, J. I., Baldock, J. A., Gélinas, Y., Lee, C., Peterson, M., & Wakeham, S. G. (2001). Evidence for non-selective preservation of organic matter in sinking marine particles. *Nature*, *409*(6822), 801-804.

Hedges, J. I. (1992). Global biogeochemical cycles: progress and problems. *Marine chemistry*, *39*(1-3), 67-93.

Heinz, M., D. Graeber, D. Zak, E. Zwirnmann, J. Gelbrecht, and M. T. Pusch. (2015). Comparison of organic matter composition in agricultural versus forest affected headwaters with special emphasis on organic nitrogen. *Environmental science & technology*, 49(4), 2081-2090.

Helms, J. R., Stubbins, A., Perdue, E. M., Green, N. W., Chen, H., & Mopper, K. (2013). Photochemical bleaching of oceanic dissolved organic matter and its effect on absorption spectral slope and fluorescence. *Marine Chemistry*, *155*, 81-91.

Helm, K. P., Bindoff, N. L., & Church, J. A. (2011). Observed decreases in oxygen content of the global ocean. *Geophysical Research Letters*, *38*(23), L23602.

Helms, J. R., Stubbins, A., Ritchie, J. D., Minor, E. C., Kieber, D. J., and Mopper, K. (2008). Absorption spectral slopes and slope ratios as indicators of molecular weight, source, and photobleaching of chromophoric dissolved organic matter. *Limnology and Oceanography*, 53(3), 955-969.

Herman, J. R. (2010). Global increase in UV irradiance during the past 30 years (1979–2008) estimated from satellite data. *Journal of Geophysical Research: Atmospheres*, *115*(D4), D04203.

Hewson, I., O'Neil, J. M., Fuhrman, J. A., & Dennison, W. C. (2001). Virus-like particle distribution and abundance in sediments and overlying waters along eutrophication gradients in two subtropical estuaries. *Limnology and Oceanography*, *46*(7), 1734-1746.

Hrudya, P. P. V. H., Varikoden, H., & Vishnu, R. N. (2021). Changes in the relationship between Indian Ocean dipole and Indian summer monsoon rainfall in early and recent multidecadal epochs during different phases of monsoon. *International Journal of Climatology*, *41*, E305-E318.

Hua, B., Dolan, F., Mcghee, C., Clevenger, T. E., & Deng, B. (2007). Water-source characterization and classification with fluorescence EEM spectroscopy: PARAFAC analysis. *International Journal of Environmental and Analytical Chemistry*, *87*(2), 135-147.

Iturriaga, R., & Zsolnay, A. (1981). Transformation of some dissolved organic compounds by a natural heterotrophic population. *Marine Biology*, *62*(2), 125-129.

Jaffé, R., McKnight, D., Maie, N., Cory, R., McDowell, W. H., & Campbell, J. L. (2008). Spatial and temporal variations in DOM composition in ecosystems: The importance of long-term monitoring of optical properties. *Journal of Geophysical Research: Biogeosciences*, *113*(G4).

James, A. K., Passow, U., Brzezinski, M. A., Parsons, R. J., Trapani, J. N., & Carlson, C. A. (2017). Elevated p CO2 enhances bacterioplankton removal of organic carbon. *PLoS One*, *12*(3), e0173145.

Johnson, D. R., Weidemann, A., Arnone, R., and Davis, C. O. (2001). Chesapeake Bay outflow plume and coastal upwelling events: physical and optical properties. *Journal of Geophysical Research: Oceans*, 106(C6), 11613-11622.

Jørgensen, L., Stedmon, C. A., Kragh, T., Markager, S., Middelboe, M., & Søndergaard, M. (2011). Global trends in the fluorescence characteristics and distribution of marine dissolved organic matter. *Marine Chemistry*, *126*(1-4), 139-148.

Jyothibabu, R., Karnan, C., Jagadeesan, L., Arunpandi, N., Pandiarajan, R. S., Muraleedharan, K. R., & Balachandran, K. K. (2017). Trichodesmium blooms and warm-core ocean surface features in the Arabian Sea and the Bay of Bengal. *Marine pollution bulletin*, *121*(1-2), 201-215.

Jyothibabu, R., Madhu, N. V., Murukesh, N., Haridas, P. C., Nair, K. K. C., & Venugopal, P. (2003). Intense blooms of Trichodesmium erythraeum (Cyanophyta) in the open waters along east coast of India. *Indian Journal of Marine Science*, *32*, 165-167.

Kalle, K. (1966). The problem of the Gelbstoff in the sea. Oceanogra. *Mar. Biol.*, *4*, 91-104.

Kamat, S. B., & Sankaranarayanan, V. N. (1975). Distribution of iron in estuarine and nearshore waters of Goa. *Indian Journal of Marine Sciences*, *4*, 30-33.

Karl, D., Letelier, R., Tupas, L., Dore, J., Christian, J., & Hebel, D. (1997). The role of nitrogen fixation in biogeochemical cycling in the subtropical North Pacific Ocean. *Nature*, *388*(6642), 533-538.

Kawasaki, N., & Benner, R. (2006). Bacterial release of dissolved organic matter during cell growth and decline: molecular origin and composition. *Limnology and Oceanography*, *51*(5), 2170-2180.

Keeling, R. F., Körtzinger, A., & Gruber, N. (2010). Ocean deoxygenation in a warming world. *Annual review of marine science*, *2*, 199-229.

Kessarkar, P. M., Suja, S., Sudheesh, V., Srivastava, S., & Rao, V. P. (2015). Iron ore pollution in Mandovi and Zuari estuarine sediments and its fate after mining ban. *Environmental monitoring and assessment*, *187*(9), 1-17.

Kessarkar, P. M., Shynu, R., Rao, V. P., Chong, F., Narvekar, T., & Zhang, J. (2013). Geochemistry of the suspended sediment in the estuaries of the Mandovi and Zuari rivers, central west coast of India. *Environmental monitoring and assessment*, *185*(5), 4461-4480.

Kessarkar, P. M., Rao, V. P., Shynu, R., Ahmad, I. M., Mehra, P., Michael, G. S., & Sundar, D. (2009). Wind-driven estuarine turbidity maxima in Mandovi Estuary, central west coast of India. *Journal of Earth System Science*, *118*(4), 369.

Kieber, R. J., Whitehead, R. F., Reid, S. N., Joan, D. (2006). Chromophoric dissolved organic matter (CDOM) in rainwater, southeastern North Carolina, USA. *Journal of Atmospheric Chemistry*, *54*(1), 21-41.

Kim, J., & Kim, G. (2015). Importance of colored dissolved organic matter (CDOM) inputs from the deep sea to the euphotic zone: Results from the East (Japan) Sea. *Marine chemistry*, *169*, 33-40.

Kinsey, J. D., Corradino, G., Ziervogel, K., Schnetzer, A., & Osburn, C. L. (2018). Formation of chromophoric dissolved organic matter by bacterial degradation of phytoplankton-derived aggregates. *Frontiers in Marine Science*, *4*, 430.

Kirk, J. T. (1994). *Light and photosynthesis in aquatic ecosystems*. Cambridge university press.

Kirk, J. T. O. (1976). Yellow substance (gelbstoff) and its contribution to the attenuation of photosynthetically active radiation in some inland and coastal south-eastern Australian waters. *Marine and Freshwater Research*, *27*(1), 61-71.

Klisch, M., & Häder, D. (2008). Mycosporine-like amino acids and marine toxins-The common and the different. *Marine drugs*, *6*(2), 147-163.

Knap, A. H., Michaels, A., Close, A. R., Ducklow, H., & Dickson, A. G. (1996). Protocols for the joint global ocean flux study (JGOFS) core measurements. JGOFS Rep. 19, 170UNESCO, Paris.

Korak, J. A., Wert, E. C., & Rosario-Ortiz, F. L. (2015). Evaluating fluorescence spectroscopy as a tool to characterize cyanobacteria intracellular organic matter upon simulated release and oxidation in natural water. *Water research*, *68*, 432-443.

Kowalczuk, P., Stoń-Egiert, J., Cooper, W. J., Whitehead, R. F., & Durako, M. J. (2005). Characterization of chromophoric dissolved organic matter (CDOM) in the Baltic Sea by excitation emission matrix fluorescence spectroscopy. *Marine Chemistry*, *96*(3-4), 273-292.

Kowalczuk, P., Cooper, W. J., Whitehead, R. F., Durako, M. J., and Sheldon, W. (2003). Characterization of CDOM in an organic-rich river and surrounding coastal ocean in the South Atlantic Bight. *Aquatic Sciences-Research Across Boundaries*, 65(4), 384-401.

Krishnakumari, L., Bhattathiri, P. M. A., Matondkar, S. G. P., & John, J. (2002). Primary productivity in Mandovi-Zuari estuaries in Goa. *Journal of Marine Biological Association India*, *44*(1&2), 1-13.

Kritzberg, E. S., Villanueva, A. B., Jung, M., & Reader, H. E. (2014). Importance of boreal rivers in providing iron to marine waters. *PLoS One*, *9*(9), e107500.

Kustka, A. B., Sañudo-Wilhelmy, S. A., Carpenter, E. J., Capone, D., Burns, J., & Sunda, W. G. (2003). Iron requirements for dinitrogen-and ammonium-supported growth in cultures of Trichodesmium (IMS 101): Comparison with nitrogen fixation rates and iron: Carbon ratios of field populations. *Limnology and Oceanography*, *48*(5), 1869-1884.

Lalonde, K., Mucci, A., Ouellet, A., & Gélinas, Y. (2012). Preservation of organic matter in sediments promoted by iron. *Nature*, *483*(7388), 198-200.

Larsson, T., Wedborg, M., & Turner, D. (2007). Correction of inner-filter effect in fluorescence excitation-emission matrix spectrometry using Raman scatter. *Analytica Chimica Acta*, *583*(2), 357-363.

Lawaetz, A. J., & Stedmon, C. A. (2009). Fluorescence intensity calibration using the Raman scatter peak of water. *Applied spectroscopy*, *63*(8), 936-940.

Levitus, S., Antonov, J. I., Boyer, T. P., & Stephens, C. (2000). Warming of the world ocean. *Science*, *287*(5461), 2225-2229.

Li, H., & Minor, E. C. (2015). Dissolved organic matter in Lake Superior: insights into the effects of extraction methods on chemical composition. *Environmental Science: Processes & Impacts*, *17*(10), 1829-1840.

Li, P., & Hur, J. (2017). Utilization of UV-Vis spectroscopy and related data analyses for dissolved organic matter (DOM) studies: A review. *Critical Reviews in Environmental Science and Technology*, *47*(3), 131-154.

Loginova, A. N., Thomsen, S., and Engel, A. (2016). Chromophoric and fluorescent dissolved organic matter in and above the oxygen minimum zone off Peru. *Journal of Geophysical Research: Oceans*, 121(11), 7973-7990.

Loiselle, S. A., Bracchini, L., Dattilo, A. M., Ricci, M., Tognazzi, A., Cózar, A., & Rossi, C. (2009). The optical characterization of chromophoric dissolved organic matter using wavelength distribution of absorption spectral slopes. *Limnology and oceanography*, *54*(2), 590-597.

Lønborg, C., Carreira, C., Jickells, T., & Álvarez-Salgado, X. A. (2020). Impacts of global change on ocean dissolved organic carbon (DOC) cycling. *Frontiers in Marine Science*, *7*, 466.

Lønborg, C., Davidson, K., Álvarez–Salgado, X. A., & Miller, A. E. (2009). Bioavailability and bacterial degradation rates of dissolved organic matter in a temperate coastal area during an annual cycle. *Marine Chemistry*, *113*(3-4), 219-226.

Lübben, A., Dellwig, O., Koch, S., Beck, M., Badewien, T. H., Fischer, S., & Reuter, R. (2009). Distributions and characteristics of dissolved organic matter in temperate coastal waters (Southern North Sea). *Ocean Dynamics*, *59*(2), 263-275.

Madhupratap, M., Nair, K. N. V., Gopalakrishnan, T. C., Haridas, P., Nair, K. K. C., Venugopal, P., & Gauns, M. (2001). Arabian Sea oceanography and fisheries of the west coast of India. *Current Science*, *81*(4), 355-361.

Mahowald, N. M., Baker, A. R., Bergametti, G., Brooks, N., Duce, R. A., Jickells, T. D., ... & Tegen, I. (2005). Atmospheric global dust cycle and iron inputs to the ocean. *Global biogeochemical cycles*, *19*(4).

Maloney, K. O., Morris, D. P., Moses, C. O., & Osburn, C. L. (2005). The role of iron and dissolved organic carbon in the absorption of ultraviolet radiation in humic lake water. *Biogeochemistry*, *75*(3), 393-407.

Manizza, M., Le Quéré, C., Watson, A. J., & Buitenhuis, E. T. (2005). Bio-optical feedbacks among phytoplankton, upper ocean physics and sea-ice in a global model. *Geophysical Research Letters*, *32*(5), 1-4.

Mannino, A., Novak, M. G., Nelson, N. B., Belz, M., Berthon, J.- F., Blough, N. V., Boss, E., Bricaud, A., Chaves, J., Del Castillo, C., Del Vecchio, R., D'Sa, E. J., Freeman S., Matsuoka, A., Miller, R. L., Neeley, A. R., Röttgers R., Tzortziou, M., and Werdell, P. J. (2019) Measurement protocol of absorption by chromophoric dissolved organic matter (CDOM) and other dissolved materials, In A. Mannino, and M. G. Novak, (Ed.), *Inherent Optical Property Measurements and Protocols: Absorption Coefficient, IOCCG Ocean Optics and Biogeochemistry Protocols for Satellite Ocean Colour Sensor Validation*, Volume ###, IOCCG, Dartmouth, NS, Canada.

Manoj, N. T., & Unnikrishnan, A. S. (2009). Tidal circulation and salinity distribution in the Mandovi and Zuari estuaries: case study. *Journal of waterway, port, coastal, and ocean engineering*, *135*(6), 278-287.

Mari, X., E. Rochelle-Newall, J. P. Torréton, O. Pringault, A. Jouon, and C. Migon. (2007). Water residence time: a regulatory factor of the DOM to POM transfer efficiency. *Limnology and Oceanography*, 52(2), 808-819.

Massicotte, P., Asmala, E., Stedmon, C., & Markager, S. (2017). Global distribution of dissolved organic matter along the aquatic continuum: Across rivers, lakes and oceans. *Science of the Total Environment*, *609*, 180-191.

Matondkar, S. G. P., Gomes, H., Parab, S. G., Pednekar, S., & Goes, J. I. (2007). Phytoplankton diversity, biomass, and production. In S.R Shetye, M Dileep Kumar, and D. Shankar (Ed.), *The Mandovi and Zuari Estuaries* (pp. 67-82). National Institute of Oceanography, Goa, India.

Maya, M. V., Karapurkar, S. G., Naik, H., Roy, R., Shenoy, D. M., and Naqvi, S. W. A. (2011a). Intra-annual variability of carbon and nitrogen stable isotopes in suspended organic matter in waters of the western continental shelf of India. *Biogeosciences*, 8, 3441-3456.

Maya, M. V., Soares, M. A., Agnihotri, R., Pratihary, A. K., Karapurkar, S., Naik, H., & Naqvi, S. W. A. (2011b). Variations in some environmental characteristics including C and N stable isotopic composition of suspended organic matter in the Mandovi estuary. *Environmental Monitoring and Assessment*, *175*(1), 501-517.

Mayer, L. M., Schick, L. L., & Loder III, T. C. (1999). Dissolved protein fluorescence in two Maine estuaries. *Marine Chemistry*, *64*(3), 171-179.

McCarthy, J., & Zachara, J. (1989). ES&T Features: Subsurface transport of contaminants. *Environmental science & technology*, *23*(5), 496-502.

McKinna, L. I. (2015). Three decades of ocean-color remote-sensing Trichodesmium spp. in the World's oceans: A review. *Progress in Oceanography*, *131*, 177-199.

McKnight, D. M., Boyer, E. W., Westerhoff, P. K., Doran, P. T., Kulbe, T., & Andersen, D. T. (2001). Spectrofluorometric characterization of dissolved organic matter for indication of precursor organic material and aromaticity. *Limnology and Oceanography*, *46*(1), 38-48.

McKnight, D. M., & Aiken, G. R. (1998). Sources and age of aquatic humus. In D. O. Hessen and L. J. Tranvik (Ed.), *Aquatic humic substances* (pp. 9-39). Springer, Berlin, Heidelberg.

Medeiros, P. M., Seidel, M., Dittmar, T., Whitman, W. B., and Moran, M. A. (2015). Drought-induced variability in dissolved organic matter composition in a marsh-dominated estuary. *Geophysical Research Letters*, 42(15), 6446-6453.

Menon, H. B., Sangekar, N. P., Lotliker, A. A., & Vethamony, P. (2011). Dynamics of chromophoric dissolved organic matter in Mandovi and Zuari estuaries—A study through in situ and satellite data. *ISPRS journal of photogrammetry and remote sensing*, *66*(4), 545-552.

Menon, H. B., Lotliker, A. A., & Nayak, S. R. (2006a). Analysis of estuarine colour components during non-monsoon period through Ocean Colour Monitor. *Estuarine, Coastal and Shelf Science*, *66*(3-4), 523-531.

Menon, H. B., Lotliker, A. A., Moorthy, K. K., & Nayak, S. R. (2006b). Variability of remote sensing reflectance and implications for optical remote sensing—A study along the eastern and northeastern waters of Arabian Sea. *Geophysical research letters*, *33*(15).

Menon, H. B., Lotliker, A., & Nayak, S. R. (2005). Pre-monsoon bio-optical properties in estuarine, coastal and Lakshadweep waters. *Estuarine, Coastal and Shelf Science*, *63*(1-2), 211-223.

Minu, P., Souda, V. P., Baliarsingh, S. K., Dwivedi, R. M., Ali, Y., & Ashraf, P. M. (2020). Assessing temporal variation of coloured dissolved organic matter in the coastal waters of South Eastern Arabian Sea. *Acta Oceanologica Sinica*, *39*(1), 102-109.

Mitchell, B. G., Kahru, M., Wieland, J., Stramska, M., & Mueller, J. L. (2002). Determination of spectral absorption coefficients of particles, dissolved material and phytoplankton for discrete water samples. *Ocean optics protocols for satellite ocean color sensor validation, Revision*, *3*(2), 231.

Mitchell, B.G., Bricaud, A., Carder, K., Cleveland, J., Ferrari, G.M., Gould, R., Kahru, M., Kishino, M., et al. (2000). Determination of spectral absorption coefficients of particles, dissolved material and phytoplankton for discrete water samples. In G. Fargion, *and* J. Mueller (Ed.), *Ocean Optics Protocols For Satellite Ocean Color Sensor Validation, Revision 2, NASA Technical Memorandum* (pp. 125–153), Chapter 12, vol. 2000-209966, SIMBIOS Proj., Goddard Space Flight Center, Natl. Aeronautics and Space Admin., Greenbelt, Md.

Mitchell, B. G., & Kiefer, D. A. (1984). Determination of absorption and fluorescence excitation spectra for phytoplankton. In *Marine phytoplankton and productivity* (pp. 157-169). Springer, Berlin, Heidelberg.

Mohanty, A. K., Satpathy, K. K., Sahu, G., Hussain, K. J., Prasad, M. V. R., & Sarkar, S. K. (2010). Bloom of Trichodesmium erythraeum (Ehr.) and its impact on water quality and plankton community structure in the coastal waters of southeast coast of India. *Indian Journal of Marine Science*, *39*(3), 323-333.

Mopper, K. and Kieber, R. J. (2002). The photochemical and cycling of carbon sulfur nitrogen and phosphorus. In *Biogeochemistry of marine dissolved organic matter*. (pp.455-507), Academic Press. Elsevier Science. San Diego, CA.

Moran, M. A., Sheldon Jr, W. M., & Zepp, R. G. (2000). Carbon loss and optical property changes during long-term photochemical and biological degradation of estuarine dissolved organic matter. *Limnology and Oceanography*, *45*(6), 1254-1264.

Morel, A., & Berthon, J. F. (1989). Surface pigments, algal biomass profiles, and potential production of the euphotic layer: Relationships reinvestigated in view of remote-sensing applications. *Limnology and oceanography*, *34*(8), 1545-1562.

Mueller, J. L., Fargion, G. S., McClain, C. R., Pegau, S.,. Zanefeld, J. R. V., Gregg Mitchell, B., Kahru, M., Wieland, J., and Stramska, M. (2003). *Ocean optics protocols for satellite ocean color sensor validation, revision 4, volume IV: Inherent optical*

properties: Instruments, characterizations, field measurements and data analysis protocols. Goddard Space Flight Center.

Muller-Karger, F. E., Varela, R., Thunell, R., Luerssen, R., Hu, C., & Walsh, J. J. (2005). The importance of continental margins in the global carbon cycle. *Geophysical research letters*, *32*(1).

Murphy, K. R., Stedmon, C. A., Wenig, P., & Bro, R. (2014). OpenFluor–an online spectral library of auto-fluorescence by organic compounds in the environment. *Analytical Methods*, *6*(3), 658-661.

Murphy, K. R., Stedmon, C. A., Graeber, D., & Bro, R. (2013). Fluorescence spectroscopy and multi-way techniques. PARAFAC. *Analytical Methods*, *5*(23), 6557-6566.

Myklestad, S. M. (1995). Release of extracellular products by phytoplankton with special emphasis on polysaccharides. *Science of the total Environment*, *165*(1-3), 155-164.

Nagata, T. (2000). Production mechanisms of dissolved organic matter. In *Microbial ecology of the oceans*. (pp. 121-151), New York: John Wiley and Sons, Inc.

Naik, R., Naqvi, S. W. A., & Araujo, J. (2017). Anaerobic carbon mineralisation through sulphate reduction in the inner shelf sediments of eastern Arabian Sea. *Estuaries and Coasts*, *40*(1), 134-144.

Naqvi, S. W. A., Naik, H., Jayakumar, A., Pratihary, A. K., Narvenkar, G., Kurian, S., Agnihotri, R., Shailaja, M. S., and Narvekar, P. V. (2009a). Seasonal anoxia over the western Indian continental shelf. *Indian Ocean Biogeochemical Processes and Ecological Variability*, 1, 333-345.

Naqvi, S. W. A., Naik, H., & Narvekar, P. V. (2009b). The Arabian Sea. In K. D. Black, G. B. Shimmield (Ed.), *Biogeochemistry of marine systems* (pp. 157-198), CRC press, USA.

Naqvi, S. W. A., Naik, H., Jayakumar, D. A., Shailaja, M. S., & Narvekar, P. V. (2006). Seasonal oxygen deficiency over the western continental shelf of India. In *Past and present water column anoxia* (pp. 195-224). Springer, Dordrecht.

Naqvi, S. W. A., Jayakumar, D. A., Narvekar, P. V., Naik, H., Sarma, V. V. S. S., D'souza, W., ... & George, M. D. (2000). Increased marine production of N2O due to intensifying anoxia on the Indian continental shelf. *Nature*, *408*(6810), 346-349.

Naqvi, S. W. A., George, M. D., Narvekar, P. V., Jayakumar, D. A., Shailaja, M. S., Sardessai, S., ... & Binu, M. S. (1998). Severe fish mortality associated with'red tide'observed in the sea off Cochin. *Current Science*, *75*(6), 543-544.

Narvekar, J., Chowdhury, R. R., Gaonkar, D., Kumar, P. D., & Kumar, S. P. (2021). Observational evidence of stratification control of upwelling and pelagic fishery in the eastern Arabian Sea. *Scientific Reports*, *11*(1), 1-13.

Nelson, N. B., & Siegel, D. A. (2013). The global distribution and dynamics of chromophoric dissolved organic matter. *Annual review of marine science*, *5*, 447-476.

Nelson, N. B., Siegel, D. A., Carlson, C. A., & Swan, C. M. (2010). Tracing global biogeochemical cycles and meridional overturning circulation using chromophoric dissolved organic matter. *Geophysical Research Letters*, *37*(3), L03610.

Nelson, N. B., Carlson, C. A., and Steinberg, D. K. (2004). Production of chromophoric dissolved organic matter by Sargasso Sea microbes. *Marine Chemistry*, 89(1), 273-287.

Nelson, N. B., & Siegel, D. A. (2002). Chromophoric DOM in the open ocean. *Biogeochemistry of marine dissolved organic matter*, 547-578.

Neveux, J., Tenírio, M. M., Dupouy, C., & Villareal, T. A. (2006). Spectral diversity of phycoerythrins and diazotroph abundance in tropical waters. *Limnology and Oceanography*, *51*(4), 1689-1698.

Nikolaou, A. D., Meric, S., Lekkas, D. F., Naddeo, V., Belgiorno, V., Groudev, S., and Tanik, A. (2008). Multi-parametric water quality monitoring approach according to the WFD application in Evros trans-boundary river basin: priority pollutants. *Desalination*, 226(1), 306-320.

Norrman, B., Zwelfel, U. L., Hopkinson Jr, C. S., & Brian, F. (1995). Production and utilization of dissolved organic carbon during an experimental diatom bloom. *Limnology and Oceanography*, *40*(5), 898-907.

Ogawa, H., Amagai, Y., Koike, I., Kaiser, K., & Benner, R. (2001). Production of refractory dissolved organic matter by bacteria. *Science*, *292*(5518), 917-920.

Okaichi, T. (1976). Identification of ammonia as the toxic principle of red tide of *Noctiluca miliaris*. *Bulletin Plankton Society Japan*, *23*, 75-80.

Omori, Y., Hama, T., Ishii, M., & Saito, S. (2011). Vertical change in the composition of marine humic-like fluorescent dissolved organic matter in the subtropical western North Pacific and its relation to photoreactivity. *Marine Chemistry*, *124*(1-4), 38-47.

Omori, Y., Hama, T., Ishii, M., & Saito, S. (2010). Relationship between the seasonal change in fluorescent dissolved organic matter and mixed layer depth in the subtropical western North Pacific. *Journal of Geophysical Research: Oceans*, *115*(C6).

Oren, A., & Gunde-Cimerman, N. (2007). Mycosporines and mycosporine-like amino acids: UV protectants or multipurpose secondary metabolites?. *FEMS microbiology letters*, *269*(1), 1-10.

Padmakumar, K. B., SreeRenjima, G., Fanimol, C. L., Menon, N. R., & Sanjeevan, V. N. (2010). Preponderance of heterotrophic Noctiluca scintillans during a multi-species diatom bloom along the southwest coast of India. *International Journal of Oceans and Oceanography*, *4*(1), 55-63.

Paerly, H. W., Bebout, B. M., & Prufert, L. E. (1989). Bacterial associations with marine oscillatoria sp.(trichodesmium sp.) Populations: ecophysiological implications. *Journal of Phycology*, *25*(4), 773-784.

Pandi, S. R., Chari, N. V. H. K., Sarma, N. S., Lotliker, A. A., Tripathy, S. C., & Bajish, C. C. (2021). Spatiotemporal variability in the optical characteristics of dissolved organic matter in the coastal Bay of Bengal. *International Journal of Environmental Science and Technology*, 1-16.

Para, J., Coble, P. G., Charrière, B., Tedetti, M., Fontana, C., & Sempere, R. (2010). Fluorescence and absorption properties of chromophoric dissolved organic matter (CDOM) in coastal surface waters of the northwestern Mediterranean Sea, influence of the Rhône River. *Biogeosciences*, *7*(12), 4083-4103.

Parab, S. G., Matondkar, S. P., Gomes, H. D. R., & Goes, J. I. (2013). Effect of freshwater influx on phytoplankton in the Mandovi estuary (Goa, India) during monsoon season: Chemotaxonomy. *Journal of Water Resource and Protection, 5*, 349- 361.

Parab, S. G., & Matondkar, S. G. P. (2012). Primary productivity and nitrogen fixation by *Trichodesmium* spp. in the Arabian Sea. *Journal of Marine Systems*, *105*, 82-95.

Parab, S. G., Matondkar, S. P., Gomes, H. D. R., & Goes, J. I. (2006). Monsoon driven changes in phytoplankton populations in the eastern Arabian Sea as revealed by microscopy and HPLC pigment analysis. *Continental Shelf Research*, *26*(20), 2538-2558.

Pednekar, S. M., Bates, S. S., Kerkar, V., & Matondkar, S. P. (2018). Environmental factors affecting the distribution of Pseudo-nitzschia in two monsoonal estuaries of Western India and effects of salinity on growth and domoic acid production by P. pungens. *Estuaries and Coasts*, *41*(5), 1448-1462.

Pednekar, S. M., Matondkar, S. G. P., and Kerkar, V. (2012). Spatiotemporal distribution of harmful algal flora in the tropical estuarine complex of Goa, India. *The Scientific World Journal*, 1-11.

Pefanis, V., Losa, S. N., Losch, M., Janout, M. A., & Bracher, A. (2020). Amplified Arctic surface warming and sea ice loss due to phytoplankton and colored dissolved material. *Geophysical Research Letters*, *47*(21), e2020GL088795.

Pegau, W. S., Cleveland, J. S., Doss, W., Kennedy, C. D., Maffione, R. A., Mueller, J. L., ... & Zaneveld, J. R. V. (1995). A comparison of methods for the measurement of the absorption coefficient in natural waters. *Journal of Geophysical Research: Oceans*, *100*(C7), 13201-13220.

Peierls, B. L., Hall, N. S., and Paerl, H. W.. (2012). Non-monotonic responses of phytoplankton biomass accumulation to hydrologic variability: a comparison of two coastal plain North Carolina estuaries. *Estuaries and coasts*, 35(6), 1376-1392.

Peter, S., Isidorova, A., & Sobek, S. (2016). Enhanced carbon loss from anoxic lake sediment through diffusion of dissolved organic carbon. *Journal of Geophysical Research: Biogeosciences*, *121*(7), 1959-1977.

Piontek, J., Borchard, C., Sperling, M., Schulz, K. G., Riebesell, U., & Engel, A. (2013). Response of bacterioplankton activity in an Arctic fjord system to elevated pCO 2: results from a mesocosm perturbation study. *Biogeosciences*, *10*(1), 297-314.

Prasanna Kumar, S., Narvekar, J., Kumar, A., Shaji, C., Anand, P., Sabu, P., ... & Nair, K. K. C. (2004). Intrusion of the Bay of Bengal water into the Arabian Sea during winter monsoon and associated chemical and biological response. *Geophysical Research Letters*, *31*(15).

Prasanna Kumar, S., Madhupratap, M., Kumar, M. D., Muraleedharan, P. M., De Souza, S. N., Gauns, M., & Sarma, V. V. S. S. (2001). High biological productivity in the central Arabian Sea during the summer monsoon driven by Ekman pumping and lateral advection. *Current Science*, 1633-1638.

Pratihary, A. K., Naqvi, S. W. A., Narvenkar, G., Kurian, S., Naik, H., Naik, R., & Manjunatha, B. R. (2014). Benthic mineralization and nutrient exchange over the inner continental shelf of western India. *Biogeosciences*, *11*(10), 2771-2791.

Qasim, S. Z., & Sen Gupta, R. (1981). Environmental characteristics of the Mandovi-Zuari estuarine system in Goa. *Estuarine, Coastal and Shelf Science*, *13*(5), 557-578.

Qasim, S. Z. (1972). Some observations on *Trichodesmium* blooms. In T.V. Desikachary (Ed.), *International Symposium on Taxonomy and Biology of Bluegreen Algae* (pp. 433–438), Bangalore Press, Madras.

Ram, A. P., Nair, S., & Chandramohan, D. (2007). Bacterial growth efficiency in a tropical estuary: seasonal variability subsidized by allochthonous carbon. *Microbial ecology*, *53*(4), 591-599.

Ramaiah, N., Rodrigues, V., Alwares, E., Rodrigues, C., Baksh, R., Jayan, S., & Mohandass, C. (2007). Sewage-pollution indicator bacteria. In S.R Shetye, M Dileep Kumar, and D. Shankar (Ed.), *The Mandovi and Zuari Estuaries* (pp. 115-120). National Institute of Oceanography, Goa, India.

Ramaswamy, V., Muraleedharan, P. M., & Babu, C. P. (2017). Mid-troposphere transport of Middle-East dust over the Arabian Sea and its effect on rainwater composition and sensitive ecosystems over India. *Scientific reports*, *7*(1), 1-8.

Rao, V. P., & Chakraborty, P., (2016). Estuarine and marine geology (2011-2015). *Proc Indian Natn Sci Acad, 82*(3), 625 -637.

Rao, V. P., Shynu, R., Singh, S. K., Naqvi, S. W. A., and Kessarkar, P. M. (2015). Mineralogy and Sr–Nd isotopes of SPM and sediment from the Mandovi and Zuari estuaries: Influence of weathering and anthropogenic contribution. *Estuarine, Coastal and Shelf Science*, 156, 103-115.

Rao, V. P., Shynu, R., Kessarkar, P. M., Sundar, D., Michael, G. S., Narvekar, T., ... & Mehra, P. (2011). Suspended sediment dynamics on a seasonal scale in the Mandovi and Zuari estuaries, central west coast of India. *Estuarine, Coastal and Shelf Science*, *91*(1), 78-86.

Rastogi, R. P., & Sinha, R. P. (2009). Biotechnological and industrial significance of cyanobacterial secondary metabolites. *Biotechnology advances*, *27*(4), 521-539.

Raymond, P. A., & Spencer, R. G. (2015). Riverine DOM. In *Biogeochemistry of marine dissolved organic matter* (pp. 509-533). Academic Press.

Reche, I., Pace, M. L., & Cole, J. J. (1999). Relationship of trophic and chemical conditions to photobleaching of dissolved organic matter in lake ecosystems. *Biogeochemistry*, *44*(3), 259-280.

Reche, I., Pace, M. L., & Cole, J. J. (1998). Interactions of photobleaching and inorganic nutrients in determining bacterial growth on colored dissolved organic carbon. *Microbial Ecology*, *36*(3-4), 270-280.

Rennella, A. M., and Quiros, R. (2006).The effects of hydrology on plankton biomass in shallow lakes of the Pampa Plain. *Hydrobiologia*, 556(1), 181-191.

Richa, R. R., Kumari, S., Singh, K. L., Kannaujiya, V. K., Singh, G., Kesheri, M., & Sinha, R. P. (2011). Biotechnological potential of mycosporine-like amino acids and phycobiliproteins of cyanobacterial origin. *Biotechnol Bioinform Bioeng*, *1*, 159-171.

Riedel, T., Zak, D., Biester, H., & Dittmar, T. (2013). Iron traps terrestrially derived dissolved organic matter at redox interfaces. *Proceedings of the National Academy of Sciences*, *110*(25), 10101-10105.

River Rejuvenation Committee (2019). Preparation of Action Plan for Rejuvenation of Polluted Stretches of Rivers in Goa, *Action Plan Report on Zuari River.* Goa, India.

Robinson, C. (2019). Microbial respiration, the engine of ocean deoxygenation. *Frontiers in Marine Science*, *5*, 533.

Rochelle-Newall, E. J., and Fisher, T. R. (2002).Chromophoric dissolved organic matter and dissolved organic carbon in Chesapeake Bay. *Marine Chemistry*, 77(1), 23-41.

Rodrigues, V., Ramaiah, N., Kakti, S., and Samant, D. (2011). Long-term variations in abundance and distribution of sewage pollution indicator and human pathogenic bacteria along the central west coast of India. *Ecological indicators*, 11(2), 318-327.

Romera-Castillo, C., Sarmento, H., Alvarez-Salgado, X. A., Gasol, J. M., & Marraséa, C. (2010). Production of chromophoric dissolved organic matter by marine phytoplankton. *Limnology and Oceanography*, *55*(1), 446-454.

Röttgers, R., Häse, C., & Doerffer, R. (2007). Determination of the particulate absorption of microalgae using a point-source integrating-cavity absorption meter: verification with a photometric technique, improvements for pigment bleaching, and correction for chlorophyll fluorescence. *Limnology and Oceanography: Methods*, *5*(1), 1-12.

Roxy, M. K., Gnanaseelan, C., Parekh, A., Chowdary, J. S., Singh, S., Modi, A., ... & Rajeevan, M. (2020). Indian Ocean Warming. In *Assessment of Climate Change over the Indian Region* (pp. 191-206). Springer, Singapore.

Roy, R., Pratihary, A., Narvenkar, G., Mochemadkar, S., Gauns, M., & Naqvi, S. W. A. (2011). The relationship between volatile halocarbons and phytoplankton pigments during a *Trichodesmium* bloom in the coastal eastern Arabian Sea. *Estuarine, Coastal and Shelf Science*, *95*(1), 110-118.

Roy, R., Pratihary, A., Mangesh, G., & Naqvi, S. W. A. (2006). Spatial variation of phytoplankton pigments along the southwest coast of India. *Estuarine, Coastal and Shelf Science*, *69*(1-2), 189-195.

Sabine, C. L., Feely, R. A., Gruber, N., Key, R. M., Lee, K., Bullister, J. L., ... & Rios, A. F. (2004). The oceanic sink for anthropogenic CO2. *science*, *305*(5682), 367-371.

Sahayak, S., Jyothibabu, R., Jayalakshmi, K. J., Habeebrehman, H., Sabu, P., Prabhakaran, M. P., ... & Nair, K. K. C. (2005). Red tide of Noctiluca miliaris off south of Thiruvananthapuram subsequent to the 'stench event'at the southern Kerala coast. *Current Science, 89*(9), 1472- 1473.

Sankaranarayanan, V. N., & Jayaraman, R. (1972). Intrusion of upwelled water in the Mandovi and Zuari estuaries. *Current Science*, *41*(6), 204-206.

Santschi, P. H., Guo, L., Means, J. C., & Ravichandran, M. (1998). Natural Organic Matter Binding of Trace Metals and Trace Organic Contaminants. In *Biogeochemistry of Gulf of Mexico Estuaries*. (pp. 347-372). John Wiley and Sons, Inc, USA.

Sanyal, P., Ray, R., Paul, M., Gupta, V.K., Acharya, A., Bakshi, S., Jana, T.K., and Mukhopadhyay, S.K. (2020) Assessing the Dynamics of Dissolved Organic Matter (DOM) in the Coastal Environments Dominated by Mangroves, Indian Sundarbans. *Front. Earth Sci*. 8:218. doi: 10.3389

Sarma, N. S., Pandi, S. R., Chari, N. V. H. K., Chiranjeevulu, G., Kiran, R., Krishna, K. S., ... & Raman, A. (2018). Spectral modelling of estuarine coloured dissolved organic matter. *Curr. Sci*, *114*(8), 1762-1767.

Satheesh, S. K., & Srinivasan, J. (2002). Enhanced aerosol loading over Arabian Sea during the pre-monsoon season: Natural or anthropogenic?. *Geophysical Research Letters*, *29*(18), 21-1.

Sathyendranath, S., and Varadachari, V.V.R. (1982). Light penetration in the coastal waters off Goa. *Indian Journal of Marine Science, 11*, 148-152.

Scholz, F., Severmann, S., McManus, J., Noffke, A., Lomnitz, U., & Hensen, C. (2014). On the isotope composition of reactive iron in marine sediments: Redox shuttle versus early diagenesis. *Chemical Geology*, *389*, 48-59.

Sellner, K. G. (1992). Trophodynamics of marine cyanobacteria blooms. In *Marine pelagic cyanobacteria: Trichodesmium and other diazotrophs* (pp. 75-94). Springer, Dordrecht.

Sen Gupta, R., & Naqvi, S. W. A. (1984). Chemical oceanography of the Indian Ocean, north of the equator. *Deep Sea Research Part A. Oceanographic Research Papers*, *31*(6-8), 671-706.

Shank, G. C., Zepp, R. G., Vähätalo, A., Lee, R., & Bartels, E. (2010). Photobleaching kinetics of chromophoric dissolved organic matter derived from mangrove leaf litter and floating Sargassum colonies. *Marine Chemistry*, *119*(1-4), 162-171.

Shanmugam, P., Varunan, T., Jaiganesh, S. N., Sahay, A., & Chauhan, P. (2016). Optical assessment of colored dissolved organic matter and its related parameters in dynamic coastal water systems. *Estuarine, Coastal and Shelf Science*, *175*, 126-145.

Shetye, S. R., Dileep Kumar, M., and Shankar, D.. (2007). *The Mandovi and Zuari Estuaries*. National Institute of Oceanography, India.

Shetye, S. R. (1999). Propagation of tides in the Mandovi and Zuari estuaries. *Sadhana*, *24*(1-2), 5-16.

Shi, T., Sun, Y., & Falkowski, P. G. (2007). Effects of iron limitation on the expression of metabolic genes in the marine cyanobacterium Trichodesmium erythraeum IMS101. *Environmental Microbiology*, *9*(12), 2945-2956.

Shukla, R. P., & Huang, B. (2016). Mean state and interannual variability of the Indian summer monsoon simulation by NCEP CFSv2. *Climate Dynamics*, *46*(11), 3845-3864.

Shynu, R., Rao, P., Sarma, V. V. S. S., Kessarkar, P. M., & Murali, R. M. (2015). Sources and fate of organic matter in suspended and bottom sediments of the Mandovi and Zuari estuaries, western India. *Current Science*, 226-238.

Shynu, R., Rao, V. P., Kessarkar, P. M., & Rao, T. G. (2012). Temporal and spatial variability of trace metals in suspended matter of the Mandovi estuary, central west coast of India. *Environmental Earth Sciences*, *65*(3), 725-739.

Siegel, D. A., Maritorena, S., Nelson, N. B., Hansell, D. A., & Lorenzi-Kayser, M. (2002). Global distribution and dynamics of colored dissolved and detrital organic materials. *Journal of Geophysical Research: Oceans*, *107*(C12), 21-1.

Singbal, S. Y. S. (1973). Diurnal variations of some physico-chemical factors in the Zuari estuary of Goa. *Indian Journal of Marine Science*, *2*, 90-93.

Sivonen, K., & Börner, T. (2008). Bioactive compounds produced by cyanobacteria. In A. Herraro, and E. Flores (Ed.), *The cyanobacteria: molecular biology, genomics and evolution*, (pp.159-197), Caister Academic Press, Norfolk.

Skoog, A. C., & Arias-Esquivel, V. A. (2009). The effect of induced anoxia and reoxygenation on benthic fluxes of organic carbon, phosphate, iron, and manganese. *Science of the total environment*, *407*(23), 6085-6092.

Skoog, A., Hall, P. O., Hulth, S., Paxéus, N., Van Der Loeff, M. R., & Westerlund, S. (1996). Early diagenetic production and sediment-water exchange of fluorescent dissolved organic matter in the coastal environment. *Geochimica et Cosmochimica Acta*, *60*(19), 3619-3629.

Smitha, B. R., Sanjeevan, V. N., Vimalkumar, K. G., & Revichandran, C. (2008). On the upwelling off the southern tip and along the west coast of India. *Journal of Coastal Research*, (24), 95-102.

Song, K., Zhao, Y., Wen, Z., Fang, C., & Shang, Y. (2017). A systematic examination of the relationships between CDOM and DOC in inland waters in China. *Hydrology and Earth System Sciences*, *21*(10), 5127-5141.

Spencer, R. G., Aiken, G. R., Wickland, K. P., Striegl, R. G., & Hernes, P. J. (2008). Seasonal and spatial variability in dissolved organic matter quantity and composition from the Yukon River basin, Alaska. *Global Biogeochemical Cycles*, *22*(4), 1-13.

Spilling, K., Kremp, A., Klais, R., Olli, K., & Tamminen, T. (2014). Spring bloom community change modifies carbon pathways and C: N: P: Chl a stoichiometry of coastal material fluxes. *Biogeosciences*, *11*(24), 7275-7289.

Stedmon, C. A., Thomas, D. N., Papadimitriou, S., Granskog, M. A., & Dieckmann, G. S. (2011). Using fluorescence to characterize dissolved organic matter in Antarctic sea ice brines. *Journal of Geophysical Research: Biogeosciences*, *116*(G3).

Stedmon, C. A., & Bro, R. (2008). Characterizing dissolved organic matter fluorescence with parallel factor analysis: a tutorial. *Limnology and Oceanography: Methods*, *6*(11), 572-579.

Stedmon, C. A., & Markager, S. (2005). Resolving the variability in dissolved organic matter fluorescence in a temperate estuary and its catchment using PARAFAC analysis. *Limnology and oceanography*, *50*(2), 686-697.

Stedmon, C. A., Markager, S., & Bro, R. (2003). Tracing dissolved organic matter in aquatic environments using a new approach to fluorescence spectroscopy. *Marine chemistry*, *82*(3-4), 239-254.

Stedmon, C. A., Markager, S., & Kaas, H. (2000). Optical properties and signatures of chromophoric dissolved organic matter (CDOM) in Danish coastal waters. *Estuarine, Coastal and Shelf Science*, *51*(2), 267-278.

Steinberg, D. K., Nelson, N. B., Carlson, C. A., & Prusak, A. (2004). Production of chromophoric dissolved organic matter (CDOM) in the open ocean by zooplankton and the colonial cyanobacterium Trichodesmium spp. *Marine Ecology Progress Series*, *267*, 45-56.

Subramaniam, A., Carpenter, E. J., & Falkowski, P. G. (1999). Bio-optical properties of the marine diazotrophic cyanobacteria *Trichodesmium spp*. II. A reflectance model for remote sensing. *Limnology and Oceanography*, *44*(3), 618-627.

Suksomjit, M., Nagao, S., Ichimi, K., Yamada, T., & Tada, K. (2009). Variation of dissolved organic matter and fluorescence characteristics before, during and after phytoplankton bloom. *Journal of Oceanography*, *65*(6), 835-846.

Suresh, T., Naik, P., Bandishte, M., Desa, E., Mascaranahas, A., & Matondkar, S. P. (2006a, November). Secchi depth analysis using bio-optical parameters measured in the Arabian Sea. In *Remote sensing of the marine environment* (Vol. 6406, p. 64061Q). International Society for Optics and Photonics.

Suresh, T., Desa, E., Mascaranahas, A., Matondkar, S. P., Naik, P., & Nayak, S. R. (2006b, November). An empirical method to estimate bulk particulate refractive index for ocean satellite applications. In *Remote Sensing of the Marine Environment* (Vol. 6406, p. 64060B). International Society for Optics and Photonics.

Suresh, T., Desa, E., Kurian, J., & Mascarenhas, A. (1998). Measurement of inherent optical properties in the Arabian Sea. *Indian Journal of Marine Sciences, 27*, 274-280.

Suresh, T., Desa, E., Desai, R. G. P., Jayaraman, A., & Mehra, P. (1996). Photosynthetically available radiation in the central and eastern Arabian Sea. *Current Science*, *71*(11), 883-887.

Swan, C. M., Siegel, D. A., Nelson, N. B., Carlson, C. A., & Nasir, E. (2009). Biogeochemical and hydrographic controls on chromophoric dissolved organic matter distribution in the Pacific Ocean. *Deep Sea Research Part I: Oceanographic Research Papers*, *56*(12), 2175-2192.

Takata, H., Kuma, K., Iwade, S., Isoda, Y., Kuroda, H., & Senjyu, T. (2005). Comparative vertical distributions of iron in the Japan Sea, the Bering Sea, and the western North Pacific Ocean. *Journal of Geophysical Research: Oceans*, *110*(C7).

Talaulikar, M., Suresh, T., Desa, E., & Inamdar, A. (2015). Optical closure of apparent optical properties in coastal waters off Goa. *Journal of the Indian Society of Remote Sensing*, *43*(1), 163-171.

Tanaka, K., Kuma, K., Hamasaki, K., & Yamashita, Y. (2014). Accumulation of humic-like fluorescent dissolved organic matter in the Japan Sea. *Scientific reports*, *4*(1), 1-7.

Tanaka, T. Y., & Chiba, M. (2006). A numerical study of the contributions of dust source regions to the global dust budget. *Global and Planetary Change*, *52*(1-4), 88-104.

Teira, E., Fernández, A., Álvarez-Salgado, X. A., García-Martín, E. E., Serret, P., & Sobrino, C. (2012). Response of two marine bacterial isolates to high CO2 concentration. *Marine Ecology Progress Series*, *453*, 27-36.

Thayapurath, S., Joshi, S., Talaulikar, M., & Desa, E. J. (2016, May). Preliminary results of algorithms to determine horizontal and vertical underwater visibilities of coastal waters. In *Remote Sensing of the Oceans and Inland Waters: Techniques, Applications, and Challenges* (Vol. 9878, p. 98781I). International Society for Optics and Photonics.

Tilstone, G. H., Lotliker, A. A., Miller, P. I., Ashraf, P. M., Kumar, T. S., Suresh, T., ... & Menon, H. B. (2013). Assessment of MODIS-Aqua chlorophyll-a algorithms in coastal and shelf waters of the eastern Arabian Sea. *Continental Shelf Research*, *65*, 14-26.

Tilstone, G. H., Moore, G. F., Sørensen, K., Doerfeer, R., Røttgers, R., Ruddick, K. D., ... & Jørgensen, P. V. (2002). Regional validation of MERIS chlorophyll products in North Sea coastal waters. *REVAMP Methodologies EVGI-CT-2001-00049*.

Timko, S. A., Gonsior, M., & Cooper, W. J. (2015). Influence of pH on fluorescent dissolved organic matter photo-degradation. *Water research*, *85*, 266-274.

Tiwari, S. P., & Shanmugam, P. (2011). An optical model for the remote sensing of coloured dissolved organic matter in coastal/ocean waters. *Estuarine, Coastal and Shelf Science*, *93*(4), 396-402.

Tomas, C. R., & Haste, G. R. (1997). *Identifying marine phytoplankton*. Academic Press. *New York*.

Twardowski, M. S., Boss, E., Sullivan, J. M., & Donaghay, P. L. (2004). Modeling the spectral shape of absorption by chromophoric dissolved organic matter. *Marine Chemistry*, *89*(1-4), 69-88.

Uher, G., Hughes, C., Henry, G., and Upstill-Goddard, R. C. (2001). Non-conservative mixing behavior of colored dissolved organic matter in a humic-rich, turbid estuary. *Geophysical Research Letters*, 28(17), 3309-3312.

Unnikrishnan, A. S., & Manoj, N. T. (2007). Numerical models. In S.R Shetye, M Dileep Kumar, and D. Shankar (Ed.), *The Mandovi and Zuari Estuaries* (pp. 39-48). National Institute of Oceanography, Goa, India.

Unnikrishnan, A. S., Shetye, S. R., & Gouveia, A. D. (1997). Tidal propagation in the Mandovi–Zuari estuarine network, west coast of India: Impact of freshwater influx. *Estuarine, Coastal and Shelf Science*, *45*(6), 737-744.

Van Baalen, C., & Brown, R. M. (1969). The ultrastructure of the marine blue green alga, *Trichodesmium erythraeum*, with special reference to the cell wall, gas vacuoles, and cylindrical bodies. *Archiv für Mikrobiologie*, *69*(1), 79-91.

Van den Meersche, K., Middelburg, J. J., Soetaert, K., Van Rijswijk, P., Boschker, H. T., & Heip, C. H. (2004). Carbon-nitrogen coupling and algal-bacterial interactions during an

experimental bloom: Modeling a 13C tracer experiment. *Limnology and Oceanography*, *49*(3), 862-878.

Vantrepotte, V., Danhiez, F. P., Loisel, H., Ouillon, S., Mériaux, X., Cauvin, A., & Dessailly, D. (2015). CDOM-DOC relationship in contrasted coastal waters: implication for DOC retrieval from ocean color remote sensing observation. *Optics express*, *23*(1), 33-54.

Veerasingam, S., Vethamony, P., ManiMurali, R., & Babu, M. T. (2015). Sources, vertical fluxes and accumulation of petroleum hydrocarbons in sediments from the Mandovi estuary, west coast of India. *International Journal of Environmental Research*, *9*(1), 179-186.

Vijith, V., and Shetye, S. R. (2012). A stratification prediction diagram from characteristics of geometry, tides and runoff for estuaries with a prominent channel. *Estuarine, Coastal and Shelf Science*, 98, 101-107.

Vijith, V., D. Sundar, and Shetye, S. R. (2009). Time-dependence of salinity in monsoonal estuaries. *Estuarine, Coastal and Shelf Science*, 85(4), 601-608.

Vodacek, A., Blough, N. V., DeGrandpre, M. D., DeGrandpre, M. D., & Nelson, R. K. (1997). Seasonal variation of CDOM and DOC in the Middle Atlantic Bight: Terrestrial inputs and photooxidation. *Limnology and Oceanography*, *42*(4), 674-686.

Wachenfeldt, E., and Tranvik, L. J. (2008). Sedimentation in boreal lakes—the role of flocculation of allochthonous dissolved organic matter in the water column. *Ecosystems*, 11(5), 803-814.

Wafar, S., Untawale, A. G., and Wafar, M. (1997). Litter fall and energy flux in a mangrove ecosystem. *Estuarine, Coastal and Shelf Science*, 44(1), 111-124.

Wafar, S. (1987). *Ecology of mangroves along the estuaries of Goa*. (Ph. D. Thesis, Karnataka University, Dharward).

Walsh, J. J. (1991). Importance of continental margins in the marine biogeochemical cycling of carbon and nitrogen. *Nature*, *350*(6313), 53-55.

Wang, L., Lin, X., Goes, J. I., & Lin, S. (2016). Phylogenetic analyses of three genes of Pedinomonas noctilucae, the green endosymbiont of the marine dinoflagellate Noctiluca scintillans, reveal its affiliation to the order Marsupiomonadales (Chlorophyta, Pedinophyceae) under the reinstated name Protoeuglena noctilucae. *Protist*, *167*(2), 205-216.

Watanabe, S., Sudo, K., Nagashima, T., Takemura, T., Kawase, H., & Nozawa, T. (2011). Future projections of surface UV-B in a changing climate. *Journal of Geophysical Research: Atmospheres*, *116*(D16).

Watson, S. J., Cade-Menun, B. J., Needoba, J. A., & Peterson, T. D. (2018). Phosphorus forms in sediments of a river-dominated estuary. *Frontiers in Marine Science*, *5*, 302.

Webb, E. A., Moffett, J. W., & Waterbury, J. B. (2001). Iron stress in open-ocean cyanobacteria (Synechococcus, Trichodesmium, and Crocosphaera spp.): identification of the IdiA protein. *Applied and Environmental Microbiology*, *67*(12), 5444-5452.

Webster, P. J., Magana, V. O., Palmer, T. N., Shukla, J., Tomas, R. A., Yanai, M. U., & Yasunari, T. (1998). Monsoons: Processes, predictability, and the prospects for prediction. *Journal of Geophysical Research: Oceans*, *103*(C7), 14451-14510.

Wetz, M. S., & Wheeler, P. A. (2007). Release of dissolved organic matter by coastal diatoms. *Limnology and Oceanography*, *52*(2), 798-807.

Whitehead, K., & Hedges, J. I. (2005). Photodegradation and photosensitization of mycosporine-like amino acids. *Journal of Photochemistry and Photobiology B: Biology*, *80*(2), 115-121.

Whittaker, S., Bidle, K. D., Kustka, A. B., & Falkowski, P. G. (2011). Quantification of nitrogenase in Trichodesmium IMS 101: implications for iron limitation of nitrogen fixation in the ocean. *Environmental Microbiology Reports*, *3*(1), 54-58.

Wiggert, J. D., Hood, R. R., Banse, K., & Kindle, J. C. (2005). Monsoon-driven biogeochemical processes in the Arabian Sea. *Progress in Oceanography*, *65*(2-4), 176-213.

Willey, J. D., Kieber, R. J., Eyman, M. S., & Avery Jr, G. B. (2000). Rainwater dissolved organic carbon: concentrations and global flux. *Global Biogeochemical Cycles*, *14*(1), 139-148.

Wu, J., Zhang, H., He, P. J., & Shao, L. M. (2011). Insight into the heavy metal binding potential of dissolved organic matter in MSW leachate using EEM quenching combined with PARAFAC analysis. *Water research*, *45*(4), 1711-1719.

Yamashita, Y., Nosaka, Y., Suzuki, K., Ogawa, H., Takahashi, K., and Saito, H. (2013). Photobleaching as a factor controlling spectral characteristics of chromophoric dissolved organic matter in open ocean. *Biogeosciences*, 10(11), 7207-7217.

Yamashita, Y., Cory, R. M., Nishioka, J., Kuma, K., Tanoue, E., & Jaffé, R. (2010). Fluorescence characteristics of dissolved organic matter in the deep waters of the Okhotsk Sea and the northwestern North Pacific Ocean. *Deep Sea Research Part II: Topical Studies in Oceanography*, *57*(16), 1478-1485.

Yamashita, Y., & Tanoue, E. (2009). Basin scale distribution of chromophoric dissolved organic matter in the Pacific Ocean. *Limnology and Oceanography*, *54*(2), 598-609.

Yamashita, Y., & Tanoue, E. (2008). Production of bio-refractory fluorescent dissolved organic matter in the ocean interior. *Nature Geoscience*, *1*(9), 579-582.

Yamashita, Y., Tsukasaki, A., Nishida, T., & Tanoue, E. (2007). Vertical and horizontal distribution of fluorescent dissolved organic matter in the Southern Ocean. *Marine Chemistry*, *106*(3-4), 498-509.

Yamashita, Y., & Tanoue, E. (2004). In situ production of chromophoric dissolved organic matter in coastal environments. *Geophysical Research Letters*, *31*(14).

Yamashita, Y., & Tanoue, E. (2003). Chemical characterization of protein-like fluorophores in DOM in relation to aromatic amino acids. *Marine Chemistry*, *82*(3-4), 255-271.

Yuan, D., Wang, H., An, Y., Guo, X., & He, L. (2019). Insight into the binding properties of carbamazepine onto dissolved organic matter using spectroscopic techniques during grassy swale treatment. *Ecotoxicology and environmental safety*, *173*, 444-451.

Zaneveld, J. R., & Pegau, W. S. (1993). Temperature-dependent absorption of water in the red and near-infrared portions of the spectrum. *Limnology and Oceanography*, *38*(1), 188-192.

Zaneveld, J. R. V., Kitchen, J. C., & Pak, H. (1981). The influence of optical water type on the heating rate of a constant depth mixed layer. *Journal of Geophysical Research: Oceans*, *86*(C7), 6426-6428.

Zhang, J., Hu, A., Wang, B., & Ran, W. (2019). Al (III)-binding properties at the molecular level of soil DOM subjected to long-term manuring. *Journal of Soils and Sediments*, *19*(3), 1099-1108.

Zhang, Y., Zhou, L., Zhou, Y., Zhang, L., Yao, X., Shi, K., ... & Zhu, W. (2021). Chromophoric dissolved organic matter in inland waters: Present knowledge and future challenges. *Science of the Total Environment*, *759*, 143550.

Zhang, Y., Yin, Y., Feng, L., Zhu, G., Shi, Z., Liu, X., & Zhang, Y. (2011). Characterizing chromophoric dissolved organic matter in Lake Tianmuhu and its catchment basin using excitation-emission matrix fluorescence and parallel factor analysis. *water research*, *45*(16), 5110-5122.

Zhang, Y., Zhang, E., Yin, Y., Van Dijk, M. A., Feng, L., Shi, Z., ... & Qina, B. (2010). Characteristics and sources of chromophoric dissolved organic matter in lakes of the Yungui Plateau, China, differing in trophic state and altitude. *Limnology and Oceanography*, *55*(6), 2645-2659.

Zhang, Y., van Dijk, M. A., Liu, M., Zhu, G., & Qin, B. (2009). The contribution of phytoplankton degradation to chromophoric dissolved organic matter (CDOM) in

eutrophic shallow lakes: field and experimental evidence. *Water research*, *43*(18), 4685-4697.

Zhao, Z., Gonsior, M., Luek, J., Timko, S., Ianiri, H., Hertkorn, N., ... & Chen, F. (2017). Picocyanobacteria and deep-ocean fluorescent dissolved organic matter share similar optical properties. *Nature communications*, *8*, 15284.

Zielinski, O., Rüssmeier, N., Ferdinand, O. D., Miranda, M. L., & Wollschläger, J. (2018). Assessing fluorescent organic matter in natural waters: towards in situ excitation–emission matrix spectroscopy. *Applied Sciences*, *8*(12), 2685.

Publications and Conference Participation

Publications

- **Dias, A.B.,** Thayapurath, S., Sahay, S., and Chauhan, P. (2017). Contrasting characteristics of colored dissolved organic matter of the coastal and estuarine waters of Goa during summer. *Indian Journal of Geo-Marine Science*, *49*(50), 860-870.
- **Dias, A.,** Kurian, S., & Thayapurath, S. (2020). Influence of environmental parameters on bio-optical characteristics of colored dissolved organic matter in a complex tropical coastal and estuarine region. *Estuarine, Coastal and Shelf Science*, *242*, 106864.
- **Dias, A.,** Kurian, S., & Thayapurath, S. (2020). Optical characteristics of colored dissolved organic matter during blooms of *Trichodesmium* in the coastal waters off Goa. *Environmental Monitoring and Assessment*, *192*(8), 1-18.
- **Dias, A.,** Kurian, S., Thayapurath, S., & Pratihary, A. K. (2021). Variations of Colored Dissolved Organic Matter in the Mandovi Estuary, Goa, During Spring Inter-Monsoon: A Comparison With COVID-19 Outbreak Imposed Lockdown Period. *Frontiers in Marine Science*. 8:638583.
- **Dias, A.,** & Kurian, S. (2022). Characterization of colored dissolved organic matter along the western continental shelf of India during the seasonal hypoxia. *Estuarine, Coastal and Shelf Science*, *265*, 107714.

Conference participations

- **Albertina Dias,** T. Suresh, Arvind Sahay, Prakash Chauhan, Manguesh Gauns. Preliminary Results Of Colored Dissolved Organic Matter (CDOM) In The Coastal And Estuarine Waters Of Goa During Summer, WOSC, Kochi, 5-8 February, 2015.
- **Albertina Dias,** T. Suresh, Manguesh Gauns, Arvind Sahay, Prakash Chauhan. Spatial and temporal variations of colored dissolved organic matter in the estuarine and coastal waters of Goa. OSICON, 22-24 March 2015.
- **Albertina Dias,** Suresh T, Siby Kurian. CDOM characteristics of *Trichodesmium* bloom observed in the coastal waters, off Goa, India. ICESAL, Mysore, 2-3 July, 2018.
- **Albertina Dias**, Siby Kurian, Suresh T. Some observations on colored dissolved organic matter during blooms in the coastal waters off Goa. WOSC, Vishakhapatnam, 25-27 February, 2019.

Estuarine, Coastal and Shelf Science 265 (2022) 107714

Contents lists available at ScienceDirect

Estuarine, Coastal and Shelf Science

journal homepage: www.elsevier.com/locate/ecss

Characterization of colored dissolved organic matter along the western continental shelf of India during the seasonal hypoxia

Albertina Dias [a,b], Siby Kurian [a,*]

[a] CSIR- National Institute of Oceanography, Dona Paula, Goa, 403004, India
[b] Goa University, Taleigao Plateau, Goa, India

ARTICLE INFO

Keywords:
Colored dissolved organic matter
Western continental shelf of India
Hypoxia
Southwest monsoon
Autochthonous

ABSTRACT

In recent years the number of hypoxic zones in the world is rising, which has been attributed to the increase in nutrients and organic matter due to anthropogenic activities. Here we present results on the variations in absorption and fluorescent characteristics of colored dissolved organic matter (CDOM) along the western continental shelf of India (WCSI) during the southwest monsoon (SWM). WCSI hosts the world's largest, natural, seasonal hypoxic zone covering 180,000 km^2. Water samples were collected along 4 transects off Kochi, Mangalore, Karwar, and Goa during SWM (June–July 2018) for CDOM and other hydrographic parameters. Also, the Goa transect was sampled during late SWM (September–November 2016 and September 2018) when the bottom waters experienced low oxygen conditions. The onset of upwelling was observed in the hydrographical parameters with low temperature and dissolved oxygen (DO) in the sub-surface waters along the Kochi transect. DO decreased with depth and was hypoxic to suboxic in the bottom waters at most of the stations. The Highest CDOM absorption was observed at the nearshore stations of the Goa transect during July 2018. The waters along the Goa transect were highly stratified during the late SWM (September 2018) with low saline waters at the surface (due to heavy rainfall), with the development of hypoxia in the bottom waters. High CDOM absorption (a_g412 m^{-1}) was observed in the bottom waters, which coincided with hypoxic/suboxic conditions. Spectral slope $S_{250\text{-}600}$ also showed a significant difference between the oxygen rich and low oxygenated waters. Three fluorescent DOM components were identified from PARAFAC analysis. Component 1 (C1) and 2 (C2) were humic-like with emissions in the longer wavelength, while component 3 (C3) was protein-like with excitation and emission in the UV region. CDOM absorption (a_g412) and humic-like fluorescent component (C1) showed a positive correlation with apparent oxygen utilization (AOU), indicating the role of microbial respiration for CDOM production. Laboratory experiments also shed light on the CDOM production in low oxygenated waters when sufficient organic matter is available. This study gives insight into understanding dissolved organic matter's cycling under varying oxygen conditions prevailing in these waters.

1. Introduction

Dissolved organic matter (DOM) is a complex mixture of reduced carbon (Hansell and Carlson, 2014) comprising the largest pool of organic carbon on the earth (Hedges and Keil, 1995). It plays an important role in the biogeochemical cycling of C, N, and P globally (Hansell et al., 2002). DOM present in the aquatic system can be either autochthonous (algal exudation, viral lysis, grazing) or allochthonous (riverine discharge, fluvial inputs) with varied composition depending on the source and its exposure to degradation processes (Hansell et al., 2002; Bauer and Bianchi, 2011). Colored DOM (CDOM) is an optically active fraction of the DOM pool that absorbs light in the visible and UV range (Rochelle-Newall and Fisher, 2002; Coble, 2007; Zhang et al., 2009). CDOM plays an important role in regulating the penetration of photosynthetically active radiation (PAR), thereby influencing the primary productivity, protecting organisms from damaging UV radiation, and contributing to the carbon cycle due to its photoreactivity (Williamson et al., 1999; Belzile et al., 2002). A fraction of CDOM emits fluorescence when excited with UV light (fluorescent-DOM, FDOM). FDOM study has received increasing interest due to its usefulness as a proxy for the bulk DOC pool (Stedmon et al., 2003; Zhou et al., 2016). Fluorescence excitation-emission matrices (EEMS) together with

* Corresponding author.
E-mail address: siby@nio.org (S. Kurian).

https://doi.org/10.1016/j.ecss.2021.107714
Received 11 May 2021; Received in revised form 30 November 2021; Accepted 18 December 2021
Available online 21 December 2021

frontiers in Marine Science

ORIGINAL RESEARCH
published: 20 May 2021
doi: 10.3389/fmars.2021.638583

Variations of Colored Dissolved Organic Matter in the Mandovi Estuary, Goa, During Spring Inter-Monsoon: A Comparison With COVID-19 Outbreak Imposed Lockdown Period

Albertina Dias[1,2], Siby Kurian[1], Suresh Thayapurath[1] and Anil K. Pratihary[1]*

[1] CSIR-National Institute of Oceanography, Panaji, India, [2] School of Earth, Ocean, and Atmospheric Sciences, Goa University, Taleigão, India

OPEN ACCESS

Edited by:
D. Swain,
Indian Institute of Technology Bhubaneswar, India

Reviewed by:
Mar Nieto-Cid,
Spanish Institute of Oceanography, Spain
Fernanda Giannini,
Federal University of Rio Grande, Brazil

***Correspondence:**
Siby Kurian
siby@nio.org

Specialty section:
This article was submitted to Marine Biogeochemistry, a section of the journal Frontiers in Marine Science

Received: *07 December 2020*
Accepted: *29 April 2021*
Published: *20 May 2021*

Citation:
Dias A, Kurian S, Thayapurath S and Pratihary AK (2021) Variations of Colored Dissolved Organic Matter in the Mandovi Estuary, Goa, During Spring Inter-Monsoon: A Comparison With COVID-19 Outbreak Imposed Lockdown Period. Front. Mar. Sci. 8:638583. doi: 10.3389/fmars.2021.638583

Colored dissolved organic matter (CDOM) is one of the important fractions of dissolved organic matter (DOM) that controls the availability of light in water and plays a crucial role in the cycling of carbon. High CDOM absorption in the Mandovi Estuary (Goa) during spring inter-monsoon (SIM) is largely driven by both *in-situ* production and anthropogenic activities. Here we have presented the CDOM variation in the estuary during SIM of 2014–2018 and compared it with that of 2020 when the COVID-19 outbreak imposed lockdown was implemented. During 2020, low CDOM absorption was observed at the mid-stream of the estuary as compared to the previous years, which could be attributed to low autochthonous production and less input from anthropogenic activities. On the other hand, high CDOM observed at the mouth during 2020 is linked to autochthonous production, as seen from the high concentrations of chlorophyll *a*. High CDOM in the upstream region could be due to both autochthonous production and terrestrially derived organic matter. Sentinel-2 satellite data was also used to look at the variations of CDOM in the study region which is consistent with *in-situ* observations. Apart from this, the concentration of nutrients (NO_3^-, NH_4^+, and SiO_4^{4-}) in 2020 was also low compared to the previous reports. Hence, our study clearly showed the impact of anthropogenic activities on CDOM build-up and nutrients, as the COVID-19 imposed lockdown drastically controlled such activities in the estuary.

Keywords: CDOM, Mandovi Estuary, COVID-19 lockdown, Sentinel-2, anthropogenic activities

INTRODUCTION

Dissolved organic matter (DOM) is one of the key pools of organic carbon in natural waters (Hedges, 1992), and colored DOM (CDOM) is that fraction of DOM that interacts with light (Blough and Del Vecchio, 2002; Nelson and Siegel, 2002; Nelson et al., 2007). CDOM controls the availability of light in water and plays an important role in regulating the chemical processes in water (Mopper and Kieber, 2002; Coble, 2007). CDOM can be produced *in-situ* by biological

Environ Monit Assess (2020) 192:526
https://doi.org/10.1007/s10661-020-08494-w

Optical characteristics of colored dissolved organic matter during blooms of *Trichodesmium* in the coastal waters off Goa

Albertina Dias · Siby Kurian · Suresh Thayapurath

Received: 6 February 2020 / Accepted: 13 July 2020

Abstract *Trichodesmium*, a marine cyanobacterium, plays a significant role in the global nitrogen cycle due to its nitrogen fixing ability. Large patches of *Trichodesmium* blooms were observed in the coastal waters, off Goa during spring intermonsoon (SIM) of 2014–2018. Zeaxanthin was the dominant pigment in the bloom region. Here, we present the spectral absorption and fluorescence characteristics of colored dissolved organic matter (CDOM) during these blooms. CDOM concentration was much higher in the bloom patches as compared with nonbloom regions. During the bloom spectral CDOM absorption had distinct peaks in the UV region due to the presence of UV-absorbing/screening compounds, mycosporine-like amino acids (MAAs) and in the visible region due to phycobiliproteins (PBPs). The spectral fluorescence signatures by the traditional peak picking method exhibited three peaks, one was protein-like, and the other two were humic-like. Apart from these, *Trichodesmium* exhibited strong protein-like fluorescence with 370/460 nm (Ex/Em), which is a signature of cyanobacteria. A parallel factor analysis (PARAFAC) on the fluorescence excitation-emission matrix (EEM) of *Trichodesmium* dataset fitted a 3-component model of which one was protein-like, and two were humic-like. The fluorescence index (FI) values during *Trichodesmium* bloom was very high (~ 3) compared with the typical range of 1.2–1.8 observed for the natural waters. Bloom degradation experiments proved that increase in tryptophan fluorescence enhances the CDOM absorption. Our study indicates that *Trichodesmium* blooms provide a rich source of organic matter in the coastal waters and long-term monitoring of these blooms is essential for understanding the health of ecosystem.

Keywords Dissolved organic matter · Photodegradation · Mycosporine-like amino acids · Phycobiliproteins · PARAFAC

A. Dias · S. Kurian (✉) · S. Thayapurath
CSIR—National Institute of Oceanography, Dona Paula, Goa 403004, India
e-mail: siby@nio.org

A. Dias
School of Earth, Ocean and Atmospheric Sciences, Goa University, Goa 403206, India

Introduction

Dissolved organic matter (DOM) is perhaps the largest repository of organic carbon in the ocean and most inland waters (Thurman 1985). It is composed of heterogeneous mixture of organic compounds originating either from allochthonous (terrestrial origin), autochthonous (algal or phytoplankton origin), or anthropogenic sources with a wide range of molecular weights ranging from less than 100 to over 300,000 Daltons (Hayase and Tsubota 1985; Ma and Ali 2009). DOM, being the most mobile and active cycling fraction of organic matter, influences a spectrum of biogeochemical processes. As it plays an important role in global biogeochemical cycles, studies on the sources of DOM, its chemical characteristics, and cycling in the aquatic environment

Published online: 16 July 2020

Estuarine, Coastal and Shelf Science 242 (2020) 106864

Contents lists available at ScienceDirect

Estuarine, Coastal and Shelf Science

journal homepage: http://www.elsevier.com/locate/ecss

Influence of environmental parameters on bio-optical characteristics of colored dissolved organic matter in a complex tropical coastal and estuarine region

Albertina Dias [a,b], Siby Kurian [a,*], Suresh Thayapurath [a]

[a] CSIR- National Institute of Oceanography, Dona Paula, Goa, 403004, India
[b] Goa University, Taleigao Plateau, Goa, India

ARTICLE INFO

Keywords:
Colored dissolved organic matter
Photobleaching
Non-conservative mixing
Autochthonous
Allochthonous

ABSTRACT

Dissolved organic matter (DOM) is an important source of carbon in aquatic ecosystems, and colored DOM (CDOM), which is smaller than 0.2 μm and interacts with ultraviolet (UV) and visible light, affects the spectral quality and quantity of light in water. In this study, the spatial and temporal variations of CDOM with changes in environmental conditions were investigated from March 2014 to May 2017 in the coastal waters and two estuaries (Zuari and Mandovi) of Goa, western India, and the major sources and sinks controlling the optical properties of these waters were identified. The CDOM absorption in the estuaries was two times higher than that of the coastal waters. It was also determined that the CDOM absorption at 412 nm (a_g412) in the coastal and estuarine waters significantly varied between seasons. The a_g412 was found to be higher in the coastal waters during the spring inter-monsoon (SIM) and fall inter-monsoon (FIM) than during the northeast monsoon (NEM). The high absorption during the SIM was of autochthonous origin, while terrigenous DOM was the primary contributor mainly during the FIM. The photobleaching of CDOM was highest during the SIM, resulting in the predominance of low-molecular-weight DOM in the coastal waters. This photobleaching of DOM also resulted in deeper UV light penetration, as indicated by the diffuse attenuation coefficient K_d at 350 nm. In the Mandovi and Zuari estuaries, higher levels of CDOM were observed during the southwest monsoon (SWM) and SIM than the FIM and NEM. The terrigenous DOM contribution was higher in the estuaries during the SWM, while phytoplankton contributed to a higher level of CDOM during the SIM. CDOM exhibited non-conservative mixing behavior in the study region, as it decreased in estuaries with lower salinities and increased at salinities between 20 and 31. Considering the importance of CDOM in the carbon cycle, this study highlights the various sources and sinks of CDOM controlling the optical properties and biogeochemical processes of coastal and estuarine waters.

1. Introduction

Dissolved organic matter (DOM) is one of the largest sources of biologically available organic carbon in aquatic ecosystems, and its dynamics affect carbon cycling at local to global scales (Battin et al., 2009). Colored DOM (CDOM) is a complex DOM pool originating from terrestrially derived materials due to plant degradation and riverine runoff (allochthonous), and from *in-situ* production by phytoplankton, microbial remineralization, excretion, and grazing within the water body (autochthonous) (Zhang et al., 2009; Loiselle et al., 2012). CDOM is operationally defined as the optically active component of DOM present in the water that is smaller than 0.2 μm and interacts with ultraviolet (UV) and visible light. CDOM plays a major role in the spectral quality and quantity of available light in water and can have a positive or negative impact on the ecosystem. Low levels of CDOM result in deeper penetration of UV light in the water, affecting marine biota, whereas high levels of CDOM will limit penetration of visible light, hampering primary productivity (Del Vecchio and Blough, 2002). CDOM can also interfere with satellite measurements of phytoplankton biomass, which affects ecosystem models (Carder et al., 1991; Vodacek et al., 1994; Nelson and Siegel, 2013). It is also an essential climate variable (ECV) that influences ocean color (Groom et al., 2019).

Rivers and estuaries are important sources of DOM during its transport from the terrestrial ecosystem to the coastal ocean. The coastal

* Corresponding author.
E-mail address: siby@nio.org (S. Kurian).

https://doi.org/10.1016/j.ecss.2020.106864
Received 5 July 2019; Received in revised form 2 May 2020; Accepted 25 May 2020
Available online 30 May 2020

Indian Journal of Geo Marine Sciences
Vol.46 (05), May 2017, pp. 860-870

Contrasting characteristics of colored dissolved organic matter of the coastal and estuarine waters of Goa during summer

Albertina Balbina Dias[1], Suresh Thayapurath[1], Arvind Sahay[2] & Prakash Chauhan[2]

[1]Marine Instrumentation Division, CSIR-National Institute of Oceanography, Dona Paula Goa, 403004, India
[2]Space Application Centre, Ahmedabad, 380015, India

[E.Mail: albertina.dias8@gmail.com ; suresh@nio.org]

Received 25 June 2015 ; revised 07 December 2015

The colored dissolved organic matter (CDOM) was investigated during the summer for the coastal and estuarine waters of Goa using the spectral absorption characteristics of CDOM. Accessions of CDOM were seen all along the estuary through multiple sources of CDOM with relatively insignificant sink, while in the coastal waters there was a sink due to photo bleaching. Measure of CDOM indicated by the absorption at reference wavelength $a_g(412)$ varied with a mean value of 0.470 m^{-1} in the Mandovi, 0.420 m^{-1} in Zuari and 0.176 m^{-1} in the coastal waters. Slope of CDOM $S_{250-600}$ was found to vary from 0.080-0.017 nm^{-1} in coastal waters and 0.017-0.020 nm^{-1} in the estuaries. High values of $S_{275-295}$ observed in the coastal waters were indicative of photobleaching. Point of inflection was observed at a distance of about 8 km from the mouth of the estuary at a salinity of about 34 psu.

[**Key words**: CDOM, Dissolved organic matter, Estuaries, Coastal waters, optical properties, resuspension, Goa]

Introduction

Dissolved organic matter (DOM) stores a large amount of organic carbon in the marine environment[1]. Colored dissolved organic matter (CDOM) which is often known as gilvin, gelbstoff, yellow substances, is defined as that component of DOM that passes through 0.2 micron filter and interacts with UV and visible light of the solar spectrum. The contribution by CDOM to dissolved organic carbon (DOC) is estimated to be the highest in the coastal and estuarine waters[2]. CDOM regulates the penetration of UV light in the water column and hence it can have a positive or negative impact on the aquatic system[3-5]. Rivers and estuaries form an important source transporting DOM from the terrestrial ecosystem to the coastal ocean. Transformations of CDOM are expected to have a significant impact on carbon cycling dynamics[6 - 8]. The coastal waters off Goa are net consumers of organic matter, rather than producers[9]. Seasonal algal blooms of which *Trichodesmium* are observed during summer, *Noctiluca* during winter and other varied species, which are episodic, have been reported in these waters[10 -15]. These blooms have an impact on the coastal waters affecting the biogeochemical cycles. These waters are affected by seasonal reversing currents, with strong temperature inversions being observed due to the transport of low salinity waters from the Bay of Bengal during winter[16]. Hypoxia is also observed in these coastal waters[17], which is of biogeochemical and environmental importance.

The Mandovi and Zuari estuaries on the west coast of India are the two estuaries of Goa, which are classified as monsoonal estuaries[18]. There is very less discharge from river runoff during the summer because of which the estuaries become an extension of the sea and remain vertically well mixed[19- 23]. During the summer, there is very less precipitation and the driving force in the estuary for mixing and circulations are solely controlled by the tides[22 24]. Although adjacent to each other the Mandovi and Zuari estuaries are influenced by different factors thus, each estuarine environment exhibits a wide variation in its physical and chemical features[25]. The estuarine waters during summer are found to be highly productive[9 11 26]. There are mangroves present all along the banks of the estuaries that form a major reservoir of organic matters. These estuaries receives